Report
R-19-17
October 2019

Groundwater flow modelling under transient ice sheet conditions in Greenland

Oliver Jaquet
Rabah Namar
Pascal Siegel
Joel Harper
Peter Jansson

SVENSK KÄRNBRÄNSLEHANTERING AB

SWEDISH NUCLEAR FUEL
AND WASTE MANAGEMENT CO

Box 3091, SE-169 03 Solna
Phone +46 8 459 84 00
skb.se

SVENSK KÄRNBRÄNSLEHANTERING

ISSN 1402-3091
SKB R-19-17
ID 1597342
October 2019

Groundwater flow modelling under transient ice sheet conditions in Greenland

Olivier Jaquet, Rabah Namar, Pascal Siegel
In2Earth Modelling Ltd

Joel Harper, University of Montana

Peter Jansson, Department of Physical Geography
and Quaternary Geology, Stockholm University

Summary

The Greenland Analogue Project (GAP), an international field and modelling study of the Greenland Ice Sheet was established in 2008, collaboratively by the Swedish, Finnish and Canadian nuclear waste management organisations; namely, SKB (Svensk Kärnbränslehantering AB), Posiva (Posiva Oy) and NWMO (Nuclear Waste Management Organisation). The aim of GAP is to advance the understanding of the impact of glacial processes on the long-term performance of a deep geologic repository. The Greenland Ice Sheet is considered to be a modern analogue with respect to size and conditions that could prevail in Fennoscandia and Canada during future glacial periods with continental-scale ice sheets. Within the framework of the GAP project, this third phase of groundwater flow modelling under transient ice sheet conditions in Greenland has enabled the assimilation of transient data from the dynamic ice sheet model SICOPOLIS into the simulations over time frames relevant to safety assessment applications. Modelling density-driven groundwater flow, heat transfer and permafrost using transient boundary conditions representing ice sheet displacement was performed during a complete glacial cycle (from -115 to -1 ka before 2000 AD) in Greenland. Detailed subglacial topography, subglacial layer, deformation zones, borehole data and talik locations were integrated in the model. For the first time, the choice for the subglacial boundary conditions (i.e. as ice overburden hydraulic pressure) could be justified by field data provided by ice boreholes drilled in the Greenland ice sheet during the GAP project. The impact of various hydraulic parametrisations for the rock domain and deformation zones was investigated based on data from three sites located in the Fennoscandian shield (Laxemar, Forsmark and Olkiluoto). Furthermore, the effect of specific glaciation scenarios given by the dynamic ice sheet model was investigated. The tracing of meltwater from the ice sheet was modelled in order to determine the depth range likely reachable by glacial meltwater for the various sensitivity cases. The subglacial layer plays a key hydraulic role in draining meltwater underneath the ice sheet. Below the surface, groundwater flow is governed by the hydraulic parametrisation of the rock domain, the deformation zones and the permafrost. Glacial meltwater is likely to reach depths that exceed 500 m whatever the glacial period considered. During the periods of glacial build-up and retreat, solely the taliks located within a few kilometres of the ice margin can be reached by glacial meltwater. Whatever the glacial period considered, for the lower hydraulic parametrisation cases (Forsmark and Olkiluoto), the flux values remains below 10 mm/a at depth. The mean depth of permafrost lies in the range 509 – 617 m when only a part of the domain is covered by the ice sheet during the periods of glacial build up and retreat. Finally, the presented groundwater flow modelling approach allowing assimilation of dynamic ice sheet model data leads to a reduction in uncertainty and consequently improves confidence when assessing selected measures of repository performance.

Sammanfattning

The Greenland Analogue Project (GAP), ett internationellt fält- och modelleringsprojekt om Grönlands inlandsis initierades 2008 av de svenska, finska och kanadensiska organisationerna för hantering av kärnavfall; nämligen SKB (Svensk Kärnbränslehantering AB), Posiva (Posiva Oy) och NWMO (Nuclear Waste Management Organization). Syftet med GAP är att främja förståelsen för inverkan av glaciala processer på den långsiktiga prestandan av djupa geologiska förvar. Grönlands inlandsis kan betraktas som en modern analog med avseende på storlek och andra förhållanden som kan råda i Fennoskandien och Kanada under framtida perioder med inlandsisar på kontinental skala. Inom ramen för GAP-projektet har denna tredje fas av grundvattenflödesmodellering med transienta inlandsisförhållanden på Grönland möjliggjort att integrera data från den dynamiska inlandsismodellen SICOPOLIS i simuleringarna för tidsperspektiv som är relevanta för säkerhetsanalysapplikationer. Modellering av densitetsdrivet grundvattenflöde, värmetransport och permafrost med användning av transienta randvillkor som representerar förändringar i inlandsisens läge och mäktighet utfördes under en komplett glaciationscykel på Grönland (från -115 till -1 ka relativt 2000 e.Kr.). Subglacial topografi, subglacialt lager, deformationszoner, borrhålsdata och läge för talikar integrerades i modellen. För första gången har valet av de subglaciala randvillkoren (dvs hydrauliskt tryck motsvarande ismassans mäktighet) kunnat motiveras med fältdata från isborrhål som borrats igenom Grönlands inlandsis under GAP-projektet. Effekterna av olika hydrauliska parametriseringar för bergmassan och deformationszoner har undersökts baserat på data från tre platser belägna i den Fennoskandiska skölden (Laxemar, Forsmark och Olkiluoto). Dessutom undersöktes effekten av specifika glaciationsscenarier som ges av den dynamiska inlandsismodellen. Spårning av smältvatten från inlandsisen modellerades för olika känslighetsfall för att bestämma det djup till vilket smältvatten från isen troligen kan nå. Det subglaciala lagret spelar en hydraulisk nyckelroll för bortledning av smältvatten under inlandsisen. I berget styrs grundvattenflödet av den hydrauliska parametriseringen av bergmassan, deformationszonerna samt av permafrosten. Glacialt smältvatten kommer sannolikt att nå djup som överstiger 500 m oavsett vilken glacial period som beaktas. Under perioderna med isuppbyggnad och isavsmältning kan endast de talikar som ligger inom några få kilometers avstånd från isfronten nås av smältvatten från isen. Oavsett vilken glacial period som beaktas för fallen med de lägre hydrauliska egenskaperna (Forsmark och Olkiluoto), förblir flödena mindre än 10 mm/år på djupet. När endast en del av domänen täcks av inlandsisen ligger det genomsnittliga djupet av permafrost i intervallet 509 – 617 m. Den presenterade strategin för grundvattenflödesmodellering, vilken inkorporerar resultat från en dynamisk inlandsismodell, leder till en minskning av osäkerheterna och förbättrar därmed förtroendet för modellen vid utvärdering av förvarets prestanda.

Contents

1 Introduction

The Greenland Analogue Project (GAP), an international field and modelling study of the Greenland Ice Sheet was established in 2008, collaboratively by the Swedish, Finnish and Canadian nuclear waste management organisations; namely, SKB (Svensk Kärnbränslehantering AB), Posiva (Posiva Oy) and NWMO (Nuclear Waste Management Organisation).

The aim of GAP is to advance the understanding of the impact of glacial processes on the long-term performance of a deep geologic repository. The Greenland Ice Sheet is considered to be a modern analogue with respect to size and conditions that could prevail in Fennoscandia and Canada during future glacial periods with continental-scale ice sheets. In addition, the bedrock in the studied domain presents some similarities in terms of composition, fracturing and age to the crystalline bedrock in Sweden, Finland and Canada.

The funding organisations together with participation of researchers from universities and geological surveys in Canada, Denmark, Finland, Sweden, Switzerland, United Kingdom and the United States want to improve scientific understanding of continental ice sheet and permafrost effects on groundwater flow and water chemistry in crystalline rocks at depths resembling those of a potential deep geological repository over time frames of 100 000 years or more.

The GAP study area is located on the west coast of Greenland close to the village of Kangerlussuaq, just north of the Polar Circle. This domain extends from the Kangerlussuaq fjord to the ice divide, measuring approximately 200 km from east to west; and 60 km from north to south. The selection criteria for the GAP study area were the following: i) the main orientation is parallel to the general ice flow direction; ii) the presence of wet and frozen conditions at the base of the ice sheet and iii) the pro-glacial domain is formed of continuous permafrost and comprises larger lakes.

This report provides contributions to the Greenland Analogue Project by answering specific questions using a numerical approach. A hydrogeological model is developed that assimilates transient data from dynamic ice sheet modelling and field data from the GAP area.

2 Objectives

The potential impact of long-term climate changes has to be evaluated with respect to repository performance and safety. In particular, glacial periods of advancing and retreating ice sheets and prolonged permafrost conditions are likely to occur over a repository site. The growth and decay of ice sheets and the associated distribution of permafrost will affect the chemical composition of the groundwater flow and its flow field. Since significant changes may take place, the understanding of groundwater flow patterns and composition during glaciations is an important safety issue for the geological disposal at long term. During a glacial period, the performance of the repository could be impacted by some of the following conditions and associated processes:

- Maximum pressure at repository depth (canister failure).
- Maximum permafrost depth (canister failure, buffer function).
- Darcy flux (buffer erosion).
- Concentration of groundwater oxygen (canister corrosion).
- Groundwater salinity and groundwater with low ionic concentrations (buffer stability).
- Glacially induced earthquakes (canister failure).

Thus, in order to advance scientific understanding of hydrological, hydrogeological and geochemical processes during glacial conditions, GAP research was focused on obtaining information that contributes to answering the following six overall project questions (Claesson Liljedahl et al. 2016):

1. Where is the meltwater generated under an ice sheet?
2. What are the hydraulic pressure conditions under an ice sheet, driving groundwater flow?
3. To what depth does glacial meltwater penetrate into the bedrock?
4. What is the chemical composition of glacial water when and if it reaches repository depth?
5. How much oxygenated water will reach repository depth?
6. Does discharge of deep groundwater occur in the investigated proglacial talik in the study area?

Therefore, with the help of numerical modelling, specific answers shall be provided that aim at further understanding of key related hydrogeological issues:

- Regional groundwater flow system under ice sheet conditions during a complete glacial cycle.
- Flow and infiltration conditions at the ice sheet bed.
- Penetration depth of glacial meltwater into the bedrock.
- Water chemical composition at repository depth in presence of glacial effects.
- Role of the taliks, located in front of the ice sheet, likely to act as potential discharge zones of deep groundwater flow.
- Influence of permafrost distribution on the groundwater flow system in relation to glacial periods of build up, completeness and retreat.

Some answers are provided by the field data and investigations; the integration of the data, the dynamic characterisation and the understanding of the key processes is obtained through numerical modelling at regional scale. Preliminary scoping calculations were performed by developing a groundwater flow model under ice sheet conditions for the region of Kangerlussuaq (Jaquet et al. 2010). These calculations have highlighted the governing importance of specific factors, such as ice boundary conditions, permafrost and taliks on the groundwater flow system.

This preliminary phase was followed by a second phase of groundwater flow modelling (Jaquet et al. 2012) that aimed at a more in depth understanding of groundwater flow conditions likely to occur underneath ice sheets. This modelling phase has enabled the development of an improved regional model that has led to a better representation of groundwater flow under ice sheet conditions. New data in relation to talik geometry and elevation, as well as to deformation zones were integrated in the numerical model. In addition, more realistic hydraulic properties were considered for groundwater flow modelling. The major improvements were related to: i) the assimilation of the subglacial boundary conditions using pressure and meltwater rates provided by a dynamic ice sheet model – describing present day conditions – that has enabled simulation of a more plausible flow field in the Eastern part of the domain, ii) the integration of all potential taliks within the modelled domain that have provided a better characterisation of the flow field under ice sheet conditions, and iii) the characterisation of the permafrost-depth distribution that was improved using a coupled description of flow and heat transfer. Finally, the tracing of glacial meltwater produced by the ice sheet was modelled for the determination of depth and lateral extent likely reachable by glacial water.

This third groundwater flow modelling phase of the GAP enables the assimilation of transient data from dynamic ice sheet modelling into the simulations over time frames relevant to the safety assessment. Modelling density-driven groundwater flow, heat transfer and permafrost using transient boundary conditions representing ice sheet displacement is performed during a complete glacial cycle in Greenland. Detailed subglacial topography, deformation zones, borehole data and talik location are integrated in the model. The impact of various hydraulic parameterisations for the rock domain and deformation zones is investigated based on data from three sites located in the Fennoscandian shield (Laxemar, Forsmark and Olkiluoto). The tracing of meltwater from the ice sheet is modelled in order to determine the depth range likely reachable by glacial water for various glaciation scenarios.

3 Conceptualisation

The regional domain of the groundwater flow model, under ice sheet conditions, is located in the SW part of Greenland near the town Kangerlussuaq (Figure 3-1). The domain extends in an EW direction, roughly parallel to ice flow and hence, inferred general glacier hydrology flow direction.

The Kangerlussuaq area is located in the Precambrian region of West Greenland (Henriksen et al. 2000) and belongs to the southern part of the Nagssugtoqidian Orogen, which consists of an approximately 1 900 to 1 800 Ma old fold belt that formed in a collision zone between two parts of a previously rifted large Archaean continent (Claesson Liljedahl et al. 2016). Between the coast and the ice sheet, the bedrock is dominated by banded gneisses which are frequently fractured and weathered. Amphibolites and pegmatitic dykes are associated with these extensively metamorphosed gneisses (Wallroth et al. 2010).

Based on lineament interpretation and field observations, over a hundred major deformation zones and faults could be revealed for this region (Engström et al. 2012, Follin et al. 2011); these zones are likely more permeable than the surrounding metamorphic rocks. This geological medium with conductive deformation zones is considered as a 3D stochastic continuum; i.e. a continuum with stochastically described hydraulic properties.

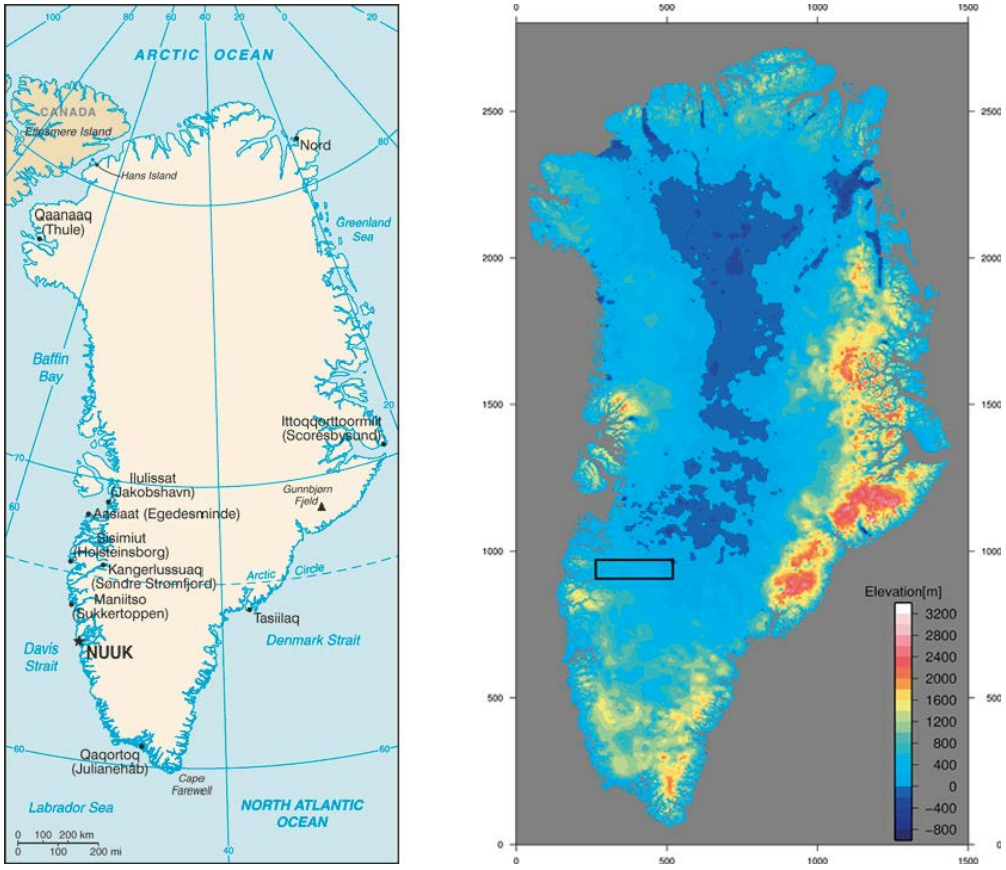

Figure 3-1. *Geography of Greenland (left; after http://wwp.greenwichmeantime.com/ time-zone/ north-america/greenland/map/index.htm) and location of the groundwater flow model in relation to the Greenland digital bed elevation model (right; after Bamber 2001).*

The boundary conditions for the groundwater flow model are taken from ice sheet simulations produced using two different ice sheet models. The SICOPOLIS *(SImulation COde for POLythermal Ice Sheets)* model that enables simulation of a full glacial cycle, involving glacial build up and retreat; i.e. transient boundary conditions, representing the ice sheet displacement, are applied for the purpose of groundwater flow modelling. And, the ice sheet model VarGlaS (*Variational Glacier Simulator*) where present day ice sheet conditions are considered in quasi-equilibrium at the investigated location; corresponding to steady state boundary conditions where the movement of the ice sheet is not taken into account.

Transient ice sheet data from SICOPOLIS are provided by the University of Stockholm (Vallot et al. 2012a, b). SICOPOLIS (Greve et al. 2011) enables simulation of large-scale dynamics and thermodynamics (ice extent, thickness, velocity, temperature, water content and age) of ice sheets in the 4 dimensional space-time domain. The shallow-ice approximation (Hutter 1983, Morland 1984) is applied as well as the rheology of an incompressible, heat-conducting, power-law fluid. The description of thermomechanical coupling is obtained by the temperature- and water-content-dependent rate factor (Greve et al. 1998). Finally, the elastic–lithosphere–relaxing–asthenosphere approach (Greve and Blatter 2009) is applied for the modelling of lithosphere isostatic effects; i.e. depression and rebound due to the changing of ice load.

Steady state ice sheet data from VarGlaS are provided by the GAP ice sheet modelling group from the University of Montana. VarGlaS (Brinkerhoff and Johnson 2013) is novel prognostic ice sheet model that uses a continuum formulation for describing thermomechanical coupling with higher order finite element. The solution to the Stokes' equations is treated as a minimisation of a scalar variational principle representing the conversion of gravitational potential energy into heat under the constraint of incompressibility. For the energy balance equations, an enthalpy formulation is applied. The three-dimensional ice sheet velocity, enthalpy, and geometry are solved through time with strong coupling of all these three variables. Regarding data assimilation, inversion of surface velocity data is performed to obtain an initial estimate of the basal traction field by using the adjoint-state method.

The data provided by the two ice sheet models SICOPOLIS and VarGlas and used as boundary conditions for groundwater flow modelling are respectively of the following types: ice thickness and temperature for the transient simulations during a complete glacial cycle in Greenland; ice thickness and meltwater rate for the steady-state cases representative of present day conditions.

The state of the Greenland ice sheet is still not well understood. Krabill et al. (2000) showed that the interior of the ice sheet thickened while peripheral parts experienced thinning. That the Greenland ice sheet is experiencing losses have also been reported from GRACE data by Chen et al. (2006), Luthcke et al. (2006), Ramillien et al. (2006), and Velicogna and Wahr (2006). The results provide a strong independent indication that mass losses from the Southern part of Greenland ice sheet has increased substantially, thus verifying more local studies from Rignot et al. (1997), Howat et al. (2005), Rignot and Kanagaratnam (2006), and Luckman et al. (2006). Much of the mass losses observed are thus from dynamic response at outlet glaciers.

The permafrost is continuous in the periglacial environment, except at the location of taliks. Beneath the ice sheet, some permafrost regions of limited extent can still occur. The depth variability of the permafrost depends on: the surface and ground thermal conditions, the groundwater flow system, and the geothermal flux from the Earth interior (Vidstrand 2003, Hartikainen et al. 2010). Glacial climate conditions are assumed during glacial build up, the vertical extent of permafrost decreases as the ice advances and recovers it; at the glacial maximum, the entire permafrost is under ice and continues to decrease, it might even disappear; finally, due to warmer climatic conditions the ice sheet retreats, the remaining permafrost is gradually eliminated as the ice sheet progresses backwards. The permafrost thickness reaches 350–400 m as measured in the boreholes DH-GAP03 and DH-GAP04 (Claesson Liljedahl et al. 2016); the former was drilled a few hundreds of meters away from the ice margin in summer 2009, and the latter, the deep research borehole that extends beneath the ice sheet was realised during summer 2011.

Based on the interpretation of seismic reflection data – carried out up to 70 km from the ice margin – basal sediment sequences of many meters thickness are likely to exist within the major troughs underneath the ice sheet (Harper et al. 2016). These basal sediment sequences constitute the subglacial layer, a discontinuous permeable layer, located at the bedrock-ice interface, which spatial distribution

in terms of geometry and hydraulic properties controls subglacial drainage. And, it potentially plays a major hydraulic contribution in carrying meltwater infiltrating in the subsurface. From the results of the ice boreholes, the subglacial layer consists of a relatively thin veneer of sand and gravel-sized sediment (Claesson Liljedahl et al. 2016).

Density-driven flow as induced by the variable salinity of the groundwater is taken into account in the current modelling phase. Since the groundwater flow model is more than 100 km away from the ocean, its influence is neglected; i.e. there are no fluctuations in ocean level as well as no supply of salt from the Davis Strait. Finally, geomechanical effects, due to ice loading, that lead to variations in hydraulic conductivity, porosity and hence fluid pressure are not considered as part of the conceptual model.

Therefore, the groundwater flow system is considered under transient conditions and governed by infiltration of glacial meltwater in heterogeneous faulted crystalline rocks, with a subglacial sedimentary layer, in the presence of permafrost (Figure 3-2). Two types of water are distinguished: glacial meltwater produced by the ice sheet and saline groundwater circulating at depth; i.e. coupled groundwater flow and transport are considered for describing variations in salinity and therefore fluid density.

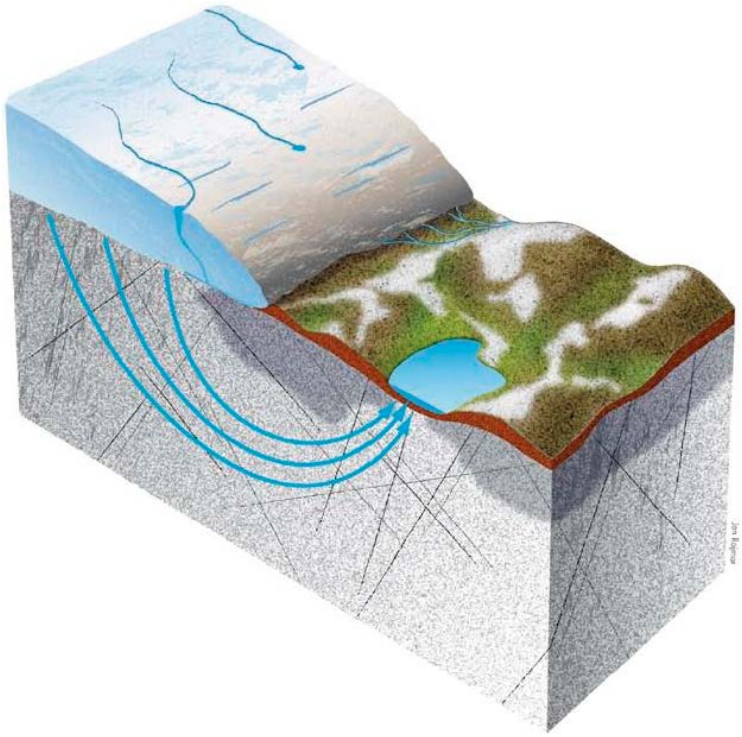

Figure 3-2. *Simplified conceptual model for the groundwater flow system – without density effects – under ice sheet conditions with talik (i.e. a lake with a permafrost free area underneath) and permafrost (in dark grey).*

4 Phenomenology

4.1 Groundwater flow

For the modelled domain, considered as a stochastic continuum, the simulation of groundwater flow with variable density, under permafrost conditions, is obtained using a modified mass conservation equation to account for liquid motion due to volume change induced by density difference between solid and liquid phases:

$$\frac{\partial \rho_f (1-ic)\phi}{\partial t} + \frac{\partial (\rho_{ice} - \rho_f) ic\phi}{\partial t} + \frac{\partial \rho_f u}{\partial x} + \frac{\partial \rho_f v}{\partial y} + \frac{\partial \rho_f w}{\partial z} = Q \qquad (4\text{–}1)$$

where:

ρ_f: fluid density
ρ_{ice}: ice density
ϕ: porosity (kinematic)
ic: proportion of ice
u, v, w: Darcy velocities
Q: source/sink term.

The pressure equation is governed by Darcy's law:

$$\rho\, u = -\frac{K_x}{g}\frac{\partial P}{\partial x}$$

$$\rho\, v = -\frac{K_y}{g}\frac{\partial P}{\partial y} \qquad (4\text{–}2)$$

$$\rho\, w = -\frac{K_z}{g}\frac{\partial P}{\partial z} - K_z(\rho_f - \rho_0)$$

where:

K_x, K_y, K_z: local hydraulic conductivities in x, y and z directions
g: gravity acceleration
P: dynamic fluid pressure; $P = p + \rho_0 g z$, with p the (total) pressure
ρ_0: reference fluid density.

with:

$\rho = \rho_f + (\rho_{ice} - \rho_f)\, ic$

4.2 Salt transport

For the description of salt transport, the following equation is applied (Ferry 2016):

$$\rho\phi\frac{\partial C}{\partial t}+\frac{\partial}{\partial x}\left(\rho_f u\,C-\rho_f\gamma D_e\quad\frac{\partial C}{\partial x}\right)+\frac{\partial}{\partial y}\left(\rho_f v\,C-\rho_f\gamma D_e\quad\frac{\partial C}{\partial y}\right)$$
$$+\frac{\partial}{\partial z}\left(\rho_f w\,C-\rho_f\gamma D_e\quad\frac{\partial C}{\partial z}\right)=\left(\frac{\partial\rho_f u}{\partial x}+\frac{\partial\rho_f v}{\partial y}+\frac{\partial\rho_f w}{\partial z}\right)C+Q_c \qquad (4–3)$$

where:

C: transported mass fraction of salt (salinity)
D_e: effective diffusion coefficient
Q_c: source/ sink term.

The pressure dependency of the porosity is expressed as follows:

$$\phi = \phi_0\,\gamma$$

where:

$$\gamma = 1+\frac{S_s}{\phi_0}\frac{P-P_0}{\rho g}$$

with:

γ: matrix compaction coefficient
S_s: specific storage
ϕ_0: reference porosity (kinematic)

4.3 Permafrost

The modelling of permafrost requires the description of heat transfer. The formulation of Ferry (2016) is adopted while neglecting the latent heat term; i.e. the contribution of water freezing to heat transfer is minor when porosity for water-saturated rocks is less than 1 % (SKB 2006).

$$\rho\phi\frac{\partial c_f T}{\partial t}+\frac{\partial(1-\phi)c_{roc}T}{\partial t}+\frac{\partial\phi c_i T}{\partial t}+\frac{\partial}{\partial x}\left(\rho_f u\,c_f T-\lambda_x\frac{\partial T}{\partial x}\right)+\frac{\partial}{\partial y}\left(\rho_f v\,c_f T-\lambda_y\frac{\partial T}{\partial y}\right)$$
$$+\frac{\partial}{\partial z}\left(\rho_f w\,c_f T-\lambda_z\frac{\partial T}{\partial z}\right)=\left(\frac{\partial\rho_f u}{\partial x}+\frac{\partial\rho_f v}{\partial y}+\frac{\partial\rho_f w}{\partial z}\right)c_f T+Q_T \qquad (4–4)$$

with: $c_i=\rho_i\left(c_{ice}-c_f\right)ic$

where:

T: temperature
c_f: mass-specific heat capacity of fluid
c_{roc}: volume-specific heat capacity of rock
c_{ice}: mass-specific heat capacity of ice
$\lambda_x,\lambda_y,\lambda_z$: equivalent thermal conductivities (i.e. rock + fluid) in x, y and z directions
Q_T: source/sink term

The proportion of ice in the pore space is obtained using the following function (Figure 4-1):

$$ic = ic_{max}\left\{1 - e^{-\left(\frac{min(T,T_L) - T_L}{W}\right)^2}\right\} \quad (4\text{–}5)$$

where:

ic: proportion of ice
ic_{max}: maximum proportion of ice (set to 1)
T_L: freezing temperature
W: temperature interval for freezing.

The following reduction in hydraulic conductivity is applied for the permafrost (cf. Figure 4-1):

$$K = max\left\{\alpha\, K_{ref}\,,\, 10^{-12}\right\} \quad (4\text{–}6)$$

with :

$$\alpha = max\left\{\alpha_{min}, (1 - ic)^a\right\}$$

where:

α: reduction factor
α_{min}: lower bound for reduction factor (i.e. maximum reduction for permeability)
a: constant related to rock type
K_{ref}: hydraulic conductivity of unfrozen rock.

And, the kinematic porosity of the frozen rock (permafrost) is obtained as follows:

$$\phi = (1 - ic)\,\phi_{ref} \quad (4\text{–}7)$$

where:

ϕ_{ref}: kinematic porosity of unfrozen rock.

Following the modelling approach applied in Sweden for the Laxemar and Forsmark sites (Vidstrand et al. 2010a, b), no dependence is assumed between the dynamic viscosity of water and the temperature. Therefore, for density-driven flow under isothermal conditions, the fluid properties are given by the following state laws:

$$\mu = \mu_0$$

$$\rho = \rho_0\left[1 + \alpha_1 C\right] \quad (4\text{–}8)$$

where:

μ: dynamic viscosity
α_1: constant parameter.

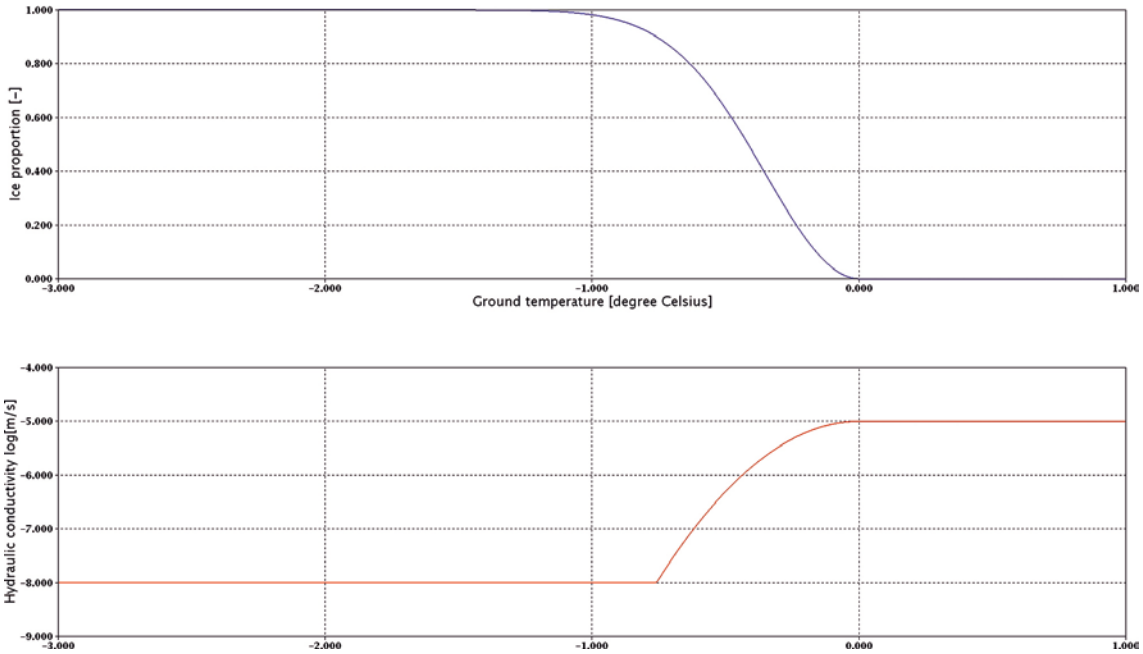

Figure 4-1. *Ice proportion and log(hydraulic conductivity) curves as function of temperature.*

4.4 Tracing of glacial meltwater

The tracing of glacial meltwater produced by the ice sheet is performed using the following transport equation (Svensson et al. 2010):

$$\rho_{mw}\left[\phi\frac{\partial C_{mw}}{\partial t}+\frac{\partial}{\partial x}\left(uC_{mw}-D_e\frac{\partial C_{mw}}{\partial x}\right)+\frac{\partial}{\partial y}\left(vC_{mw}-D_e\frac{\partial C_{mw}}{\partial y}\right)+\frac{\partial}{\partial z}\left(wC_{mw}-D_e\frac{\partial C_{mw}}{\partial z}\right)\right] \quad (4\text{–}9)$$
$$= \rho_{mw}\left(\frac{\partial u}{\partial x}+\frac{\partial v}{\partial y}+\frac{\partial w}{\partial z}\right)C_{mw}+Q_{C_{mw}}$$

where:

ρ_{mw}: density of meltwater
C_{mw}: transported mass fraction of meltwater
Qc_{mw}: source/ sink term.

The application of Equation (4-9) assumes that the description of the medium heterogeneity in terms of a stochastic continuum enables the characterisation of the spatial variability for the fluid velocity and therefore captures the effects of kinematic dispersion. The effects of matrix diffusion could not be considered in the present modelling phase, due to numerical problems.

5 Geomodelling

5.1 Model domain

The longest dimension of the 3D domain for the groundwater flow model extends about 150–200 km beneath the ice sheet and roughly 50 km in front of the ice sheet margin (Figure 5-1). The width of the model is approximately 60 km and its depth is set to about 5 km. The EW orientation of the domain, i.e. its long axis, coincides with the main ice flow direction. These dimensions are identical to those selected for the first and second modelling phases (Jaquet et al. 2010, 2012).

5.2 Topographic data and taliks

During GAP, the subglacial topography was mapped, at high spatial resolution (250 to 500 m), with the help of 1 500 km of radar profiles using two ground-based impulse radar systems. GAP Digital Elevation Models (DEMs) of ice thickness and bedrock topography were obtained by kriging interpolation using the GAP data set, and other available datasets including the ICEbridge and the Danish Technical University (DTU) datasets (Claesson Liljedahl et al. 2016). The estimated uncertainty for the DEMs is about 20 m (Lindbäck et al. 2014). With respect to the domain of the groundwater flow model, the area of the ice sheet covered by the GAP DEMs, starting for the ice margin, extends about 100 km eastwards. For the remaining eastern part of the model domain, the refined Bamber data set available at 1 km resolution (Bamber et al. 2013) was used as subglacial topography. The land topography of the model domain, west of the ice margin, was described using the Greenland Mapping Project (GIMP) surface elevation model (Howat et al. 2014), with a resolution of 30 m (Harper et al. 2016), constructed from a combination of ASTER and SPOT-5 DEMs. The interpolation of the various data sets on the surface grid of the groundwater flow model was performed by Uppsala University using kriging interpolation. The bedrock elevation was estimated by subtracting the ice thickness from the surface elevation in each node of the grid. Detailed maps of bedrock elevation and ice thickness were obtained at 500 m resolution for the model domain (Figure 5-2). For the groundwater flow modelling, the topography described by bedrock elevation is assumed to be representative for the complete glacial cycle.

125 lakes were considered as through taliks by SKB for the model domain located west of the ice margin. Through taliks extend through the entire permafrost thickness and are assumed to react as either discharge or recharge flow paths for groundwater flow.

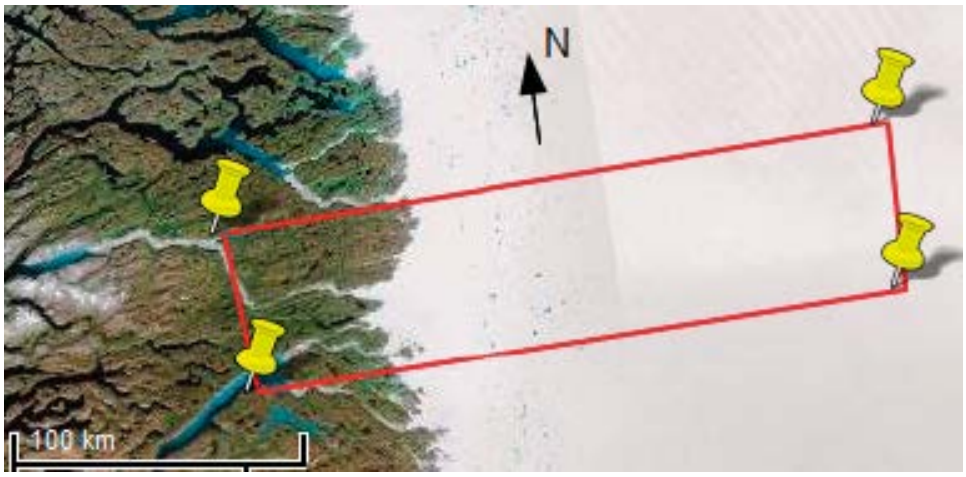

Figure 5-1. *Location of the groundwater flow model with respect to the ice margin (red rectangle with an area of about 250 × 60 km^2).*

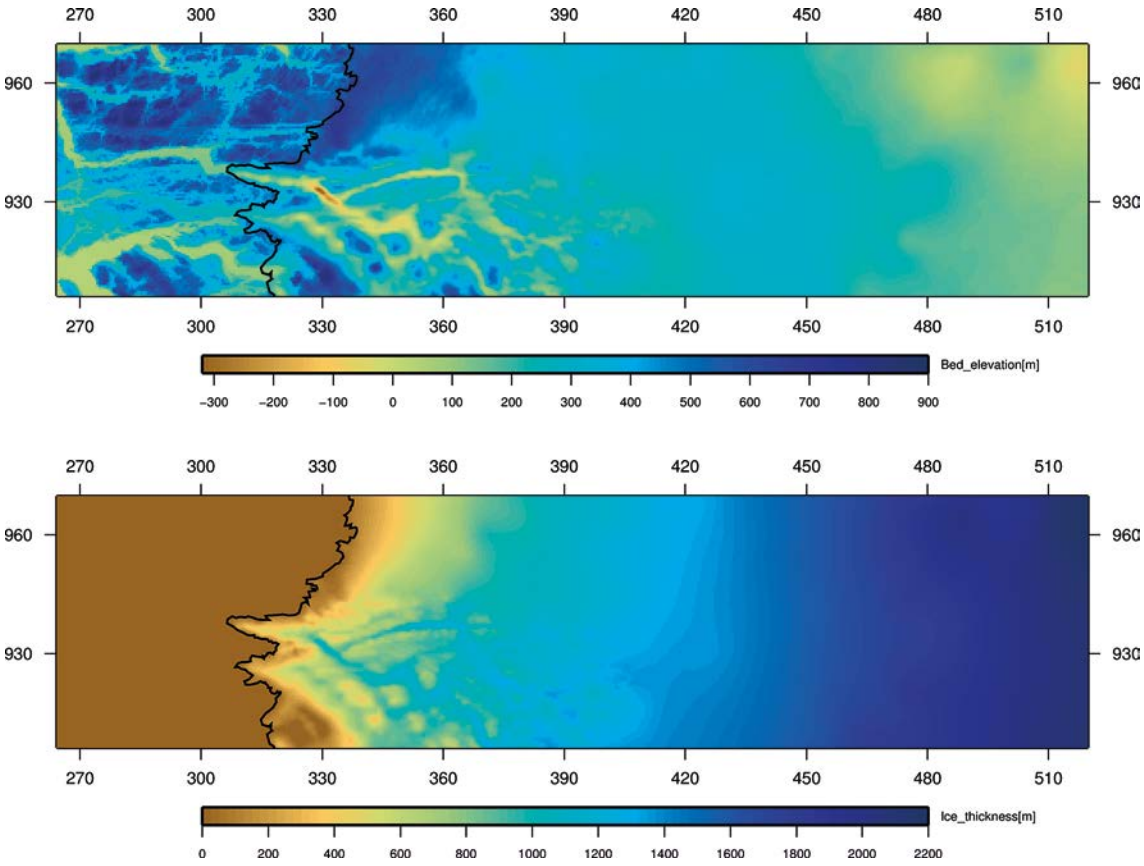

Figure 5-2. *GAP DEMs: bedrock elevation (above) with some remarkable deep troughs, around −300 m elevation, discovered underneath the ice sheet; and, ice thickness (below) for the model domain (coordinates in km).*

These potential through taliks were selected on the basis of their size, i.e. a lake was considered as a through talik, if it had a diameter larger than 400 m. The "Talik lake" is the lake with approximate dimensions of 1 200 × 400 m under which borehole DH-GAP01 is drilled. This borehole has confirmed the existence of a through talik beneath the "Talik lake" in an area of continuous permafrost (Claesson Liljedahl et al. 2016, Johansson et al. 2015).

The description of the perimeter of these through taliks was obtained using LANDSAT satellite data (Figure 5-3). The surface elevation for the taliks was estimated by Aberystwyth University with the help of ASTER GDEM satellite data and adjusted by SKB to the DEM values. The resulting elevation ranges from 93 to 760 m; the given vertical accuracy is 20 m at 95 % confidence, at global scale (ASTER 2009).

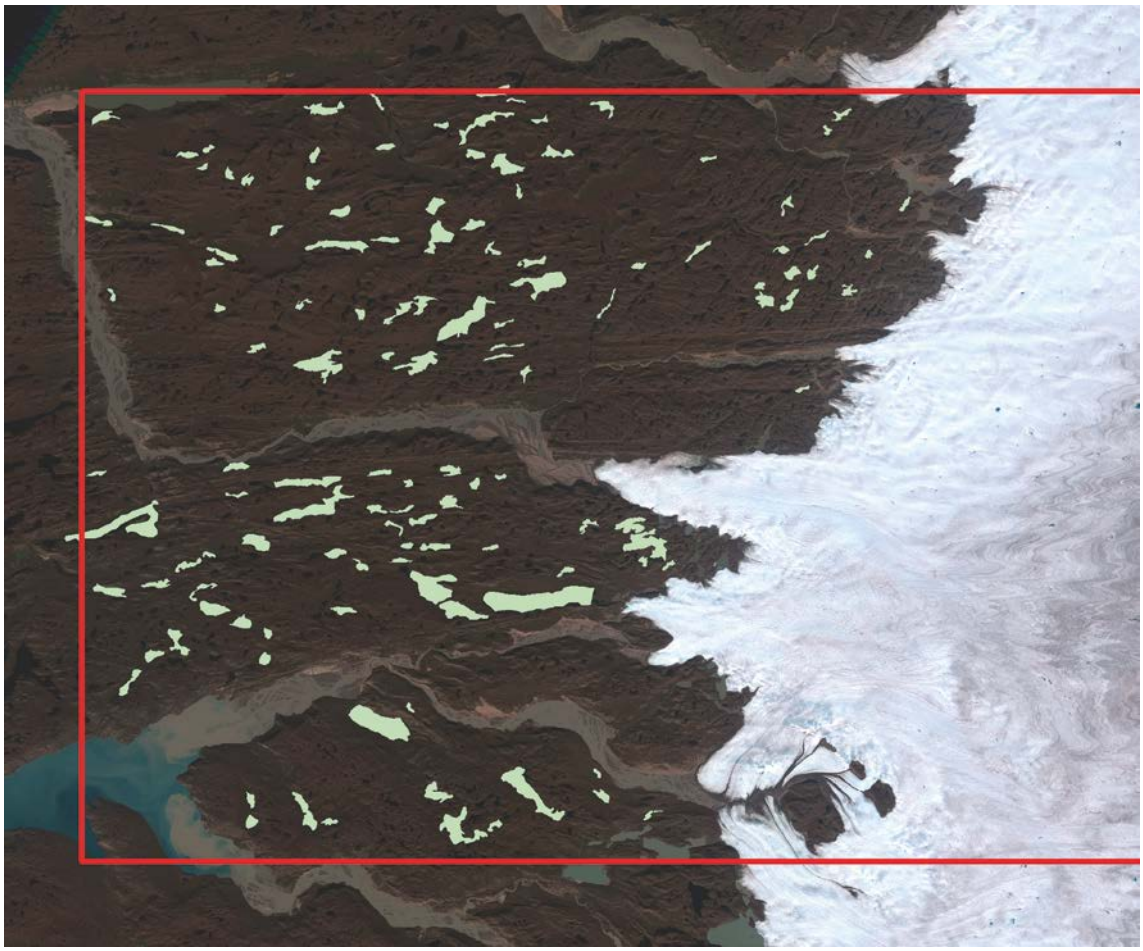

Figure 5-3. *Landsat image with potential through talik location (light green), ice sheet and groundwater flow model boundary (red line).*

5.3 Deformation zones

For the description of the deformation zones, a geological model – called Geomodel version 1 (Engström et al. 2012) – has been developed at regional scale and covers some area under the ice (Figure 5-4). This model integrates all topographical, geological and geophysical (aeromagnetic data from GEUS) information available, as well as the fracture data from the boreholes DH-GAP01 and DH-GAP03. Based on lineament interpretation supported by field observations, the Geomodel version 1 integrates a total of 158 potential deformation zones and faults (Figure 5-5) that were classified in four different sets, characterised by steep to moderate dip 75°. The Eastern area of the groundwater flow model is not covered by the Geomodel version 1. Therefore, deformation zones and faults are duplicated towards the central part of the ice sheet, in order to introduce them in the groundwater flow model (Figure 5-6). A fifth set of sub-horizontal deformation zones, hydraulically important, was also identified by Engström et al. (2012) in boreholes DH-GAP01and DH-GAP03 and more recently also in borehole DH-GAP04; since its distribution is insufficiently constrained, this set was not included in Geomodel version 1. Therefore, a stochastic method was applied for the description of the geometric and hydraulic properties of this fifth set (cf. Section 5.9).

A through talik is often a sign of a discharge area. These are generally found in topographic lows, which in turn often coincide where there is an outcropping deformation zone. Therefore, through taliks are likely to be located on deformation zones. The obtained map shows that more than 75 % of the through taliks are associated to deformation zones (Figure 5-7).

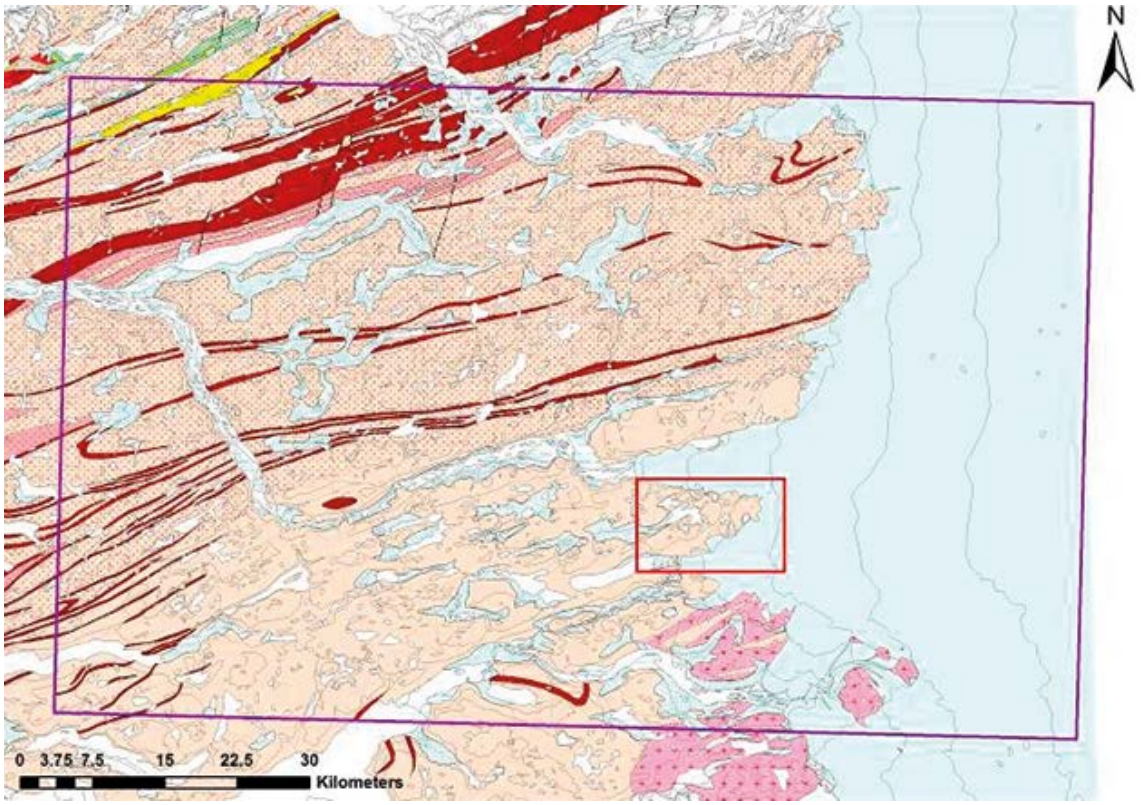

Figure 5-4. *Regional area of Geomodel version 1 (purple box) and GAP site scale area (red box), after Engström et al. (2012).*

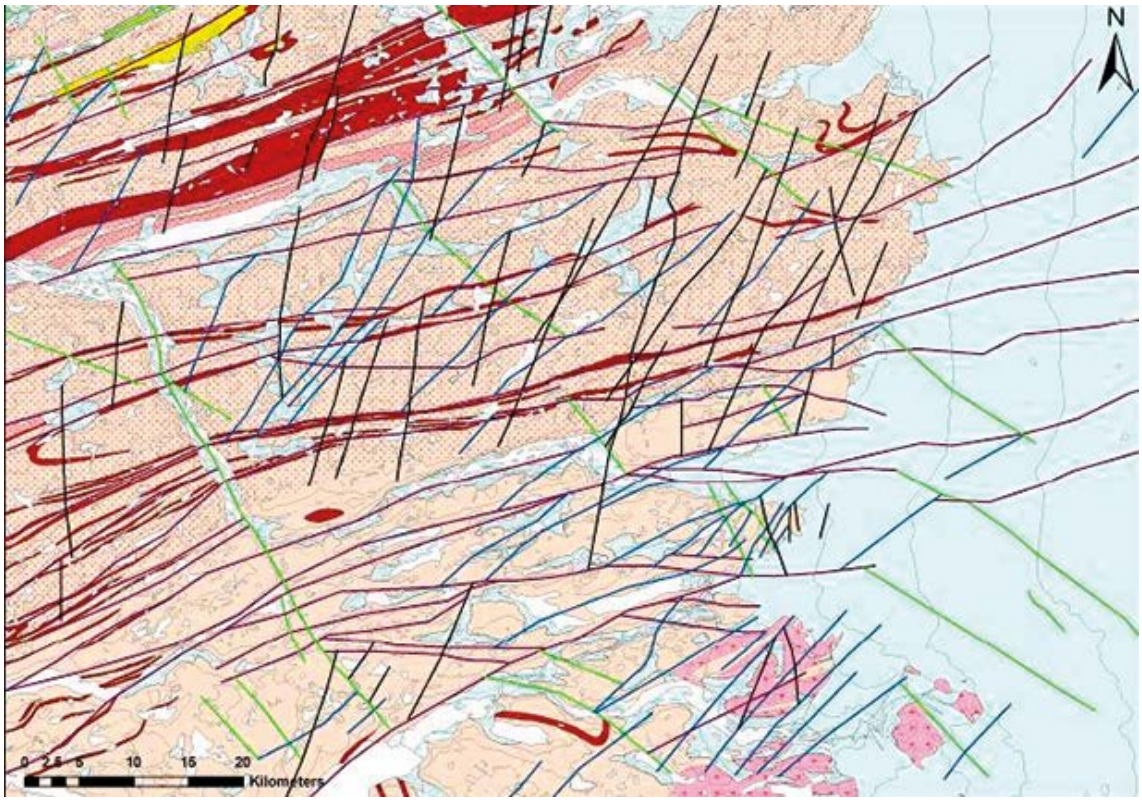

Figure 5-5. *Geomodel version 1 map with four different types of deformation zones and faults: Type 1=Lilac (oldest), Type 2=Green, Type 3=Blue and Type 4=Black (youngest). After Engström et al. (2012).*

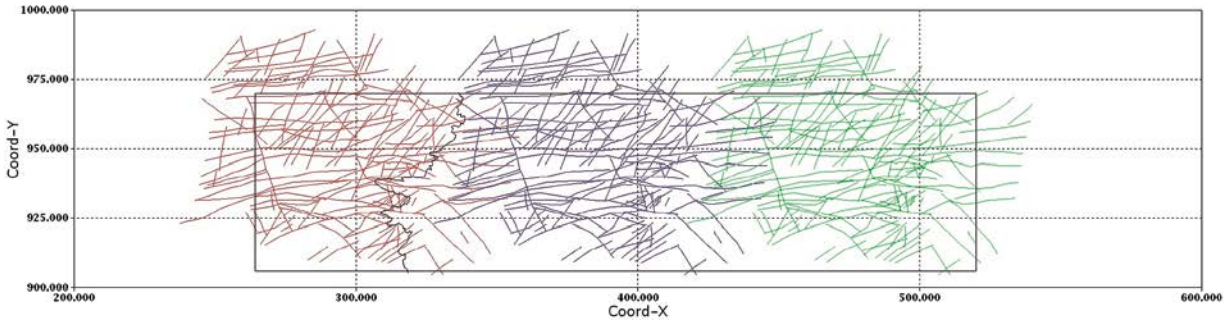

Figure 5-6. *Groundwater flow model area (black box) with ice margin and duplicated deformation zones and faults taken from Geomodel version 1 (coordinates in km).*

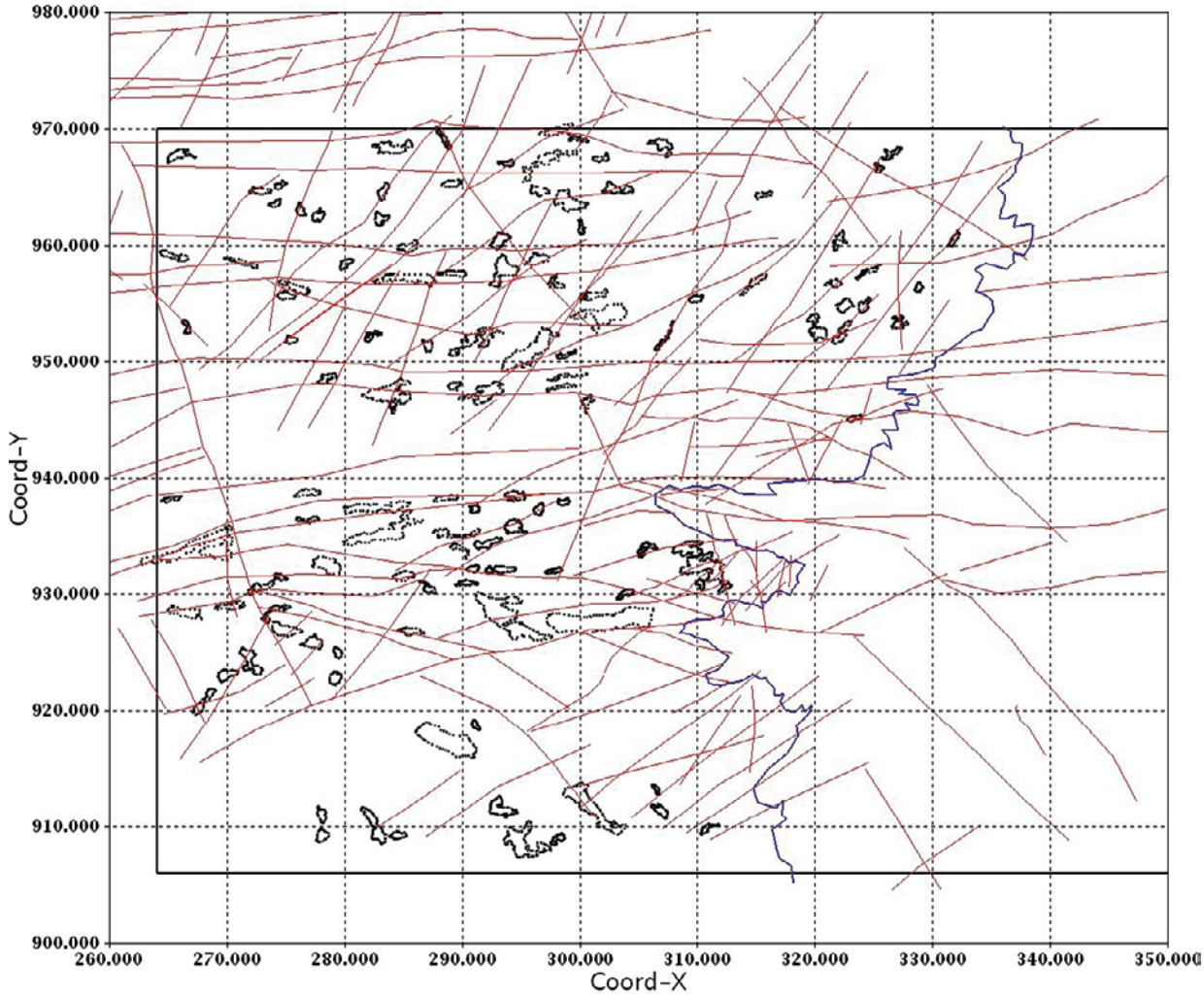

Figure 5-7. *Location of deformation zones (red) and taliks (black), west of the ice margin (blue), (coordinates in km).*

5.4 The ice-bedrock boundary

The conditions at the interface between the ice and underlying bed of the Greenland Ice Sheet are central to establishing the regional groundwater flow. The characteristics of the interface can be divided into two relevant components based on whether (1) the interface is at the melting point or is sub-freezing and (2) the interface is a rock-ice contact or rock-sediment-ice contact. The first component determines whether liquid water can flow at the interface (melting conditions) or not, whereas the second component concerns whether or not water flows within a sediment aquifer. If water is present, a third line of information becomes relevant concerning the pressure, distribution, and flux of the liquid water at the interface.

The following sections provide a brief overview of Greenland ice sheet's basal thermal conditions, basal framework, and subglacial water conditions. The focus is on the GAP model domain (cf. Figure 5-1). Note that this chapter is not intended to be a comprehensive literature review, but simply a condensed synopsis intended to provide context for the remainder of this report. Despite numerous remaining uncertainties regarding the basal conditions within the GAP study domain, this region is one of the most highly studied ice sheet locations in the world and is therefore much better constrained than the remainder of the Greenland ice sheet.

Basal Thermal Conditions

Temperature at the ice sheet bed is a function of boundary conditions introducing heat at the ice surface and bed, advection and diffusion processes that transport heat through the ice mass, and internal heat sources. Geothermal heat flux introduces energy directly at the bed and is therefore a strong control on basal ice temperature (e.g. Waddington 1987). Where ice slides over the bed, basal friction also generates heat at the bed (Cuffey and Paterson 2010). Internal heating within the ice mass can occur through strain heating as the ice deforms. Where meltwater penetrates the ice and refreezes, large amounts of latent heat are released (e.g. Jarvis and Clarke 1974). The collective heat sources and transport processes determine the thermal state of the bed. Confident determination of bed temperature conditions is limited to direct temperature measurements. Elsewhere, assessment of basal temperature must be inferred from indirect observations and numerical modelling; results from the latter remain uncertain owing to poor constraints on the heat sources and boundaries described above.

Direct temperature measurements are available in 20 boreholes drilled to the ice sheet bed in the ablation zone as part of the GAP and ICE projects. Measurements in each of these boreholes reveal basal conditions that are consistently temperate (Harrington et al. 2015, Hills et al. 2016). Boreholes were drilled in locations representing a range of ablation zone conditions: in bedrock troughs and over bed topographic highs, and at sites <1 km from the ice margin where ice thickness is 100 m, to 46 km from the Isunnguata Sermia terminus in ice 830 m thick. While it is possible that borehole sites were influenced by localized warming that is not pervasive over the ablation zone, measurement of temperate bed conditions in all holes strongly suggests that the bed is in a homogeneous melted state below ~1 100 m surface elevation over the study domain, and thermal conditions are insensitive to large changes in bed topography. Moreover, because boreholes drilled 10s to 100s of meters apart at each site all measure basal temperature at the pressure melting point; the data do not support a patchy framework of melted and frozen conditions at the local scale. These findings are consistent with observations of copious meltwater penetrating the ice sheet to the bed. The water releases latent heat by refreezing when it encounters cold ice, and it facilitates the generation of heat from sliding motion. Sufficient energy is thus available to warm all areas of the bed.

Further inland, beyond the borehole locations, assessment of basal thermal conditions can only be made using numerical models and indirect observations. The inland extent of melted conditions here is sensitive to geothermal heat flux (Brinkerhoff et al. 2011). Model results with prescription of the basal thermal boundary informed by the heat flux value computed in GAP-DH04 reveal melted bed conditions extending deep in to the ice sheet interior, to within some 10s of km of the ice sheet divide (Meierbachtol et al. 2015). These results are consistent with a recently published synthesis of results from a suite of numerical models and inferences from remote data, which conclude that thawed conditions at the bed are highly likely to extend to within 10s of km of the ice sheet divide (MacGregor et al. 2016). In summary, the growing body of direct measurements and indirect observations and modelling support the presence of melted bed conditions extending nearly 200 km from the ice sheet edge to within 10s of km of the ice divide in the study area.

Basal framework

Unlike temperature, the sediment structure of the bed is not a state variable and typically, must be assumed based on indirect information or reasoning. Certain aspects of the physical structure of the ice/bed interface can be obtained from geophysical surveys and modelling of seismic data. Drill holes provide direct observation, but for very limited areas. Conditions under the ice can be conjectured from observations of proglacial areas, or can be inferred from observations of the ice motion. While the nature of the sediment and bedrock under the ice sheet is difficult to ascertain, this is the framework which dictates all water flow and therefore is fundamentally important.

A layer of basal sediment with unknown thickness likely covers the ice/ bed interface across the region encompassing the interior ice divide. The ice motion here has a strong vertical component, and both modelling and direct evidence suggests the ice frozen to the bed (MacGregor et al. 2016). The frozen conditions would likely prevent stripping of sediment on the bed by ice sliding or by flushing with water. Samples from the bottom of ice cores along the divide have indeed, detected sediment at the basal interface (e.g. Gow and Meese 1996). Further away from the ice divide, the bed is melted and copious water moves through the subglacial drainage system. This could potentially influence the conditions for the generation and preservation (or lack thereof) of sediment at the bed.

One study examined the basal conditions of the GAP study region using a network of 32 boreholes drilled along a 46 km long transect starting at Isunnguata Sermia terminus (Harper et al. 2016, 2017). The action of a hot water drill stem as it intersected the bed, penetrometer experiments, hydrological impulse tests, and basal sampling were used to investigate the interface. This study found no evidence for a thick sediment cover on the bed, but rather a relatively hard bed with only a thin mantling of sediment (i.e., a 0 to ~2 m thick layer). This is consistent with the hard bed conditions interpreted from analysis of the seasonal changes in surface velocity (e.g. Sundal et al. 2011, Bartholomew et al. 2012) and assumed in models for subglacial drainage development along the margins of Greenland (Schoof 2010, Hewitt 2013, Werder et al. 2013). As this study is limited to just point measurements in boreholes, however, the findings of other geophysical studies elsewhere in the region should also be considered.

Both seismic experiments and borehole drilling have been used to infer thick sediment at the bed in an area north of the Jakobshavn Isbræ trough (Ryser et al. 2014, Walter et al. 2014). However, a drilling study at a separate location closer to the trough detected a hard bed (Lüthi et al. 2002). Closer to the GAP study region, two different seismic studies conducted 10s of km away concluded that the bed is covered by a till layer. Booth et al. (2012) used seismic amplitude versus angle methods to characterize bed reflections at a site located south and ~70 km inland. The acoustic impedance was indicative of a lodged till deposit with low porosity, but Poisson's ratio suggested a highly water-saturated substrate. Their explanation for this apparent discrepancy was that a thin (<2m) layer of dilatant till rests on top of a thicker lodged till; the thin layer is unresolvable, but interferes with seismic wavelets. Similarly, a study conducted 13 km from the Russel Glacier terminus suggested a layer of porous sediment was present at the ice bed interface, although its thickness was undetermined (Dow et al. 2013).

This apparent discrepancy between studies may have several explanations. First, none of the observations are coincident in space and so do not necessarily disagree. The bed conditions need not be restricted to a single structural makeup across the entire ice sheet. The underlying geologic framework, historical ice variations, current and historical ice flow dynamics and climate conditions are among the many factors that likely contribute to the derivation of particular bed conditions. Second, the GAP area drilling study did not intersect the deepest troughs in the region. Perhaps the areas adjacent to the troughs generate little sediment relative to the troughs, or any sediment generated is quickly routed to the troughs, which is an obvious water routing pathway.

Basal Water

The state of the basal drainage system dictates the coupling of ice sheet hydrology dynamics to underlying groundwater processes. Specifically, the water pressure in the basal drainage network and its configuration (i.e. coverage as a fraction of the bed) are critical boundary couplings.

The spatial coverage of water at the bed remains unknown, but borehole tests provide some bounding constraints. Water pressure responses to pumping tests in boreholes have illustrated basal water flow through spatially variable and discrete elements at the bed (Harper et al. 2016). Responses in the test holes commonly displayed evidence of connection to drainage elements with high drainage capacity, but responses in neighbouring boreholes just 10s of m away were variable, and in some cases entirely absent. Other observational evidence has shown that potentially large areas of the bed are likely to be covered by basal meltwater that is isolated from an active drainage system. For instance, dye injected in a borehole persisted for >10 days, revealing connection to an isolated water pocket at the bed (Meierbachtol et al. 2016). Dilution of the initial dye concentration, coupled with thermal dissipation during drilling, suggested the volume of this basal cavity was on the order of cubic meters. Such a volume of basal melt water could cover 10s of m^2 along the bed. Collectively, these observations rule out two end member coverage scenarios: complete and uniform water coverage over the bed, as might be expected in a thick package of saturated till (see above) is unsupported, and water coverage at the bed is not limited to sparse meltwater channels. Rather, borehole measurements in the study area support a drainage configuration at the bed that is composed of a network of active drainage elements, interspersed with isolated pockets of water that can be spatially extensive. Quantitative constraints on fractional water coverage at the bed, however, remain elusive and unmeasurable.

Existing observations illustrate basal water pressure conditions which vary over a range of spatial and temporal scales. This is owing to the spatially discrete nature of the drainage network, and because surface meltwater forcing and basal drainage processes vary in time and space. During the melt season, the response of the basal drainage network to diurnally varying surface melt inputs can cause significant changes in basal pressure. Near the ice sheet margin, measured pressures have been observed to vary diurnally by up to 70 % of overburden pressure Wright et al. (2016). Elsewhere, particularly further inland, diurnal pressure variations persist but become smaller: Wright et al. (2016) showed that diurnal variability in 12 of 13 boreholes in the study area was restricted to between 80–110 % of ice overburden pressure (this high value for the pressure corresponds to a water column equal to the thickness of the ice and was achieved where boreholes were entirely filled with water, from the bed to the surface; Harper et al. 2016). This may reflect changes in surface input, but is also likely influenced by thick ice and smaller gradients in surface elevation, which collectively limit the rapid growth and persistence of basal melt conduits (Meierbachtol et al. 2013) and therefore inhibit large drops in drainage system pressure.

While observations illustrate substantial variability in basal pressure during the melt season, it is important to note that low pressure exists for only a small portion of the day. Further, this variability is limited to a ~3–4 month period during the melt season. Measurements at the study area during the winter months identified consistently high pressure, remaining near ice overburden levels (Wright et al. 2016). Consequently, when averaged over an annual time scale, measured basal water pressure over the transect of boreholes was 96 % of overburden pressure (Wright et al. 2016). The basal water pressure across the transect therefore generally mimics the ice thickness field, suggesting that over the time scales of ice sheet advance and retreat, ice sheet thickness changes are a first order control on the water pressure field.

Modelling the subglacial layer geometry

On the basis of these data and the conceptual elements developed for the basal framework, the subglacial layer is conceptualised as a discontinuous permeable layer, located at the bedrock-ice interface, likely to exist within the major troughs underneath the ice sheet. Using this concept, a model for the geometry of the subglacial layer is developed based on the data from the subglacial topography.

During GAP, the subglacial topography was mapped, at high spatial resolution (cf. Section 5.2), but with respect to the domain of the groundwater flow model, such data was solely available for the western part of the domain (Figure 5-8).

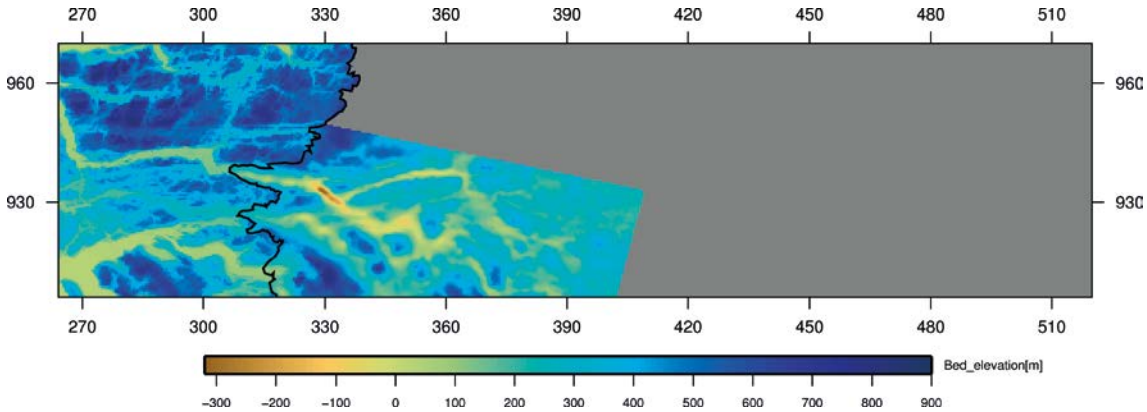

Figure 5-8. *Bedrock elevation data at high spatial resolution available for the model domain (coordinates in km). The black line delineates the current location of the ice margin.*

Due to the lack of high spatial resolution data towards the eastern part of the model domain, a stochastic method is needed for the simulation of the subglacial topography for this region. The stochastic simulation method starts from the following decomposition (Chilès and Delfiner 2012):

$$Z(x) = Z^k(x) + \left[Z(x) - Z^k(x)\right] \quad (5\text{–}1)$$

where $Z^k(x)$ is the kriging estimator of the bedrock elevation at location x using the high resolution data; and, the term $\left[Z(x)-Z^k(x)\right]$ is the interpolation (kriging) error. As the true value of the elevation, $Z(x)$, is unknown, the same equation is considered in terms of simulation:

$$Z^s(x) = Z^{sk}(x) + \left[Z^s(x) - Z^{sk}(x)\right] \quad (5\text{–}2)$$

where $Z^s(x)$ is the simulation of $Z(x)$ and $Z^{sk}(x)$ is the kriging estimator using only the simulated values at the location of the data, and then the kriging error in Equation (5-1) is replaced by its simulation:

$$Z^{cs}(x) = Z^k(x) + \left[Z^s(x) - Z^{sk}(x)\right] \quad (5\text{–}3)$$

where $Z^{cs}(x)$ is the conditional simulation of the elevation; i.e. at a data location, the value of the kriging estimator corresponds to the observed elevation and the simulation of the kriging error is equal to zero, then the conditional simulation of value at a data location is by construction the observed value. The conditional simulation method allows the generation of stochastic simulations for the all model domain while reproducing the data in the western part of the domain.

For the first step, the simulation of $Z^s(x)$, the turning bands method (Lantuéjoul 2002, Emery and Lantuéjoul 2006) is applied which enables Gaussian simulation using a given variogram model for the elevation. As the data were not Gaussian distributed, a simulation matching the observed elevation histogram is obtained using a non-linear (bijective) transformation – named Gaussian anamorphosis (Chilès and Delfiner 2012) – applied to the elevation data. By performing variogram analysis, an anisotropic exponential-sine model (Emery and Lantuéjoul 2006) is fitted to the elevation data; the practical ranges at which spatial variability occurs are estimated at about 85 km and 5 km in the E–W and N–S directions respectively. Then, in the second step, the simulation becomes conditional using Equation (5-3). The obtained conditional simulation of elevation (Figure 5-9), while respecting the data in the western part of the domain, provides a simplified description for the topography in the eastern part with potential troughs having some of the statistical properties of those of the western part.

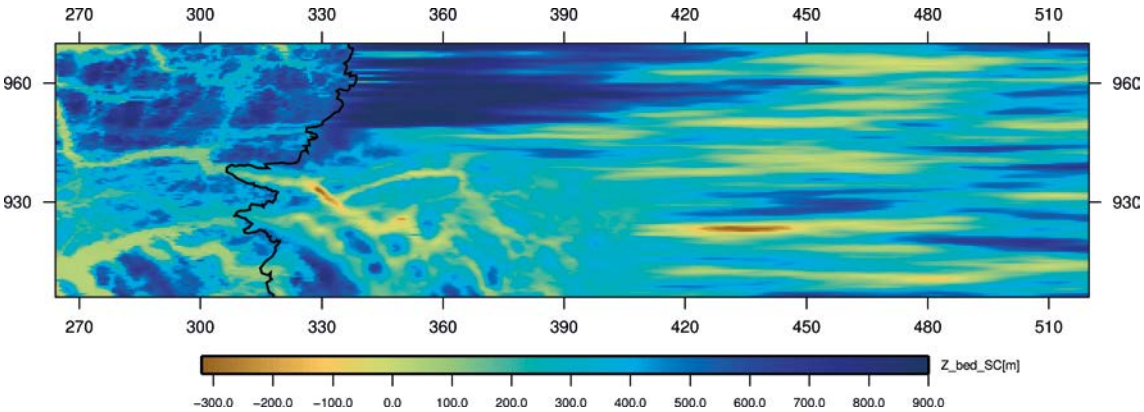

Figure 5-9. *Conditional simulation of bedrock elevation data at high spatial resolution for the entire model domain (coordinates in km). The black line delineates the current location of the ice margin.*

The third step is the determination of the geometry for the subglacial layer based on its conceptualisation. The idea is to apply a threshold to the conditional simulation of bedrock elevation in order to construct a categorical variable. Values for the conditional simulation below that threshold are set to zero and values above to one; i.e. using this categorical variable, locations with value equal to 0 belong to the subglacial layer and those with values set to one are outside. A value of 260 m was chosen for the elevation threshold which enables to preserve the main troughs observed in the high resolution data (cf. Figure 5-8) and the creation of elongated subglacial layer zones towards the east; and, moreover, the geometrical connectivity for the subglacial layer is guaranteed in the E–W direction (Figure 5-10).

The stochastic simulation of the subglacial layer is carried out in 2 dimensions in the horizontal plane. In order to guarantee face connectivity between neighbouring cells of the subglacial layer cells, developments were undertaken for the generation of a connective subglacial layer, located at the top of the 3D model grid.

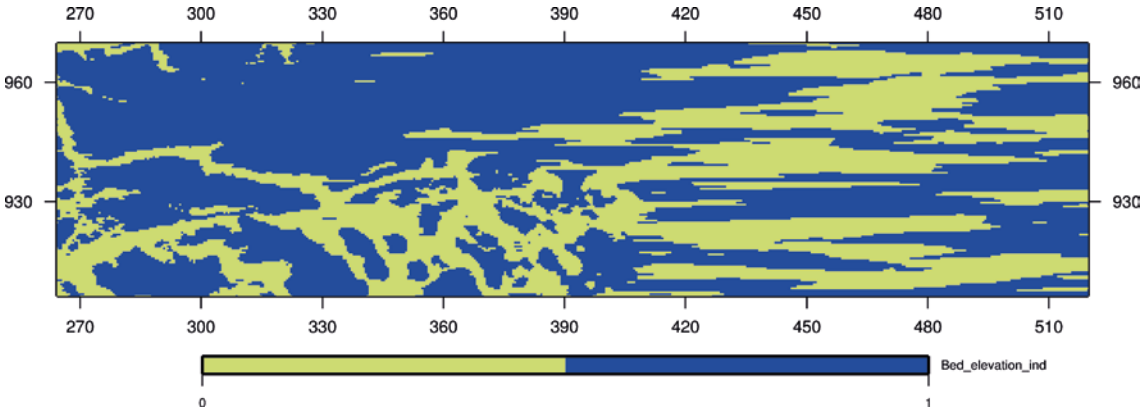

Figure 5-10. *Geometry of the subglacial layer (in yellow-grey colour; subglacial proportion equals 0.37 of the studied domain), (coordinates in km).*

5.5 Hydraulic properties

In order to meet modelling data needs, the hydraulic properties for the groundwater flow model were provided by Follin et al. (2011). They were compiled from the two Swedish sites of Laxemar and Forsmark, as well as from the site of Olkiluoto in Finland.

For the three sites considered, the rock mass domain is divided either in three or four hydrogeological units for which statistical parameters are available (Tables 5-1, 5-2 and 5-3). The hydraulic conductivity is assumed to follow a log-normal distribution with an anisotropic exponential variogram. The correlation scale is assumed to remain constant for the hydrogeological units considered.

Table 5-1. Rock mass domain hydraulic parameters according to Laxemar site.

Lithology	Depth [m]	Geometric mean of hydraulic conductivity[1] [m/s] [log value] (scale of hydraulic test in m)	Standard deviation [log 10]	Correlation scales (x,y,z) [m]
Crystalline	0–200	1.1×10^{-7} [−6.96] (100)	1.04	(775, 775, 275[2])
Crystalline	200–450	1.5×10^{-8} [−7.81] (100)	1.63	(775, 775, 275)
Crystalline	450–700	8.9×10^{-10} [−9.05] (100)	1.78	(775, 775, 275)
Crystalline	700–5 000[3]	2.2×10^{-10} [−9.66] (100)	1.70	(775, 775, 275)

Table 5-2. Rock mass domain hydraulic parameters according to Forsmark site.

Lithology	Depth [m]	Geometric mean of hydraulic conductivity[1] [m/s] [log value] (scale of hydraulic test in m)	Standard deviation [log 10]	Correlation scales (x,y,z) [m]
Crystalline	0–225	2.3×10^{-9} [−8.63] (100)	1.44	(775, 775, 275[2])
Crystalline	225–425	3.2×10^{-11} [−10.50] (100)	1.07	(775, 775, 275)
Crystalline	425–5 000[3]	1.0×10^{-11} [−11.00] (100)	1.12	(775, 775, 275)

Table 5-3. Rock mass domain hydraulic parameters according to Olkiluoto site.

Lithology	Depth [m]	Geometric mean of hydraulic conductivity[1] [m/s] [log value] (scale of investigation[4])	Standard deviation [log 10]	Correlation scales (x,y,z) [m]
Crystalline	0–118	1.0×10^{-9} [−9.00] (100)	0.90	(775, 775, 275[2])
Crystalline	118–218	7.1×10^{-10} [−9.15] (100)	0.74	(775, 775, 275)
Crystalline	218–418	4.0×10^{-10} [−9.40] (100)	0.74	(775, 775, 275)
Crystalline	418–5 000[3]	9.1×10^{-11} [−10.04] (100)	0.74	(775, 775, 275)

[1] Equal to the mean of the log-conductivity values.

[2] The correlation scale along the z-direction corresponds to the range of the spherical isotropic variogram used by Rhén et al. (1997). The value for the horizontal correlation scales is taken from Jaquet et al. (2012).

[3] Values are assumed beyond 1 000 m depth.

[4] The maximum value is assumed for the scale of investigation.

The corresponding hydraulic properties for the deformation zones are also taken from the Laxemar and Forsmark sites. The depth dependency of the in-plane transmissivity, T_r, for the deformation zones is described using an exponential model (Follin et al. 2011), expressed as:

$$T_r\left(z \geq -1000\ m\right) = max\left\{ T_r(0)\, 10^{\frac{z}{k}}, 10^{-9} \right\} \qquad (5\text{–}4)$$

$$T_r\left(z < -1000\ m\right) = T_r\left(z = -1000\ m\right)$$

where:

$T_r(z)$: transmissivity of deformation zone

$T_r(0)$: transmissivity at zero elevation; in the range $1.0 \cdot 10^{-5}$-$8.5 \cdot 10^{-5}$ m^2/s for Laxemar; and, $2.5 \cdot 10^{-7}$-$2.2 \cdot 10^{-4}$ m^2/s for Forsmark.

k: depth interval giving one order magnitude of decrease in transmissivity; the values applied for k ranges from 365.0–534.8 m for Laxemar; and for Forsmark, the value of k equals 232.5 m (Follin et al. 2011).

For the Olkiluoto site, the depth dependency of the in-plane transmissivity for the deformation zones is described using the following exponential model (Follin et al. 2011):

$$T_r\left(z \geq -500m\right) = \left\{ T_{r1}(0) 10^{\frac{z}{k_1}} \right\}$$

$$T_r\left(-500m > z \geq -700m\right) = \left\{ T_{r2}(0) 10^{\frac{z}{k_2}} \right\} \qquad (5\text{–}5)$$

$$T_r\left(z < -700m\right) = 1.0 \cdot 10^{-9}$$

where:

$T_r(z)$: transmissivity of deformation zone

$T_{r1}(0)$, $T_{r2}(0)$: transmissivity at zero elevation;, $T_{r1}(0) = 2.5 \cdot 10^{-4}\ m^2/s$, $T_{r2}(0) = 5.0 \cdot 10^{-2}\ m^2/s$

k_1, k_2: depth interval giving one order magnitude of decrease in transmissivity; the values applied for k_1 and k_2 respectively equal 185.3 m and 100.0 m, for Olkiluoto (Follin et al. 2011).

Finally, the hydraulic conductivity of the subglacial layer is attributed spatially, according to the geometrical model (cf. Section 5.4) using the following hydraulic conductivity values (Näslund J-O 2013, personal communication, Vidstrand et al. 2010b): $K_x = K_y = 10^{-2}\ m/s$; $K_z = 10^{-3}\ m/s$. Regarding the specific storage, a value equal to 10^{-9} m^{-1} is taken for all cases, following the approach of Vidstrand et al. (2010b).

5.6 Thermal and permafrost parameters

The thermal and permeability reduction parameter for the modelling of permafrost are given in Tables 5-4 and 5-5; these parameter values correspond to the values taken for the Laxemar and Forsmark sites (Vidstrand et al. 2010a, b) and for the Olkiluoto site (Kukkonen et al. 2011). The exception being the geothermal heat flux value (0.0348 W m^{-2}) which is taken from the borehole DH-GAP03 (Harper et al. 2016) and corrected for depth using a relation given by Hartikainen et al. (2010).

Table 5-4. Thermal parameters.

Site	Equivalent thermal conductivity (rock+ fluid) [W m^{-1} K^{-1}]	Mass-specific heat capacity of fluid [J kg^{-1} K^{-1}]	Mass-specific heat capacity of ice [J kg^{-1} K^{-1}]	Volume-specific heat capacity of rock [J m^{-3} K^{-1}]	Geothermal heat flux at 5000 m depth [W m^{-2}]
Laxemar	2.75	4 182	2 110	2.23×10^{6}	0.0234
Forsmark	3.45	4 182	2 110	2.07×10^{6}	0.0234
Olkiluoto	2.91	4 182	2 110	1.93×10^{6}	0.0234

Table 5-5. Hydraulic conductivity reduction parameters (Laxemar, Forsmark and Olkiluoto).

Freezing temperature T_L [°C]	Freezing temperature interval W [°C]	Maximum reduction α_{min} [−]	Rock type constant a[−]
0	0.5	10^{-3}	3

5.7 Transport parameters

The transport parameters used for glacial meltwater tracing are given in Table 5-6 for the different sites. The value for the molecular diffusion coefficient is taken from de Marsily (1981). Following the formulation of Svensson et al. (2010), the effective diffusion coefficient is equal to the product of the molecular diffusion coefficient by the mean (arithmetic) value of the kinematic porosity, estimated from the porosity values, derived from the hydraulic conductivity (Equation 5-6) of the stochastic simulation (cf. Section 5.9).

Table 5-6. Transport parameters.

Site	Molecular diffusion coefficient [m^2 s^{-1}]	Mean (kinematic) porosity [−]	D_e [m^2 s^{-1}]
Laxemar	10^{-9}	2.8×10^{-3}	2.8×10^{-12}
Forsmark	10^{-9}	2.2×10^{-3}	2.2×10^{-12}
Olkiluoto	10^{-9}	2.2×10^{-3}	2.2×10^{-12}

The kinematic porosity is calculated from the hydraulic conductivity using the following equation (Rhén et al. 1997, Follin et al. 2011), with a lower bound as to avoid non-physical low values for kinematic porosity (Selroos J-O 2013, personal communication):

$$\phi = 34.87K^{0.753} \quad with \quad 2 \cdot 10^{-4} \leq \phi \leq 0.05 \tag{5–6}$$

For the subglacial layer, a constant kinematic porosity is applied using a value equal to 0.25 (Vidstrand et al. 2010b).

5.8 Discretisation

The discretisation is performed using an unstructured Cartesian grid system. The grid resolution is 500 m in the horizontal directions. The discretisation in the vertical direction varies between 25, 50 or 100 m when approaching the topographic surface. The model contains about 4 338 000 cells. The Cartesian coordinate system of Bamber (2001), cf. Figure 3-1, is used for all the calculations, thus matching the coordinates of the different data sets.

The elevation of the top surface of the model domain is mapped directly on the model grid using the GAP Digital Elevation Model of bed topography obtained at 500 m resolution (cf. Section 5.2). This direct mapping was implemented for improving the discretisation resolution; i.e. it presents the advantage to avoid the smoothing related to the triangulation method of DarcyTools when processing DEM data.

In addition, all the potential through taliks located west of the ice margin within the studied domain were discretised, in terms of geometry and elevation, for groundwater flow modelling (cf. section 5.2). Some of the taliks are regrouped with other ones, due to their small size.

5.9 Stochastic simulation of hydraulic properties and porosity

Rock mass domain and vertical deformation zones

The description of the spatial variability of the hydraulic conductivity for the rock mass domain is obtained at the cell scale by a stochastic simulation using the turning bands method (Matheron 1973, Lantuéjoul 2002). The details of the stochastic methodology applied are given in Appendix A. A Gaussian standard normalised simulation of the hydraulic conductivity logarithm is carried out using an anisotropic exponential variogram (cf. Section 5.5). Then, this simulation is scaled according to the mean and standard deviation of the hydraulic conductivity given to the hydrogeological units (cf. Tables 5-1 to 5-3) associated to the three different sites (Laxemar, Forsmark and Olkiluoto).

In the next step, the deformation zones are introduced in the model domain using the geometric parameters of Geomodel version1 (cf. Section 5.3) and their corresponding site hydraulic parameters (cf. Section 5.5). For Laxemar and Forsmark, the simulation of the lateral in-plane variability of the deformation zone transmissivity (Follin et al. 2011) is obtained by adding a stochastic residual – without spatial correlation – to the exponential model (cf. Equation 5-4):

$$T_r\left(z \geq -1000\ m\right) = max\left\{ T_r(0)\, 10^{\frac{z}{k}+Y_R}, 10^{-9} \right\} \qquad (5\text{–}7)$$

$$T_r\left(z < -1000\ m\right) = T_r\left(z = -1000\ m\right)$$

where:

Y_R: log-residual with Gaussian distribution (mean = 0 and standard deviation = 1.35, for Laxemar; and standard deviation = 0.63, for Forsmark).

For Olkiluoto, the simulation of the lateral in-plane variability of the deformation zone transmissivity (Follin et al. 2011) is achieved using a similar model with slightly different parameters (cf. Equation. 5-5):

$$T_r\left(z \geq -500m\right) = \left\{ T_{r1}(0) 10^{\frac{z}{k_1} + Y_R} \right\}$$

$$T_r\left(-500m > z \geq -700m\right) = \left\{ T_{r2}(0) 10^{\frac{z}{k_2} + Y_R} \right\} \quad (5\text{–}8)$$

$$T_r\left(z < -700m\right) = 1.0 \cdot 10^{-9}$$

where:

Y_R: log-residual with Gaussian distribution (mean = 0 and standard deviation = 1.22, for Olkiluoto).

The deformation zones are integrated into the cells discretising the rock mass domain using the GEHYCO method (Svensson et al. 2010); i.e. for each cell face, the hydraulic conductivity is calculated to take into account the contribution of the intercepting deformation zones. Then, the joint effect of deformation zones and rock mass domain is considered by calculating equivalent hydraulic conductivities for each cell face, as follows (Figure 5-11):

$$K_i = mean\left\{ K_i^{DZ}, K_i^{RD} \right\} \quad (5\text{–}9)$$

where:

K_i^{DZ}: hydraulic conductivity related to deformation zone(s) at face i (i = x, y or z)

K_i^{RD}: hydraulic conductivity related to rock mass domain at face i (i = x, y or z).

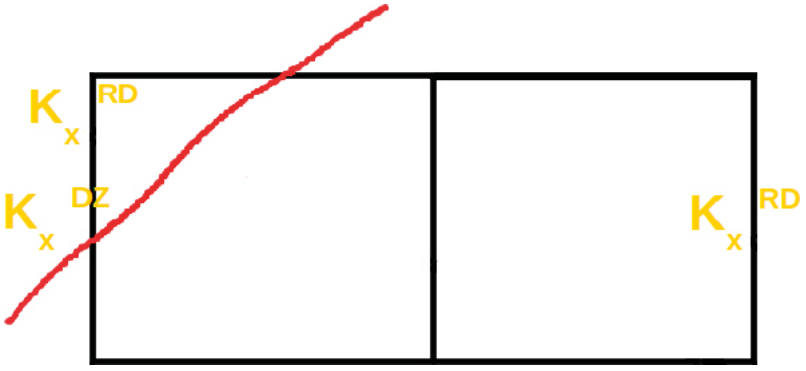

Figure 5-11. *Example of equivalent hydraulic conductivity for face x using K_x^{DZ} and K_x^{RD}, for the left cell intersected by a deformation zone.*

Finally, the calculation of the equivalent porosity, at cell scale, is obtained using a sum of the weighted volume of rock mass domain porosity and the deformation zone porosity, obtained using Equation 5-6.

Horizontal deformation zones

Due to lack of data, Geomodel version 1 does not include sub-horizontal or horizontal lineaments/ deformation zones (cf. Section 5.3). Due to their potential hydraulic importance (cf. Appendix B), it was decided to include them in the groundwater flow model by modifying the current hydraulic conductivity and porosity fields. Therefore, a conceptual model was elaborated by Pere T, Engström J and Follin S (2012, personal communication) where the horizontal deformation zones are described by horizontal patches of a few square kilometres in size; the number of horizontal patches decreases with depth; and, the value of the hydraulic conductivity for the patches is increased by a factor 10, in comparison to its previous value.

On the basis of this conceptual model, a stochastic model was applied for the characterisation of the geometry, hydraulic and transport properties of the horizontal patches. A truncated Gaussian simulation (Lantuéjoul 2002) is performed for the modelling of the spatial distribution of patches presenting a size of about 5 km (Figure 5-12). Such size is obtained by the selection of a specific variogram type (Gaussian) whose increased correlation scale values exhibit similar anisotropic ratio as the underlying conductivity field. The proportion of the patches is rendered non stationary with depth and varies as follows: 0.3, 0.2, 0.1 at respective depth intervals: 0–200 m; 200–400 m; 400–600 m. Finally, the horizontal components of the hydraulic conductivity patches were increased by a factor 10; to the dominant effect of the vertical deformation zones in terms of hydraulic conductivity is added a secondary contribution due to the horizontal deformation zones (Figure 5-13). And finally, the porosity of the horizontal deformation zones was recalculated according to these increased values using Equation 5-6.

The stochastic simulations obtained for the sites Laxemar, Forsmark and Olkiluoto with the integration of rock domain, deformation zones (horizontal and vertical) and the subglacial layer are displayed in Figures 5-14 to 5-16. For numerical reasons related to convergence issues, the range of the hydraulic conductivity had to be set to 10^{-12}-10^{-2} m/s; i.e. the values located outside of this range have received the corresponding limit value.

The differences in spatial behaviour for the hydraulic conductivity are remarkable when comparing the three sites. The site of Laxemar presents the strongest variability in hydraulic conductivity characterised by permeable deformation zones extending at depth (cf. Figure 5-14). Besides, the sites of Forsmark and Olkiluoto exhibit less variability for the hydraulic conductivity with limited extension at depth of the hydraulic signature of their deformation zones (cf. Figures 5-15 and 5-16).

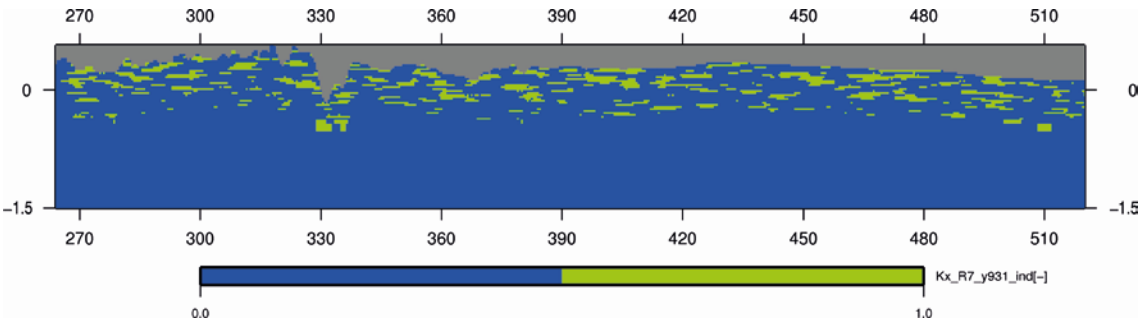

Figure 5-12. *Truncated Gaussian simulation: geometry of the horizontal deformation zones or patches (in yellow-green colour),* ***W-E vertical cut*** *at Y = 931 km (coordinates in km).*

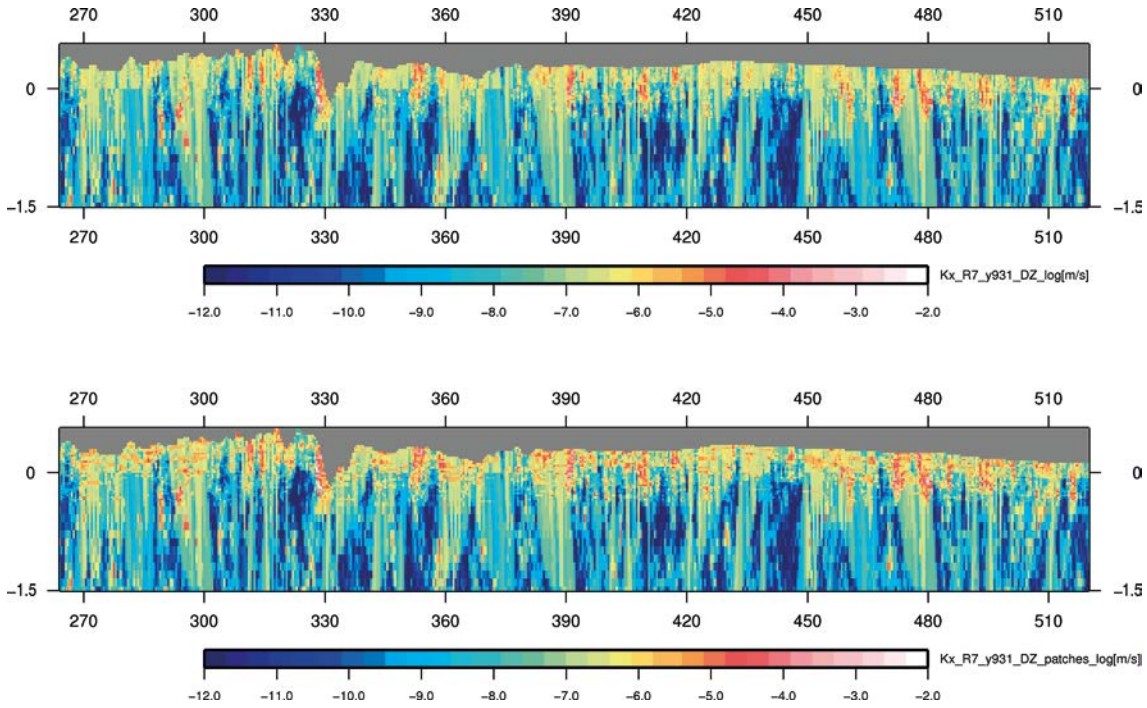

Figure 5-13. *Laxemar: stochastic simulation of log-conductivity field, with vertical deformation zones (above), and with vertical and horizontal deformation zones (below), W-E vertical cut at Y = 931 km (coordinates in km).*

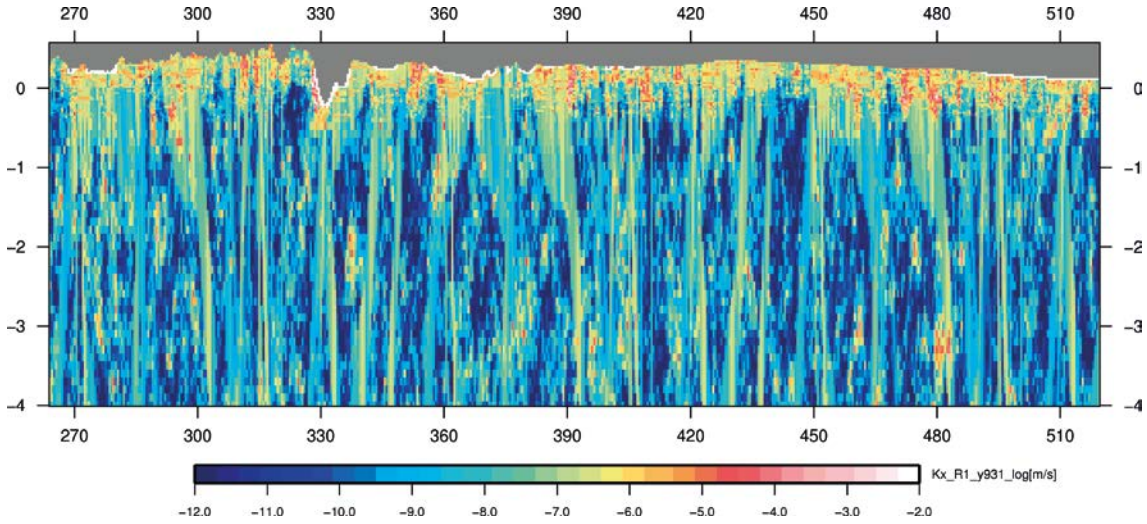

Figure 5-14. Laxemar*: stochastic simulation of log-conductivity field (white represents the sugblacial layer, located at the top, with $K_x = 10^{-2}$ m/s),* ***W-E vertical cut*** *at Y = 931 km (coordinates in km).*

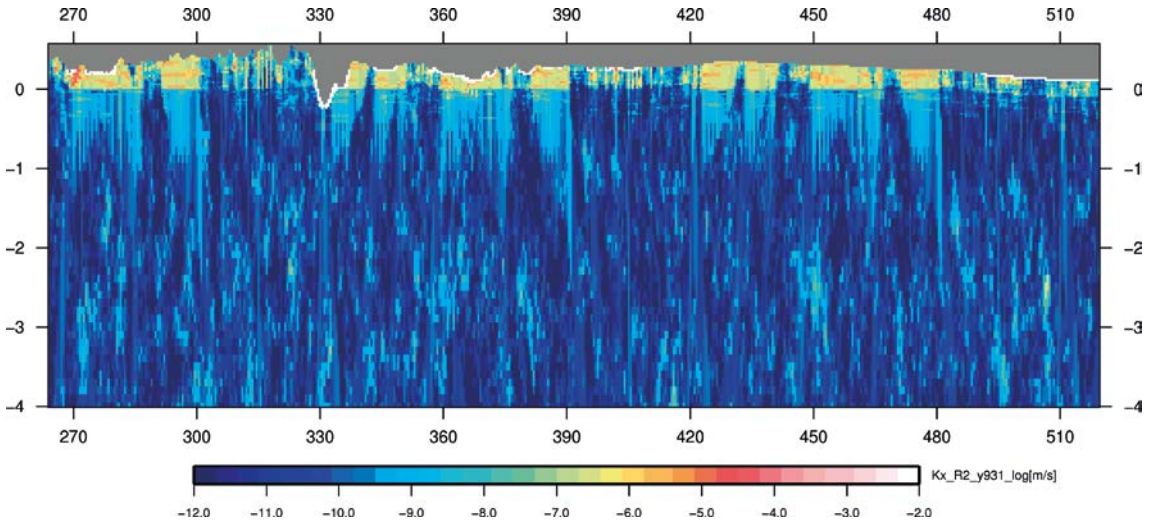

Figure 5-15. Forsmark: ***s****tochastic simulation of log-conductivity field (white represents the sugblacial layer, located at the top, with* $K_x = 10^{-2}$ *m/s),* ***W-E vertical cut*** *at Y = 931 km (coordinates in km).*

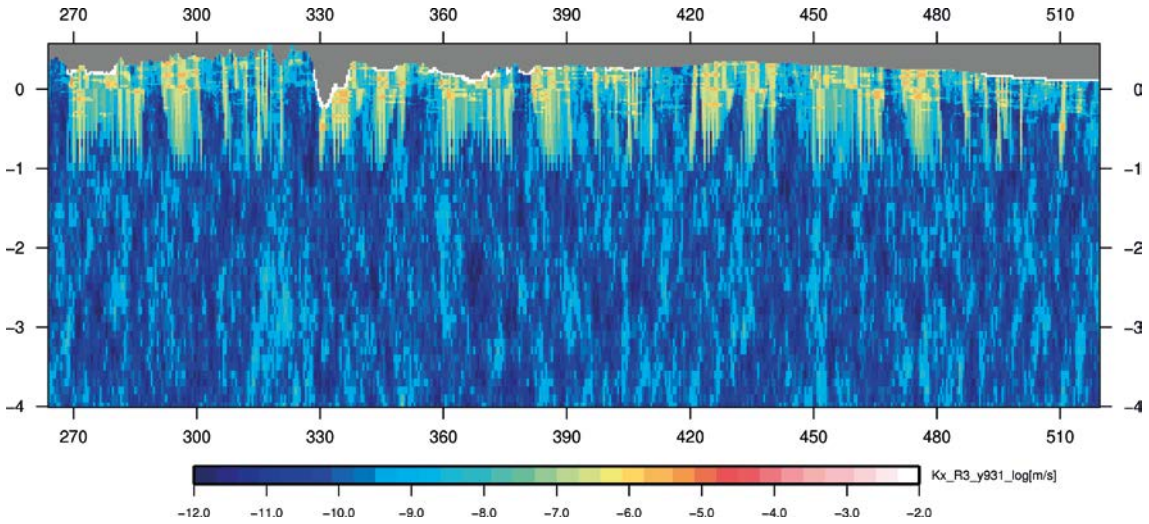

Figure 5-16. Olkiluoto: ***s****tochastic simulation of log-conductivity field (white represents the subglacial layer, located at the top, with* $K_x = 10^{-2}$ *m/s),* ***W-E vertical cut*** *at Y = 931 km (coordinates in km).*

6 Groundwater flow modelling

The modelling of density-driven groundwater flow, heat transfer and permafrost using transient boundary conditions representing ice sheet displacement is performed during a complete glacial cycle.

Five transient cases are considered whose specific characteristics are given in Table 6-1. The cases 1, 2 and 3 have their hydraulic properties respectively taken from the sites of Laxemar, Forsmark and Olkiluoto. Finally, the cases 4 and 5 consider alternative glaciation scenarios associated with Laxemar hydraulic properties.

Table 6-1. Specifications for the five transient modelling cases.

Case	Processes	Hydraulic properties + Geomodel version 1	Transient boundary conditions (ice sheet)	Objectives
1	Flow transient, transport, heat	Laxemar[1)]	Prescribed pressure from ice sheet model (glaciation scenario I)	Sensitivity to hydraulic properties Penetration depth of meltwater
2	Flow transient, transport, heat	Forsmark[1)]	Prescribed pressure from ice sheet model (glaciation scenario I)	Sensitivity to hydraulic properties Penetration depth of meltwater
3	Flow transient, transport, heat	Olkiluoto[1)]	Prescribed pressure from ice sheet model (glaciation scenario I)	Sensitivity to hydraulic properties Penetration depth of meltwater
4	Flow transient, transport, heat	Laxemar[1)]	Prescribed pressure from ice sheet model (glaciation scenario II with low value for the positive degree-day factor)	Sensitivity to boundary conditions from ice sheet model Penetration depth of meltwater
5	Flow transient, transport, heat	Laxemar[1)]	Prescribed pressure from ice sheet model (glaciation scenario III with high value for the positive degree-day factor)	Sensitivity to boundary conditions from ice sheet model Penetration depth of meltwater

[1)] Presence of subglacial layer and horizontal deformation zones.

Furthermore, two additional cases are considered under steady state ice sheet conditions (Table 6-2). Case 6 is a variation for the reference case of modelling phase II (Jaquet et al. 2012), with the GAP subglacial topography (cf. Section 5.2) and the latest steady state ice sheet boundary conditions for present day conditions (cf. Section 3). And, case 7 is characterised by the presence of horizontal deformation zones (cf. Section 5.9). For these two cases, the permafrost is not calculated, as in the previous cases, but is imposed with a fixed thickness. The results in relation to the cases 6 and 7 are given in Appendix B.

The applied parameters were defined in the preceding sections. All calculations were performed using the DarcyTools simulator, version 4.0.11 (Svensson et al. 2010). The details of the procedure applied for the numerical resolution of the system of non linear equations are given in Appendix D.

Table 6-2. Specifications for the two additional modelling cases (cf. Appendix B).

Case	Processes	Hydraulic properties	Steady state boundary conditions (ice sheet)	Objectives
6	Flow steady state	Laxemar[2)] (without horizontal deformation zones)	Prescribed meltrate from ice sheet model (scenario 0 – present day conditions)	Sensitivity to subglacial topography and ice sheet boundary conditions
7	Flow steady state	Laxemar[2)] (with horizontal deformation zones)	Prescribed meltrate from ice sheet model (scenario 0 – present day conditions)	Sensitivity to horizontal deformation zones

[2)] Presence of (fixed) permafrost and absence of subglacial layer.

6.1 Case 1

The case 1 utilises the hydraulic and thermal properties of the Laxemar site and the vertical deformation zones are described by the GAP Geomodel version 1. And, as for the other transient cases, case 1 is characterised by the presence of a subglacial layer and horizontal deformation zones. The initial and boundary conditions applied for case 1 are defined below.

Initial conditions

The initial flow conditions are calculated using hydrostatic pressure conditions with a fixed salinity profile (cf. salinity initial conditions below) in the absence of the ice sheet. The choice of this procedure was motivated by a rather fast reacting flow field at the scale of the time step considered for transient simulation.

The initial salinity conditions are taken from the Laxemar site (Vidstrand et al. 2010b):

- Ground surface to Z = −150 m: salinity is 0 %.
- Z = −150m to Z = −2 100 m: salinity linearly increases to 7.2 %.
- Below Z = −2 100 m: salinity is set to 7.2 %.

And, the following initial temperature conditions are attributed in the absence of the ice sheet (Vidstrand et al. 2010b):

- Ground surface: 1 ºC
- Depth gradient; 0.015 ºC/m.

These initial temperature conditions are needed to calculate permafrost conditions in the absence of ice. Using these initial conditions, a first simulation – applying as boundary conditions, the (negative) surface temperature field at −115 000 years derived from central-Greenland ice core (cf. Section 6.1) – is performed in order to reach pseudo steady-state permafrost conditions. This state constitutes the basis for coupled groundwater flow, heat and transport simulations with ice sheet advance and retreat coupled with progressive formation/ melting of the permafrost.

Hydraulic boundary conditions

In relation to the presence of the ice sheet and model geometry, the transient flow boundary conditions are applied as follows.

Surface of the model: the displacement of the ice sheet is described by the space-time variation of the ice thickness; i.e. the ice thickness values are provided by the SICOPOLIS ice sheet model (Vallot et al. 2012a, b and cf. Section 3) for a glacial cycle involving ice sheet build up, completeness and retreat for two periods from −115 to −80 ka and −20 to −1 ka (Figures 6-1 to 6-3).

"*The first time period captures the regrowth of the ice sheet from its last-interglacial minimum to its full last-glacial size. The second time period captures the shrinkage of the ice sheet from the Last Glacial Maximum to almost the present day"* (Vallot et al. 2012a, b). The SICOPOLIS data, available according to 10-km grid spacing, with a time step of 500 years, were downscaled at the grid cell centres of the groundwater flow model using a spline interpolation method (Vallot et al. 2012a, b). About one third of the model presents a detailed topography, the remaining part of the domain shows a smooth topography due to DEM data available at a lower resolution (cf. Section 5.2). Therefore, since the main part of the domain exhibits a smooth topography, no filtering of the ice thickness was performed in relation to topographical effects. In addition, for the areas of detailed topography, the absence of filtering allows to obtain more realistic hydraulic gradients during the periods of glacial build up and retreat, in relation to areas with low ice thickness.

Then, the ice thickness is added to the topographic contribution and expressed in terms of dynamic fluid pressure, which is used as boundary conditions:

$$P_{BC}^{surface}(x,t) = \rho_{ice}\ g\ h_{ice}(x,t) + \rho\ g\ z \qquad (6\text{–}1)$$

where:

ρ_{ice}: ice density (= 917 kg/m^3)
$h_{ice}(x,t)$: ice thickness from SICOPOLIS
z: topography elevation.

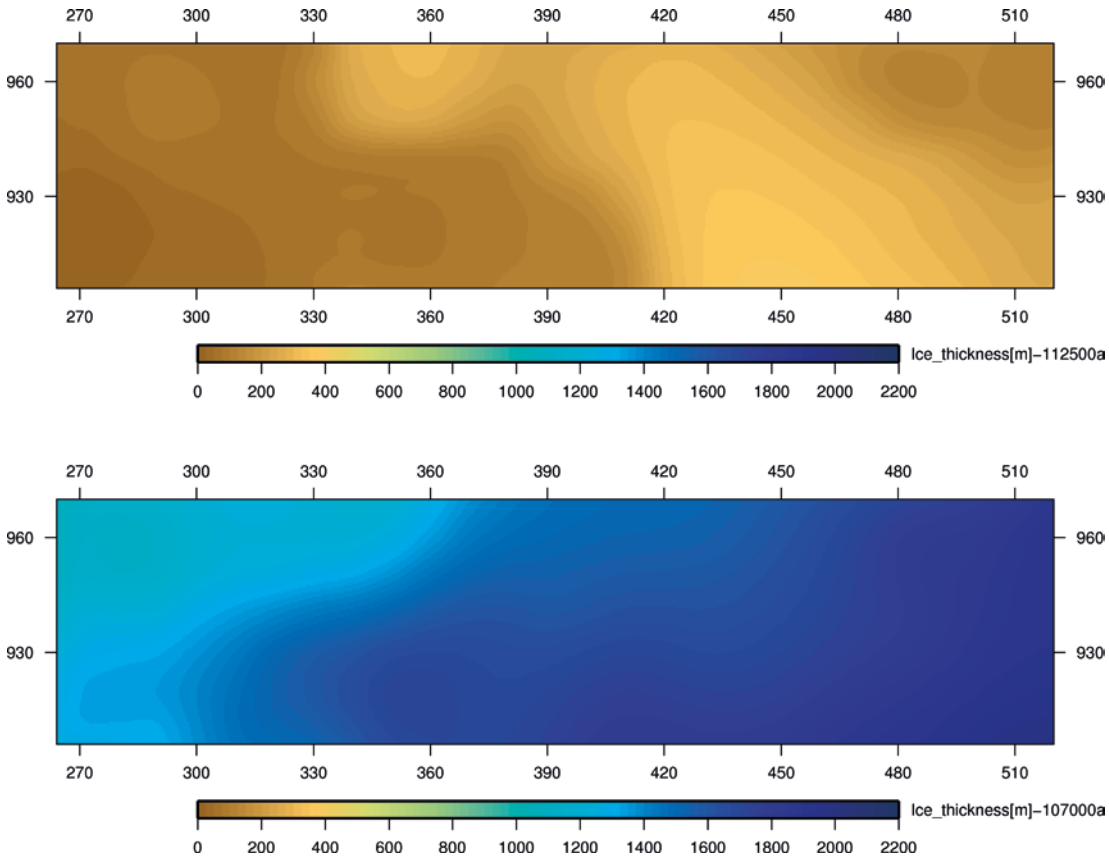

Figure 6-1. Ice sheet build up: *ice thickness [m] from SICOPOLIS ice sheet model (scenario I), at −112.5 ka (above) before 2000 AD and −107 ka (below) before 2000 AD (coordinates in km).*

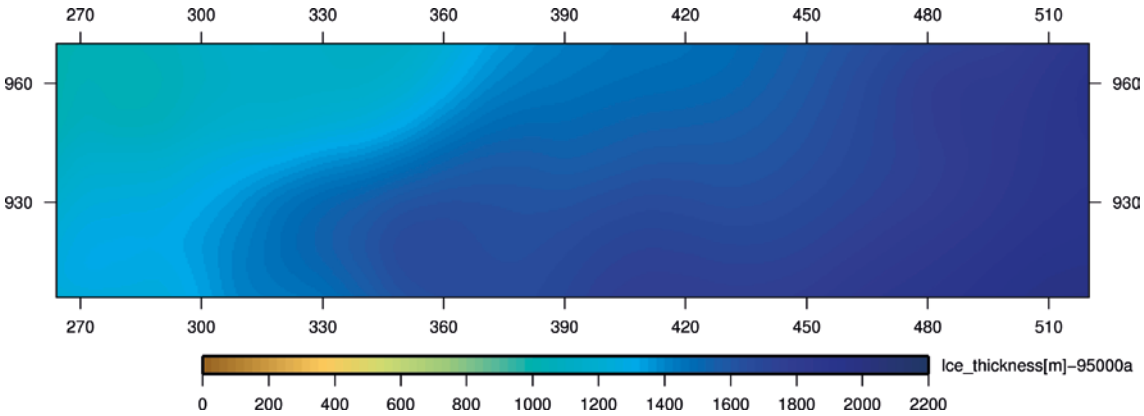

Figure 6-2. Ice sheet completeness*: ice thickness [m] from SICOPOLIS ice sheet model (scenario I), at −95 ka before 2000 AD (coordinates in km).*

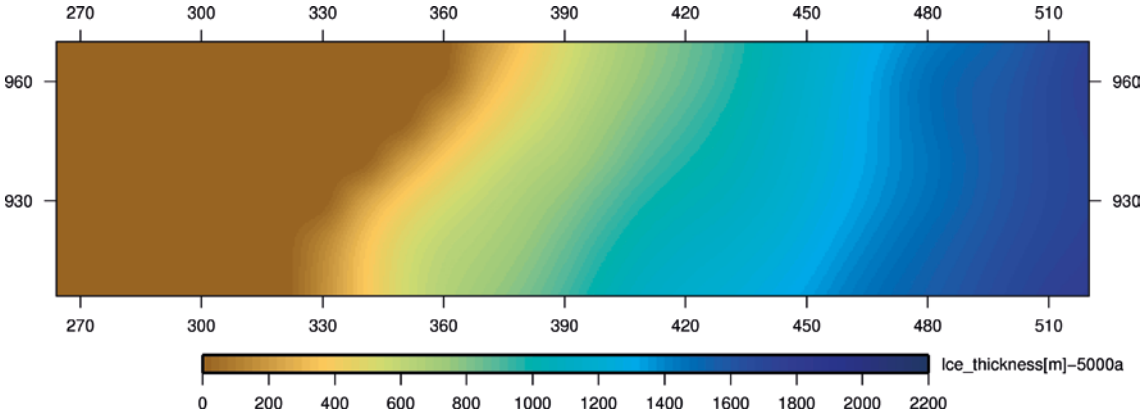

Figure 6-3. Ice sheet retreat*: ice thickness [m] from SICOPOLIS ice sheet model (scenario I), at −5 ka before 2000 AD (coordinates in km).*

In the absence of the ice sheet, solely the pressure contribution related to the elevation of the topography applies (cf. Equation 6-1). The selection of this type of boundary is the consequence of the latest findings, developed through GAP in relation to the conceptual understanding of the basal drainage system for the ice sheet (Claesson Liljedahl et al. 2016): *"Hydraulic measurements and analyses from the ice boreholes imply that ice overburden hydraulic pressure (i.e. a hydraulic head corresponding to 92 % of ice thickness) provides an appropriate description of the basal hydraulic pressure as an average value for the entire ice sheet over the year"*. Based on observations (cf. Section 5.4) and conceptual considerations from the glaciologists of the GAP project, it was assumed that such hydraulic boundary conditions (92 % of ice thickness) can be applied for groundwater flow modelling during the different periods of a glacial cycle. From the modelling point of view, more details in relation to the choice of this type of subglacial boundary conditions are given in Appendix C.

Lateral west boundary: a hydrostatic condition is prescribed using a dynamic fluid pressure where the surface elevation z is set to a constant value equal to 37.5 m; this value corresponds to the mean elevation of the topography along the boundary. When ice is present, the mean ice thickness along the boundary is added:

$$P_{BC}^{west}(t) = \rho_{ice}\ g\ mean\left(h_{ice}\left(x_B, t\right)\right) + \rho\ g\ 37.5 \qquad (6\text{–}2)$$

Lateral north+south+east and bottom boundaries: no-flow conditions are prescribed. Such choice is accordance with the current state of information. In presence of additional (new) information, the type of these boundaries shall be modified accordingly.

Thermal boundary conditions

The following transient thermal boundary conditions are applied in relation to the presence of the ice sheet and model geometry.

Surface of the model: in the absence of the ice sheet, the prescribed temperature results from the extraction of climate data from the central-Greenland ice core (Figure 6-4). The ice core was drilled in 1990–92, by the joint European Greenland Ice-core Project (GRIP) at the very top of the Greenland ice sheet. The time series of temperature anomaly is based on the GRIP ice core oxygen isotope record (Dansgaard et al. 1993, Johnsen et al. 1997). In order to be applied as boundary conditions for groundwater flow modelling, the time series is corrected according to the elevation of model grid cells in relation to the summit temperature using altitude and temperature parameters taken from Dansgaard et al. (1993) and Fausto et al. (2009), and finally estimated using a 500 year time step (Figure 6-5).

At talik locations, the prescribed temperature is equal to 4 ºC (Vidstrand et al. 2010b, Harper et al. 2016). The talik conditions are assumed to disappear when they are covered by the ice sheet. Regarding the subglacial layer, its temperature is always prescribed at 0.1 ºC (Figure 6-6), even when located underneath the ice sheet; i.e. it never freezes in order to maintain remarkable flow within the subglacial layer. This concept is based on the GAP results stating that: *...the frozen areas extends many tens of kilometres away from the ice divide, but greater than 75 % of the studied sector of the Greenland ice sheet is subject to basal melting conditions (*Claesson Liljedahl et al. 2016).

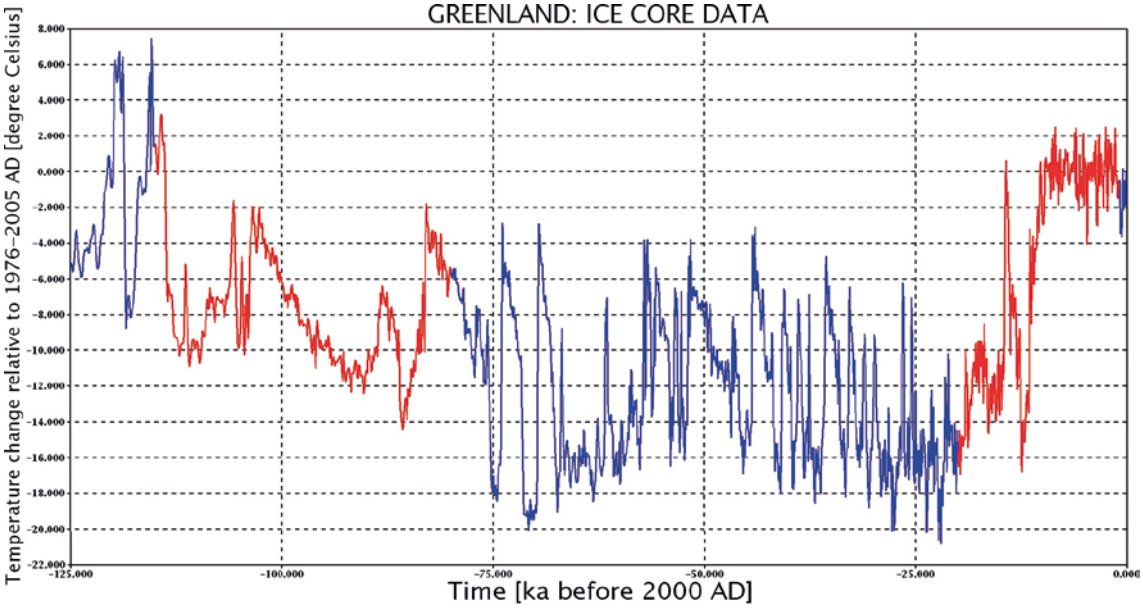

Figure 6-4. *Ice core data from central-Greenland: the temperature curves for the modelled periods (−115 to −80 ka; −20 to −1 ka) are in red colour. Temperature [ºC] change is relative to the mean annual 1976–2005 AD temperature.*

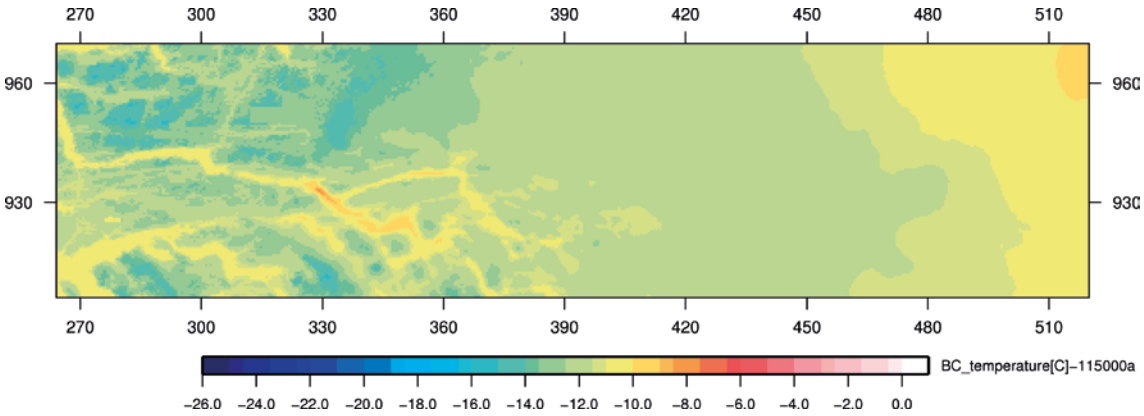

Figure 6-5. *Temperature [ºC] field at −115 ka, based on ice core data, applied as surface boundary conditions (coordinates in km).*

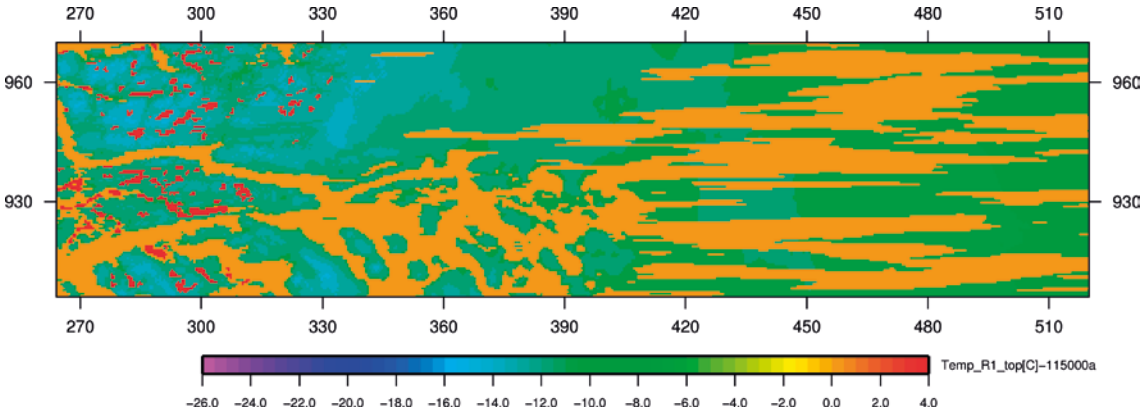

Figure 6-6. *Temperature [ºC] field at −115 ka, based on ice core data, with prescribed taliks (red) and subglacial layer (orange) applied as surface boundary conditions (coordinates in km).*

Surface of the model (underneath the ice sheet): when the ice sheet is present, the prescribed temperature values are provided by the SICOPOLIS ice sheet model (Vallot et al. 2012a, b and cf. Section 3) for the two periods −115 to −80 ka and −20 to −1 ka (Figures 6-7 to 6-9), available with a 500 years time step.

Lateral north+south+west+east boundaries: the boundary conditions are prescribed as follows;

$$\frac{\partial T}{\partial x} = 0, \quad \frac{\partial T}{\partial y} = 0 \tag{6-3}$$

Bottom boundary: the value for the prescribed geothermal heat flux is provided by GAP borehole data (0.0348 W m^{-2}) and corrected for depth (cf. Section 5.6).

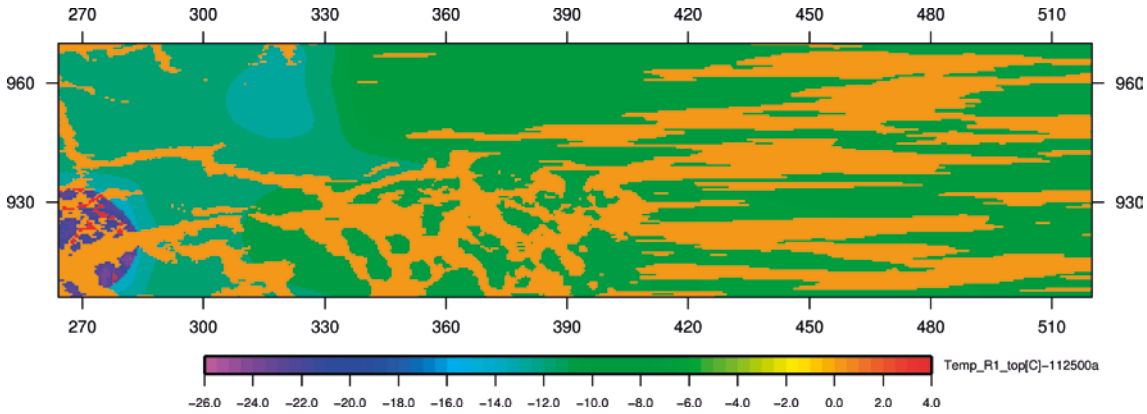

***Figure 6-7. Ice sheet build up**: basal temperature [ºC] from SICOPOLIS ice sheet model (scenario I), at -112.5 ka before 2000 AD (coordinates in km). In the south-west corner of the domain, the low temperature zone (purple) with taliks (red patches) indicates the absence of the ice sheet.*

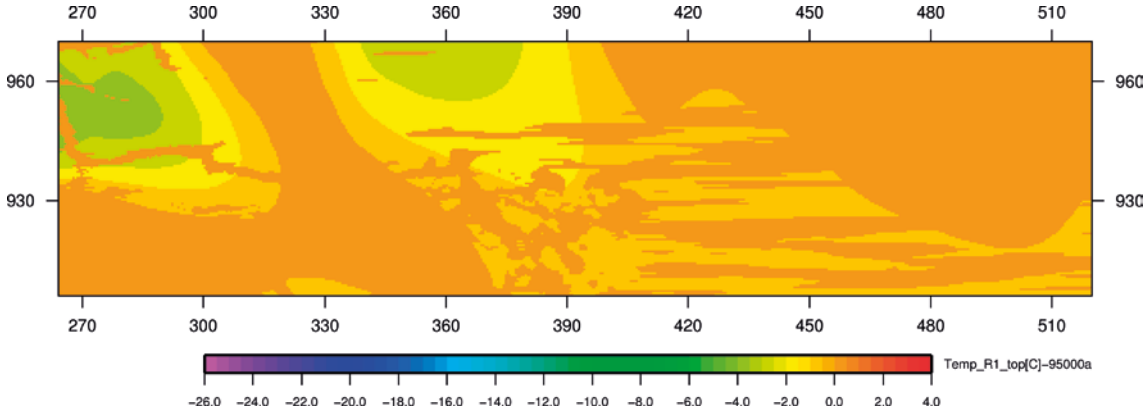

***Figure 6-8. Ice sheet completeness:** basal temperature [ºC] from SICOPOLIS ice sheet model (scenario I), at -95 ka before 2000 AD (coordinates in km). Solely, the subglacial layer remains as boundary condition.*

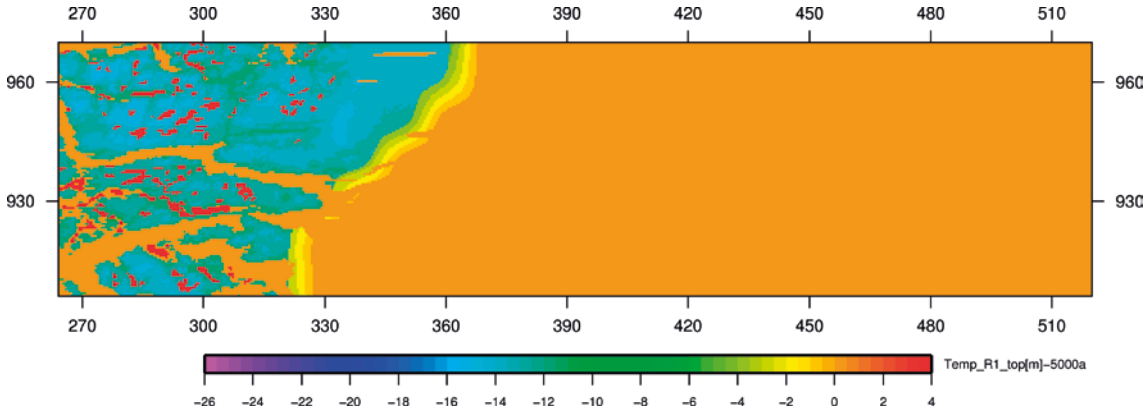

***Figure 6-9. Ice sheet retreat**: basal temperature [ºC] from SICOPOLIS ice sheet model (scenario I), at -5 ka before 2000 AD (coordinates in km). The western part of domain (yellow-blue) is marked by the absence of the ice sheet and the reappearance of the taliks (red).*

Salinity boundary conditions

The salinity boundary conditions, applied in relation to the presence of the ice sheet and model geometry, are the following.

Surface of the model: in the absence of the ice sheet, a no dispersive flux boundary is imposed for the salinity;

$$\frac{\partial C}{\partial z} = 0 \tag{6-4}$$

Surface of the model (underneath the ice sheet): when the ice sheet is present, the influx of meltwater is prescribed with a salinity equal to 0.

Lateral North+South+East boundaries: the prescribed flux boundary conditions are no dispersive;

$$\frac{\partial C}{\partial x} = 0, \quad \frac{\partial C}{\partial y} = 0 \tag{6-5}$$

Bottom boundary: a salinity value of 7.2 % is prescribed (Vidstrand et al. 2010b).

Boundary conditions for the period −80 to −20 ka

For the period between −80 to −20 ka, no data from SICOPOLIS were made available, since during this time interval little variation of ice volume was encountered by the ice sheet simulations (Figure 6-10).

Therefore, steady state boundary conditions can be considered for the period −80 to −20ka. And, the modelling domain is assumed fully covered by the ice sheet, since ice is present everywhere at −80 ka and −20 ka and during the period −80 to −20ka, no major variation in ice volume was encountered according to the results of ice sheet modelling (Applegate et al. 2012).

Flow boundary conditions

Surface of the model (underneath the ice sheet): the spatially variable ice thickness is obtained using an average value between the −80 and −20 ka time steps, taken from the SICOPOLIS model and then prescribed as a dynamic fluid pressure (cf. Equation 6-1).

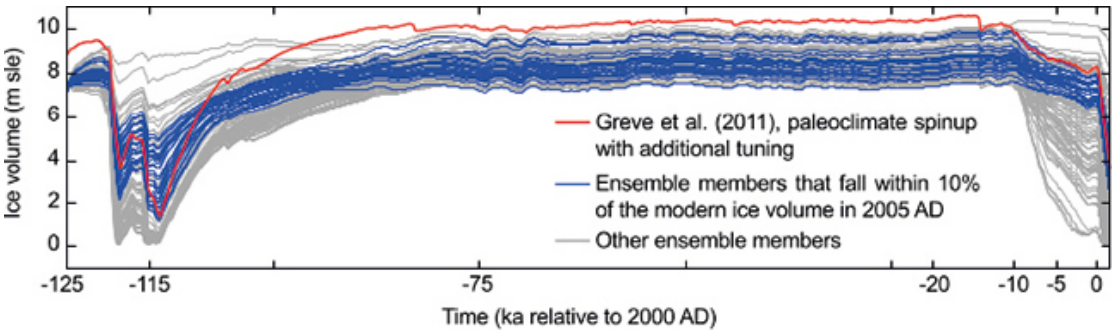

Figure 6-10. *Greenland Ice Sheet: simulated ice volume with SICOPOLIS, expressed in meters of sea level equivalent (m sle): 100 ensemble members with approximately unvarying ice volume and rather similar behaviour during the period -80 to -20 ka (after Applegate et al. 2012).*

Thermal boundary conditions

Surface of the model (underneath the ice sheet): like before, the spatially variable temperature is prescribed using an average value between the −80 and −20 ka time steps taken from the ice sheet model.

The other boundary conditions for the period −80 to −20 ka remain identical to the ones of the surrounding periods (−115 to −80 ka and −20 to −1 ka); cf. Section 6.1.

Simulation

For the case 1, groundwater flow coupled with salt transport and heat transfer is performed during the time interval from −115 to −1ka, using boundary conditions given by the ice sheet model SICOPOLIS, and corresponding to a complete glacial cycle. Due to size of the model and the number of time steps needed, the numerical solution of the heat transfer flow, salt transport and equations is weakly coupled by linearising the equations. At each iteration, the simulation is carried out in three stages: (a) solving of heat transfer under permafrost conditions, then modifications of hydraulic conductivity and porosity according to the temperature field, (b) resolution of flow with update of density according to salinity, and (c) resolution of salt transport. This iterative procedure is repeated sequentially for each time step. It is stopped when the values for the criteria of convergence are reached for each time step during the simulation (additional details can be found in Appendix D).

The glacial cycle considered for the groundwater flow simulation comprises three different ice sheet periods: build up, completeness and retreat, each of them having its specific duration (Table 6-3). This glacial cycle also comprises the Last Glacial Maximum that occurred around 20 ka ago (SKB 2014). The bounds of the periods of advance and retreat are related to the behaviour of the mean ice thickness estimated over the model domain for each time step, using values of ice thickness given by the ice sheet model (Figures 6-11 and 6-12).

Table 6-3. Glacial cycle: ice sheet periods.

Behaviour of ice sheet	Build up	Duration [ka]	Completeness	Duration [ka]	Retreat	Duration [ka]
Time*	**−115.0 to −106.5**	8.5	**−106.0 to −11.0**	95.5	**−10.5 to −1.0**	10.0
Ice sheet data* (500 years time step)	**−115.0 to −80.0**		**−20.0 to −1.0**			

*ka before 2000 AD.

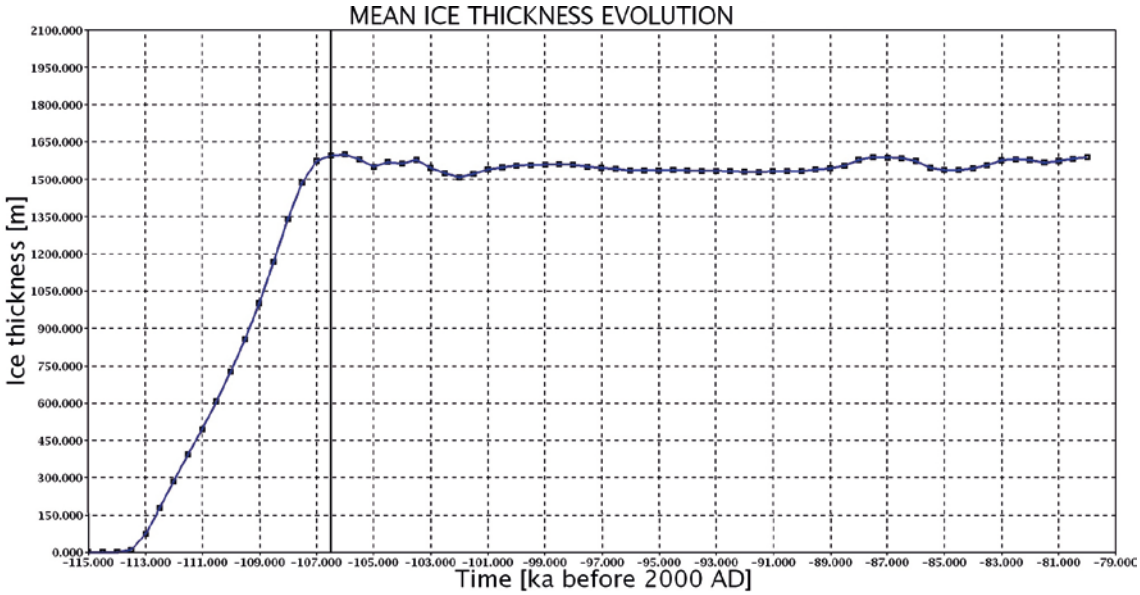

Figure 6-11. *Evolution of mean ice thickness [m] over the model surface, using SICOPOLIS data (scenario I) from −115 to −80ka. The end of the glacial build up period is at −106.5 ka (vertical black line).*

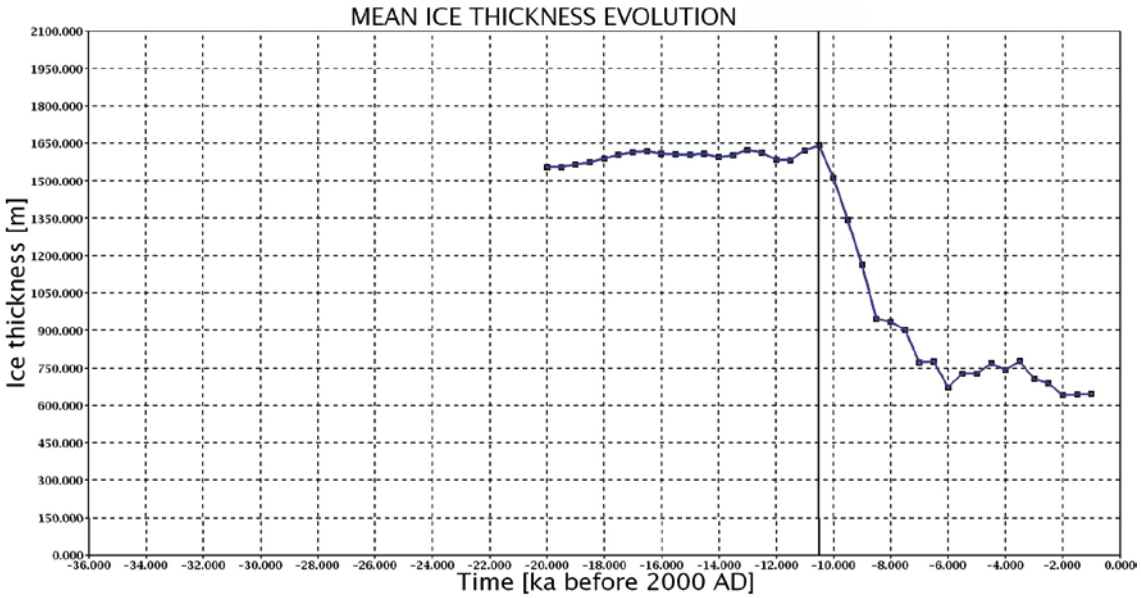

Figure 6-12. *Evolution of mean ice thickness [m] over the model surface, using SICOPOLIS data (scenario I) from −20 to −1 ka. The onset of the glacial retreat period is at −10.5 ka (vertical black line).*

During the period of ice sheet build up – with regional components predominantly from eastern and south eastern directions – the first patches of ice sheet begin to appear at −113.5 ka (cf. Figure 6-11). Then, the ice sheet gradually fills up the studied domain according to the various directions; at −110 ka, the entire domain is covered by the ice sheet. Then, until the end of the glacial build up period, thickening of the ice sheet occurs until −106.5 ka (cf. Figure 6-11). The period of glacial completeness lasts from −106 to −11 ka.

Then, the beginning of the ice sheet retreat is at −10.5 ka, and the ice margin appears at −9 ka; the ice sheet displacement is rather fast towards the east, and this partial retreat period terminates with some east-west oscillations of the ice margin, from approximately −6 to −1 ka (cf. Figure 6-12).

A time step of 500 years is applied for groundwater simulation during the time intervals −115 to −80 ka and −20 to −1 ka matching the SICOPOLIS data. Between these intervals, a larger time step is chosen (6 000 years), since no variation in boundary conditions occurs between −80 and −20 ka (cf. Section 6.1).

Therefore, the simulation results are examined for selected time steps with respect to the displacement of the ice sheet. At −114 ka, before the appearance of the ice sheet, the flow results – expressed in terms of dynamic fluid pressure in kPa; hereinafter called pressure – show the driving effects of the topography, in particular in the area of the main trough located in the middle western part of the model (X=330 km; Figure 6-13). This trough was discovered by the radar investigations during the GAP project (cf. Section 5.2).

With the arrival of the ice sheet, drastic modifications of the flow patterns are observed due to the increase of the pressure in relation to the ice thickness (Figure 6-14).

When the period of glacial completeness – from −106 to −11 ka – is reached (Figure 6-15), the flow approximately stabilizes, only minor variations are observed, likely related to the spatial distribution of the permafrost that varies in response to the temperature field reigning underneath the ice sheet. The magnitude of the regional hydraulic gradient, orientated towards the west, is mainly influenced by the variation of the ice sheet thickness that increases towards the east (cf. Figure 6-2); and, in the western part by the more variable topography (cf. Figure 6-15: e.g. the red zones located in the south).

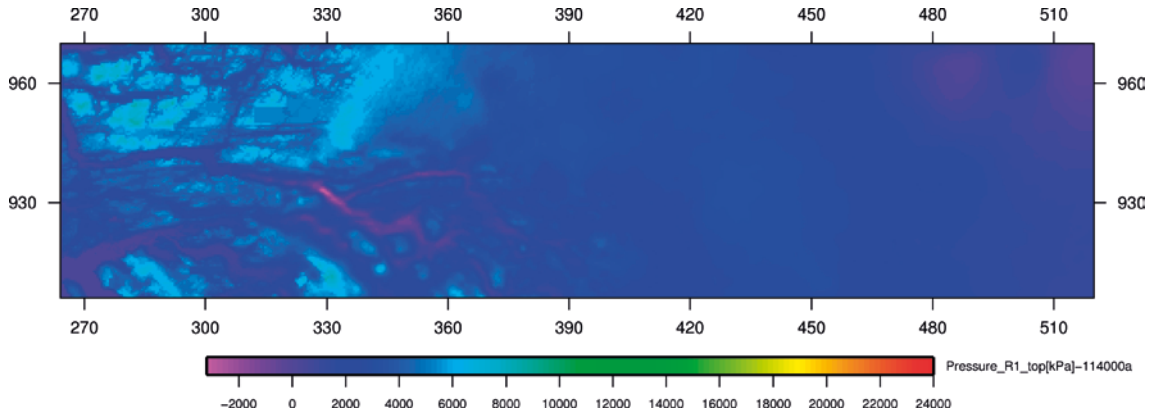

Figure 6-13. *Case 1: pressure [kPa] at −114 ka with the* ***absence of ice sheet****, projected top horizontal cut (coordinates in km).*

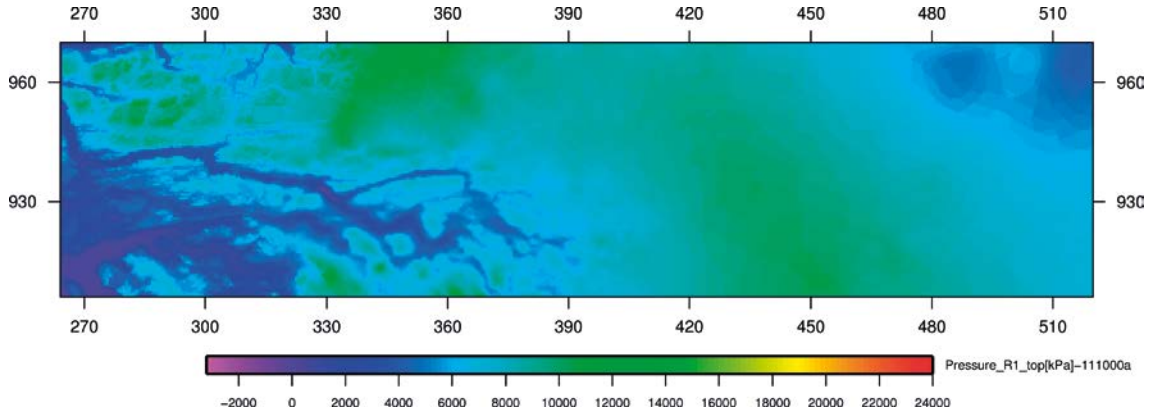

Figure 6-14. *Case 1: pressure [kPa] at −111 ka,* ***period of glacial build up****, projected top horizontal cut (coordinates in km).*

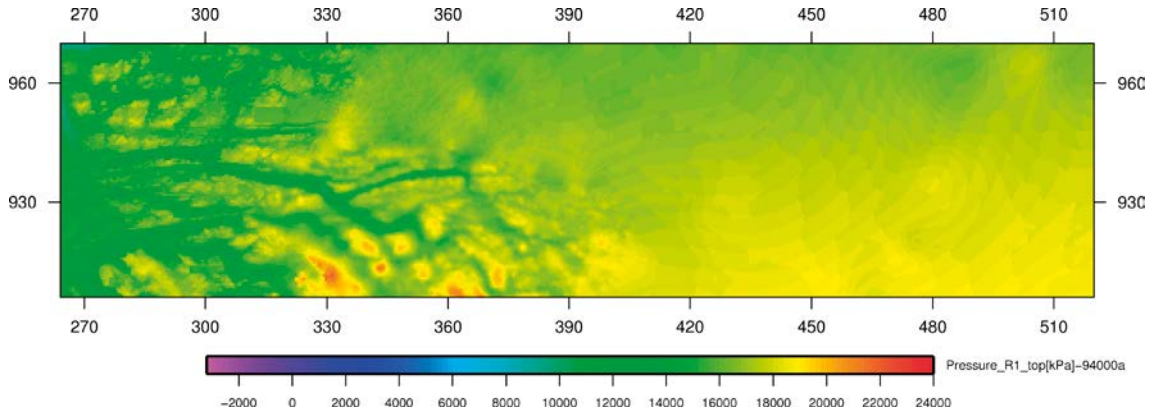

Figure 6-15. *Case 1: pressure [kPa] at −94 ka,* ***period of glacial completeness****, projected top horizontal cut (coordinates in km).*

With the beginning of glacial retreat at −10.5 ka, followed by the appearance of an ice sheet margin at −9 ka, the ice sheet moves rapidly towards the east (Figure 6-16), and this period ends up with some east-west oscillations of the ice margin, from approximately −6 to −1 ka. Due to the rapid displacement of the ice sheet (towards the east) during glacial retreat, the magnitude of the regional gradient is likely stronger during that period.

The mean temperature, estimated over the model surface, decreases remarkably with the ice sheet appearance at −113.5 ka (Figures 6-17 and 6-18). Then, during glacial build up and beyond, the mean temperature presents a gradual increase to about −105 ka (cf. Figure 6-17). During glacial completeness, the value of the mean temperature remains negative, but large zones underneath the ice sheet can occur with positive temperature values (Figure 6-19); and, during that period, the behaviour of the mean temperature is rather stable up to −11 ka. The onset of glacial retreat, at −10.5 ka (Figure 6-20 and 6-21), is marked by a slight increase in mean temperature; at −9.5 ka, the mean temperature even becomes positive, followed by a smooth decrease up to −5.5 ka and ending again with a relative stabilisation of temperature towards −1 ka (Figure 6-22).

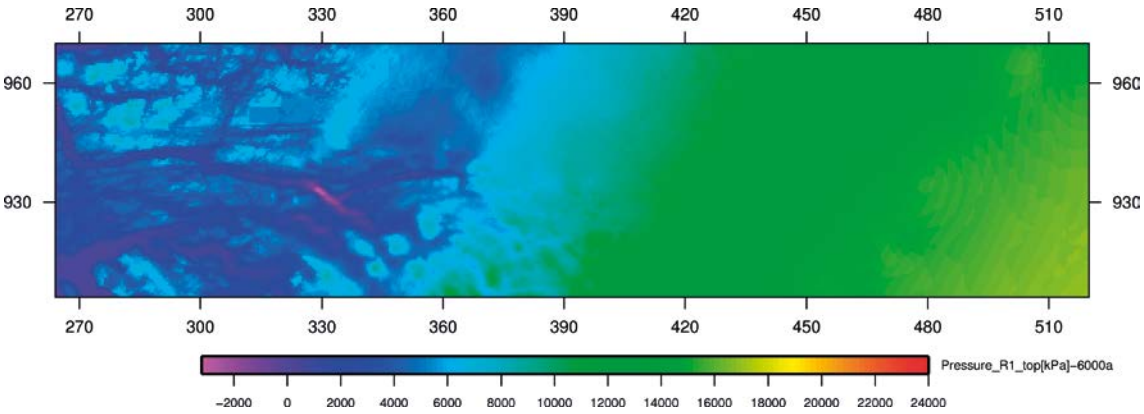

Figure 6-16. *Case 1: pressure [kPa] at −6 ka,* ***period of glacial retreat****, projected top horizontal cut (coordinates in km).*

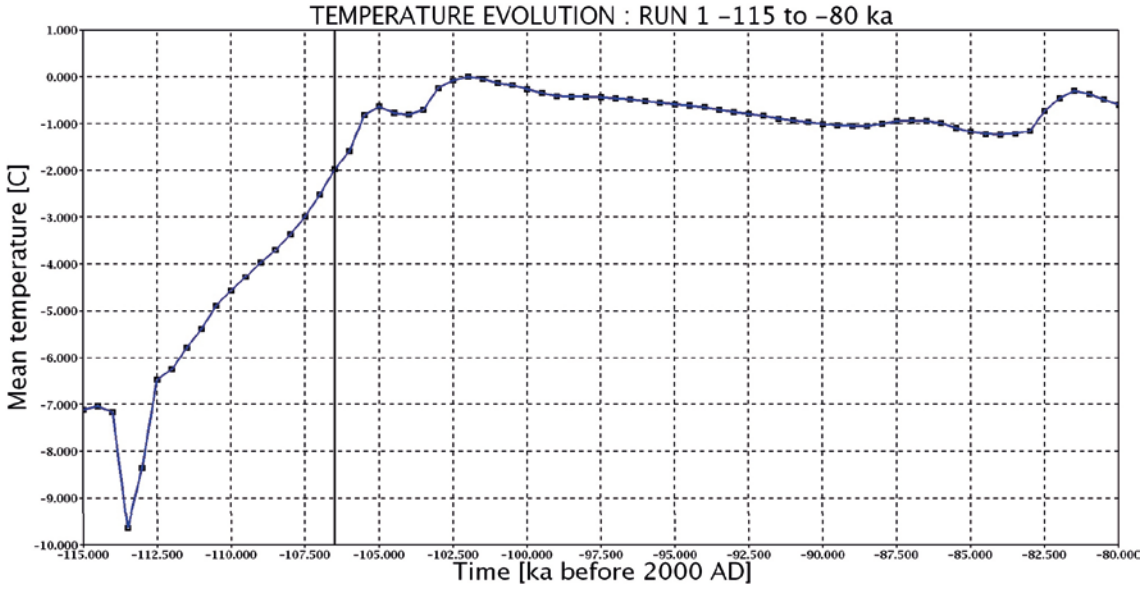

Figure 6-17. *Case 1: evolution of mean temperature [ºC] over the model surface, from −115 to −80 ka. The end of glacial build up is at −106.5 ka (vertical black line).*

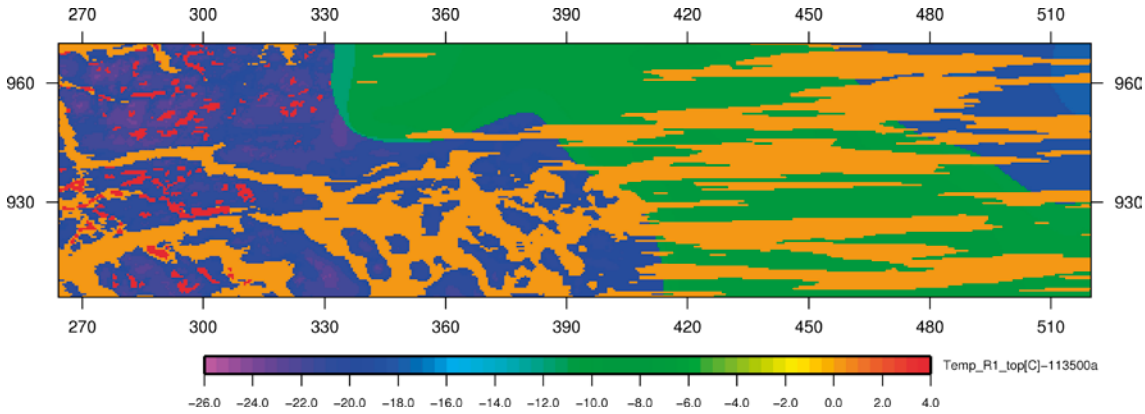

Figure 6-18. *Case 1: temperature [ºC] at −113.5 ka,* ***period of glacial build up****, projected top horizontal cut (coordinates in km).*

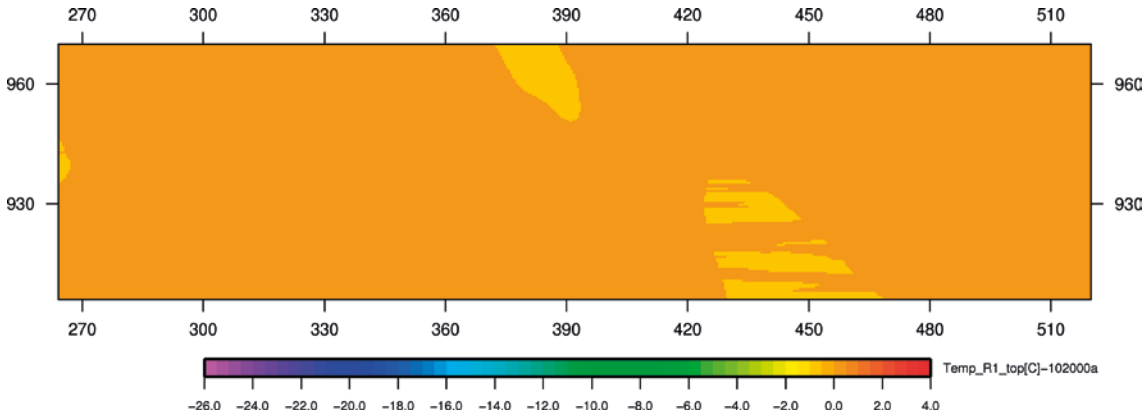

Figure 6-19. *Case 1: temperature [ºC] at −102 ka,* ***period of glacial completeness****, projected top horizontal cut (coordinates in km).*

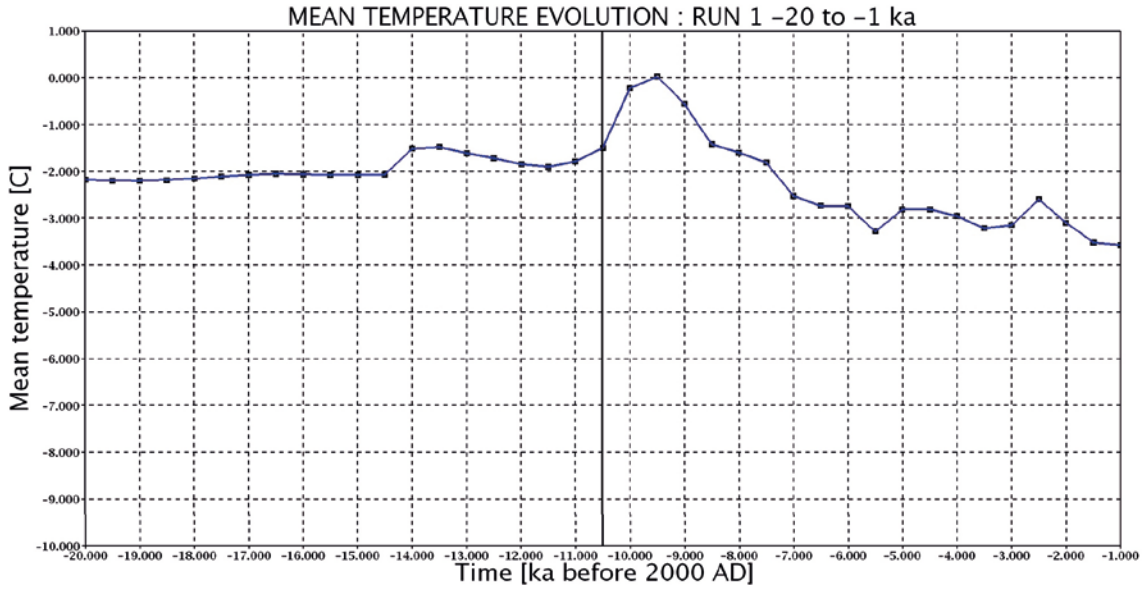

Figure 6-20. *Case 1: evolution of mean temperature [ºC] over the model surface, from −20 to −1 ka. The onset of glacial retreat is at −10.5 ka (vertical black line).*

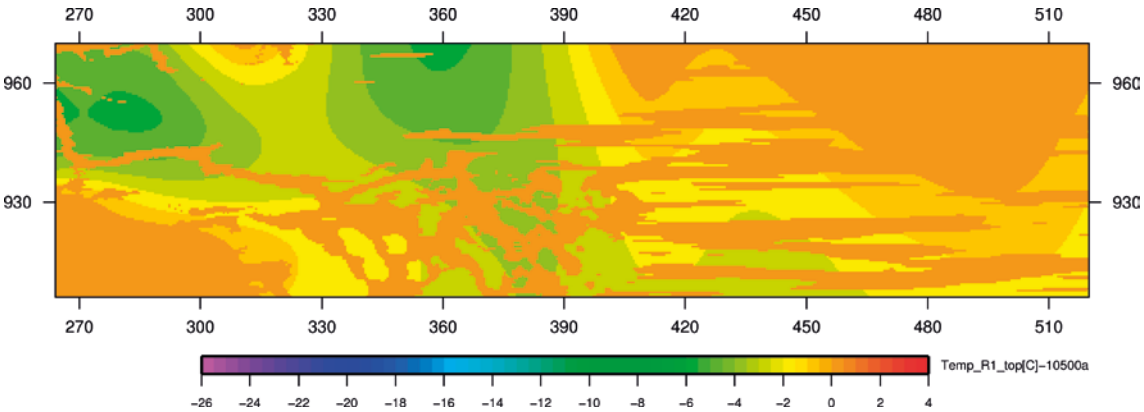

Figure 6-21. *Case 1: temperature [ºC] at −10.5 ka,* ***onset of glacial retreat****, projected top horizontal cut (coordinates in km).*

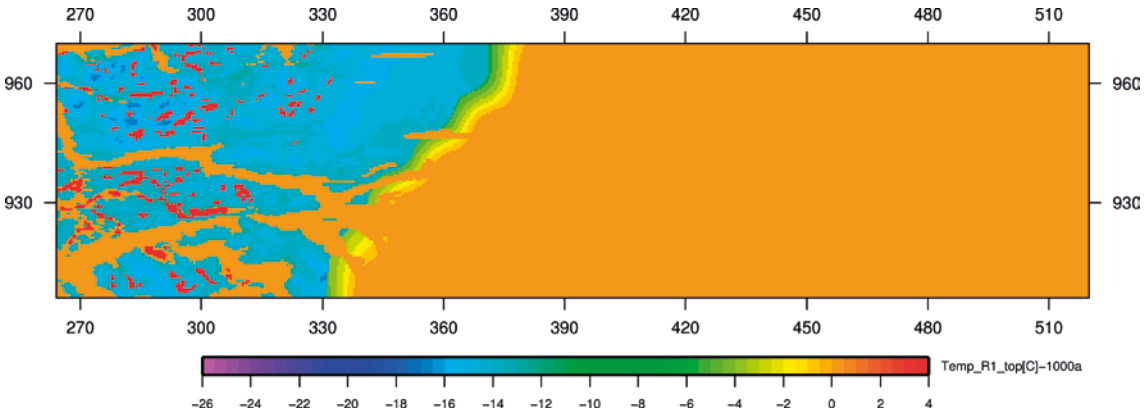

Figure 6-22. *Case 1: temperature [ºC] at −1 ka,* ***period of glacial retreat****, projected top horizontal cut (coordinates in km).*

During the glacial cycle, the evolution of the spatial distribution for the permafrost is mainly controlled by the temperature regime (periglacial and subglacial) of the ice sheet periods. At the beginning of the build up period (Figure 6-23), the surface proportion of the permafrost remains rather constant and suddenly starts to diminish at −106.5 ka (Figure 6-23), to reach a low value at −102 ka (Figure 6-25), with a few remaining patches, in response to the warmer temperature encountered underneath the ice sheet. Then, during the period of ice completeness, the regions of permafrost gradually grow under the ice with some fluctuations and then they reach a kind of plateau until the onset of glacial retreat. This last period experiences a sharp decrease of the permafrost proportion (Figure 6-26); starting at −10.5 ka (Figure 6-27), the subglacial permafrost has quasi disappeared totally under the ice sheet 1 000 years later (Figure 6-28), before the apparition of the ice margin at −9 ka (Figure 6-29). Finally, from −7 to −1 ka, the permafrost is no longer present underneath the ice sheet.

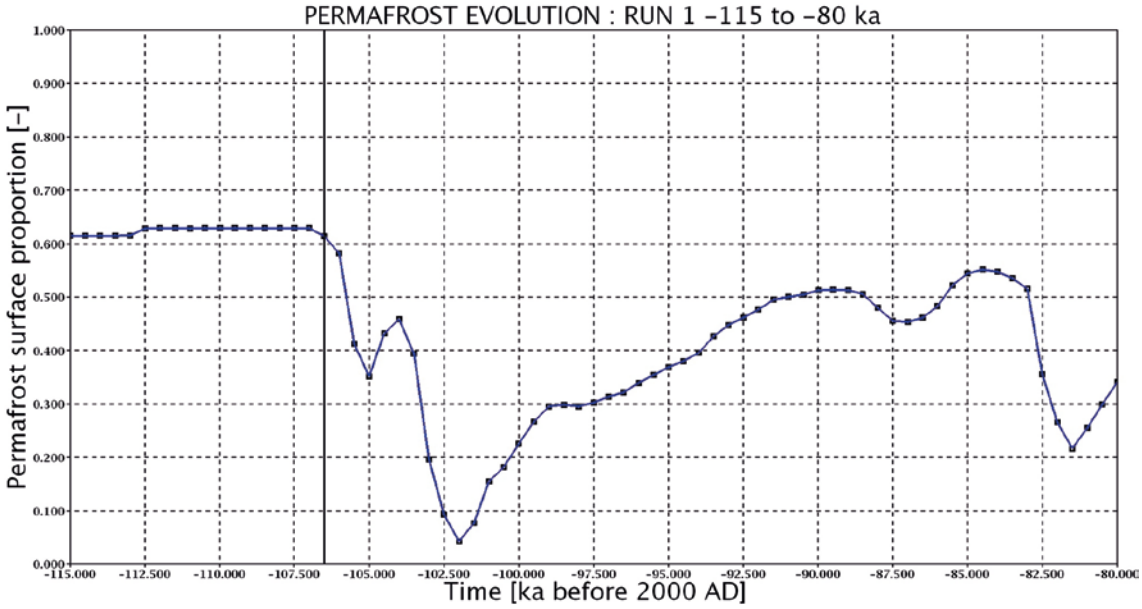

Figure 6-23. *Case 1: evolution of permafrost proportion [−] over the model surface, from −115 to −80 ka. The end of glacial build up is at −106.5 ka (vertical black line); the lowest value of permafrost proportion during ice completeness occurs at −102 ka.*

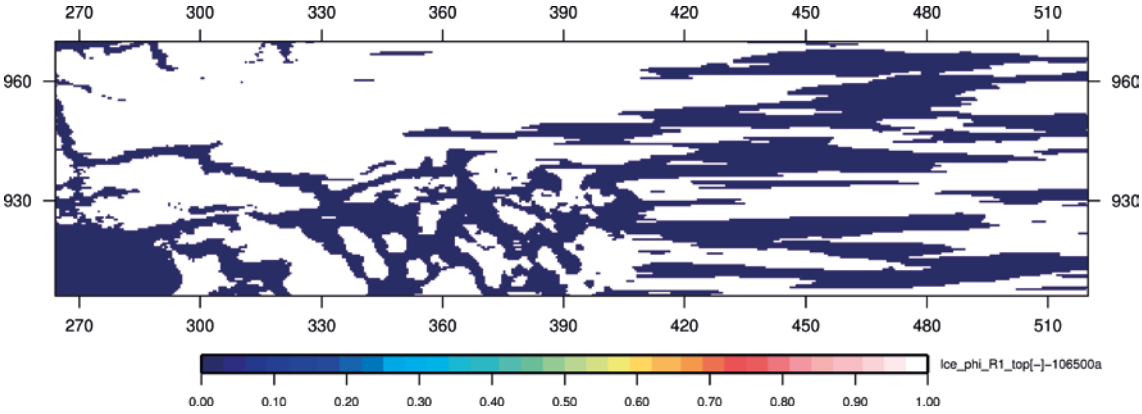

Figure 6-24. *Case 1: permafrost (white) at −106.5 ka (expressed as ice proportion [−]);* ***end of glacial build up****, projected top horizontal cut (coordinates in km).*

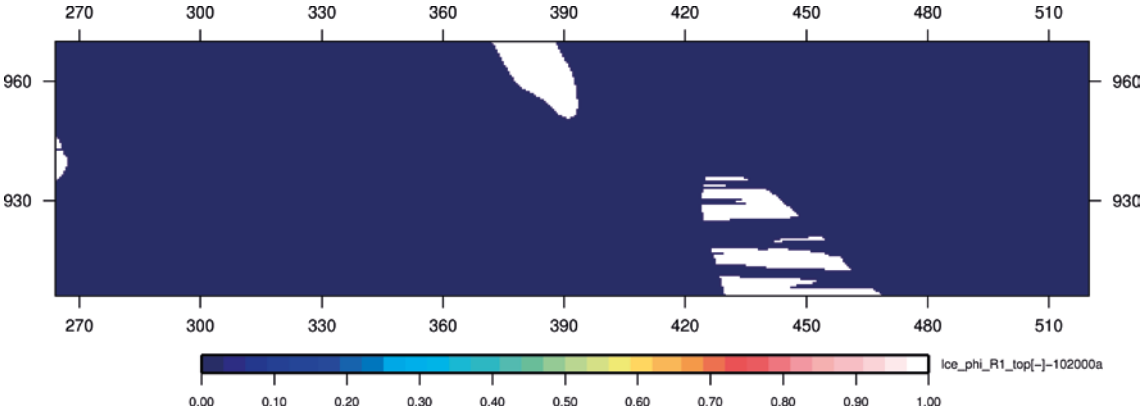

Figure 6-25. *Case 1: permafrost (white) at −102 ka (expressed as ice proportion [−]);* ***period of glacial completeness*** *with lowest permafrost proportion, projected top horizontal cut (coordinates in km).*

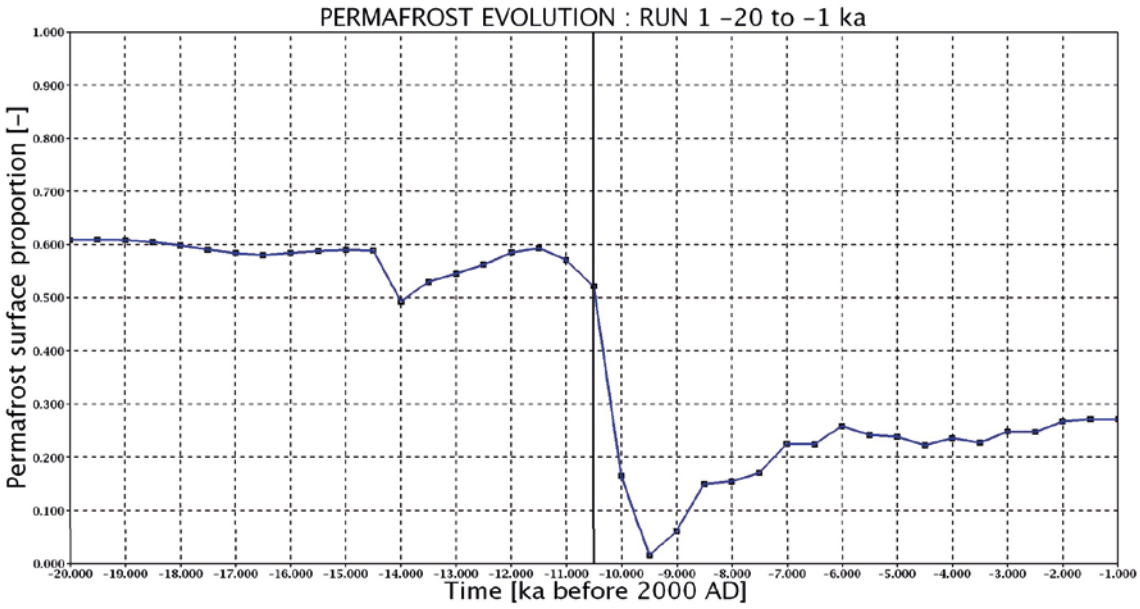

Figure 6-26. *Case 1: evolution of permafrost proportion [−] over the model surface, from −20 to −1 ka. The onset of glacial retreat is at −10.5 ka (vertical black line). The lowest value of permafrost proportion during glacial retreat occurs at −9.5 ka. From −7 to −1 ka, the permafrost is no longer present under the ice sheet.*

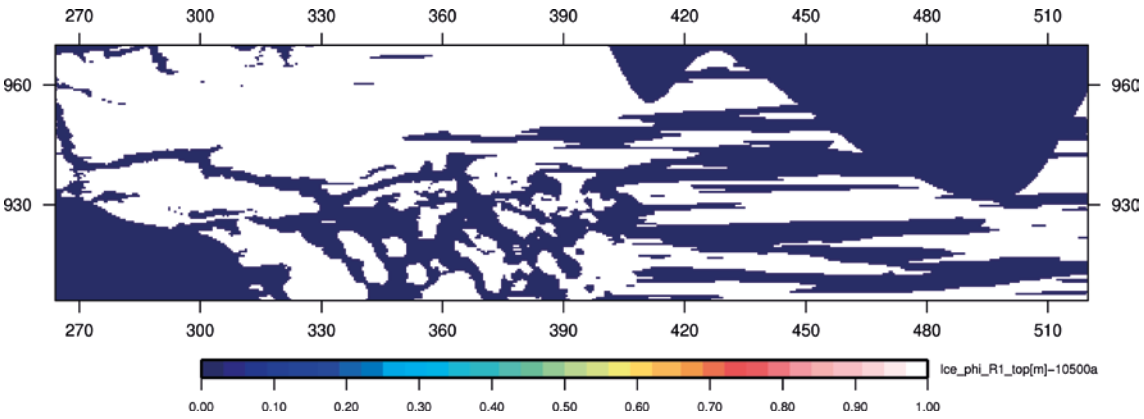

Figure 6-27. *Case 1: permafrost (white) at −10.5 ka (expressed as ice proportion [−]);* ***onset of glacial retreat****, projected top horizontal cut (coordinates in km).*

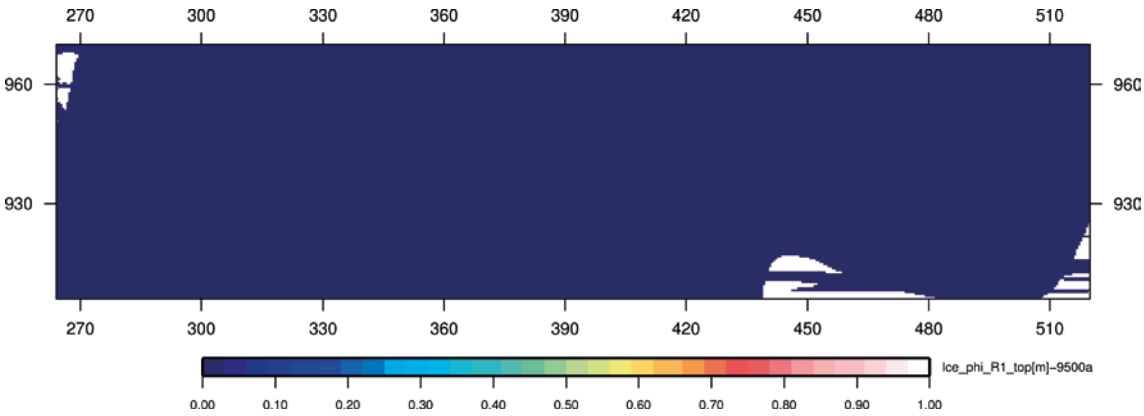

Figure 6-28. *Case 1: permafrost (white) at −9.5 ka (expressed as ice proportion [−]);* ***period of glacial retreat*** *with lowest permafrost proportion, projected top horizontal cut (coordinates in km).*

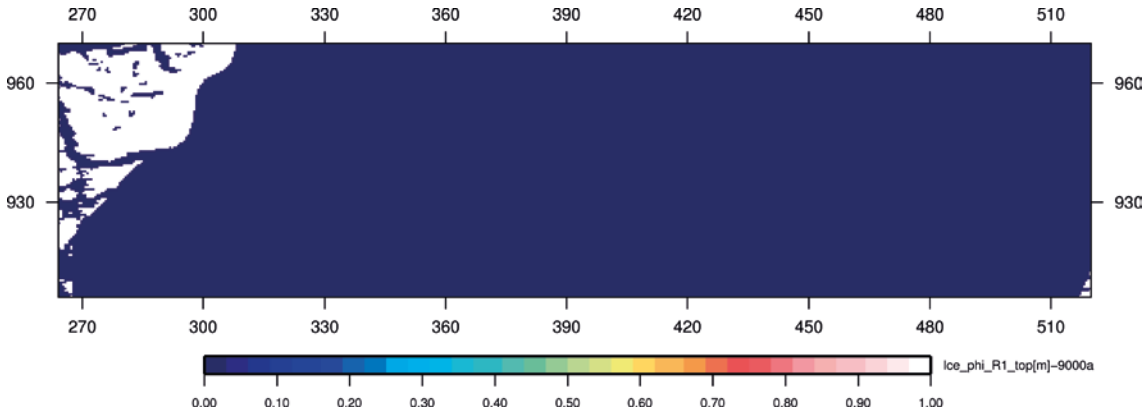

Figure 6-29. *Case 1: permafrost (white) at −9 ka (expressed as ice proportion [−]);* ***period of glacial retreat*** *with apparition of ice margin (west), projected top horizontal cut (coordinates in km).*

The evolution of the mean salinity, estimated over the model domain at 500 and 1 000 meter depths, presents a rather monotonic behaviour in time (Figures 6-30 and 6-32). After a rapid decrease of the mean salinity that occurs during the first part of the glacial build up, a relatively stable behaviour is observed for the salinity up to −1 ka (Figures 6-33 and 6-34). The variability of the permafrost proportion (cf. Figures 6-23 and 6-26) seems to have no influence on the salinity distribution at depth. The beginning of the glacial retreat at −10.5 ka is slightly visible, as shown by a smooth decrease on the salinity profile at 500 meter depth (cf. Figure 6-31).

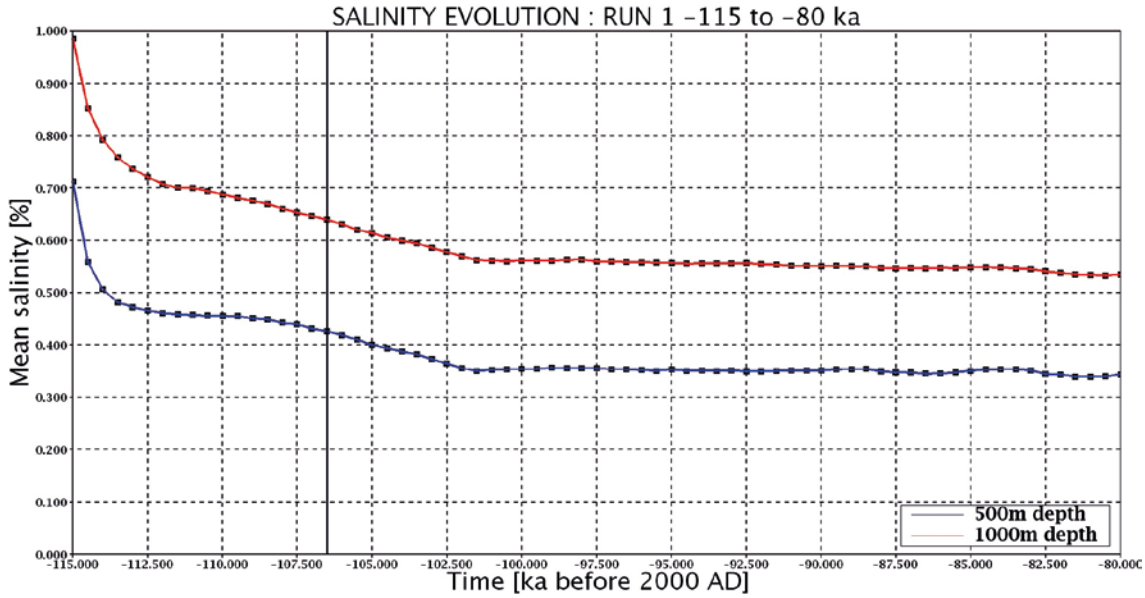

Figure 6-30. *Case 1: evolution of mean salinity [%] at 500 and 1000 meter depth over the model domain, from −115 to −80ka. The end of glacial build up is at −106.5 ka (vertical black line).*

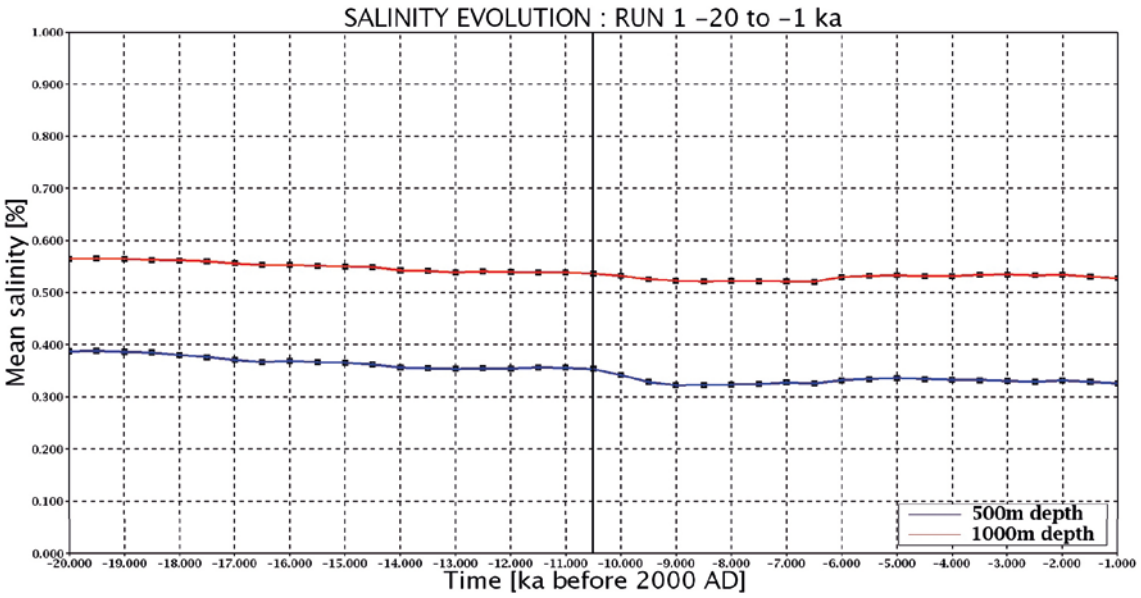

Figure 6-31. *Case 1: evolution of mean salinity [%] at 500 and 1000 meter depth over the model domain, from −20 to −1ka. The onset of glacial retreat is at −10.5 ka (vertical black line).*

The variability of the salinity is mainly controlled by the hydraulic conductivity of the rock domain, the deformation zones, and by the hydraulic gradient with an enhanced topographic effect, particularly visible in the western part of the domain (cf. Figures 6-32 to 6-36), in relation to the presence of hills and deep troughs (cf. Figure 5-2). For the case 1, flushing of salt can occur locally to the bottom boundary. Such effect is already occurring before the appearance of the ice sheet, in particular in the western part of the model that presents irregular topography (cf. Figure 6-32). The flushing effect is due to the high stochastic variability of the hydraulic conductivities related to the Laxemar rock domain and deformation zones, likely to extend high values to the bottom of the model domain (cf. Figure 5-14). To overcome such effect would have required the application of a larger grid in the vertical direction, leading to unacceptable run-times. Since flushing occurs locally in the western part of the domain, the obtained results can still be considered relevant for the larger part of the modelled domain.

Due to the presence of the ice sheet, local variations in the salinity distribution are also observable, in particular at a depth of 500 meters (cf. Figure 6-35 and Figure 6-36).

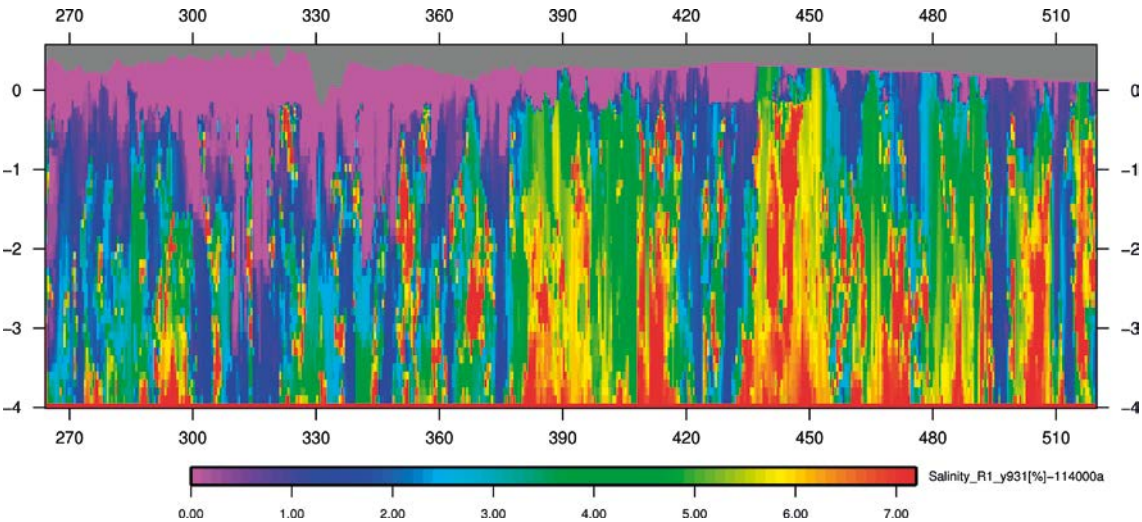

Figure 6-32. *Case 1: salinity [%] at −114 ka with the* ***absence of ice sheet****, E-W vertical at Y = 931 km (coordinates in km).*

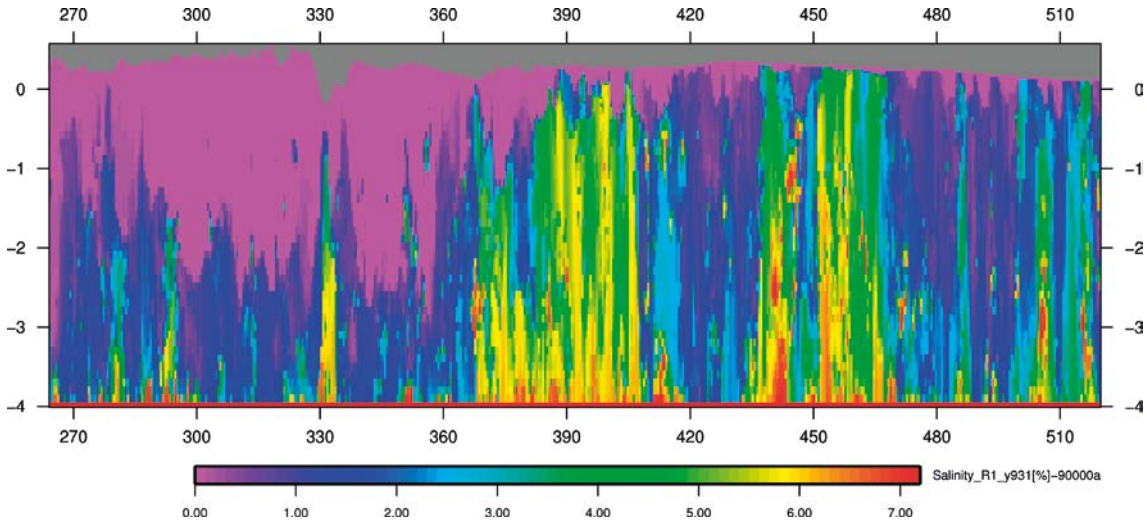

Figure 6-33. *Case 1: salinity [%] at −90 ka,* ***period of glacial completeness****, E-W vertical at Y=931 km (coordinates in km).*

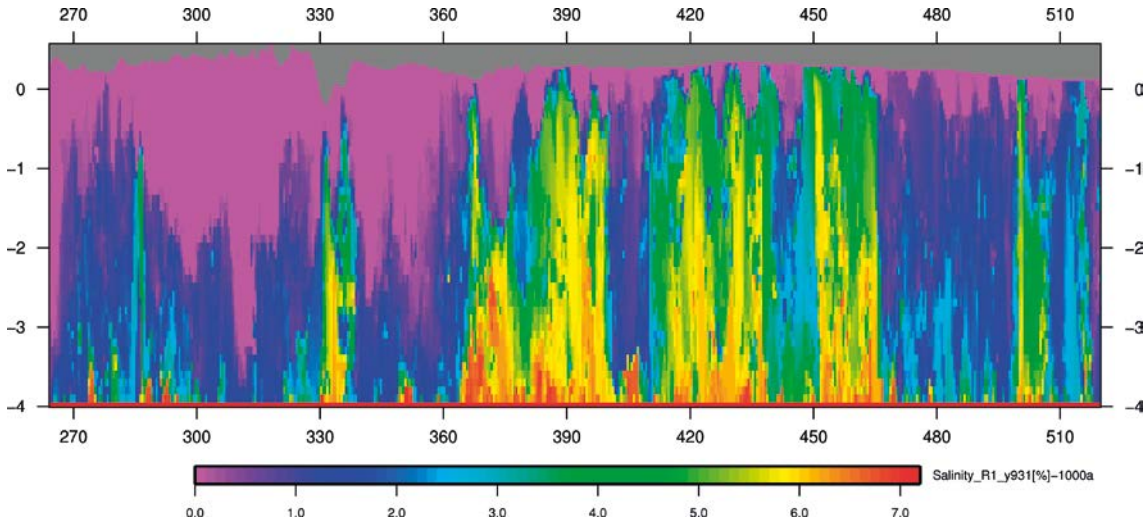

Figure 6-34. *Case 1: salinity [%] at −1 ka,* ***period of glacial retreat****, E-W vertical at Y=931 km (coordinates in km).*

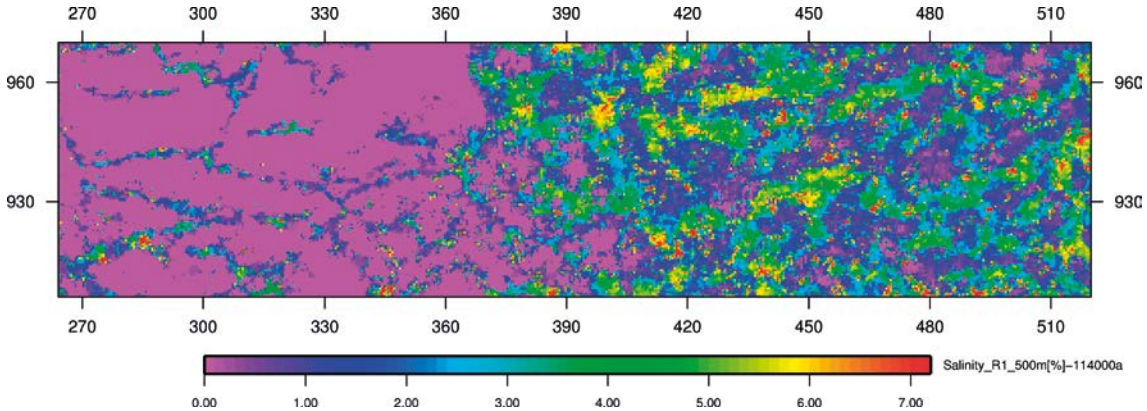

Figure 6-35. *Case 1: salinity [%] at −114 ka with the* ***absence of ice sheet****, projected horizontal cut at 500 meter depth (coordinates in km).*

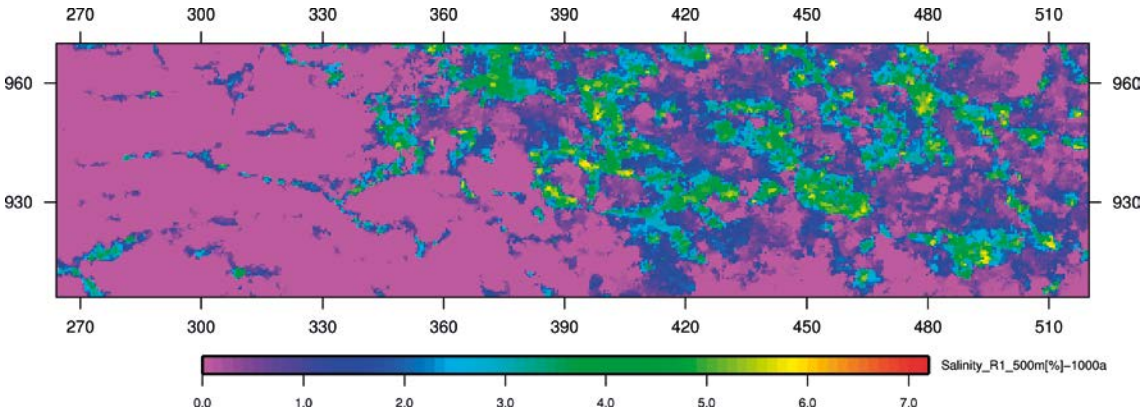

Figure 6-36. *Case 1: salinity [%] at −1 ka,* ***period of glacial retrea****t, projected horizontal cut at 500 meter depth (coordinates in km).*

The module of the Darcy velocity is calculated for selected time steps likely to present the highest hydraulic gradients and hydraulic conductivity; i.e. when large variations of ice thickness and quasi absence of permafrost occur. The corresponding time steps are −102 ka (glacial completeness: Figure 6-37) and −9 ka (glacial retreat with apparition of ice margin: Figure 6-38); these two time steps present differences in their spatial distribution of permafrost belonging to distinct glacial periods. But, they show similar values for the velocity module calculated at the surface of the model domain, with an average value around 10^{-7} m/s for the areas without permafrost; and for the permafrost zones, this average value is about 3–4 orders of magnitude lower. A similar behaviour is also observed for the subglacial layer of these two time steps (i.e. elongated zones with yellow-reddish colours); it displays a major hydraulic role in draining meltwater underneath the ice sheet, due to its high value hydraulic conductivity, and, the encountered values for the velocity module are in the range 10^{-4}–10^{-2} m/s.

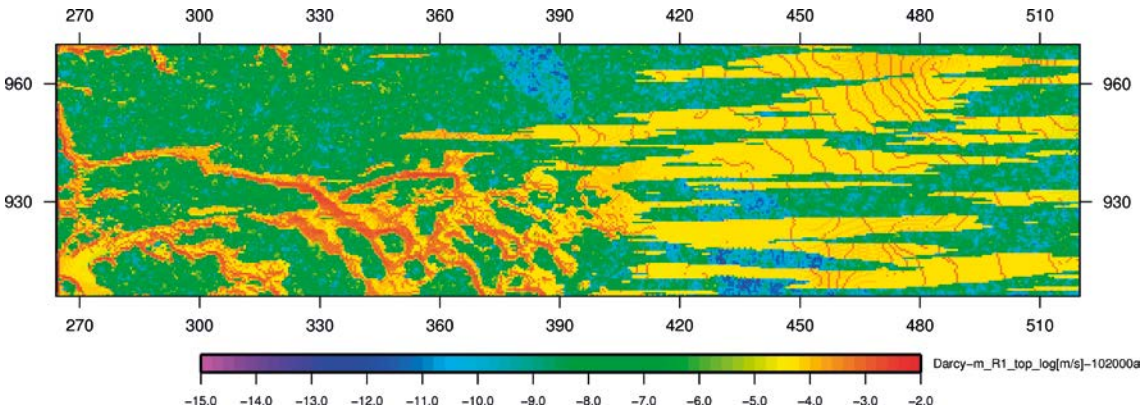

Figure 6-37. *Case 1: Darcy velocity module, log[m/s] at −102 ka;* ***period of glacial completeness*** *with lowest permafrost proportion, projected top horizontal cut (coordinates in km).*

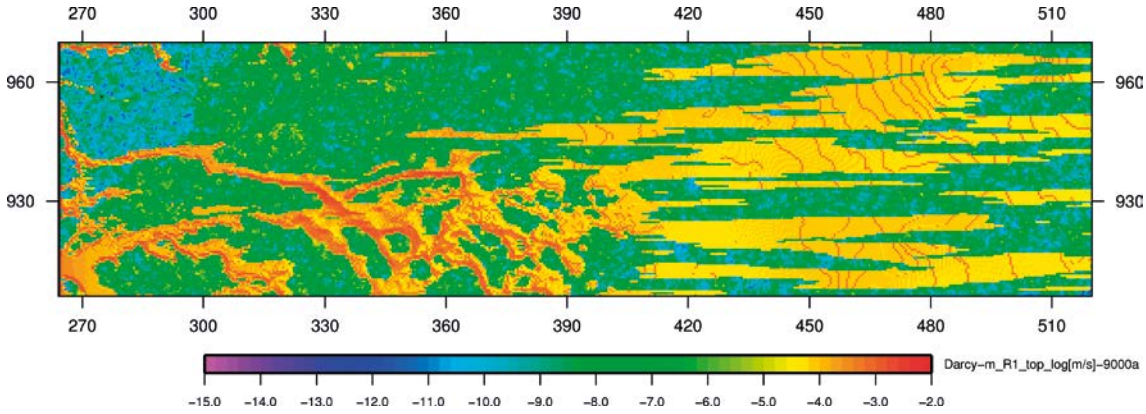

Figure 6-38. *Case 1: Darcy velocity module, log[m/s] at −9 ka;* ***period of glacial retreat*** *with apparition of ice margin (west), projected top horizontal cut (coordinates in km).*

The comparison with the −114 ka time step displays in a remarkable manner the major impact of the ice sheet on the surface velocity field (Figure 6-39); i.e. the presence of the ice sheet leads to an increase of several orders of magnitude for the Darcy velocity module. This ice sheet impact is attenuated when the velocity module is compared at depth of 500 meters for the selected time steps; some effects are still observed due to the permeable deformation zones that extend at depth (Figures 6-40 to 6-42). The appearance of the ice margin can be guessed in the northwest corner of the domain at −9 ka (cf. Figure 6-41).

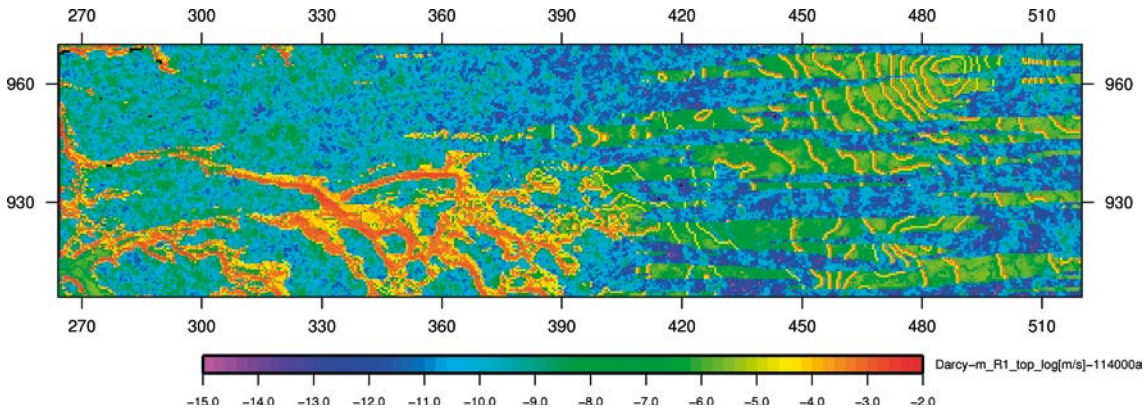

Figure 6-39. *Case 1: Darcy velocity module, log[m/s] at −114 ka with the* ***absence of ice sheet****, projected top horizontal cut (coordinates in km).*

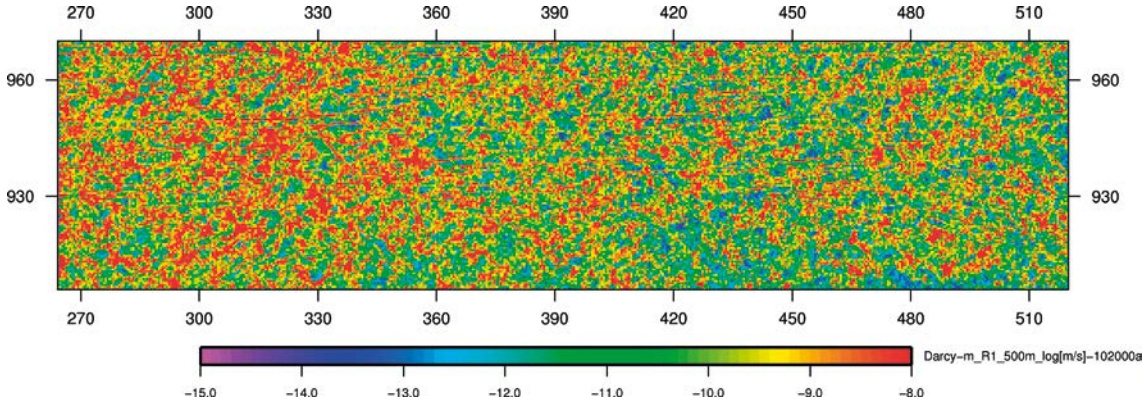

Figure 6-40. *Case 1: Darcy velocity module, log[m/s] at −102 ka;* ***period of glacial completeness*** *with lowest permafrost proportion, projected horizontal cut at 500 meter depth (coordinates in km).*

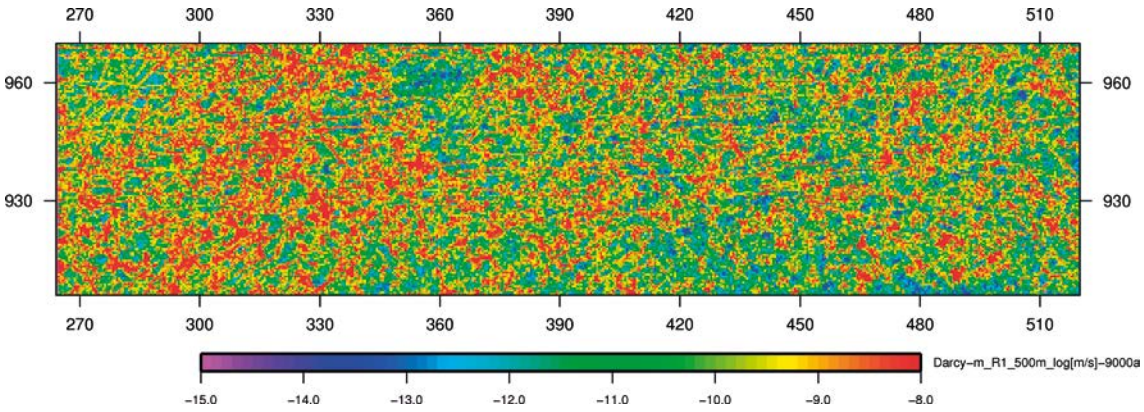

Figure 6-41. *Case 1: Darcy velocity module, log[m/s] at −9 ka;* ***period of glacial retreat****, projected horizontal cut at 500 meter depth (coordinates in km).*

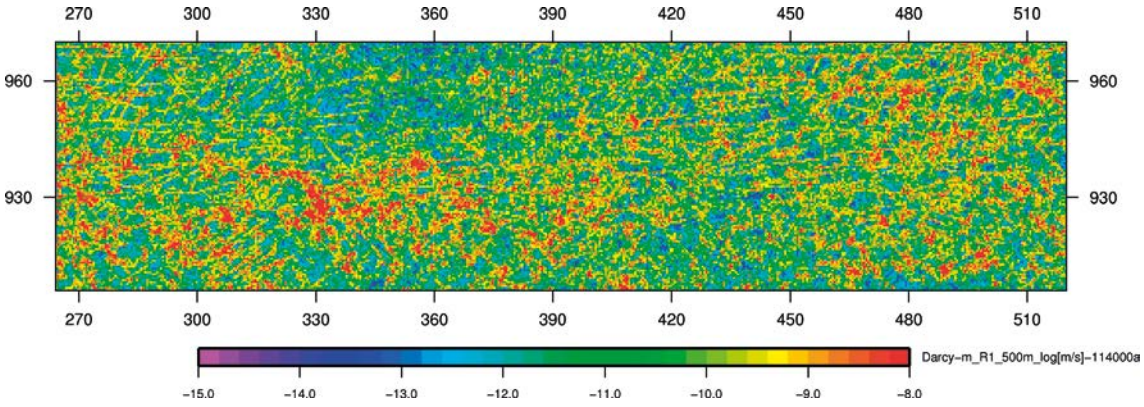

Figure 6-42. *Case 1: Darcy velocity module, log[m/s] at −114 ka with the* ***absence of ice sheet****, projected horizontal cut at 500 meter depth (coordinates in km)*

6.2 Case 2

The case 2 comprises the hydraulic and thermal properties of the Forsmark site with vertical deformation zones described by the GAP Geomodel version 1; and, is as well characterised by the presence of a subglacial layer and horizontal deformation zones. The initial and boundary conditions applied for case 2 are identical to case 1 (cf. Section 6.1), except for the salinity initial conditions which are taken as such (Vidstrand et al. 2010a):

- Ground surface to Z = -350 m: salinity is 0 %.
- Z = -350 m to Z = -1 500 m: salinity linearly increases to 7.2 %.
- Below Z = −1 500 m: salinity is set to 7.2 %.

Simulation

For the case 2, groundwater flow coupled with salt transport and heat transfer is simulated during the complete glacial cycle; from the time interval −115 to −1 ka.

The pressure field of case 2 during the period of glacial build up, compared to the case 1, presents less disturbances at depth (Figures 6-43 and 6-44), since the hydraulic effect of its deformation zones is of limited vertical extent (cf. Figure 5-15). And, the appearance of stronger hydraulic gradients towards the east is likely related to the lower and less variable hydraulic conductivity encountered at depth for case 2 (cf. Table 5-2).

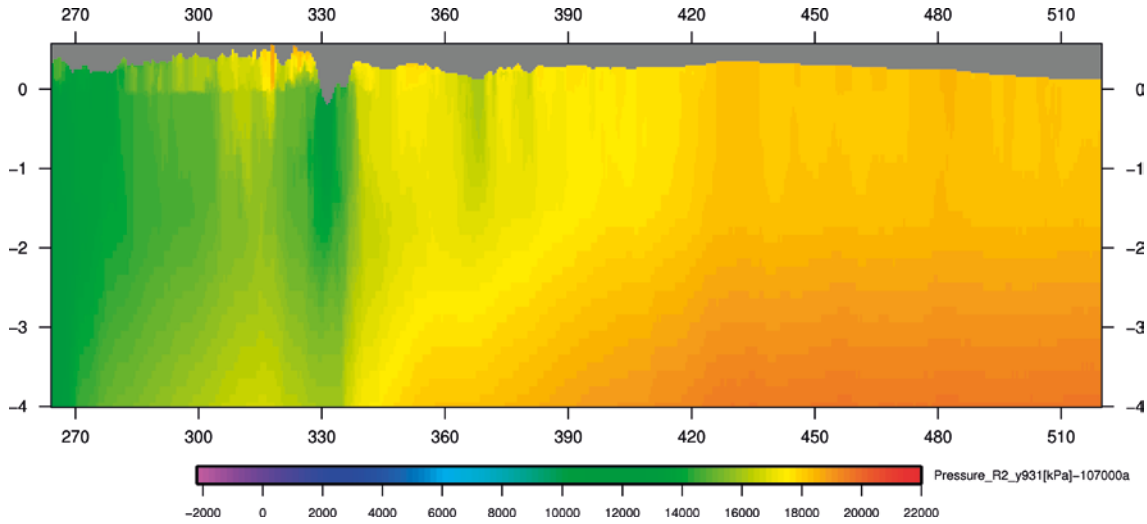

Figure 6-43. *Case 2: pressure [kPa] at −107 ka,* ***period of glacial build up****, E-W vertical at Y = 931 km (coordinates in km).*

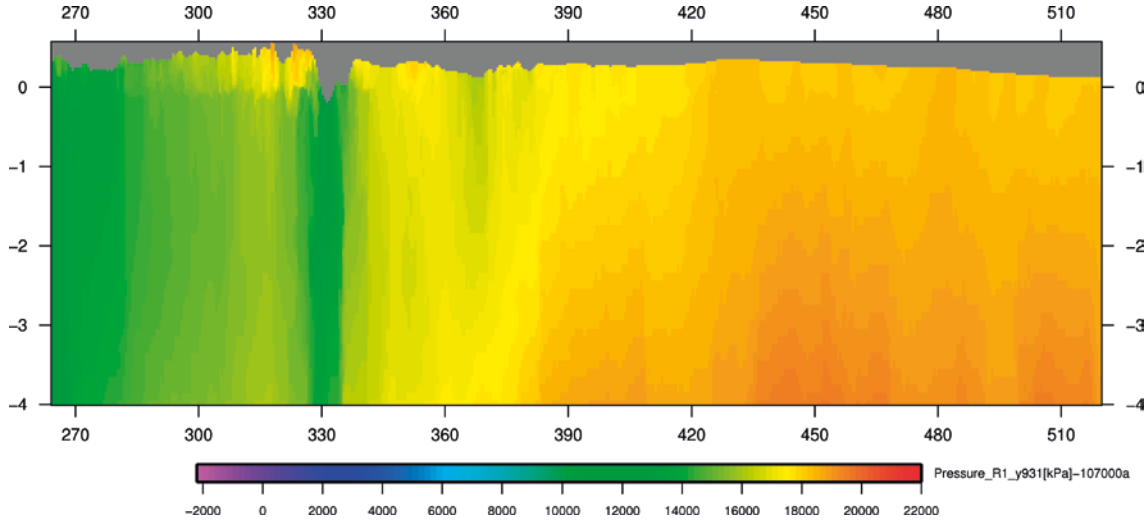

Figure 6-44. *Case 1: pressure [kPa] at −107 ka,* ***period of glacial build up****, E-W vertical at Y = 931 km (coordinates in km).*

The evolution of permafrost proportion over the model surface for the case 2 is identical to the case 1 (cf. Figures 6-23 and 6-26) since their thermal boundary conditions are the same; i.e. the proportion of permafrost in the top layer of the model, due to the fixed (imposed) temperature in this layer remains the same. Even if differences in fluxes are likely to occur due to variations in hydraulic conductivity between the two cases; in this layer, groundwater flow cannot influence temperature that governs permafrost. But, in the upper layers, their hydraulic conductivity values – reduced by about two orders of magnitudes (up to about 400 meter depth; cf. Tables 5-2 and 5-1) compared to the case 1 – have some influence on the development of permafrost at depth; and, to a likely minor extent, its differences in thermal parameters (cf. Table 5-4). The specific top hydraulic conductivity values of case 2 generally leads to thinner permafrost during glacial completeness and to its faster disappearance during glacial retreat (Figure 6-45 and 6-46). This outcome is mainly due to the reduced capability for the water to transfer heat (i.e. cold conditions) from the topographic surface to depth, in presence of lower hydraulic conductivity values in the top layers.

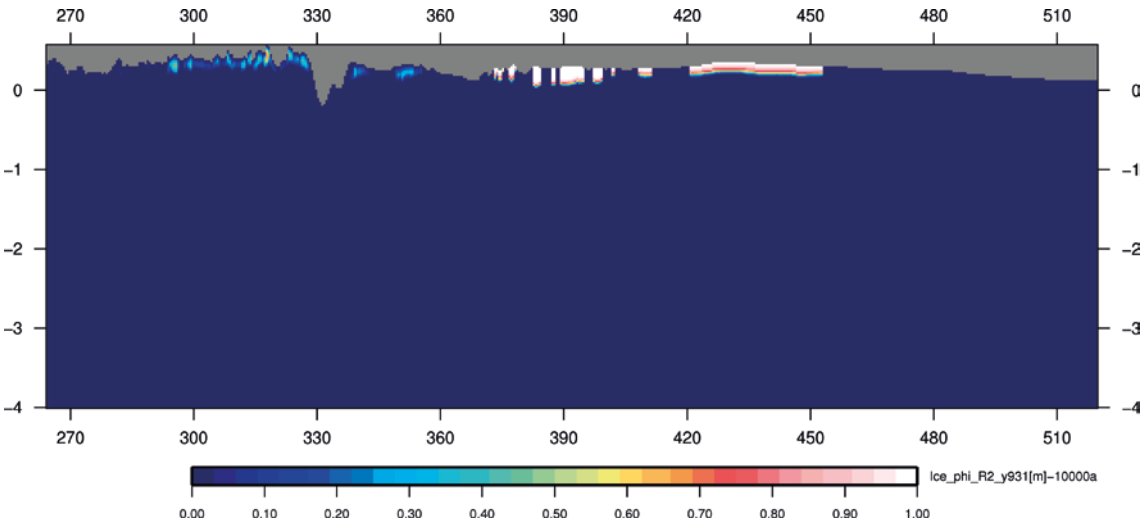

Figure 6-45. *Case 2: permafrost (white) at −10 ka (expressed as ice proportion [−]),* ***period of glacial retreat****, E-W vertical at Y = 931 km (coordinates in km).*

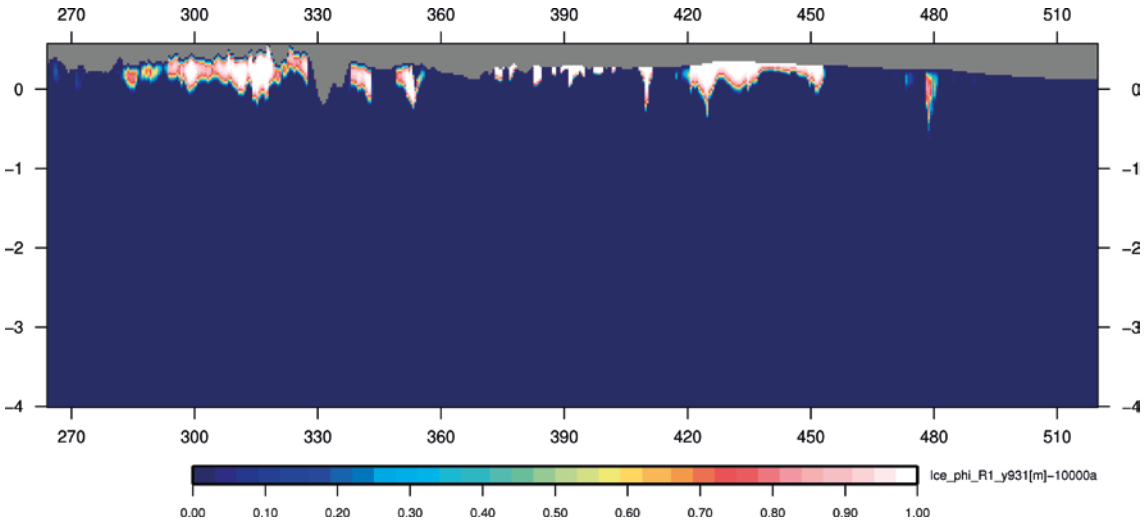

Figure 6-46. *Case 1: permafrost (white) at −10 ka (expressed as ice proportion [−]),* ***period of glacial retreat****, E-W vertical at Y = 931 km (coordinates in km).*

The mean salinity, estimated at 500 meter depth, over the model domain, displays a weak increase during the period of glacial build up (Figure 6-47 and 6-48); its behaviour is remarkably stable during most of the period of glacial completeness and then the mean salinity decreases in a monotonic manner for the remaining glacial retreat period. This weak increase during the period of glacial build up can be interpreted as an upconing effect of the saline groundwater, as an opposite decreasing trend occurs during glacial retreat. Regarding the mean salinity at 1 000 meter depth, no observable trend can be spotted except for the period of glacial retreat where a minor decrease is likely to occur. When comparing salinity profiles at −90 ka (glacial completeness; Figure 6-49) and −1 ka (glacial retreat; Figure 6-50) with those of the case 1 (cf. Figures 6-33 and 6-34); a large (red) zone of values with maximum salinity values remains at depth for case 2. The mean salinity at depth is less sensitive to the presence of the ice sheet, since for case 2, the deformation zones present a limited vertical extend and smaller hydraulic conductivity values are encountered with depth; i.e. 10^{-11} m/s from about 400 meter depth (cf. Tables 5-2 and 5-1; cf. Figures 5-15 and 5-14).

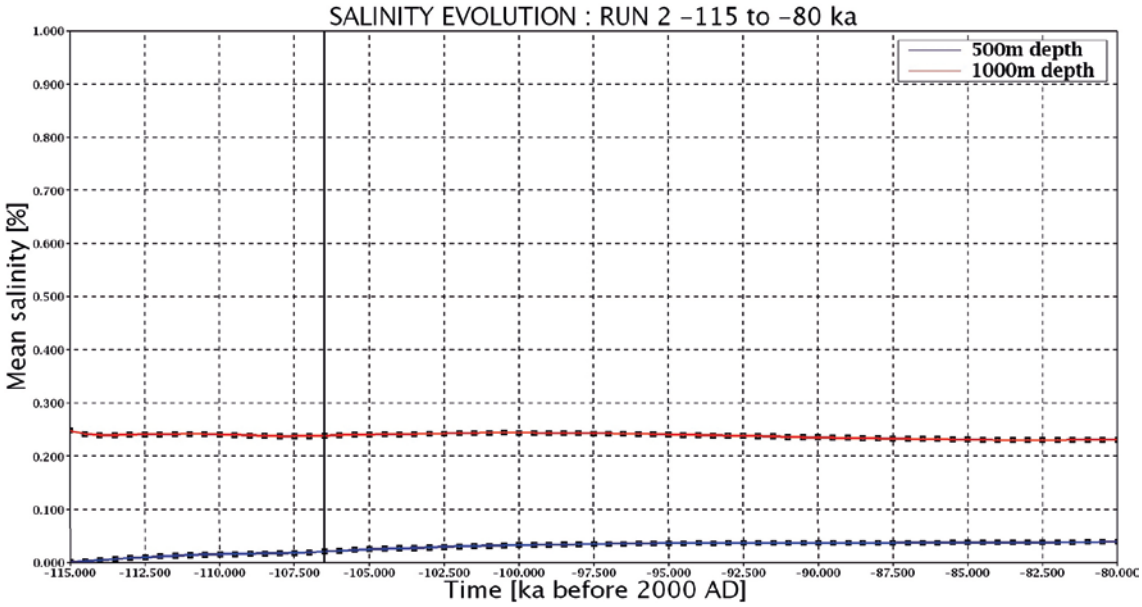

Figure 6-47. *Case 2: evolution of mean salinity [%] at 500 and 1000 meter depth over the model domain, from −115 to −80ka. The end of glacial build up is at −106.5 ka (vertical black line).*

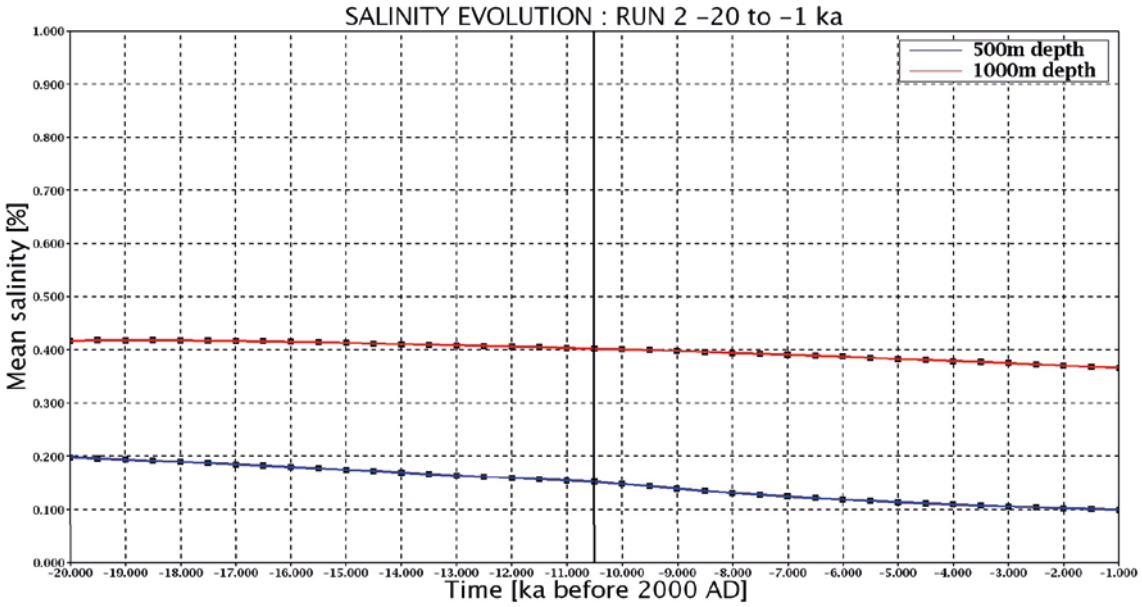

Figure 6-48. *Case 2: evolution of mean salinity [%] at 500 and 1000 meter depth over the model domain, from −20 to −1ka. The onset of glacial retreat is at −10.5 ka (vertical black line).*

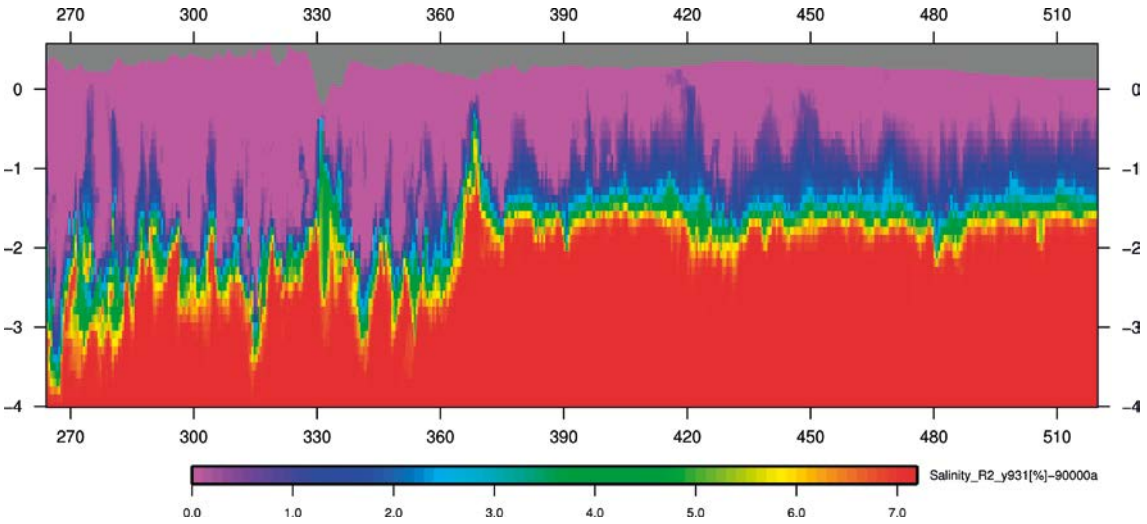

Figure 6-49. *Case 2: salinity [%] at −90 ka,* ***period of glacial completeness****, E-W vertical at Y=931 km (coordinates in km).*

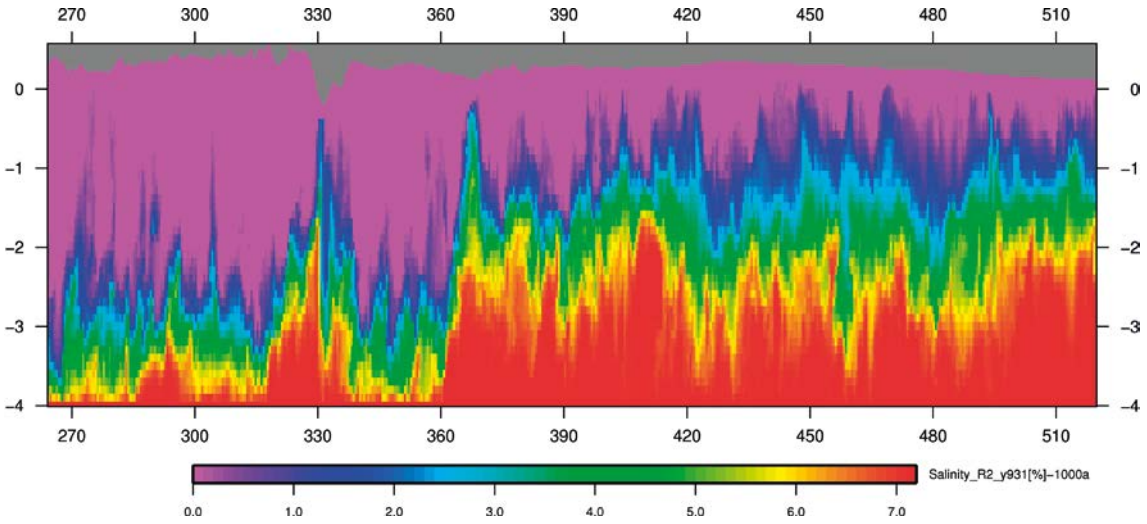

Figure 6-50. *Case 2: salinity [%] at −1 ka,* ***period of glacial retreat****, E-W vertical at Y=931 km (coordinates in km).*

A decrease in the module of the Darcy velocity (Figure 6-51) is observed in comparison to the case 1 due to smaller hydraulic conductivity values in the top surface for case 2. This effect is particularly visible at 500 meter depth (Figure 6-52; and, cf. Figure 6-40; case 1), due to a stronger decrease of hydraulic conductivity values with depth in comparison to the case 1 (cf. Tables 5-2 and 5-1).

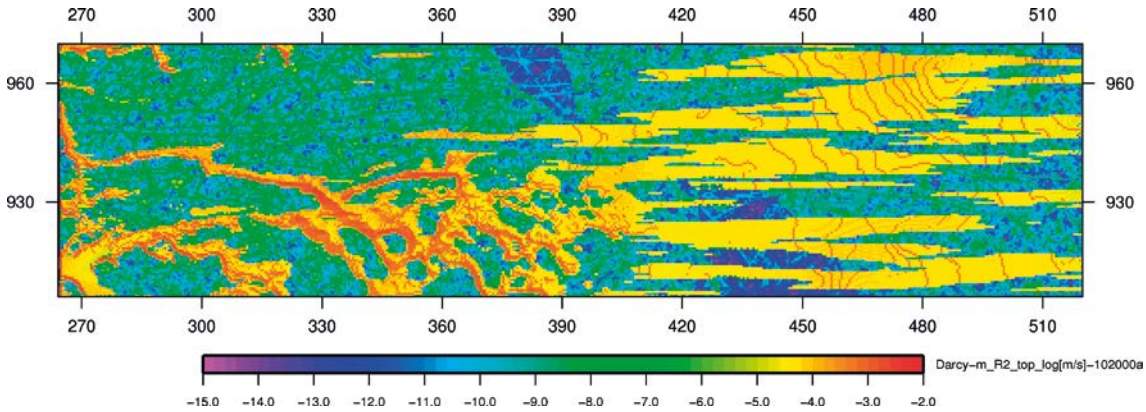

Figure 6-51. *Case 2: Darcy velocity module, log[m/s] at −102 ka;* ***period of glacial completeness*** *with lowest permafrost proportion, projected top horizontal cut (coordinates in km).*

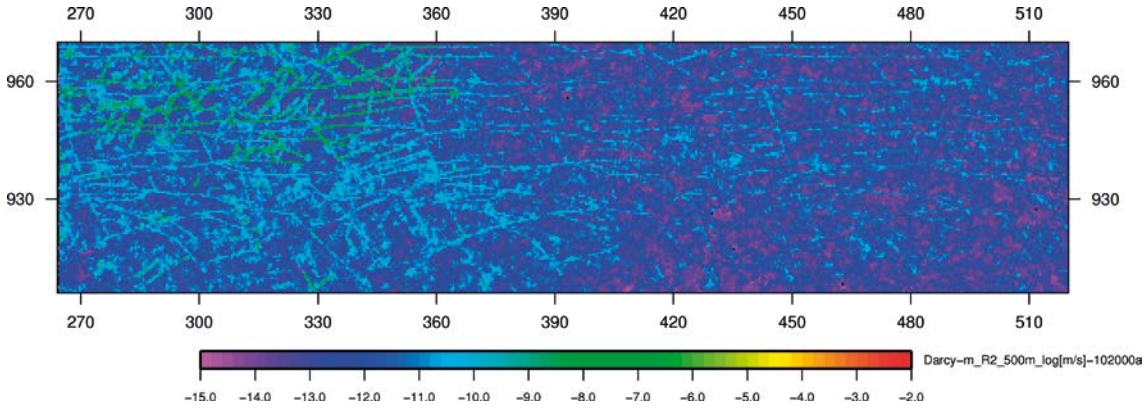

Figure 6-52. *Case 2: Darcy velocity module, log[m/s] at −102 ka;* ***period of glacial completeness*** *with lowest permafrost proportion, projected horizontal cut at 500 meter depth (coordinates in km).*

6.3 Case 3

The case 3 incorporates the hydraulic and thermal properties of the Olkiluoto site with vertical deformation zones described by the GAP Geomodel version 1; and, is also characterised by the presence of a subglacial layer and horizontal deformation zones. The initial and boundary conditions applied for case 3 are the same as the case 1 (cf. Section 6.1), except for the salinity initial conditions. These conditions were taken and summarised from the Table 2-1 of Hellä et al. (2014) and from Smellie et al. (2014):

- Ground surface to Z = -30 m: salinity is 0 %.
- Z = -30 m to Z = -400 m: salinity is 1 %.
- Below Z = −400 m: salinity is set to 8.1 %.

And, for the boundary conditions at the bottom, where a salinity value of 8.1 % is prescribed.

Simulation

For the case 3, groundwater flow coupled with salt transport and heat transfer is simulated during the complete glacial cycle; from the time interval −115 to −1 ka.

The pressure field of case 3, compared to the case 1, also presents less disturbances at depth (Figure 6-53 and cf. Figure 6-44), since the hydraulic effect of its deformation zones is of limited vertical extent (cf. Figure 5-16). And, the appearance of stronger and regular hydraulic gradients towards the east is likely related to the less variable hydraulic conductivity encountered at depth for case 3 (cf. Table 5-3).

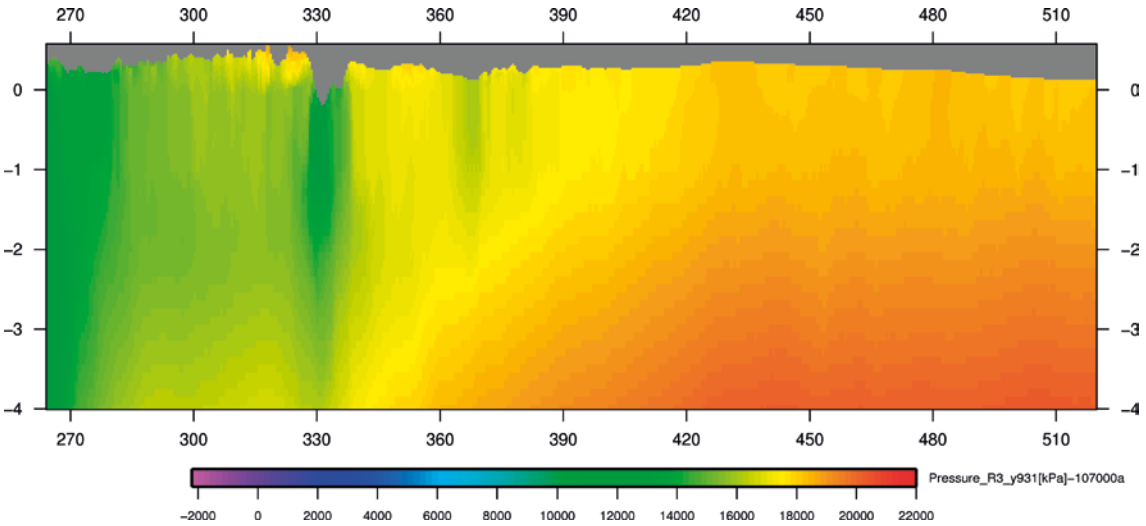

Figure 6-53. *Case 3: pressure [kPa] at −107 ka,* ***period of glacial build up****, E-W vertical at Y = 931 km (coordinates in km).*

As for the previous case, the evolution of permafrost proportion over the model surface for the case 3 is identical to the case 1 (cf. Figures 6-23 and 6-26), since their thermal boundary conditions are identical. Case 3 also presents in the top layers a reduction of about two orders of magnitude in hydraulic conductivity values compared to the case 1 (up to about 400 meter depth; cf. Tables 5-3 and 5-1). Therefore, leading for case 3, as well to thinner permafrost during glacial completeness (Figure 6-54) and to its faster disappearance during glacial retreat, due to the reduced heat transfer capability of water under such hydraulic conductivity conditions.

In comparison to the case 1, the evolution of salinity at depth for case 3 never reaches a steady behaviour during the periods of glacial completeness and retreat; i.e. its type is monotonically decreasing for the entire period of simulation (Figures 6-55 and 6-56). Such behaviour is caused by the lesser vertical extension of the deformation zones (cf. Figures 5-16 and 5-14) and the lower hydraulic conductivity values for the rock mass domain in the top layers of case 3 (i.e. about two orders of magnitude at depth below 200 meters; cf. Tables 5-3 and 5-1); i.e. meltwater provided by the ice sheet gradually replaces saline water in the upper part of the domain during the glacial cycle (Figures 6-57 and 6-58).

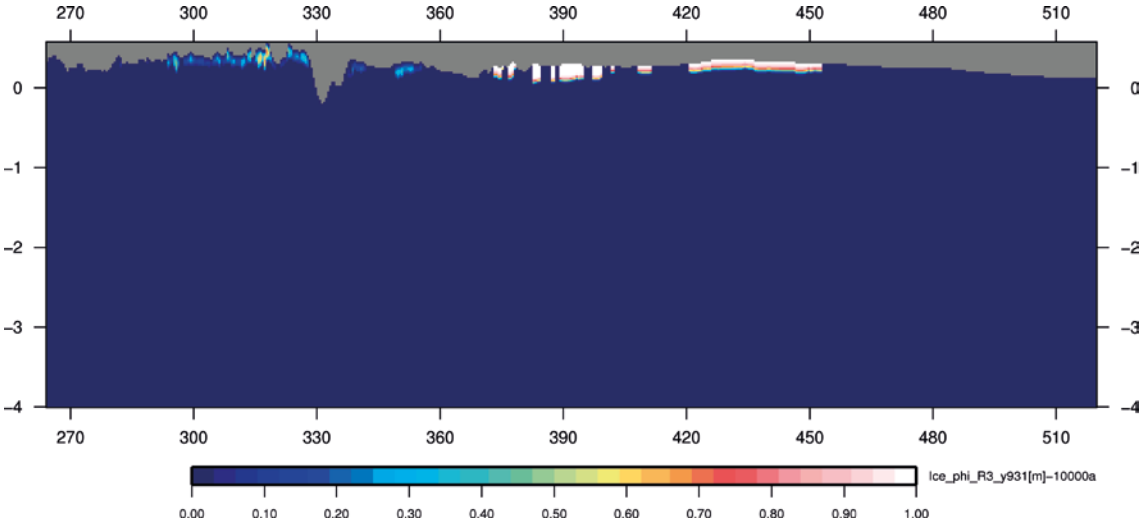

Figure 6-54. *Case 3: permafrost (white) at −10 ka (expressed as ice proportion [−]),* ***period of glacial retreat****, E-W vertical at Y = 931 km (coordinates in km).*

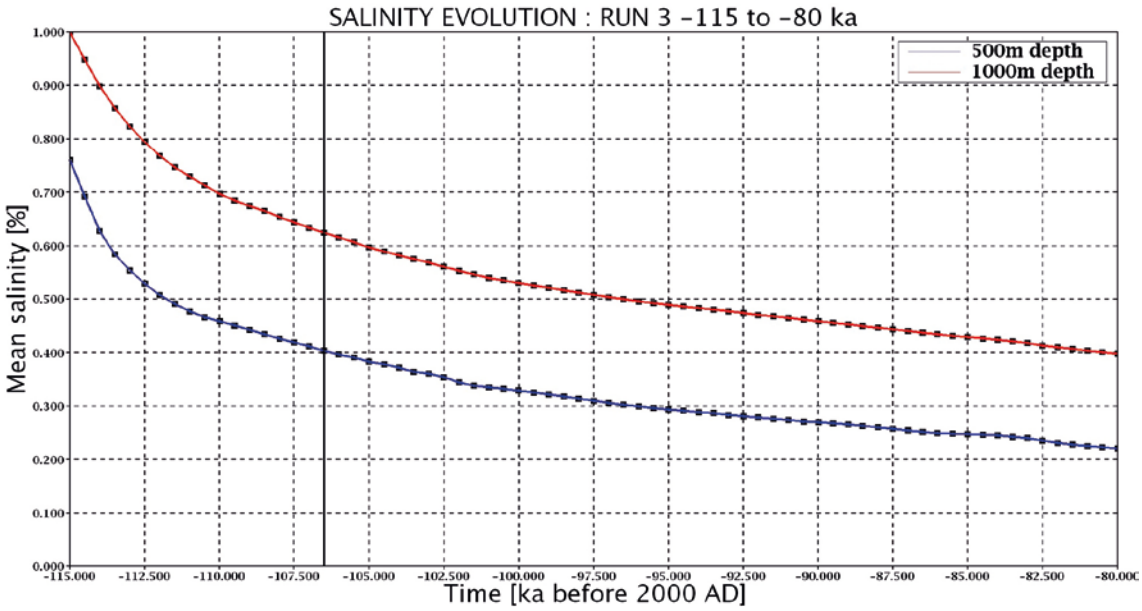

Figure 6-55. *Case 3: evolution of mean salinity [%] at 500 and 1000 meter depth over the model domain, from −115 to −80ka. The end of glacial build up is at −106.5 ka (vertical black line).*

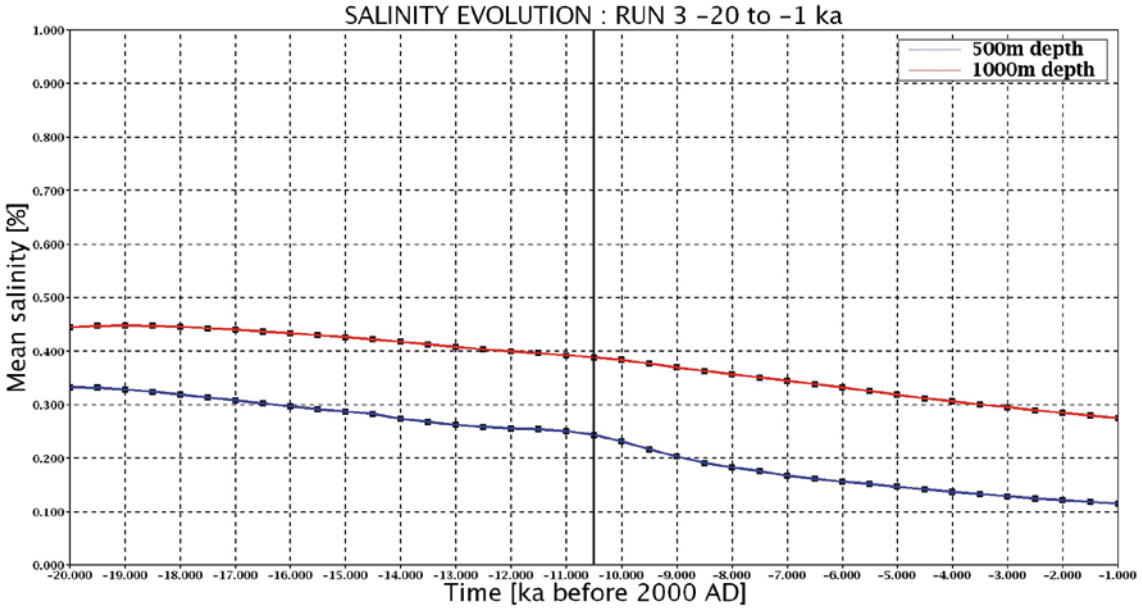

Figure 6-56. *Case 3: evolution of mean salinity [%] at 500 and 1000 meter depth over the model domain, from −20 to −1ka. The onset of glacial retreat is at −10.5 ka (vertical black line).*

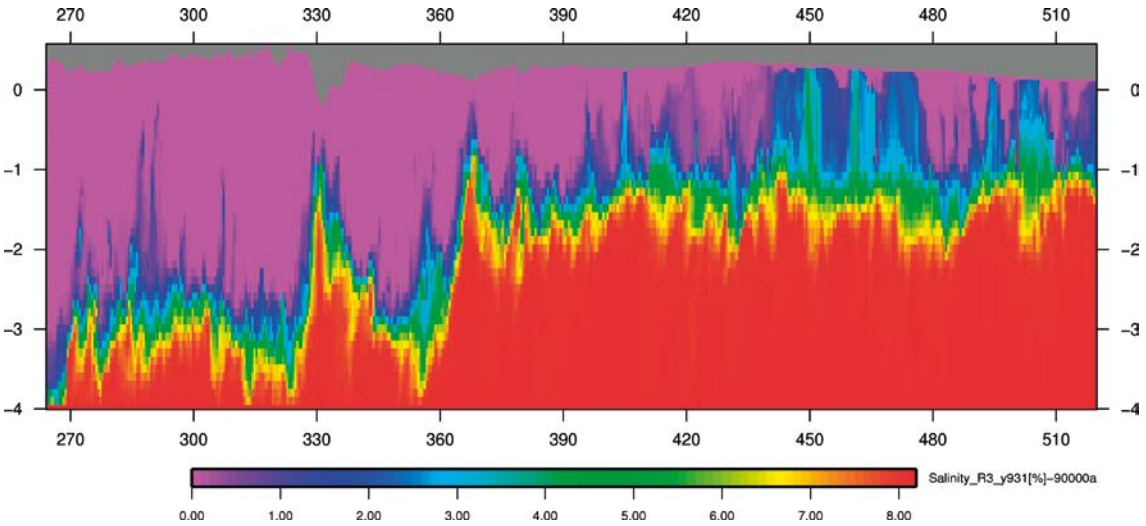

Figure 6-57. *Case 3: salinity [%] at −90 ka,* ***period of glacial completeness****, E-W vertical at Y=931 km (coordinates in km).*

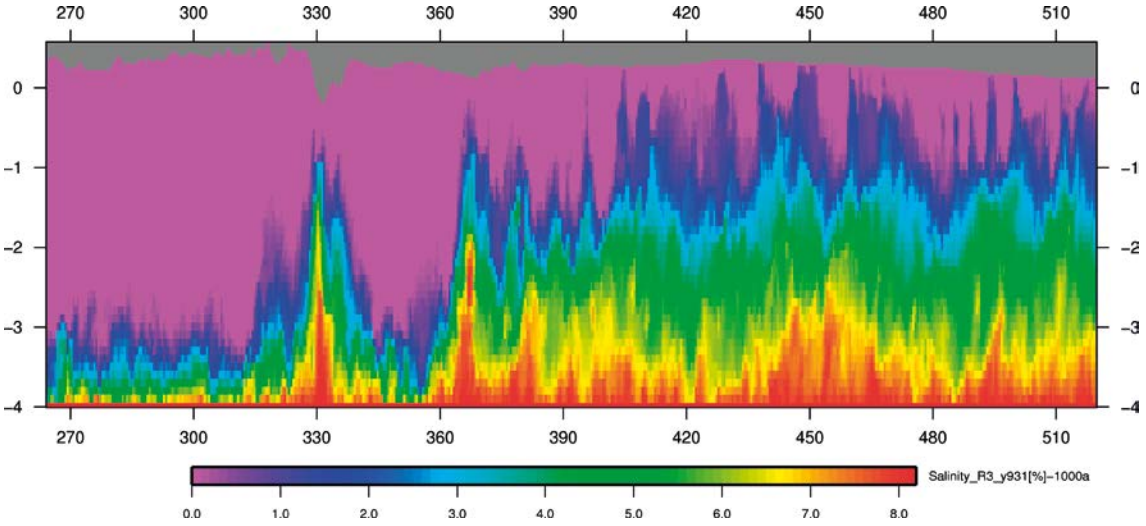

Figure 6-58. *Case 3: salinity [%] at −1 ka,* ***period of glacial retreat****, E-W vertical at Y=931 km (coordinates in km).*

Such transient behaviour for the salinity is not observed for case 2, because of the limited vertical extension of the deformation zone, below 500 m depth (cf. Figure 5-15), combined with the lowest upper layers hydraulic conductivity in comparison to the other two cases (cf. Table 5.2); i.e. the mean salinity over the model domain at depths 500 and 1 000 m is only weakly influenced during the ice sheet periods considered (cf. Figures 6-47 and 6-48).

During the first time steps (−115 to −114 ka) before the arrival of the ice sheet, the salinity field undergoes rapid changes (cf. Figure 6-55) that significantly differentiates it from the initial conditions. Such changes are related to these initial condition, taken from the Olkiluoto site where the prevailing flow boundary conditions are related to a very smooth topography. A similar behaviour for the first time steps was also observed for the case 1 (cf. Figure 6-30).

For case 3 in comparison to the case 1 (cf. Figure 6-37), a decline in the module of the Darcy velocity (Figure 6-59) is observed due to smaller hydraulic conductivity values in the surface layer (cf. Tables 5-3 and 5-1). This effect is also visible at 500 meter depth, where the contrast in hydraulic conductivity between the rock mass domain and the deformation zones is remarkably visible (Figure 6-60).

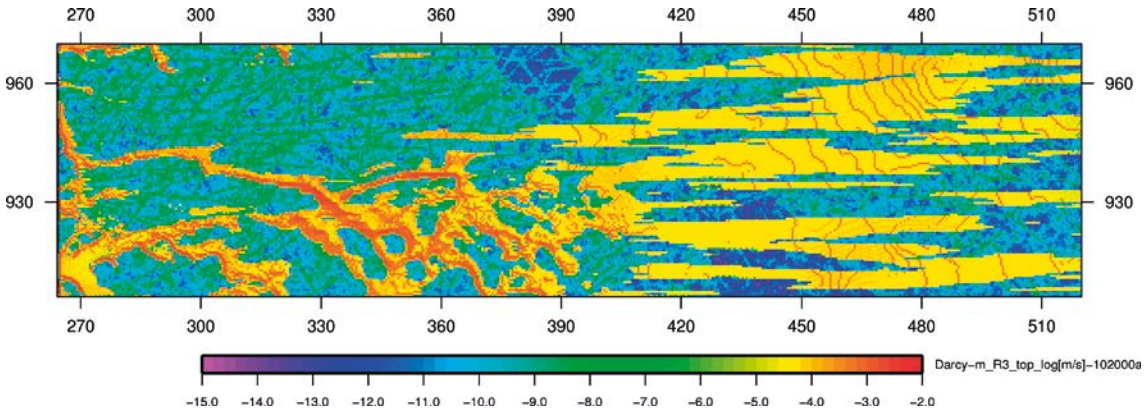

Figure 6-59. *Case 3: Darcy velocity module, log[m/s] at −102 ka;* ***period of glacial completeness*** *with lowest permafrost proportion, projected top horizontal cut (coordinates in km).*

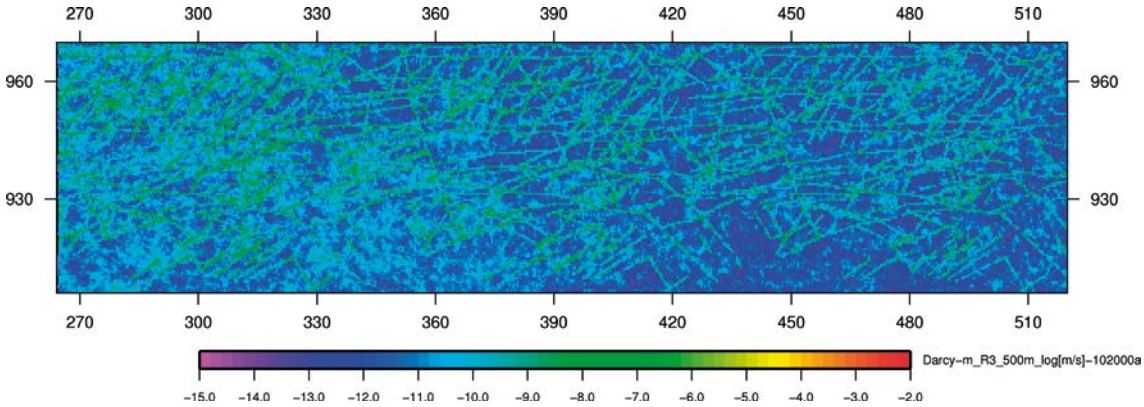

Figure 6-60. *Case 3: Darcy velocity module, log[m/s] at −102 ka;* ***period of glacial completeness*** *with lowest permafrost proportion, projected horizontal cut at 500 meter depth (coordinates in km).*

6.4 Case 4

The case 4 comprises the hydraulic and thermal properties of the Laxemar site with vertical deformation zones described by the GAP Geomodel version 1; and, is also characterised by the presence of a subglacial layer and horizontal deformation zones. The initial and boundary conditions applied for case 4 are identical to the case 1 (cf. Section 6.1), except for the boundary conditions given by the SICOPOLIS ice sheet model; i.e. the ice thickness and the temperature. These boundary conditions corresponds to the glaciation scenario II that present a lower value for the positive degree-day factor (Vallot et al. 2012a, b) compared to the case 1. This model parameter affects how much surface melting occurs on the ice sheet for a given temperature.

Simulation

The simulation of groundwater flow coupled with salt transport and heat transfer is performed for case 4, during the complete glacial cycle; from the time interval −115 to −1 ka.

For case 4, the evolution of the mean ice thickness over the model domain is similar to the case 1 for the glacial periods of build up and completeness. Differences occur during the period of glacial retreat where the ice sheet remains longer in relation to the lower value of the positive degree-day factor in comparison to the case 1 (Figures 6-61, 6-62 and 6-63).

During the period of glacial retreat, when examining the pressure field, the ice margin is located about 10-30 km more towards the west in comparison to the case 1 (Figures 6-64 and 6-65). This fact is also emphasized when observing the evolution of the ice sheet proportion over the model domain during the period of glacial retreat; i.e. for this period, a larger proportion of ice occupies the studied domain (cf. Figure 6-63).

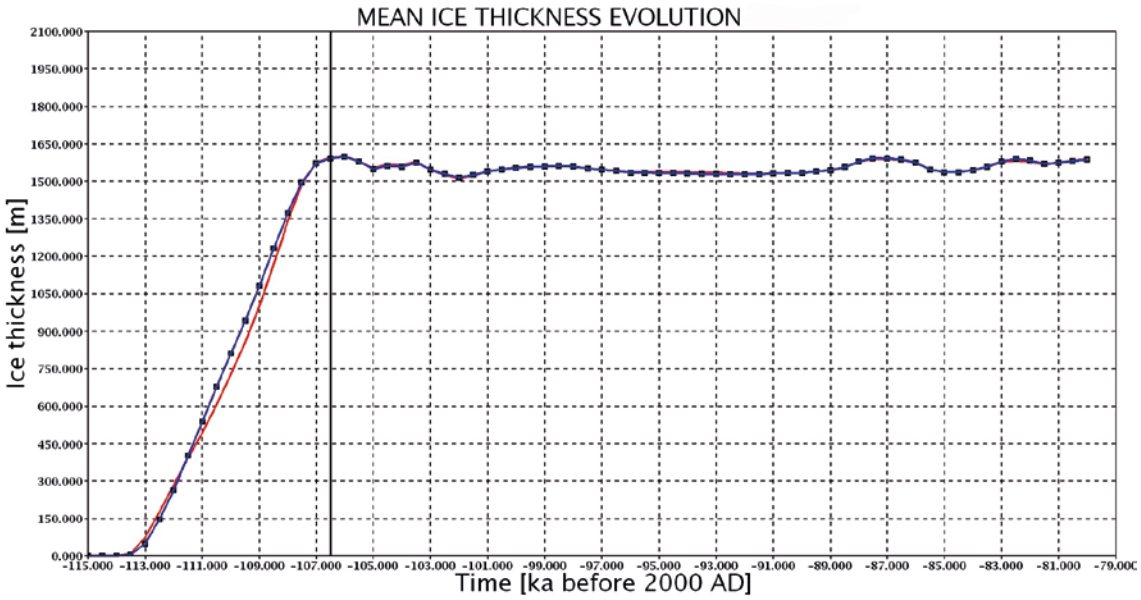

Figure 6-61. *Evolution of mean ice thickness [m] over the model surface, using SICOPOLIS data (case 4: blue line; case 1 : red line) from −115 to −80ka. The end of the glacial build up period is at −106.5 ka (vertical black line).*

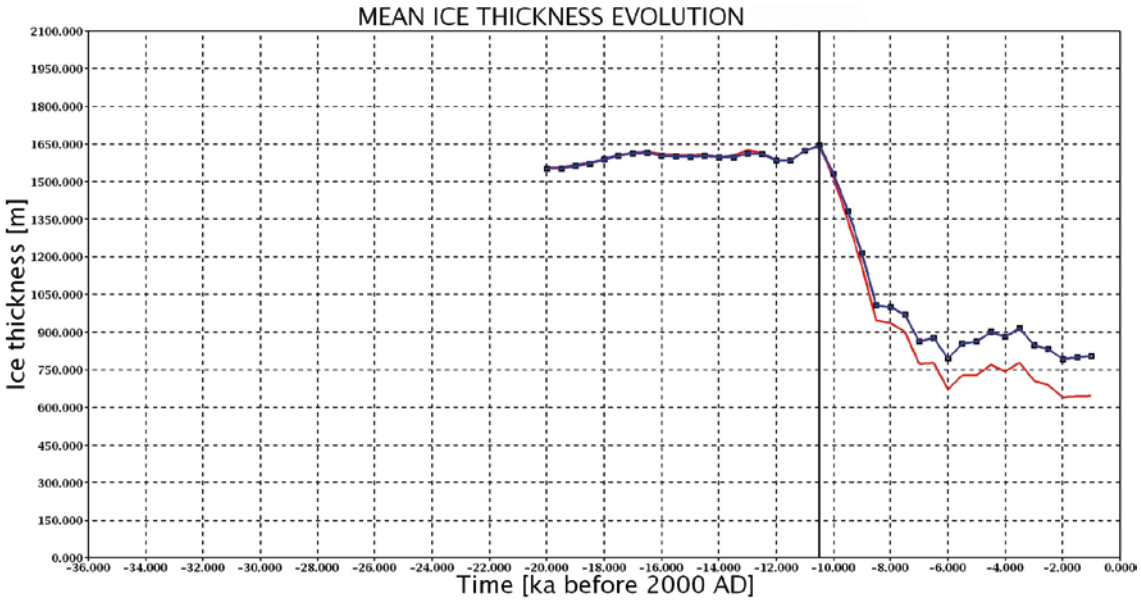

Figure 6-62. *Evolution of mean ice thickness [m] over the model surface, using SICOPOLIS data (case 4: blue line; case 1: red line) from −20 to −1ka. The onset of the glacial retreat period is at −10.5 ka (vertical black line).*

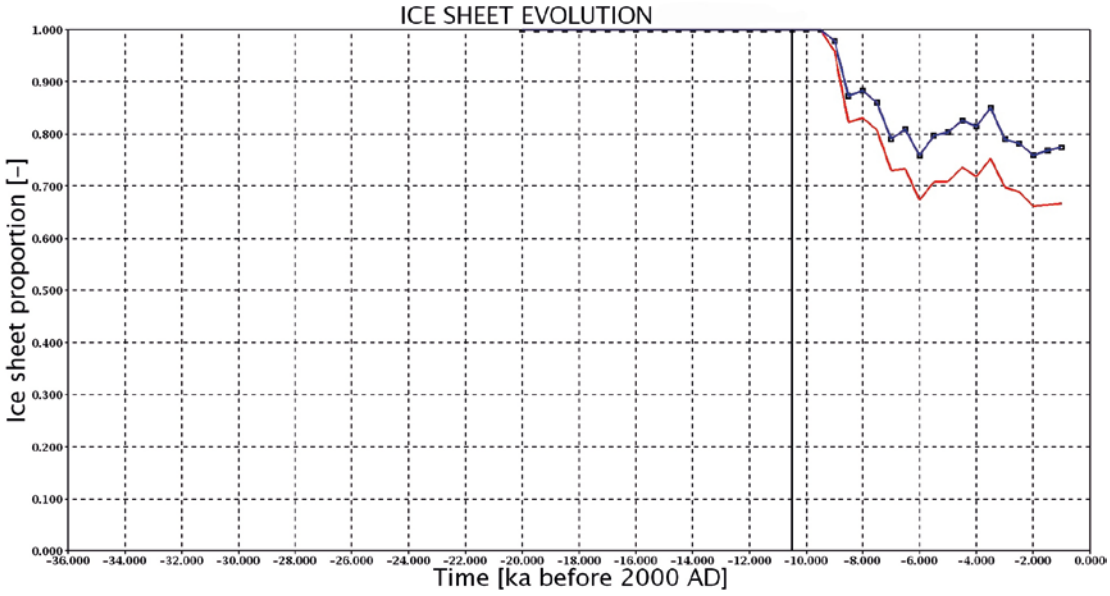

Figure 6-63. *Evolution of ice sheet proportion [−] over the model surface, using SICOPOLIS data (case 4: blue line; case 1: red line) from −20 to −1ka. The onset of the glacial retreat period is at −10.5 ka (vertical black line).*

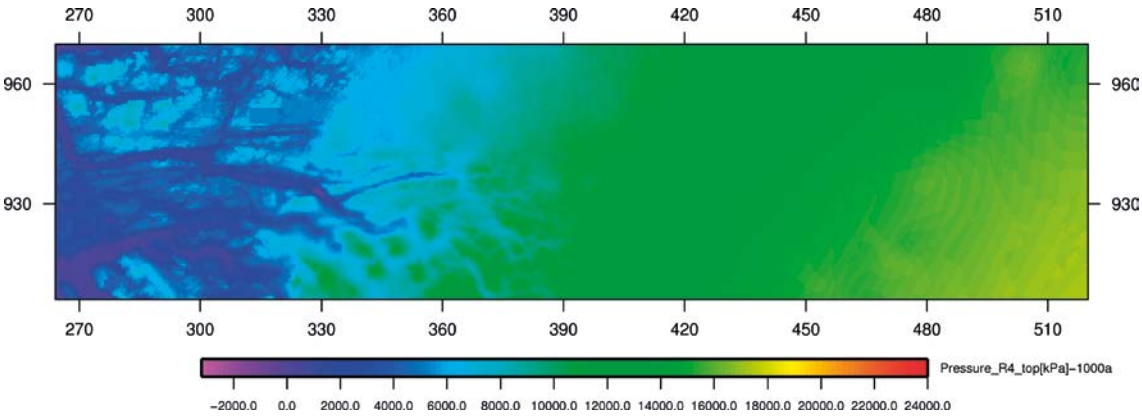

Figure 6-64. *Case 4: pressure [kPa] at −1 ka,* ***period of glacial retreat****, projected top horizontal cut (coordinates in km).*

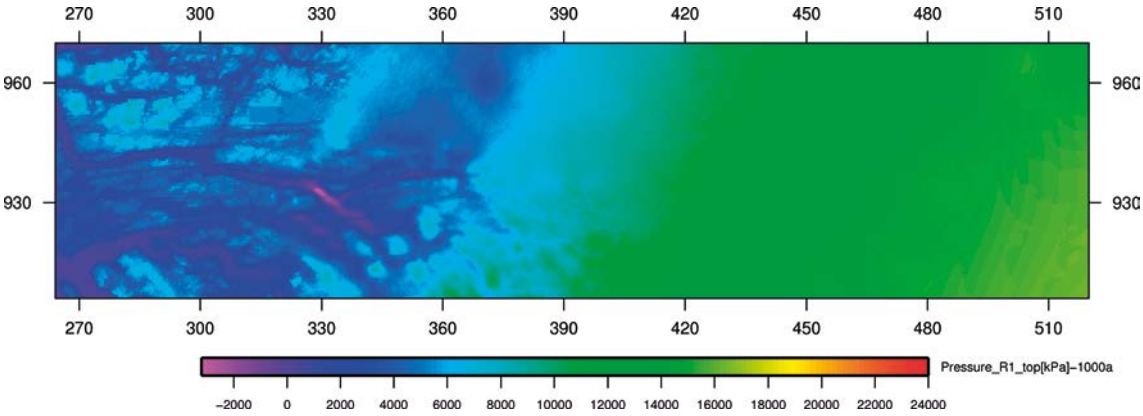

Figure 6-65. *Case 1: pressure [kPa] at −1 ka,* **period of glacial retreat***, projected top horizontal cut (coordinates in km).*

During the periods of glacial build up and completeness, the mean temperature of case 4 – estimated over the model surface – is slightly inferior to the case 1 (Figures 6-66 and 6-67). These minor differences are likely linked to variations in the geothermal heat flux and the intensity of basal sliding between the runs of the ice sheet model (Vallot et al. 2012a, b) selected among 100 ensemble members (Applegate et al. 2012). Such differences in the runs of the ice sheet model are not considered as representative variations between the glaciation scenarios applied for the groundwater flow modelling. At the time of glacial retreat, an additional effect comes into play; i.e. the higher mean temperature encountered (cf. Figure 6-67) is also due to the presence of a larger surface of ice sheet (cf. Figure 6-63) that isolates the bedrock from the colder climatic variations.

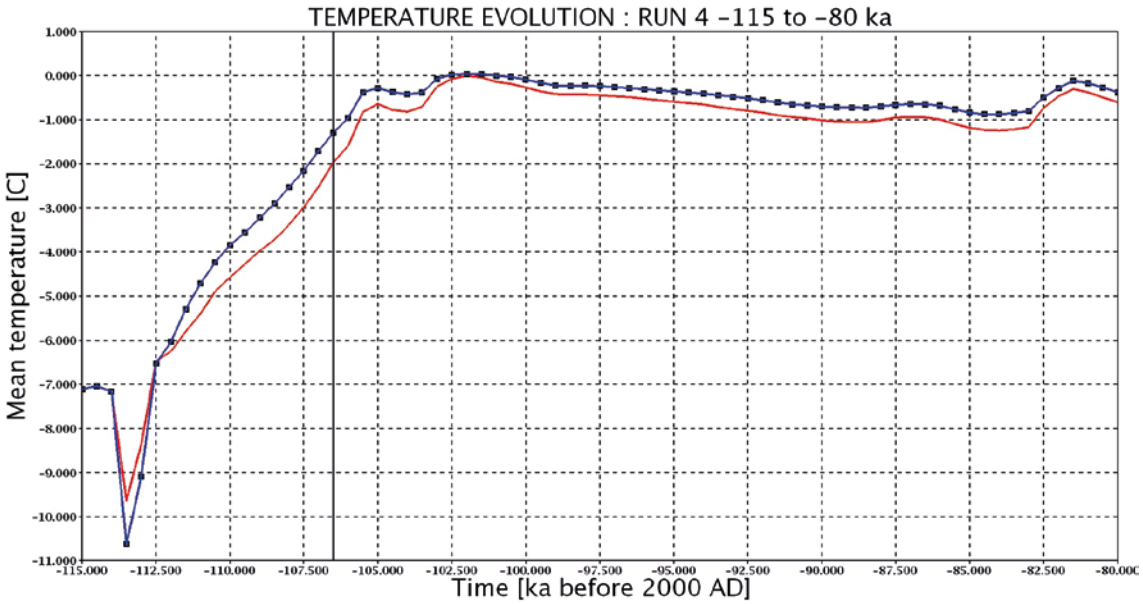

Figure 6-66. *Case 4: evolution of mean ice temperature [°C] over the model surface (blue line) in comparison to the case 1 (red line) from −115 to −80 ka. The end of the glacial build up period is at −106.5 ka (vertical black line).*

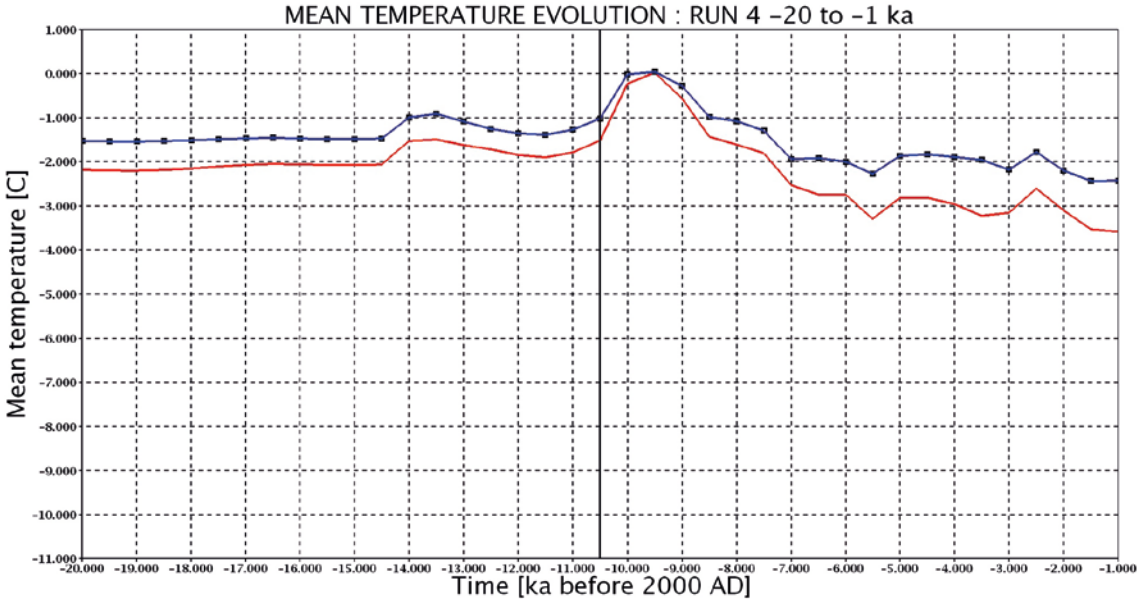

Figure 6-67. *Case 4: evolution of mean ice temperature [°C] over the model surface (blue line) in comparison to the case 1 (red line) from −20 to −1 ka. The onset of glacial retreat is at −10.5 ka (vertical black line).*

Despite small temperature differences, large variations in permafrost proportion can occur for case 4 (Figures 6-68 to 6-71) in comparison to the case 1; in particular, when surface temperature lies in the range between 0 and −1 degree; i.e. the variation domain that governs permafrost proportion (cf. Figure 4-1). During the periods of glacial completeness and retreat, permafrost temporarily disappears completely from the surface of the modelled domain, at −102 ka and −9.5ka. Rare relics of limited extent may remain below the surface (Figure 6-72).

The mean salinity curves at 500 and 1 000 meter depth over the model domain presents a very similar behaviour to the case 1 (cf. Figures 6-30 and 6-31). Small local variations of limited extent are observable at 500 m depth (Figure 6-73 and 6-74), likely in response to the changes in the boundary conditions. The permafrost proportion seems to have little influence on the salinity at depth.

For the top surface of the studied domain, during the period of glacial completeness, the module of the Darcy velocity for case 4 is similar to the case 1; the exception being related to the zones with spatial variations of permafrost occurrences (Figure 6-75 and cf. Figure 6-37). At a depth of 500 m, the behaviour of the Darcy velocity module remains quasi identical to the case 1 (Figure 6-76 and cf. Figure 6-40); i.e. the minor changes in boundary conditions, related to ice thickness and surface temperature (cf. Figure 6-61 and Figure 6-66) do not affect the flow field at depth. The only slight difference appears during the period of glacial retreat where the displacement of the ice margin seems to occur at a slower pace when compared to the case 1 (Figure 6-77 and cf. Figure 6-38).

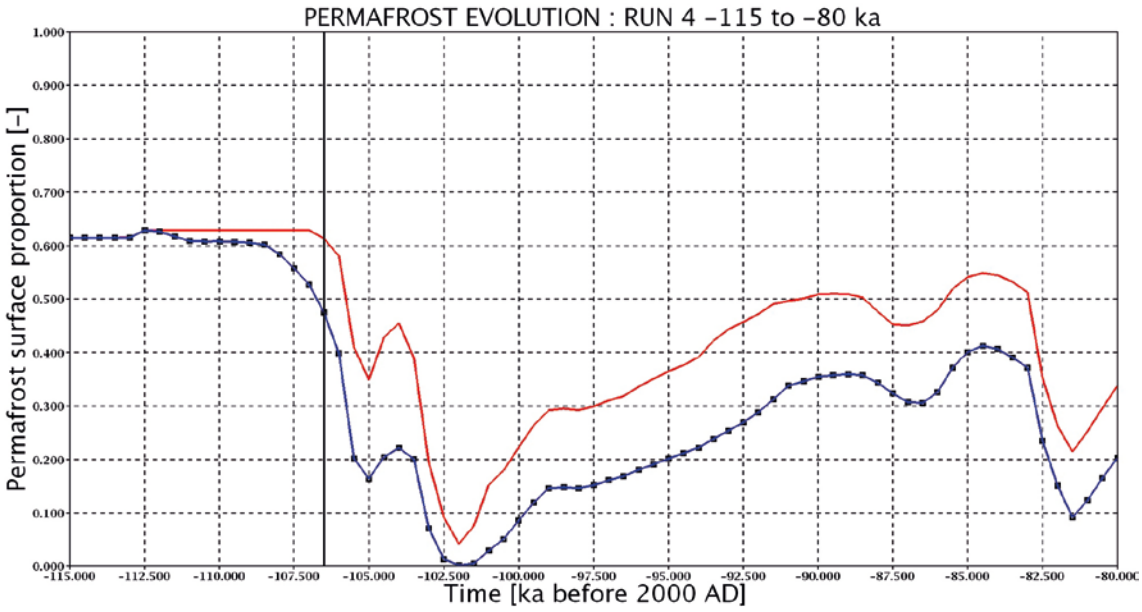

Figure 6-68. *Case 4: evolution of permafrost proportion [−] over the model surface (blue line) in comparison to the case 1 (red line) from −115 to −80 ka. The end of glacial build up is at −106.5 ka (vertical black line); the lowest value of permafrost proportion during ice completeness occurs at −102 ka.*

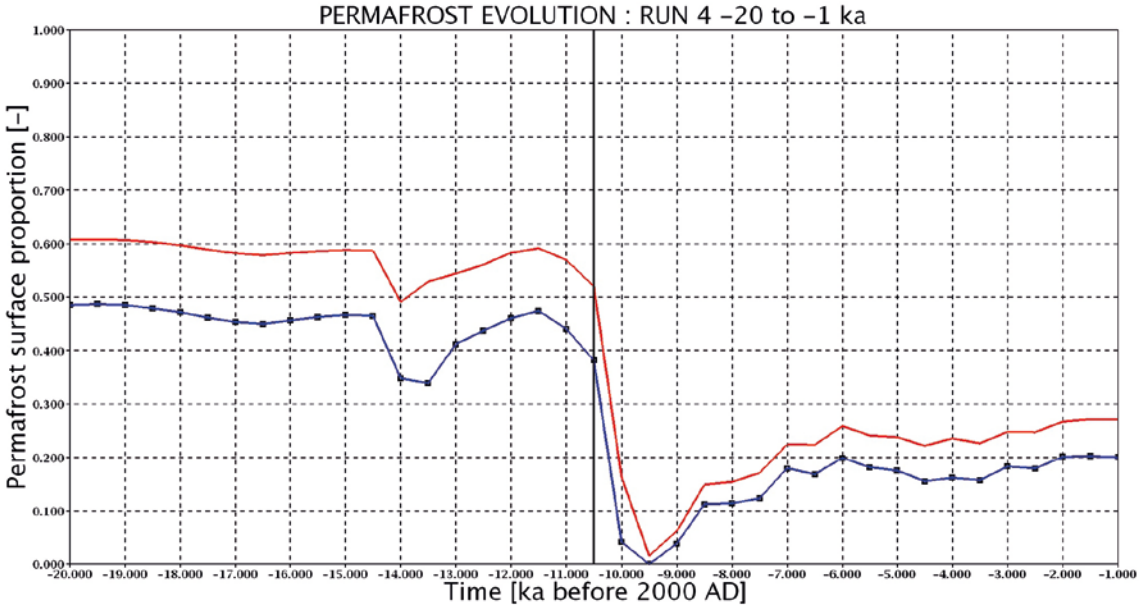

Figure 6-69. *Case 4: evolution of permafrost proportion [−] over the model surface (blue line) in comparison to the case 1 (red line) from −20 to −1ka. The onset of glacial retreat is at −10.5 ka (vertical black line). The lowest value of permafrost proportion during glacial retreat occurs at −9.5 ka. From −9.5 to −1ka, the permafrost is no longer present under the ice sheet.*

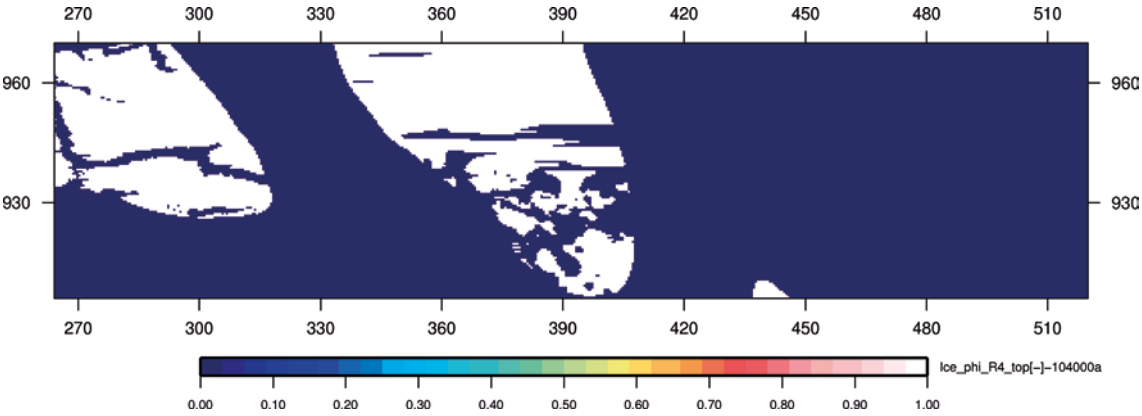

Figure 6-70. *Case 4: permafrost (white) at −104 ka (expressed as ice proportion [−]), about 0.22 of model surface;* ***period of glacial completeness****, projected top horizontal cut (coordinates in km).*

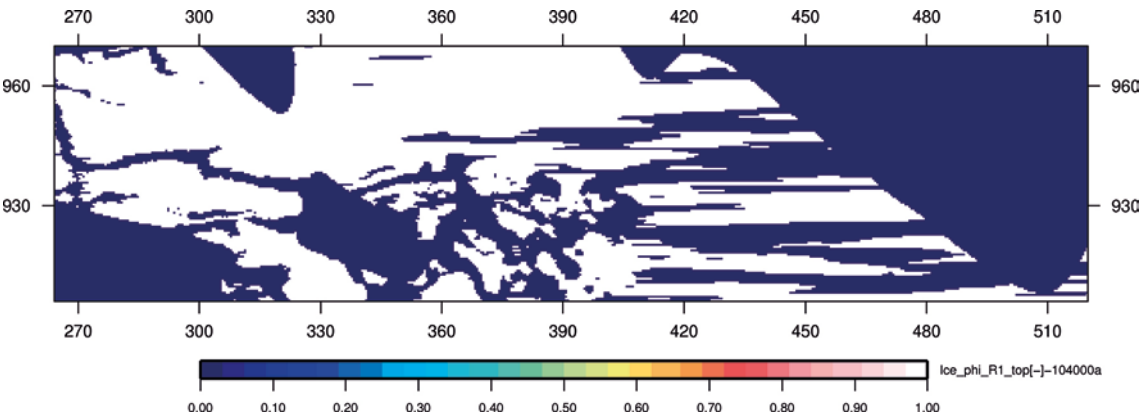

Figure 6-71. *Case 1: permafrost (white) at −104 ka (expressed as ice proportion [−]), about 0.45 of model surface;* ***period of glacial completeness****, projected top horizontal cut (coordinates in km).*

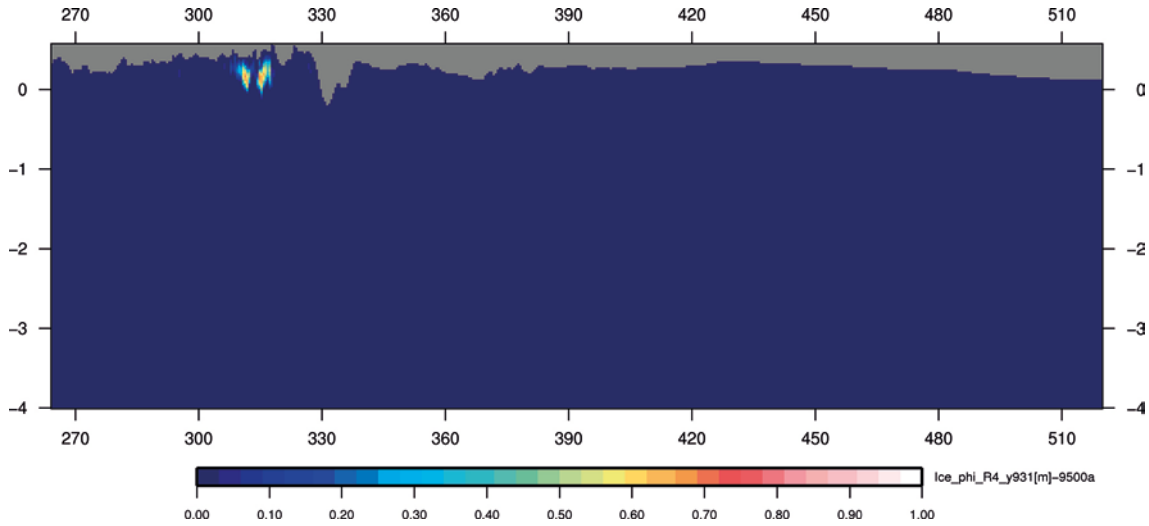

Figure 6-72. *Case 4: relics of permafrost (white), below the surface, at −9.5 ka (expressed as ice proportion [−]),* ***period of glacial retrea****t, E-W vertical at Y = 931 km (coordinates in km).*

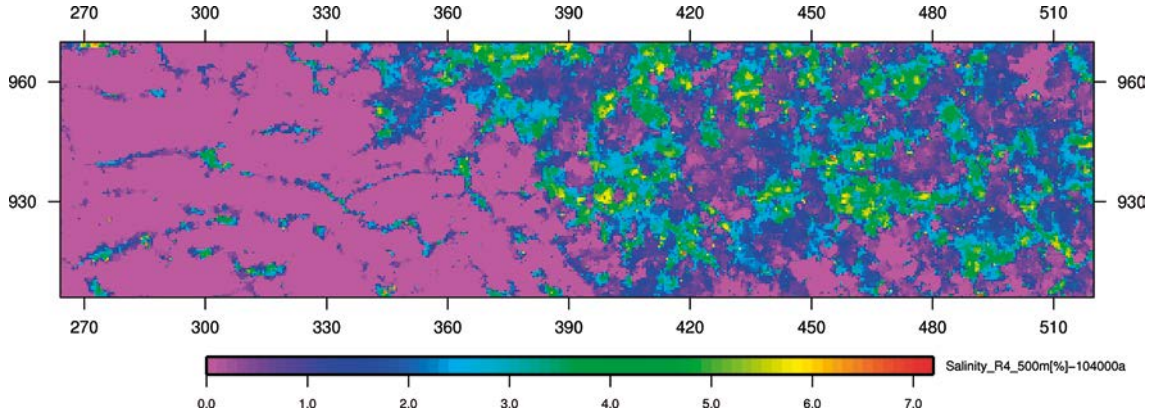

Figure 6-73. *Case 4: salinity [%] at −104 ka,* ***period of glacial completeness,*** *projected horizontal cut at 500 meter depth (coordinates in km).*

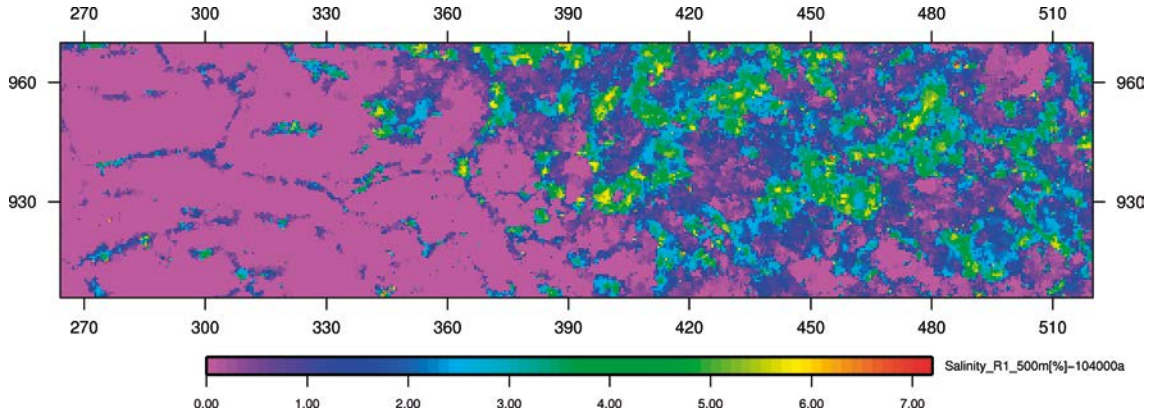

Figure 6-74. *Case 1: salinity [%] at −104 ka,* ***period of glacial completeness****, projected horizontal cut at 500 meter depth (coordinates in km).*

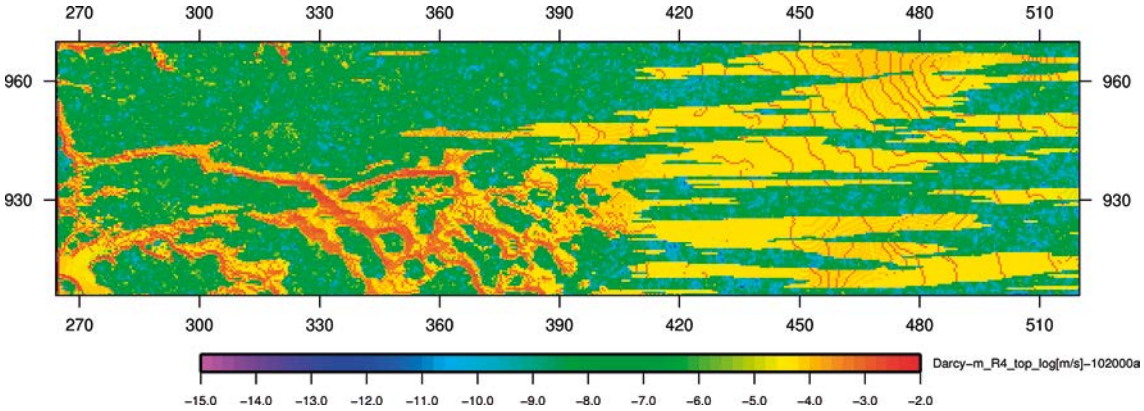

Figure 6-75. *Case 4: Darcy velocity module, log[m/s] at −102 ka;* ***period of glacial completeness*** *with permafrost proportion equal to zero, projected top horizontal cut (coordinates in km).*

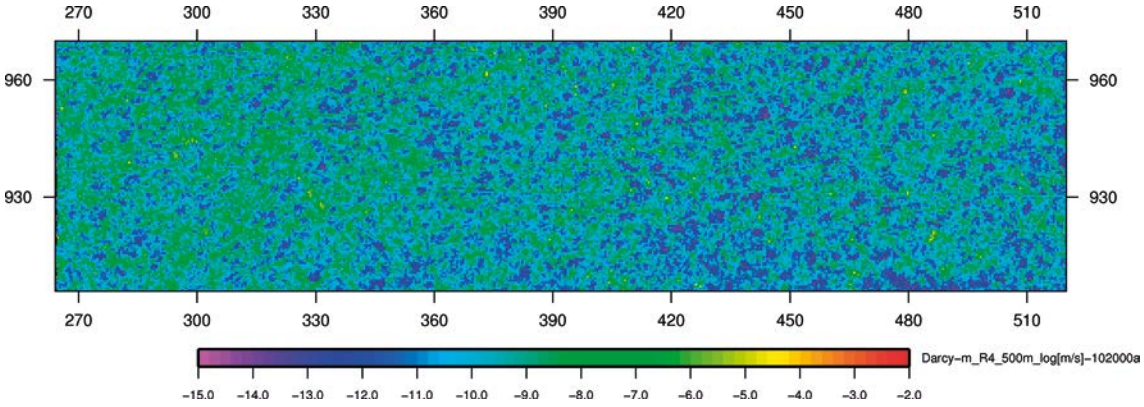

Figure 6-76. *Case 4: Darcy velocity module, log[m/s] at −102 ka;* ***period of glacial completeness*** *with permafrost proportion equal to zero, projected horizontal cut at 500 meter depth (coordinates in km).*

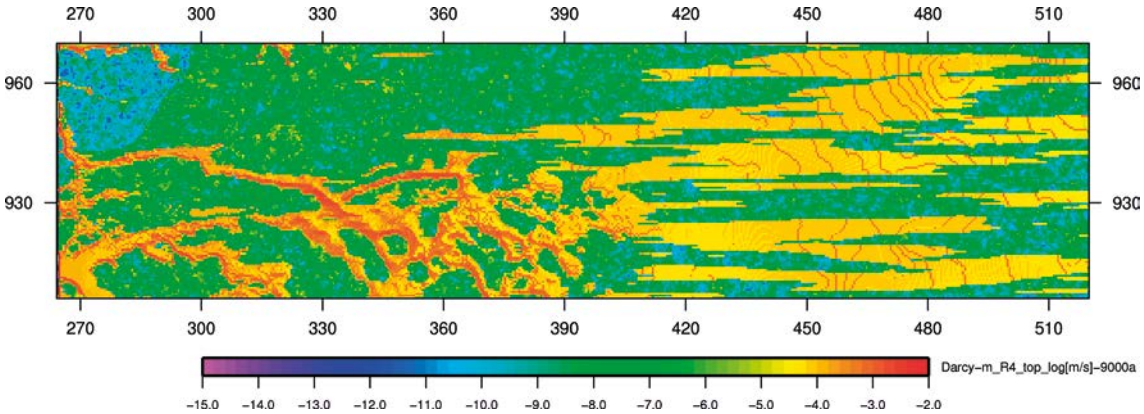

Figure 6-77. *Case 4: Darcy velocity module, log[m/s] at −9 ka;* ***period of glacial retreat*** *with appearance of ice margin (west), projected top horizontal cut (coordinates in km).*

6.5 Case 5

Like the previous case, the case 5 incorporates the hydraulic and thermal properties of the Laxemar site with vertical deformation zones described by the GAP Geomodel version 1; and, includes as well a subglacial layer and horizontal deformation zones. The initial and boundary conditions applied for case 5 are identical to the case 1 (cf. Section 6.1), except for the boundary conditions given by the SICOPOLIS ice sheet model; i.e. the ice thickness and the temperature. These boundary conditions correspond to the glaciation scenario III that present a higher value for the positive degree-day factor (Vallot et al. 2012a, b) compared to the case 1.

Simulation

As for the cases before, simulation of groundwater flow coupled with salt transport and heat transfer is performed for case 5, during the complete glacial cycle; from the time interval −115 to −1 ka.

For case 5, the transient behaviour of the mean ice thickness over the model domain is comparable to the case 1 for the different glacial periods (Figures 6-78 and 6-79). The main difference is that during the period of glacial completeness, the mean ice thickness stabilises at a higher level – about 200 meters thicker – in comparison to the case 1. This increase of ice thickness is related to the variability of ice volume investigated by Appelgate et al. (2012) using Latin hypercube ensemble methods; they performed an assessment of the Greenland Ice Sheet behaviour using the SICOPOLIS ice sheet model with a variation of five key model parameters among 100 ensemble members. Therefore, variation in ice thickness can arise between the three glaciation scenarios selected – for groundwater flow modelling – among 100 ensemble members (Figure 6-80). During the period of glacial completeness, the effect of ice thickness increase is observed when comparing the pressure field of case 5 with the one of the case 1 (Figures 6-81 and 6-82).

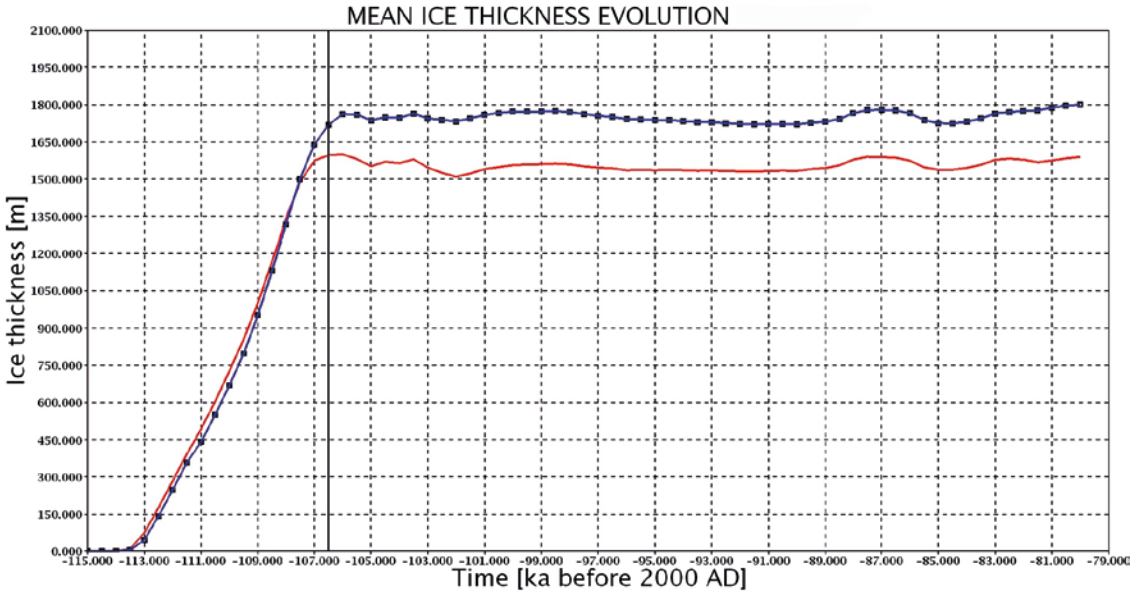

Figure 6-78. *Evolution of mean ice thickness [m] over the model surface, using SICOPOLIS data (case 5: blue line; case 1: red line) from −115 to −80 ka. The end of the glacial build up period is at −106.5 ka (vertical black line).*

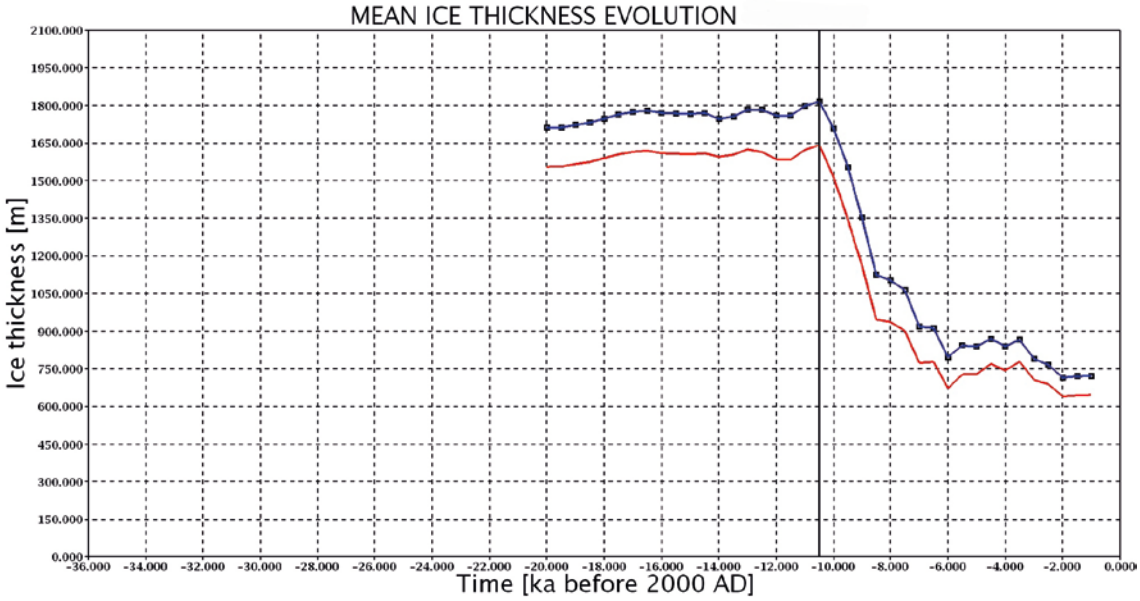

Figure 6-79. *Evolution of mean ice thickness [m] over the model surface, using SICOPOLIS data (case 5: blue line; case 1: red line) from −20 to −1 ka. The onset of the glacial retreat period is at −10.5 ka (vertical black line).*

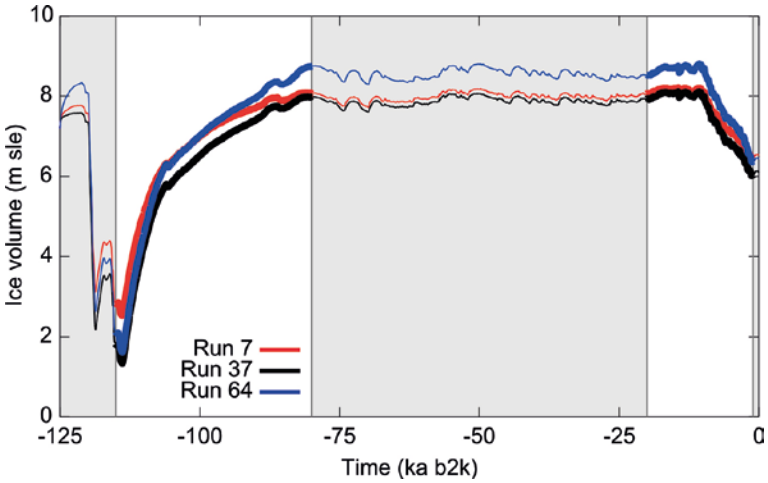

Figure 6-80. *Greenland Ice Sheet: simulated ice volume with SICOPOLIS, expressed in meters of sea level equivalent [m sle] for the three scenarios selected for groundwater flow modelling: black thick line for cases 1, 2 and 3; red thick line for case 4; blue thick line for case 5 (after Vallot et al. 2012a, b).*

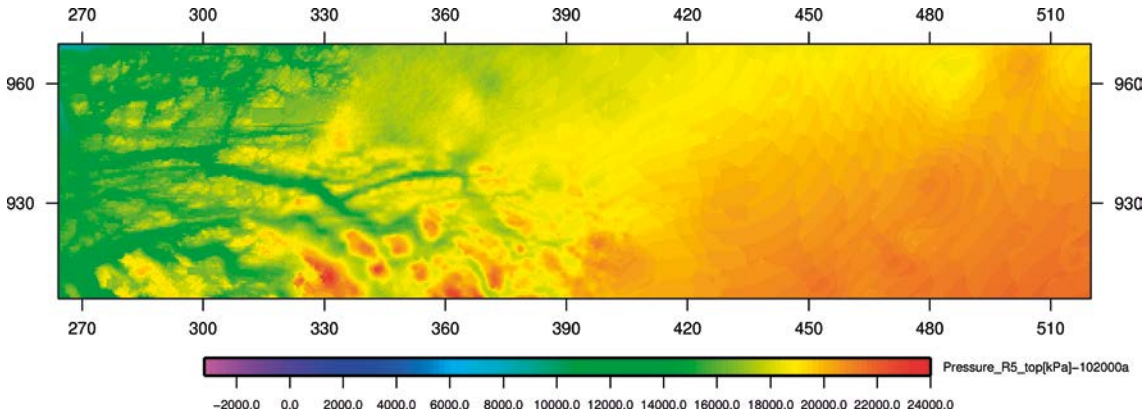

Figure 6-81. *Case 5: pressure [kPa] at −102 ka,* ***period of glacial completeness****, projected top horizontal cut (coordinates in km).*

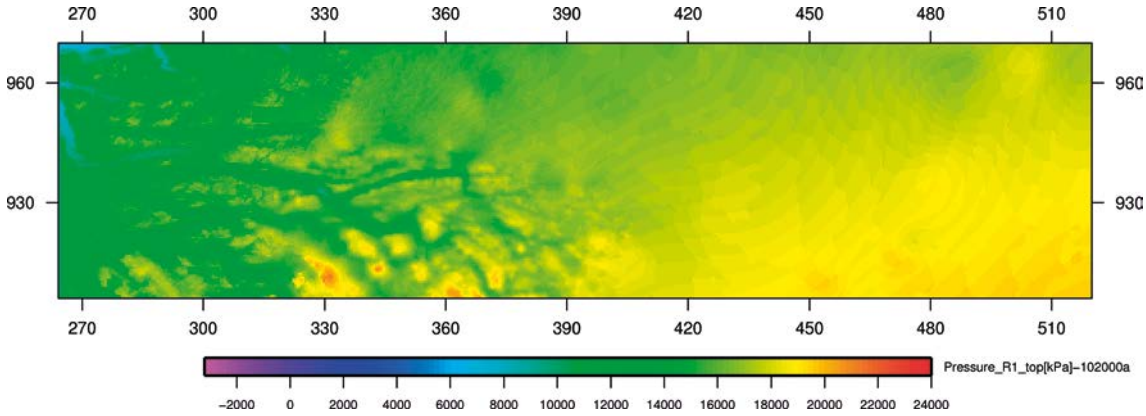

Figure 6-82. *Case 1: pressure [kPa] at −102 ka,* ***period of glacial completeness****, projected top horizontal cut (coordinates in km).*

During the period of completeness, the mean temperature of case 5 – estimated over the model surface – is generally about 1 degree above the mean temperature of the case 1 (Figures 6-83 and 6-84). As for the previous case, these differences are possibly associated to variations in geothermal heat flux or basal sliding intensity between the glaciation scenarios (Vallot et al. 2012a, b) selected among 100 ensemble members (Applegate et al. 2012).

This temperature lying in the range between 0 and −1 degree leads to large variations in the spatial distribution of permafrost proportion (Figures 6-85 to 6-87) during the period of completeness in comparison to the case 1. During two time intervals, permafrost melts away from the surface of the modelled domain: from −103 to −100 ka; from −82 to −81 ka. And, during the period of glacial retreat, the permafrost vanishes at −10 ka and then, from −9.5 to −1ka, becomes present only in front of the ice margin.

The mean salinity curves at 500 and 1 000 meter depth over the model domain exhibits a similar behaviour to the case 1 (cf. Figures 6-30 and 6-31). Tiny local variations of limited extent are observable at 500 m depth (Figure 6-88 and cf. Figure 6-74), probably in response to the modifications in the boundary conditions. The thicker ice sheet and the permafrost proportion seem to have little influence on the salinity at depth.

During the period of glacial completeness and retreat, the module of the Darcy velocity for case 5 is similar to the case 1, for the top surface of the studied domain; the exception being related to the zones with spatial variations of permafrost occurrences during the period of glacial completeness (Figure 6-89 and cf. Figure 6-37). At a depth of 500m, the behaviour of the Darcy velocity module for the case 5 remains quasi identical to the case 1; i.e. the changes in boundary conditions, related to ice thickness and surface temperature do not affect the flow field at depth.

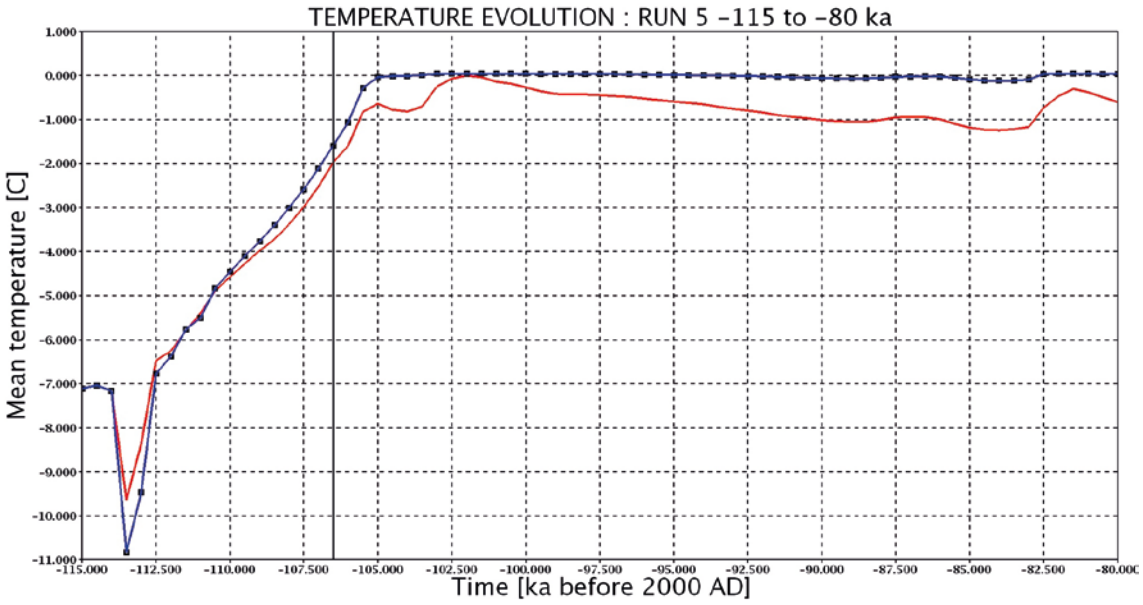

Figure 6-83. *Case 5: evolution of mean ice temperature [ºC] over the model surface (blue line) in comparison to the case 1 (red line) from −115 to −80 ka. The end of the glacial build up period is at −106.5 ka (vertical black line).*

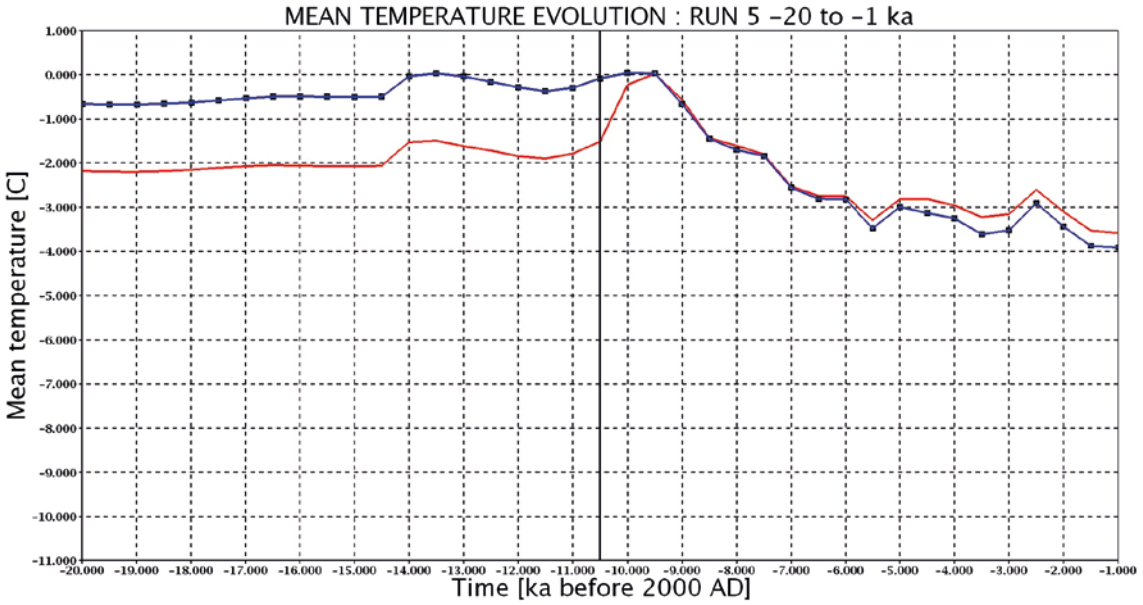

Figure 6-84. *Case 5: evolution of mean ice temperature [ºC] over the model surface (blue line) in comparison to the case 1 (red line) from −20 to −1 ka. The onset of glacial retreat is at −10.5 ka (vertical black line).*

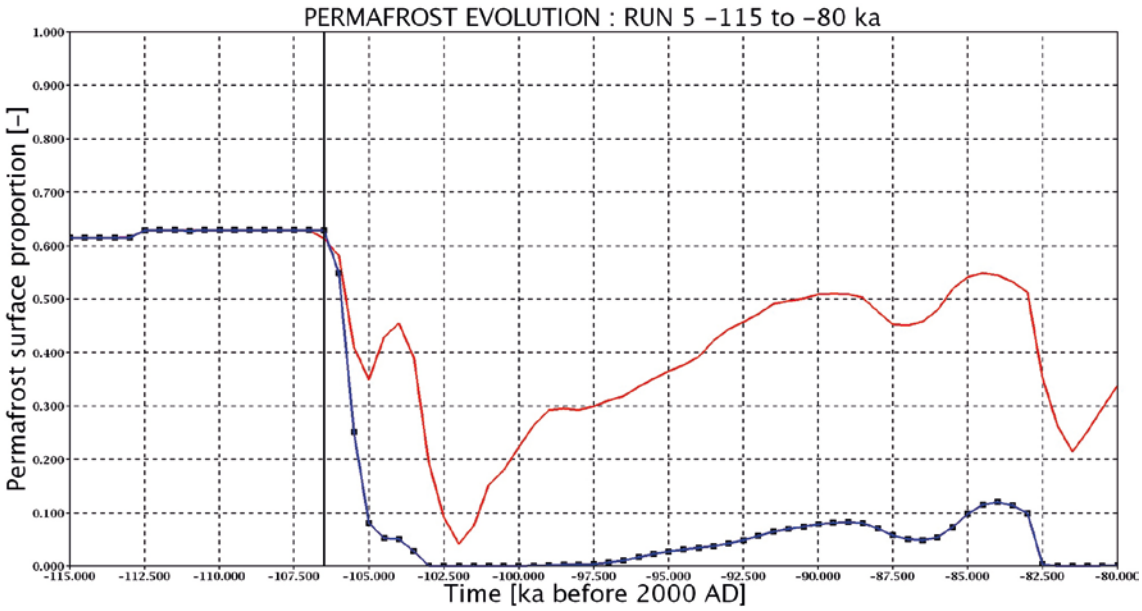

Figure 6-85. *Case 5: evolution of permafrost proportion [−] over the model surface (blue line) in comparison to the case 1 (red line) from −115 to −80 ka. The end of glacial build up is at −106.5 ka (vertical black line); the lowest values of permafrost proportion during ice completeness occur from −103 to −100 ka; and, from −82 to 81 ka.*

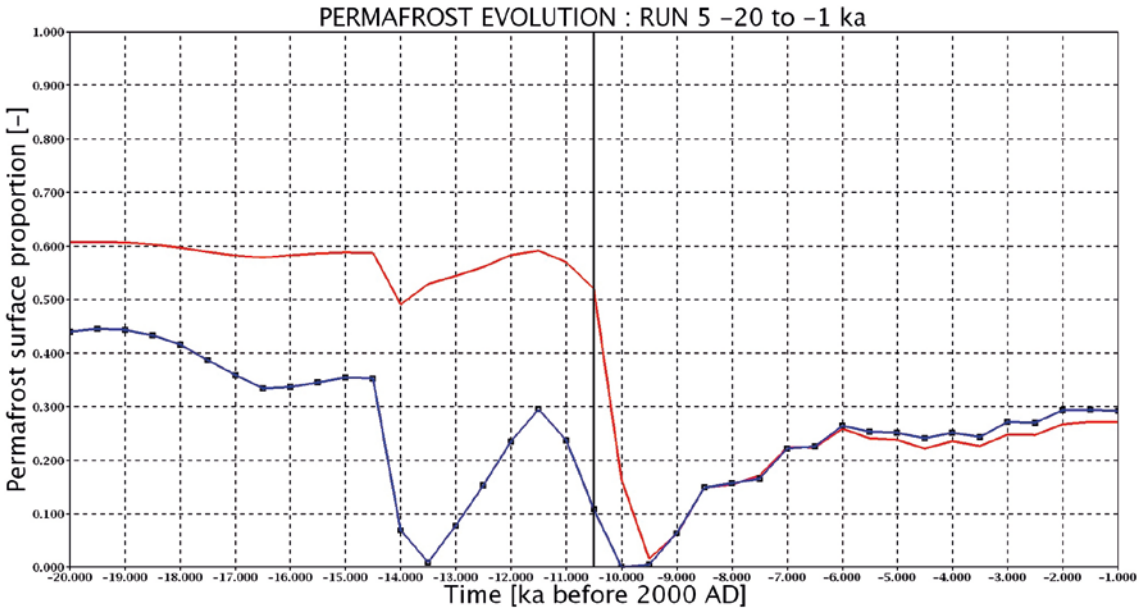

Figure 6-86. *Case 5: evolution of permafrost proportion [−] over the model surface (blue line) in comparison to the case 1 (red line) from −20 to −1 ka. The onset of glacial retreat is at −10.5 ka (vertical black line). The lowest value of permafrost proportion during glacial retreat occurs at −10 ka. From −9.5 to −1 ka, the permafrost is no longer present under the ice sheet.*

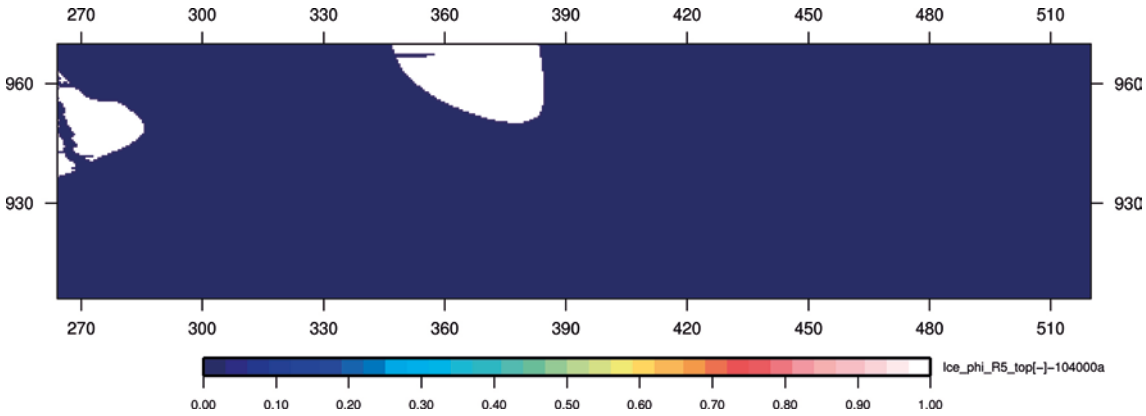

Figure 6-87. *Case 5: permafrost (white) at −104 ka (expressed as ice proportion [−]), about 0.05 of model surface);* ***period of glacial completeness****, projected top horizontal cut (coordinates in km).*

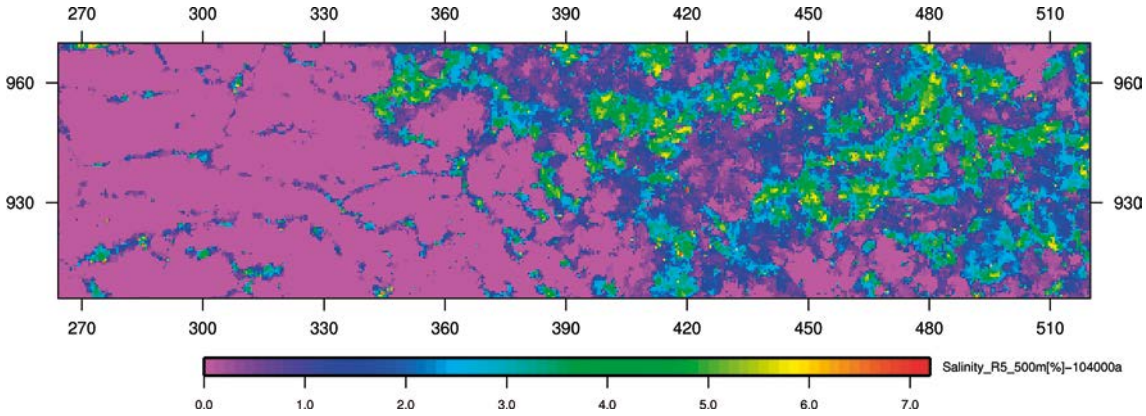

Figure 6-88. *Case 5: salinity [%] at −104 ka,* ***period of glacial completeness****, projected horizontal cut at 500 meter depth (coordinates in km).*

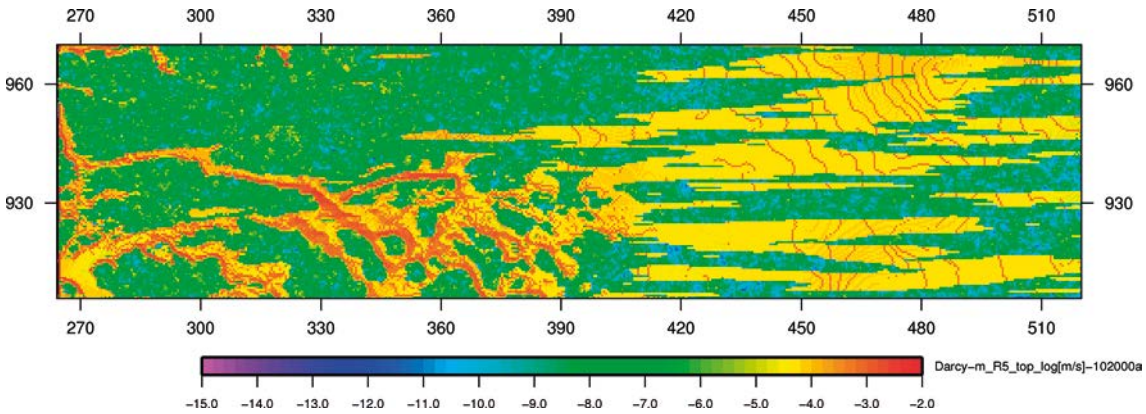

Figure 6-89. *Case 5: Darcy velocity module, log[m/s] at −102 ka;* ***period of glacial completeness*** *with permafrost proportion equal to zero, projected top horizontal cut (coordinates in km).*

7 Performance measures

Several performance measures, in relation to repository depth, and their sensitivity are investigated using specific simulation results and transport calculation. For the different cases, flux calculations are performed at selected elevations; and, the spatial variability for the permafrost depth is estimated west of the ice margin, as well as underneath the ice sheet. For the entire model domain, the penetration depth and concentration of glacial meltwater is studied using transport simulations for all of the five cases. Finally, the concentration of meltwater at taliks is also analysed at selected time steps.

7.1 Fluxes

Regarding flux calculations, average recharge and average discharge are calculated for specific time steps over the studied domain, for horizontal planes at a given elevation. The elevations of the horizontal planes are located between −200 m and −1 000 m; and, these horizontal planes are selected every 100 m. The upper elevation (−200 m) for the selected horizontal planes is selected on the basis of the low surface elevations (below sea level), in order to avoid the main holes in the planes linked to the deep troughs with negative elevation values (cf. Figure 5-2). The obtained results are given at selected time step, in terms of average recharge/ discharge curves as function of elevation.

The different signatures expressed in terms of fluxes are observable when comparing cases 2 and 3 with the case 1 for the periods of glacial build up, completeness and retreat (Figures 7-1, 7-2 and 7-3). These behaviours are related to the differences in hydraulic properties encountered at low elevation; in particular, for case 2 (cf. black and light blue curves of Figures 7-1, 7-2 and 7-3) that presents the lowest hydraulic conductivity values at depth (cf. Table 5-2). At depth, flux values for cases 2 and 3 are below 10 mm/a and around 10 mm/a for case 1, except during the periods of glacial build up and retreat where the discharge values of case 1 are near 100 mm/a (cf. Figures 7-1 and 7-3). Since stronger hydraulic gradients occur during glacial build up and retreat, this latter discharge values are likely related to the larger vertical extension of the deformation zones for the case 1, leading to larger fluxes at depth during this period.

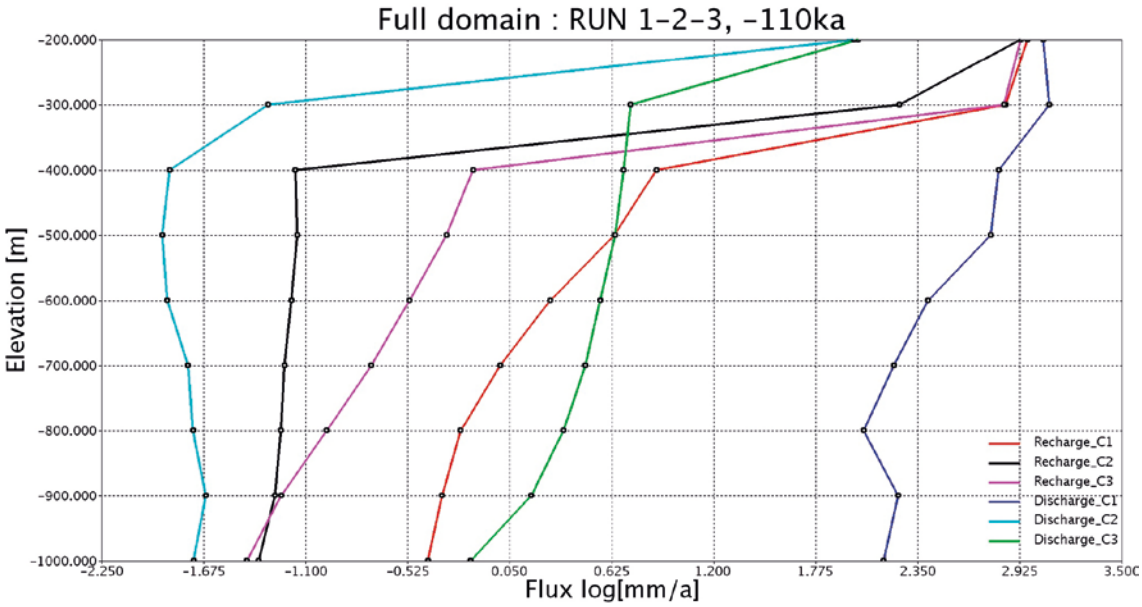

Figure 7-1. *Cases 1, 2 and 3 at −110 ka,* ***period of glacial build up****, average recharge/ discharge, log[mm/a], in terms of elevation for the modelled domain.*

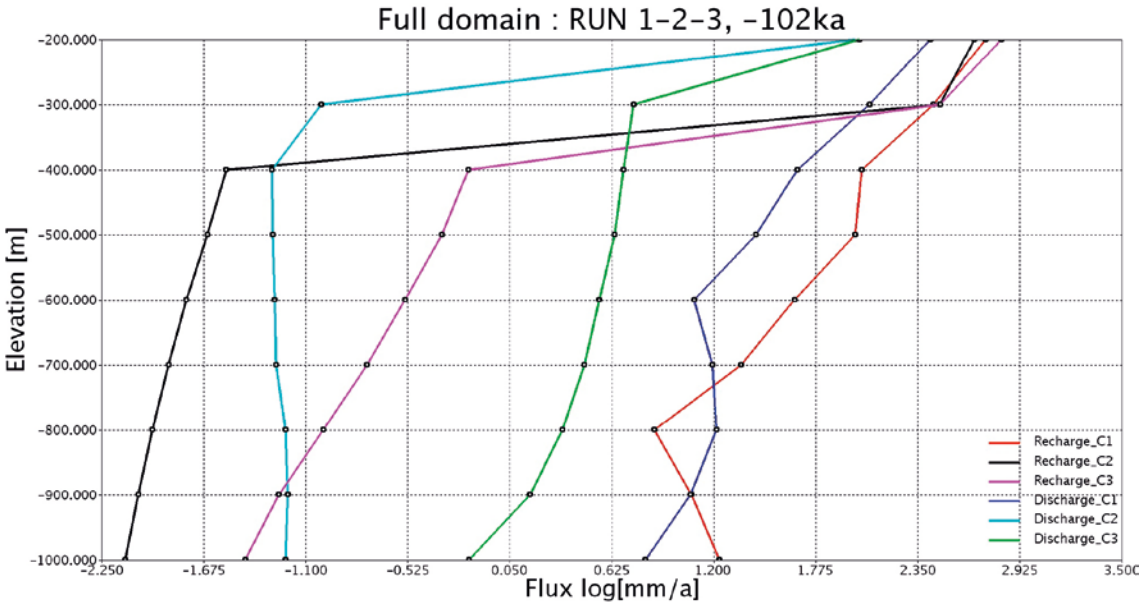

Figure 7-2. *Cases 1, 2 and 3 at −102 ka,* ***period of glacial completeness****, average recharge/ discharge, log[mm/a], in terms of elevation, for the modelled domain.*

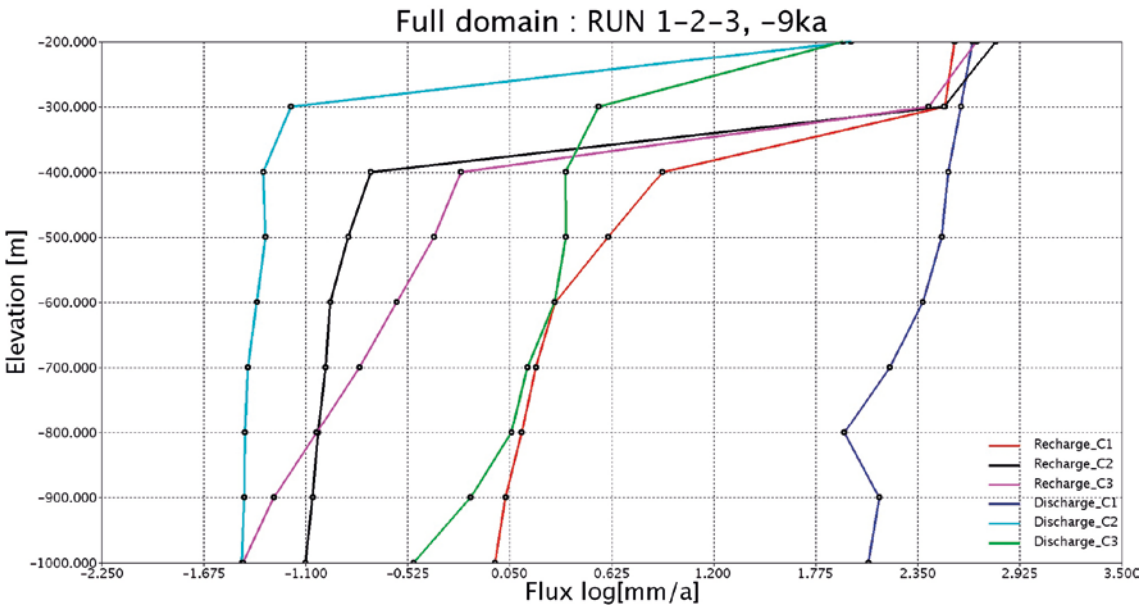

Figure 7-3. *Cases 1, 2 and 3 at −9 ka,* ***period of glacial retreat*** *(with apparition of ice margin), average recharge/ discharge, log[mm/a], in terms of elevation, for the modelled domain.*

During the period of glacial completeness, cases 4 and 5 exhibit analogous flux behaviours (Figure 7-5); the difference in behaviour for the case 1 is related to its larger proportion of surface permafrost (cf. Figures 6-68 and 6-85) – with lower hydraulic conductivity values – influencing flux results. The comparison of cases 4 and 5 with the case 1 during the periods of glacial build up and retreat shows similar behaviour for their recharge and discharge behaviour with depth (Figures 7-4 and 7-6); i.e. the fluxes are likely not sensitive to variations in boundary conditions given by the SICOPOLIS ice sheet model. For all the cases, the high flow rates observed at the top are related to the presence of the subglacial layer (more details related to recharge and subglacial boundary conditions can be found in Appendix C) and the horizontal deformation zones which display a major hydraulic role in draining meltwater underneath the ice sheet, due to their high values of hydraulic conductivity.

The variability of the recharge versus the discharge between the cases and the different glacial periods considered is due the variability of the different hydraulic conductivity fields and to the transient effects linked to the displacement of the ice sheet in presence of enhanced topographic effects in the western part of the model where water can escape the domain; since, the lateral west boundary is prescribed using a dynamic fluid pressure (cf. Section 6.1).

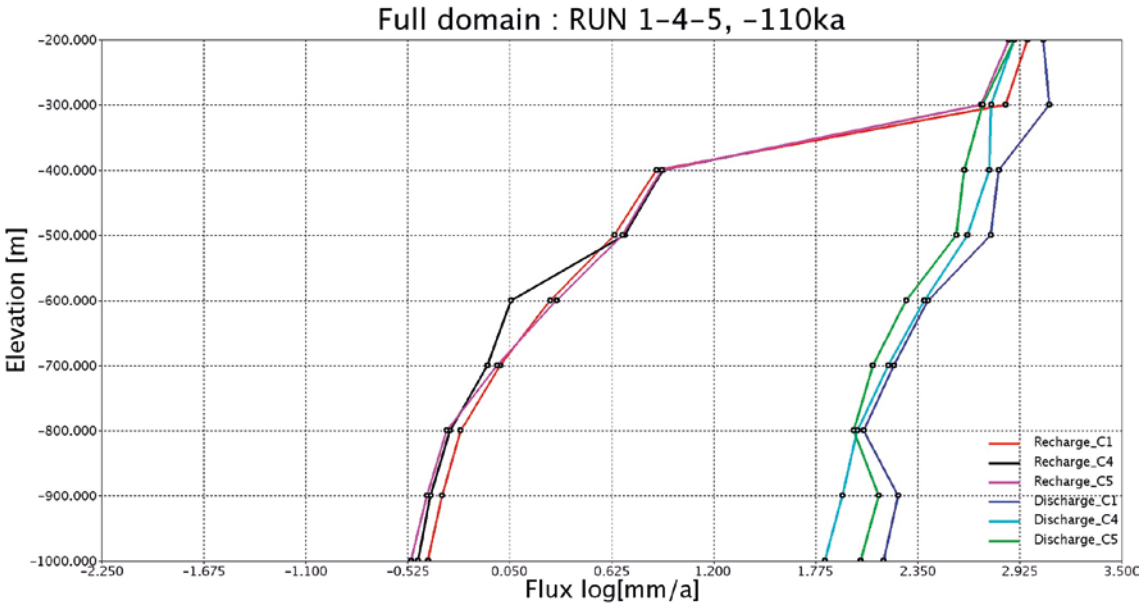

Figure 7-4. *Cases 1, 4 and 5 at −110 ka,* ***period of glacial build up****, average recharge/ discharge, log[mm/a], in terms of elevation, for the modelled domain.*

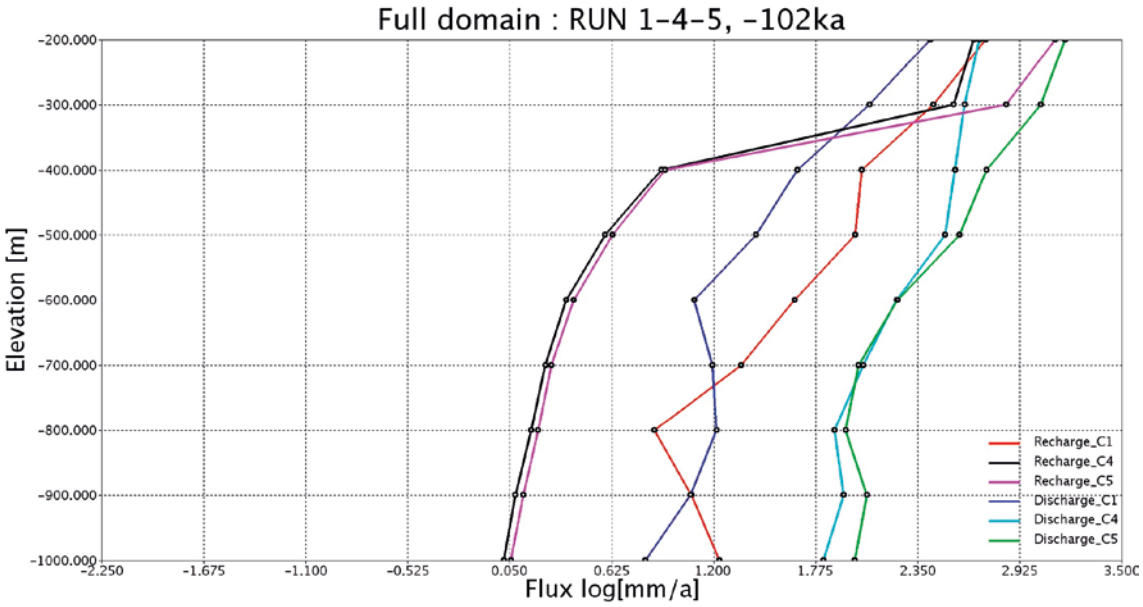

Figure 7-5. *Cases 1, 4 and 5 at −102 ka,* ***period of glacial completeness****, average recharge/ discharge, log[mm/a], in terms of elevation, for the modelled domain.*

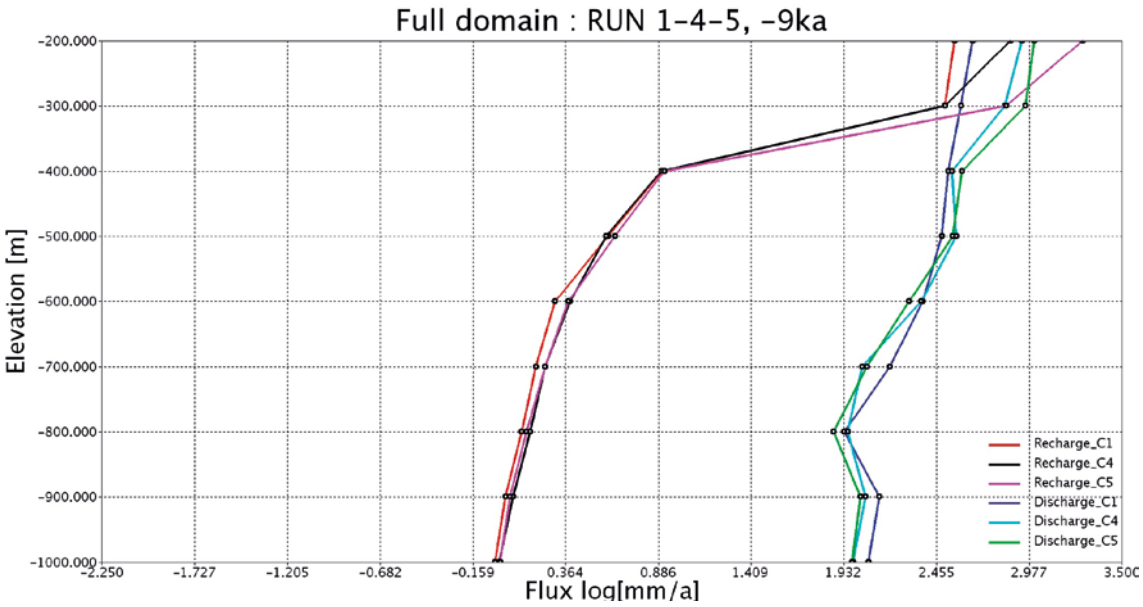

Figure 7-6. *Cases 1, 4 and 5 at −9 ka,* ***period of glacial retreat*** *(with apparition of ice margin), average recharge/ discharge, log[mm/a], in terms of elevation, for the modelled domain.*

7.2 Depth of permafrost

For each of the five cases, the depth of permafrost is evaluated at two selected time steps (−113 and −1 ka) during the periods of glacial build up and retreat; these time steps characterised by low average temperature values are expected to produce maximum values of permafrost depth when only a portion of the domain is covered by the ice sheet.

The mean depth of permafrost, lying in the range 509–617 m, appears to be slightly sensitive to the hydraulic conductivity field when comparing the differences between cases 1, 2 and 3 (Tables 7-1 and 7-2); in particular, during glacial retreat. Cases 4 and 5 present similar results for glacial build up and retreat; but, they only differ significantly from the case 1 during glacial retreat. This outcome is likely due to the distinct location of the ice margin between the different cases at time step −1ka.

For the period of glacial build up, the mean values of permafrost depth for the different cases are lower when compared to the mean values for the period of glacial retreat (cf. Tables 7-1 and 7-2).

Table 7-1. Statistics for permafrost depth at time step −113 ka (period of glacial build up).

Performance Measure	Case	Mean[1] [m]	Standard deviation	P5	P25	P50[2]	P75	P95	P_{ice}[3]
Permafrost depth [m]	1	508.5	266.4	237.5	412.5	512.5	612.5	762.5	0.56
Permafrost depth [m]	2	557.3	288.9	262.5	462.5	562.5	662.5	812.5	0.56
Permafrost depth [m]	3	511.0	267.6	287.5	412.5	512.5	612.5	737.5	0.56
Permafrost depth [m]	4	513.2	266.7	237.5	437.5	512.5	612.5	737.5	0.47
Permafrost depth [m]	5	513.6	266.2	237.5	437.5	512.5	612.5	737.5	0.41

[1] Arithmetic mean for permafrost depth when neglecting zero values.
[2] Percentile at 50 %: e.g. for case 1, 50 % of the depth values are below 512.5 m.
[3] Proportion of ice sheet (e.g. P_{ice} = 1; the whole domain is covered by the ice sheet).

Table 7-2. Statistics for permafrost depth at time step −1 ka (period of glacial retreat).

Performance Measure	Case	Mean[1] [m]	Standard deviation	P5	P25	P50[2]	P75	P95	P_{ice}[3]
Permafrost depth [m]	1	617.0	330.3	187.5	487.5	637.5	762.5	912.5	0.67
Permafrost depth [m]	2	579.7	274.5	187.5	512.5	612.5	687.5	787.5	0.67
Permafrost depth [m]	3	550.2	260.4	162.5	487.5	587.5	662.5	737.5	0.67
Permafrost depth [m]	4	556.7	245.5	152.5	437.5	587.5	712.5	837.5	0.77
Permafrost depth [m]	5	565.4	281.1	187.5	437.5	587.5	712.5	837.5	0.63

[1] Arithmetic mean for permafrost depth when neglecting zero values.
[2] Percentile at 50 %: e.g. for case 1, 50 % of the depth values are below 637.5 m.
[3] Proportion of ice sheet (e.g. P_{ice} = 1; the whole domain is covered by the ice sheet).

As one would expect the opposite result, this finding is a priori surprising and can be explained by the spatial variability of the permafrost in response to the temperature field. During the cold climatic period of glacial build up, the thin ice sheet that enters the model domain presents a basal temperature around −8 °C (Figure 7-7); permafrost can be distributed over the entire domain, with thinner depth values underneath the ice sheet (Figure 7-8). However, during glacial retreat under warmer climatic conditions (cf. Figure 6-22), the ice sheet with above zero temperature leaves the domain and permafrost occurs only in the western part of the domain, leading to a thicker mean value for the permafrost (Figure 7-9).

Permafrost can partially remain underneath the ice sheet during glacial completeness (cf. Section 6.1). During glacial retreat, newly formed permafrost occurs (cf. Figure 6-26), with however some old remains from glacial completeness; and, this permafrost is capable to expand under the ice sheet, starting from the ice margin (cf. Figure 7-9). This observation is obtained for all the cases considered, and new permafrost is likely to be found up to tens of kilometres under the ice sheet (Figure 7-10).

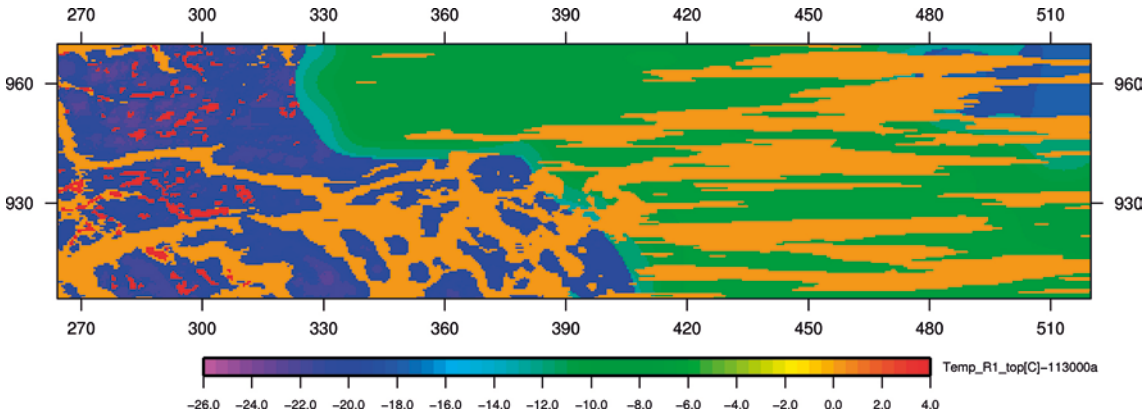

Figure 7-7. *Case 1: temperature [°C] at −113 ka,* ***period of glacial build up****, projected top horizontal cut (coordinates in km).*

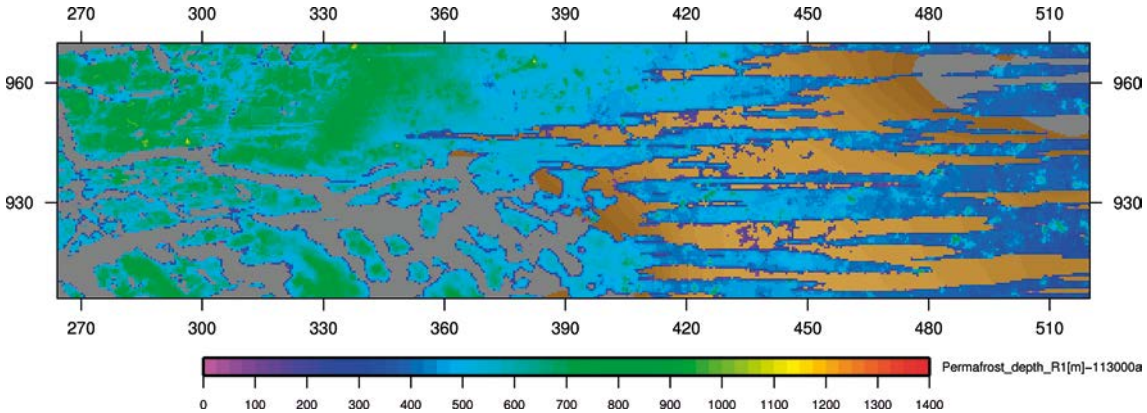

Figure 7-8. *Case 1: permafrost depth [m] at −113 ka,* ***period of glacial build up****, projected top horizontal cut from underneath the ice sheet (coordinates in km); brown colours depict the ice sheet location (cf. Figure 7-7).*

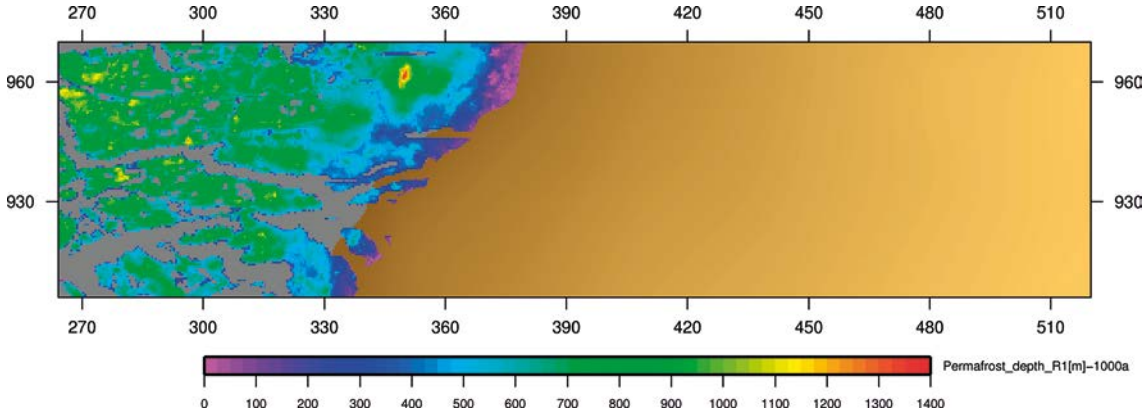

Figure 7-9. *Case 1: permafrost depth [m] at −1 ka,* ***period of glacial retreat****, projected top horizontal cut from underneath the ice sheet; brown colours, towards the east, depict the location of the ice sheet with increasing thickness (coordinates in km). Near the ice margin, patches (in colours) of permafrost can be located underneath the ice sheet (in brown).*

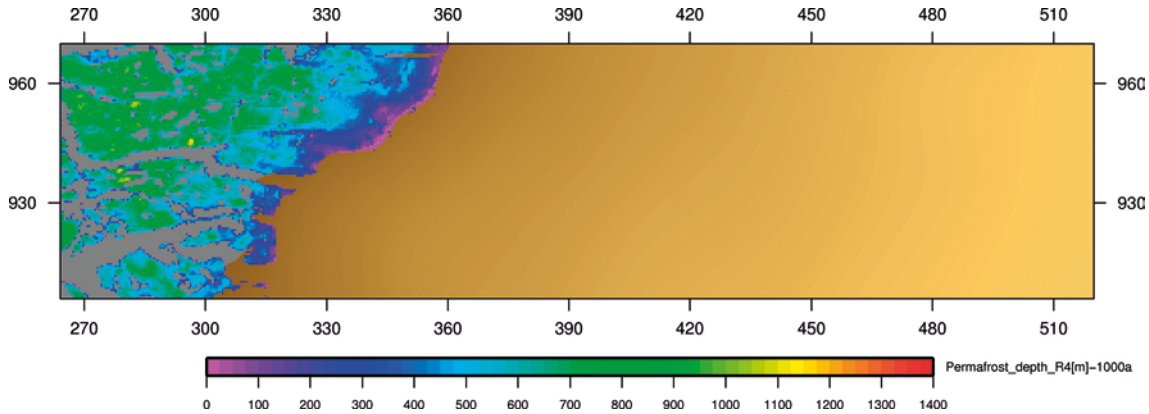

Figure 7-10. *Case 4: permafrost depth [m] at −1 ka,* ***period of glacial retreat****, projected top horizontal cut from underneath the ice sheet; brown colours, towards the east, depict the location of the ice sheet with increasing thickness (coordinates in km). Near the ice margin, patches (in colours) of permafrost can be located underneath the ice sheet (in brown).*

7.3 Tracing of glacial meltwater

The tracing of glacial meltwater as a tracer is performed by transport modelling using the velocity fields simulated for the five different cases (cf. Section 6). In addition to the hydraulic, thermal and salinity boundary conditions, the following transport boundary conditions are applied for tracing glacial meltwater:

- **Surface of the model (west of the ice margin)**: $\frac{\partial C_{mw}}{\partial z} = 0$ is prescribed for the mass fraction of the glacial meltwater. The application of no dispersive flux boundary conditions implies that the mass fraction of glacial meltwater can exit only by advection through the model surface. This boundary remains physically acceptable as advective transport is dominant within the model domain. For the range of Darcy velocity, in relation to the value of the effective diffusion coefficient, the transport is advective dominant and then the importance of the diffusive effects becomes negligible at the time and spatial scales of interest. In addition, the tracing simulation results are not sensitive to various values tested for the effective diffusion coefficient.
- **Surface of the model (underneath the ice sheet)**: the influx of glacial meltwater is prescribed with a mass fraction equal to one. No dispersive flux boundary conditions are applied for discharge conditions as well as for permafrost zones.
- **Lateral and bottom boundaries**: $\frac{\partial C_{mw}}{\partial x} = 0$, $\frac{\partial C_{mw}}{\partial y} = 0$ and $\frac{\partial C_{mw}}{\partial z} = 0$ are respectively prescribed.

Since the transport of glacial meltwater occurs at a scale of a few centuries, the concentration field of the glacial meltwater is stabilized; i.e. it presents steady behaviour at the level of a time step (500 years) of the transient groundwater flow model. Then, it is assumed that the depth reached by glacial meltwater is representative when its evaluation is performed using a steady state velocity field. Therefore, specific time steps of the transient groundwater flow model are selected with their corresponding velocity fields, which are taken as steady state, for transport calculations during 500 years. The following time steps, in relation to the glacial periods, are chosen for tracing glacial meltwater: −110 ka (glacial build up); −102 ka (glacial completeness with minimum proportion of permafrost); −9.5 ka (glacial retreat with minimum proportion of permafrost) and −2 ka (glacial retreat).

Case 1

For the case 1, the obtained results show that after 500 years, glacial meltwater is likely to reach depths that exceed 500 m whatever the glacial period considered (Figures 7-11 to 7-15). These results are in accordance with the findings of the GAP project (Claesson Liljedahl et al. 2016): *"The isotopic signature of the groundwaters sampled at three location indicates glacial meltwaters, or cold climate waters, are able to penetrate to depth of at least 500 m… Glacial melt infiltration at the GAP site may have been taking place continuously for hundreds of thousand years, even millions of years"*. One must emphasize that greater depths are attained towards the west, in relation to the strong hydraulic gradients induced by the more variable topography of the bedrock surface. The largest depth values encountered are during the period of glacial completeness (cf. Figure 7-13). At −2 ka, the meltwater disappears from the western part of the model domain, since the ice sheet retreated eastward (cf. Figure 7-15).

In addition, the comparison of the salinity distribution with the meltwater concentration provides a complementary description; the former delivers the location of total freshwater (groundwater + meltwater) while the latter shows solely the distribution of meltwater at depth (Figure 7-16; cf. Figure 7-13).

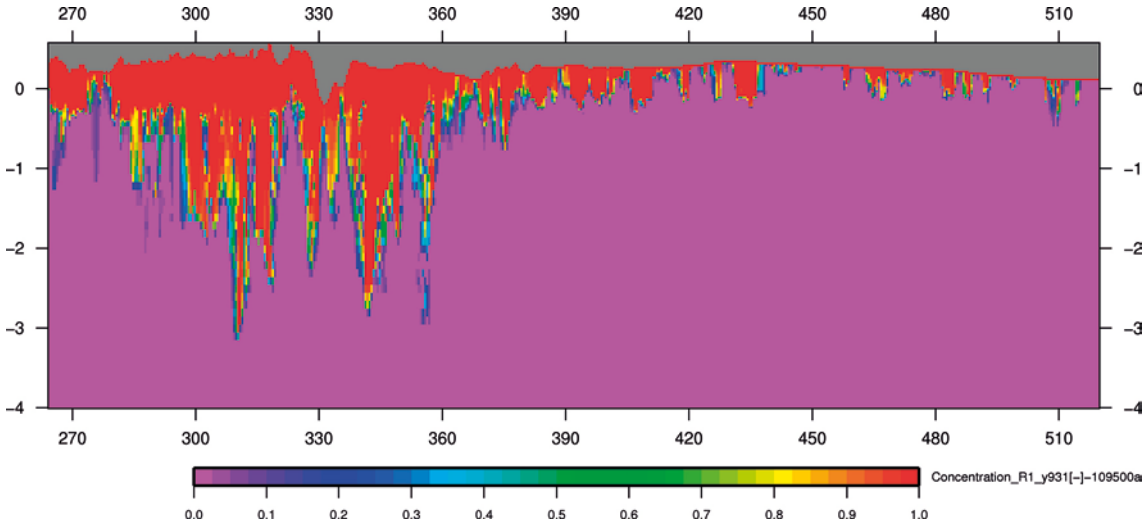

Figure 7-11. *Case 1: glacial meltwater concentration (expressed in mass fraction [−]), at −110 ka, after 500 years of transport,* ***period of glacial build up****, E-W vertical at Y = 931 km (coordinates in km).*

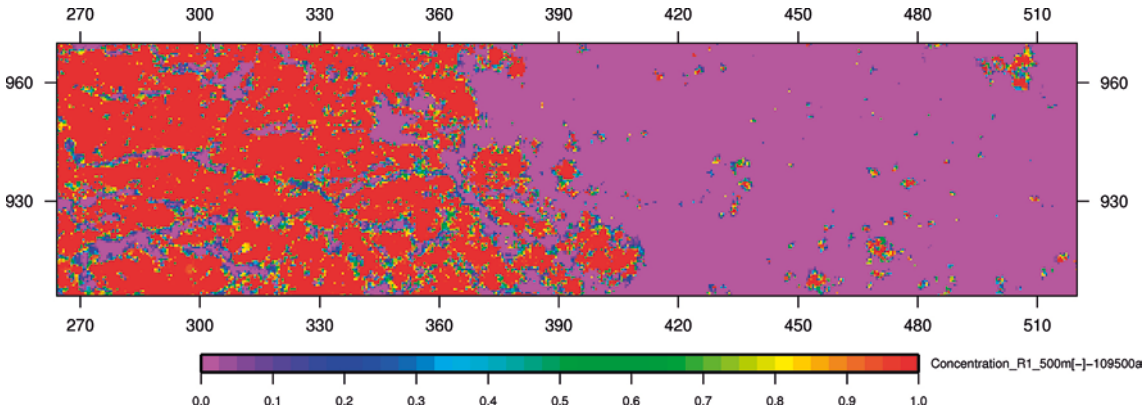

Figure 7-12. *Case 1: glacial meltwater concentration (expressed in mass fraction [−]) at −110 ka, after 500 years of transport,* ***period of glacial build up****, projected horizontal cut at 500 meter depth (coordinates in km).*

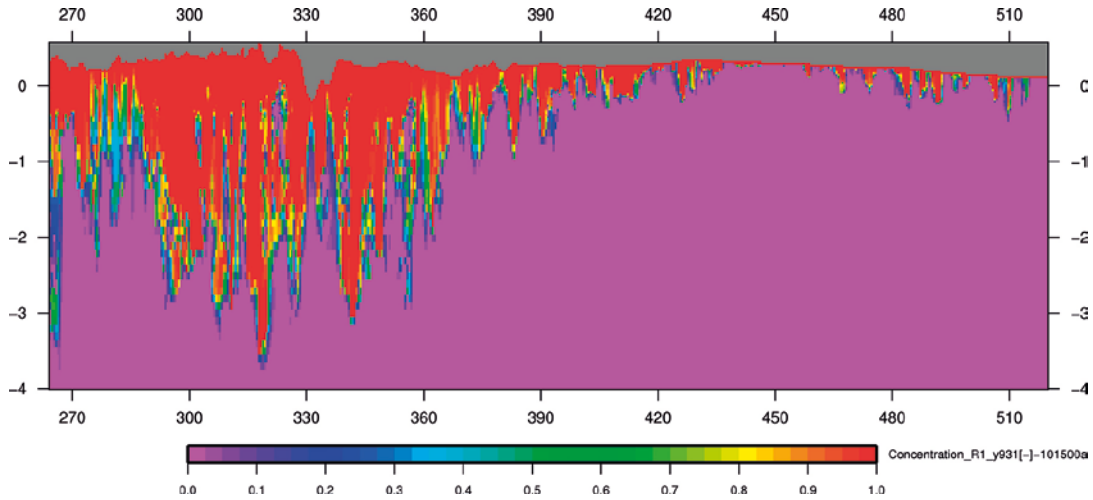

Figure 7-13. *Case 1: glacial meltwater concentration (expressed in mass fraction [−]), at −102 ka, after 500 years of transport,* ***period of glacial completeness****, E-W vertical at Y = 931 km (coordinates in km).*

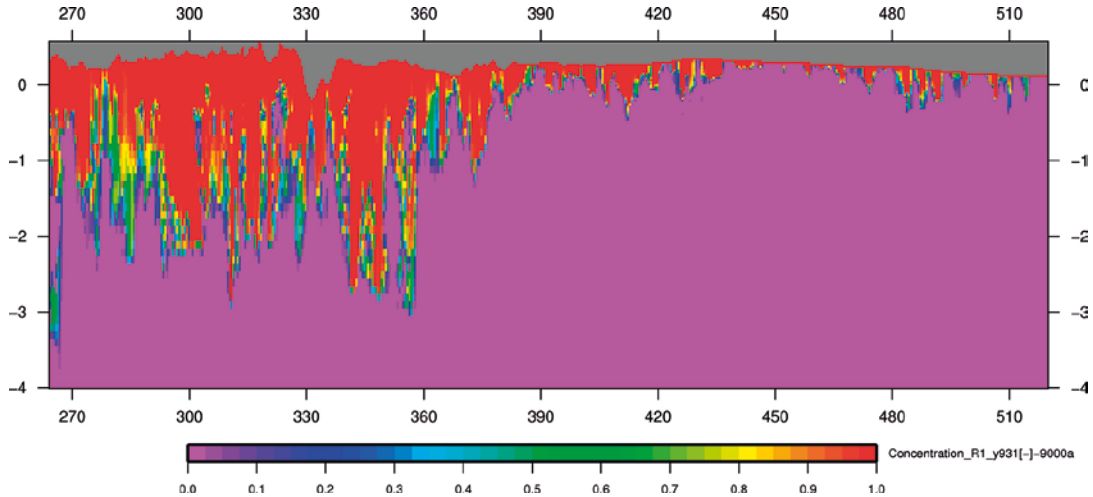

Figure 7-14. *Case 1: glacial meltwater concentration (expressed in mass fraction [−]), at −9.5 ka, after 500 years of transport,* ***period of glacial retreat****, E-W vertical at Y = 931 km (coordinates in km).*

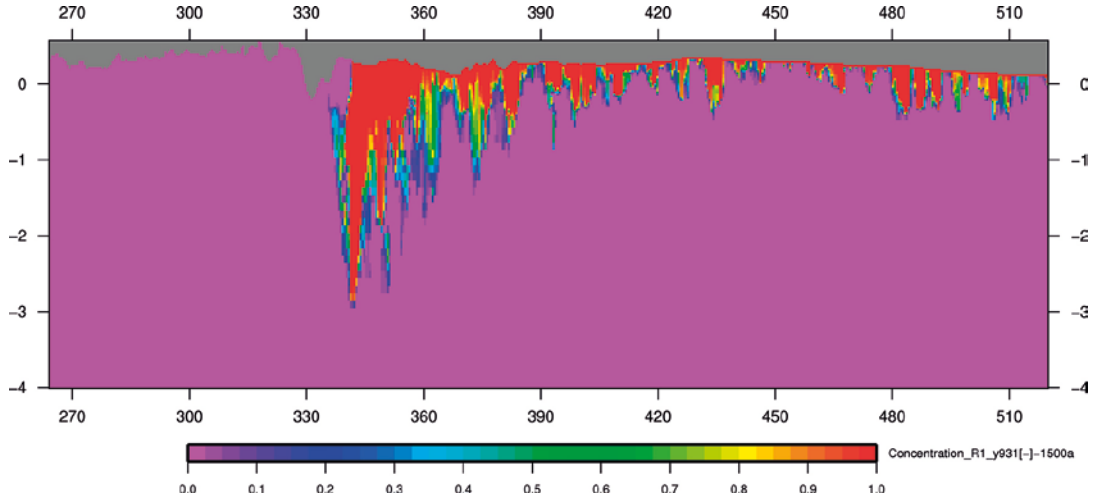

Figure 7-15. *Case 1: glacial meltwater concentration (expressed in mass fraction [−]), at −2 ka, after 500 years of transport, period of glacial retreat, E-W vertical at Y = 931 km (coordinates in km).*

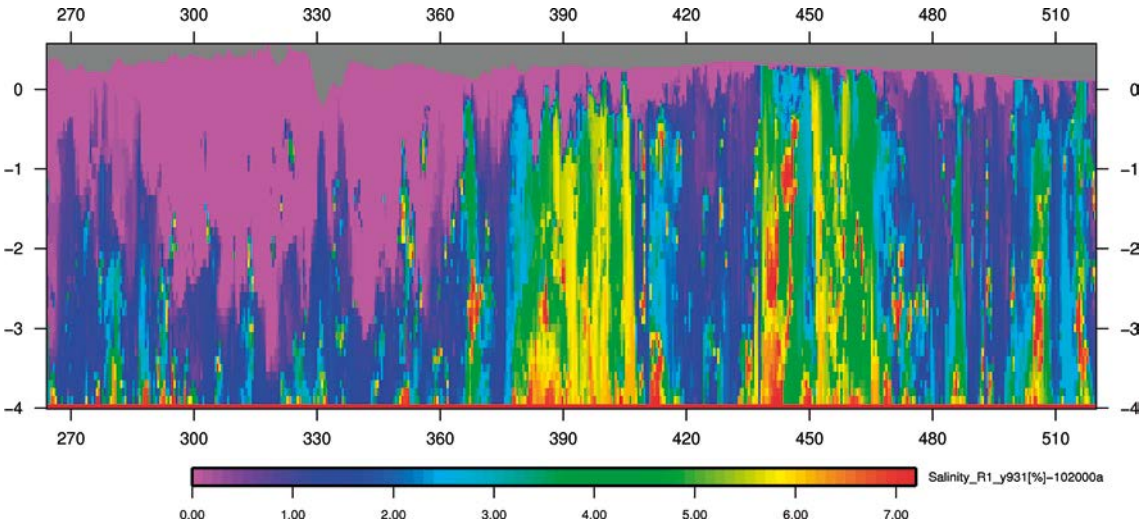

Figure 7-16. *Case 1: salinity [%], at −102 ka,* ***period of glacial completeness****, E-W vertical at Y = 931 km (coordinates in km).*

Cases 2 and 3

The comparison of the glacial meltwater concentration for cases 2 and 3 (Figures 7-17 and 7-18) with the case 1 (cf. Figure 7-13) reveals the role played by the hydraulic conductivity. For case 2, the hydraulic conductivity values in the top layers for the rock mass domain is reduced by about two orders of magnitudes (up to about 400 meter depth; cf. Tables 5-2 and 5-1) compared to the case 1. And for case 3, a similar behaviour occurs to a lesser extent; i.e. with lower hydraulic conductivity values for the rock mass domain in the top layers (i.e. about two orders of magnitude at depth below 200 meters; cf. Tables 5-3 and 5-1) associated to the lesser vertical extension of the deformation zones (cf. Figures 5-16 and 5-14). These differences in hydraulic conductivity for cases 2 and 3 lead to a reduction of the depth likely reachable by the glacial meltwater in comparison to the case 1; in particular for case 2, a much lesser amount of glacial meltwater is expected to attain the depth of 500 m (cf. Figure 7-17).

As shown previously for the case 1, a complementary description is provided by the comparison of the salinity distribution with the meltwater concentration; the former shows the location of total freshwater (groundwater+meltwater; in purple colour in Figure 7-18) while the latter indicates solely the distribution of meltwater at depth (cf. Figure 7-17).

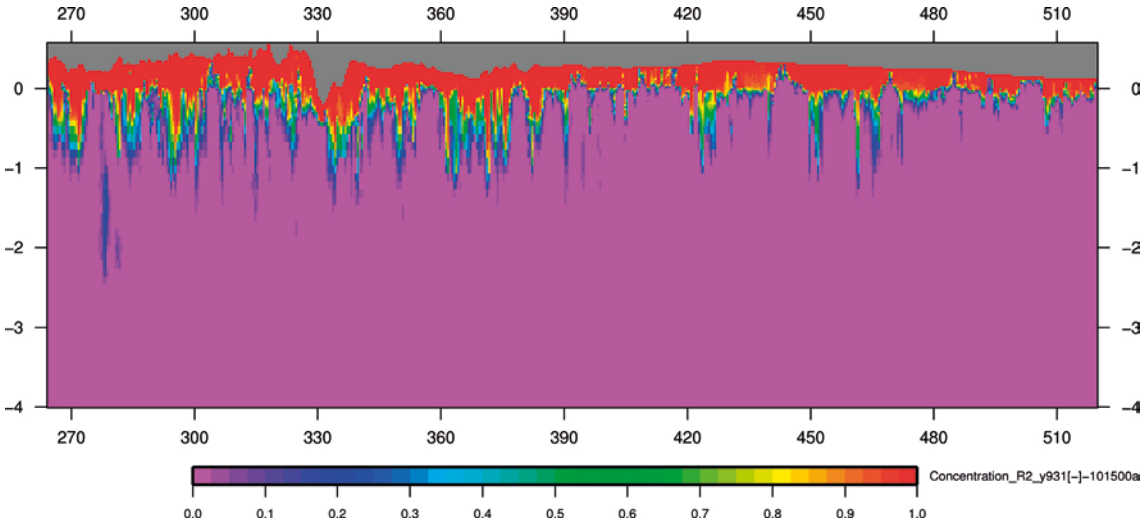

Figure 7-17. *Case 2: glacial meltwater concentration (expressed in mass fraction [−]), at −102 ka, after 500 years of transport,* ***period of glacial completeness****, E-W vertical at Y = 931 km (coordinates in km).*

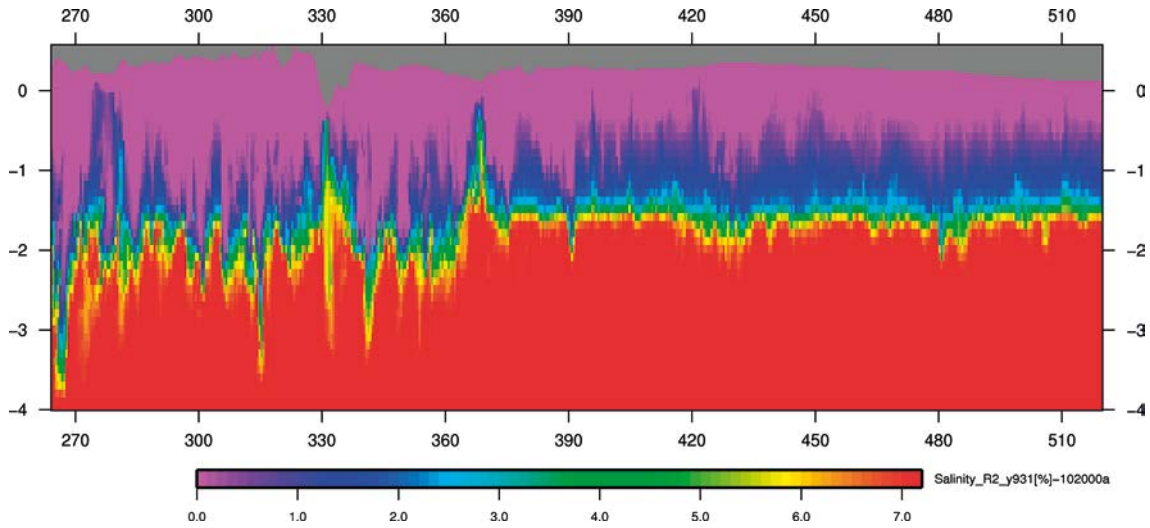

Figure 7-18. *Case 2: salinity [%], at −102 ka,* ***period of glacial completeness****, E-W vertical at Y = 931 km (coordinates in km).*

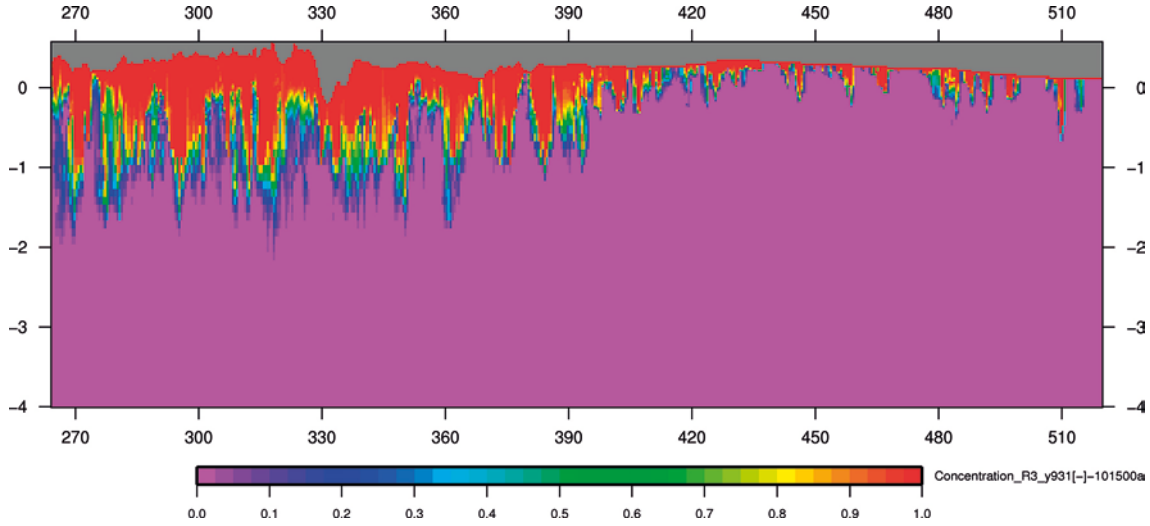

Figure 7-19. *Case 3: glacial meltwater concentration (expressed in mass fraction [−]), at −102 ka, after 500 years of transport,* ***period of glacial completeness****, E-W vertical at Y = 931 km (coordinates in km).*

Cases 4 and 5

The cases 4 and 5, corresponding to alternative glaciation scenarios, present meltwater concentration results similar to the case 1; i.e. the glacial meltwater is likely to reach depths that exceed 500 m whatever the glacial period considered. Differences are observed during the period of glacial retreat, the ice sheet moves at a different velocity depending on the glaciation scenario (Figures 7-20, 7-21 and cf. Figure 7-15).

Concentration of glacial meltwater at 500 m depth

The glacial meltwater concentration occurring at a depth of 500 m, and after 500 years, is obtained for all the five cases, using the four time steps considered: −110 ka (glacial build up); −102 ka (glacial completeness with minimum proportion of permafrost); −9.5 ka (glacial retreat with minimum proportion of permafrost) and −2 ka (glacial retreat). The resulting statistics of meltwater concentration are given in Tables 7-3 and 7-4. The range of variability for the mean concentration of glacial meltwater lies in the range 0.082–0.398. For each of the five cases, a low variability is observed in the mean value of meltwater concentration for their respective first three time steps (−110, −102 and −9.5 ka); the main differences are observed by comparing the periods of glacial build up and

completeness (cf. Figure 7-12 and Figure 7-22); the latter presenting the highest mean values. This effect is likely linked to the lower permafrost proportion at −102 ka; except for case 2, where the opposite effect is observed, at −110 ka, the permafrost leads to a reduction in porosity (cf. Equation 4-7) towards its lower bound that favors penetration depth of meltwater. The lowest mean values occur during the period of glacial retreat when the ice margin appears on the domain; e.g. for the time step at −2 ka (Figure 7-23).

The mean meltwater concentration values of cases 2 and 3 is significantly reduced compared to the case 1, due to the differences in their respective hydraulic conductivity fields (cf. Tables 5-1, 5-2 and 5-3); in particular, the spatial variability of meltwater concentration value of case 2 (Figure 7-24; cf. 7-22) differs remarkably from the case 1 (about a factor two, in terms of mean value).

Regarding cases 4 and 5, the only noticeable spatial differences in meltwater concentration compared to the case 1 appear during glacial retreat in relation to the location of the ice margin; e.g. for case 5, where the ice sheet retreated the most easterly (Figures 7-25; cf. 7-23).

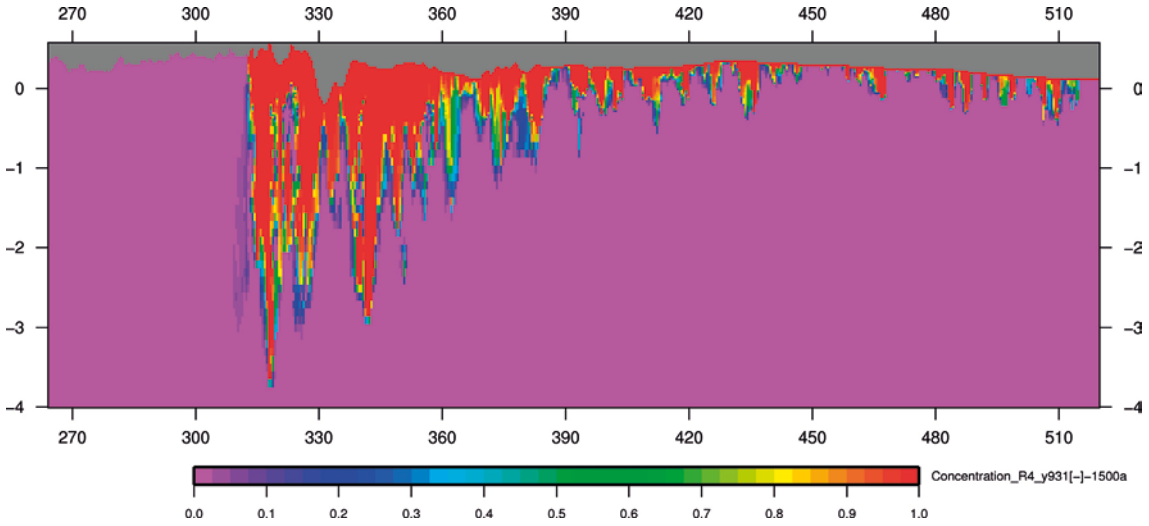

Figure 7-20. *Case 4: glacial meltwater concentration (expressed in mass fraction [−]), at −2 ka, after 500 years of transport,* ***period of glacial retreat****, E-W vertical at Y = 931 km (coordinates in km).*

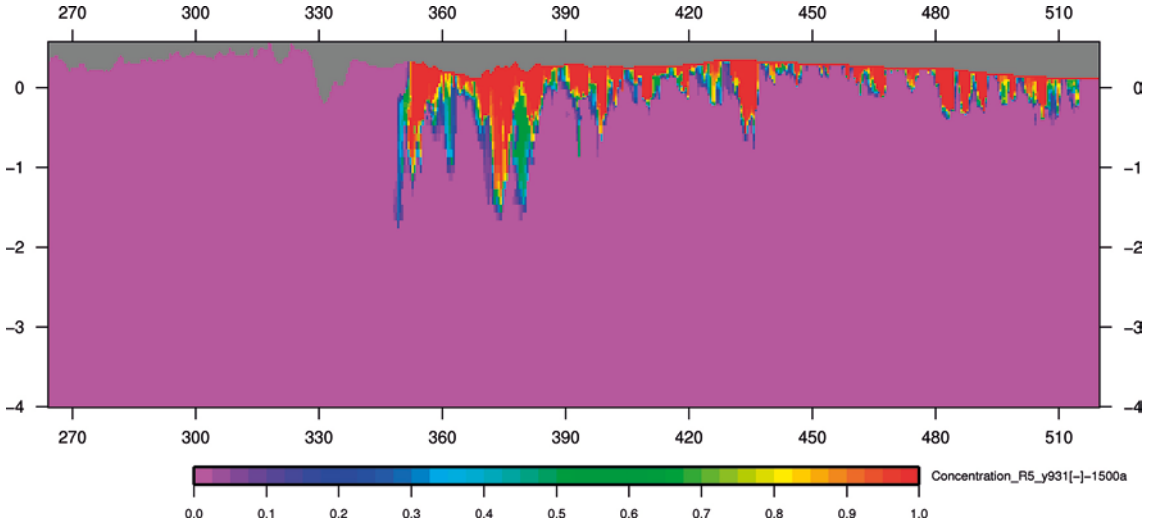

Figure 7-21. *Case 5: glacial meltwater concentration (expressed in mass fraction [−]), at −2 ka, after 500 years of transport,* ***period of glacial retreat****, E-W vertical at Y = 931 km (coordinates in km).*

Table 7-3. Cases 1, 2, 3: statistics of glacial meltwater concentration at 500 m depth (entire domain).

Performance Measure	Case	Time step [ka]	Mean[1)] [−]	Standard deviation	P5	P25	P50[2)]	P75	P95
Concentration [−]	1	−110	0.376	0.460	0.000	0.000	0.001	0.996	1.000
Concentration [−]	1	−102	0.394	0.455	0.000	0.000	0.022	0.989	1.000
Concentration [−]	1	−9.5	0.379	0.451	0.000	0.000	0.013	0.981	1.000
Concentration [−]	1	−2	0.148	0.324	0.000	0.000	0.000	0.008	0.996
Concentration [−]	2	−110	0.223	0.359	0.000	0.000	0.003	0.201	0.964
Concentration [−]	2	−102	0.179	0.311	0.000	0.000	0.003	0.201	0.964
Concentration [−]	2	−9.5	0.323	0.389	0.000	0.001	0.082	0.711	0.998
Concentration [−]	2	−2	0.082	0.204	0.000	0.000	0.000	0.019	0.634
Concentration [−]	3	−110	0.274	0.400	0.000	0.000	0.000	0.662	0.994
Concentration [−]	3	−102	0.288	0.390	0.000	0.000	0.008	0.665	0.991
Concentration [−]	3	−9.5	0.316	0.400	0.000	0.000	0.032	0.748	0.997
Concentration [−]	3	−2	0.149	0.301	0.000	0.000	0.000	0.073	0.962

[1)] Arithmetic mean for concentration expressed in mass fraction [−].
[2)] Percentile at 50 %: e.g. for case 1, 50 % of the concentration values are below 0.001.

Table 7-4. Cases 1, 4, 5: statistics of glacial meltwater concentration at 500 m depth (entire domain).

Performance Measure	Case	Time step [ka]	Mean[1)] [−]	Standard deviation	P5	P25	P50[2)]	P75	P95
Concentration [−]	1	−110	0.376	0.460	0.000	0.000	0.001	0.996	1.000
Concentration [−]	1	−102	0.394	0.455	0.000	0.000	0.022	0.989	1.000
Concentration [−]	1	−9.5	0.379	0.451	0.000	0.000	0.013	0.981	1.000
Concentration [−]	1	−2	0.148	0.324	0.000	0.000	0.000	0.008	0.996
Concentration [−]	4	−110	0.376	0.459	0.000	0.000	0.002	0.996	1.000
Concentration [−]	4	−102	0.386	0.452	0.000	0.000	0.020	0.984	1.000
Concentration [−]	4	−9.5	0.372	0.448	0.000	0.000	0.012	0.975	1.000
Concentration [−]	4	−2	0.214	0.378	0.000	0.000	0.000	0.202	0.999
Concentration [−]	5	−110	0.354	0.450	0.000	0.000	0.001	0.983	1.000
Concentration [−]	5	−102	0.396	0.454	0.000	0.000	0.029	0.987	1.000
Concentration [−]	5	−9.5	0.398	0.453	0.000	0.000	0.043	0.986	1.000
Concentration [−]	5	−2	0.127	0.299	0.000	0.000	0.000	0.004	0.986

[1)] Arithmetic mean for concentration expressed in mass fraction [−].
[2)] Percentile at 50 %: e.g. for case 1, 50 % of the concentration values are below 0.001.

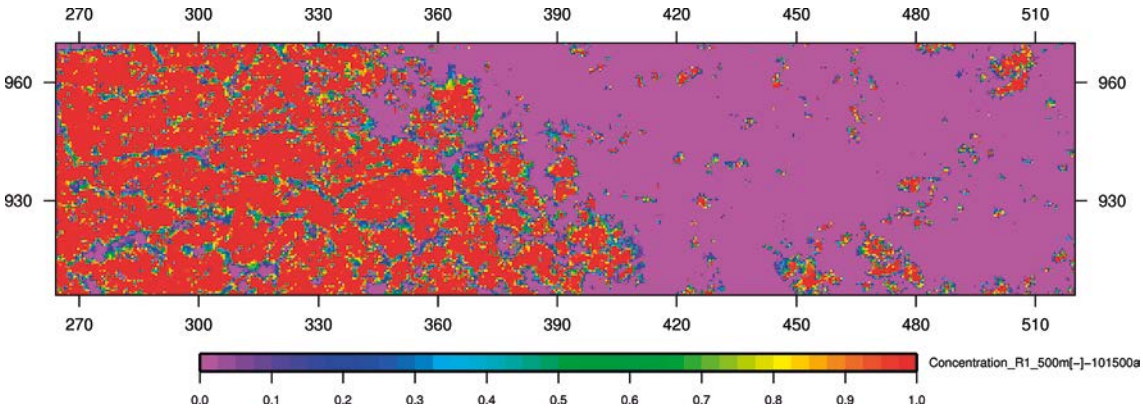

Figure 7-22. *Case 1: glacial meltwater concentration (expressed in mass fraction [−]) at −102 ka, after 500 years of transport,* ***period of glacial completeness****, projected horizontal cut at 500 meter depth (coordinates in km).*

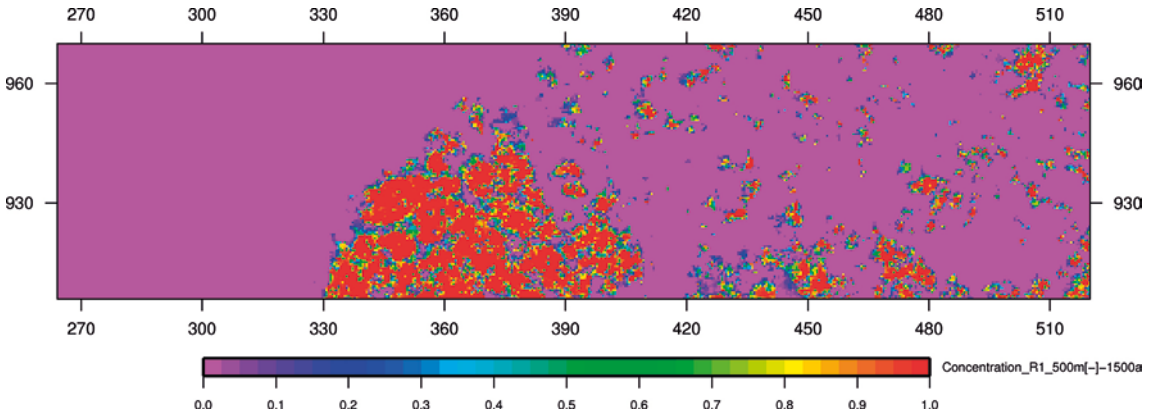

Figure 7-23. *Case 1: glacial meltwater concentration (expressed in mass fraction [−]) at −2 ka, after 500 years of transport,* ***period of glacial retrea****t, projected horizontal cut at 500 meter depth (coordinates in km).*

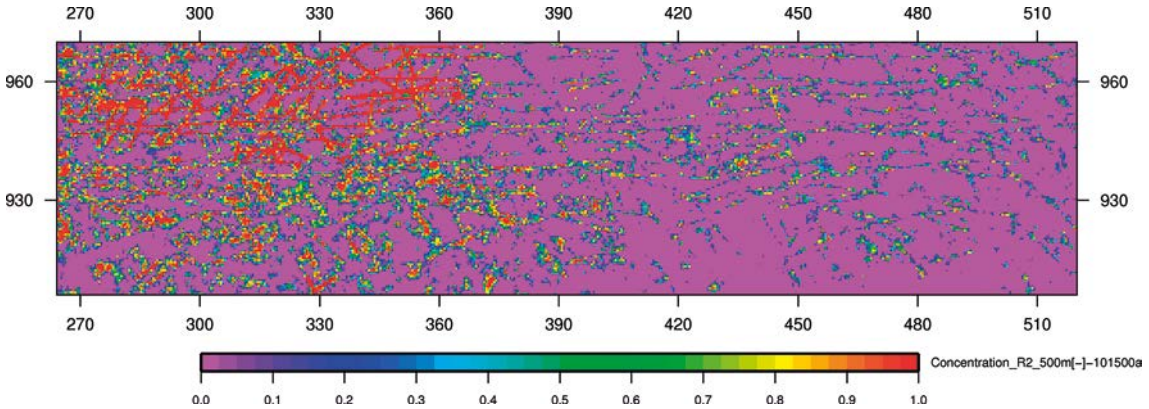

Figure 7-24. *Case 2: glacial meltwater concentration (expressed in mass fraction [−]) at −102 ka, after 500 years of transport,* ***period of glacial completeness****, projected horizontal cut at 500 meter depth (coordinates in km).*

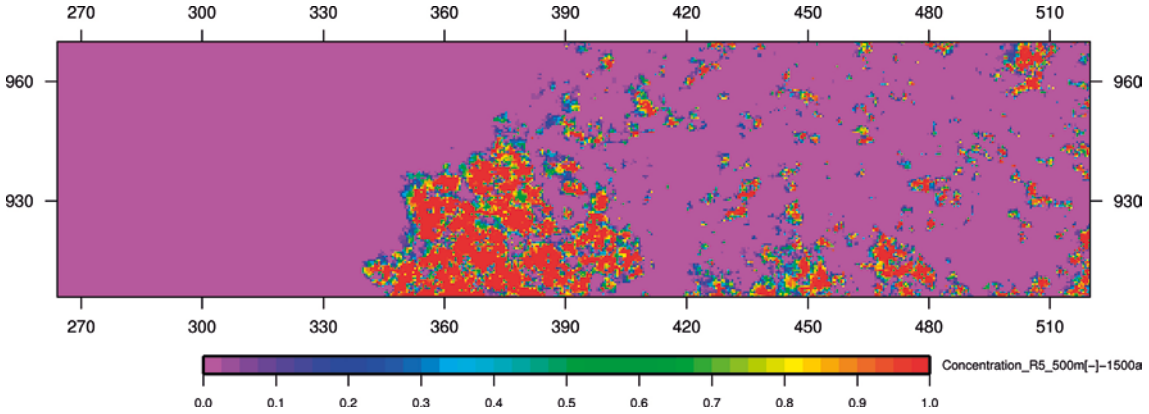

Figure 7-25. *Case 5: glacial meltwater concentration (expressed in mass fraction [−]) at −2 ka, after 500 years of transport,* ***period of glacial retreat****, projected horizontal cut at 500 meter depth (coordinates in km).*

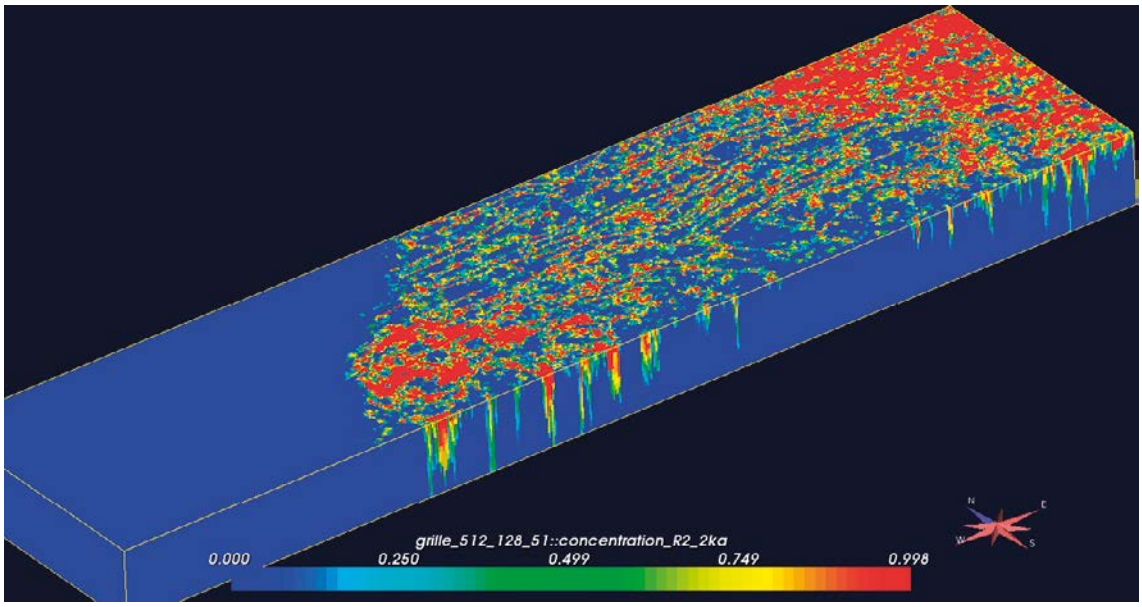

Figure 7-26. *Case 2: glacial meltwater concentration (expressed in mass fraction [−]) at −2 ka, after 500 years of transport,* ***period of glacial retreat****, model top at −55 meter elevation. The high concentration values in the NE are due to a topographic effect; i.e. the elevation values of the bedrock are close to zero and shallow depth values are encountered in the NE part of the domain.*

7.4 Concentration of glacial meltwater at taliks

The mean value of glacial meltwater concentration, estimated at each talik after 500 years, is obtained for all the five cases, using the following two time steps for which the ice sheet covers only part of the domain: −113 ka (glacial build up) and −7.5 ka (glacial retreat), and corresponding to climatic conditions with low temperature (for the areas free of ice) and with taliks close enough to the ice margin so that they can become accessible by meltwater.

The resulting statistics of meltwater concentration are given in Table 7-5. Only the taliks located within a few kilometres of the ice margin are reached by glacial meltwater. The mean value of concentration of glacial meltwater at taliks is systematically larger for the period of glacial retreat, because the hydraulic gradient, related to the increase of ice thickness, becomes stronger for that period (Figures 7-27 and 7-28); and, that leads as well to an augmentation in the number of taliks reached by glacial meltwater.

Table 7-5. Cases 1, 2, 3, 4, 5: statistics of glacial meltwater concentration at taliks.

Performance Measure	Case	Time step [ka]	Mean_t[1] [−]	Standard deviation	P25	P50[2]	P75	P95	n_t[3]
Concentration [−]	1	−113	0.125	0.175	$4.0\cdot10^{-5}$	0.061	0.379	0.379	3.4 (4)
Concentration [−]	1	−7.5	0.441	0.248	$1.2\cdot10^{-6}$	0.542	0.653	0.653	5.3 (6)
Concentration [−]	2	−113	0.287	0.342	$2.8\cdot10^{-2}$	0.057	0.772	0.772	4.2 (5)
Concentration [−]	2	−7.5	0.469	0.261	$2.0\cdot10^{-3}$	0.515	0.698	0.698	5.3 (6)
Concentration [−]	3	−113	0.009	0.006	$7.0\cdot10^{-4}$	0.010	0.015	0.015	3.4 (4)
Concentration [−]	3	−7.5	0.505	0.272	$2.8\cdot10^{-3}$	0.618	0.726	0.726	5.3 (6)
Concentration [−]	4	−113	0.035	0.059	$7.6\cdot10^{-6}$	0.002	0.103	0.103	2.4 (3)
Concentration [−]	4	−7.5	0.236	0.298	$1.6\cdot10^{-4}$	0.076	0.541	0.746	16.1 (14)
Concentration [−]	5	−113	$2.7\cdot10^{-4}$	0.000	$2.7\cdot10^{-4}$	$2.7\cdot10^{-4}$	$2.7\cdot10^{-4}$	$2.7\cdot10^{-4}$	0.8 (1)
Concentration [−]	5	−7.5	0.333	0.282	$3.9\cdot10^{-2}$	0.303	0.623	0.716	6.8 (8)

[1] Mean_t: mean value of taliks concentration with values greater or equal to 10^{-6}, where the concentration is expressed in mass fraction [−].

[2] Percentile at 50 %: e.g. for case 1, 50 % of the concentration values are below 0.061.

[3] Percentage of taliks with concentration greater or equal to 10^{-6}; with the number of taliks in ().

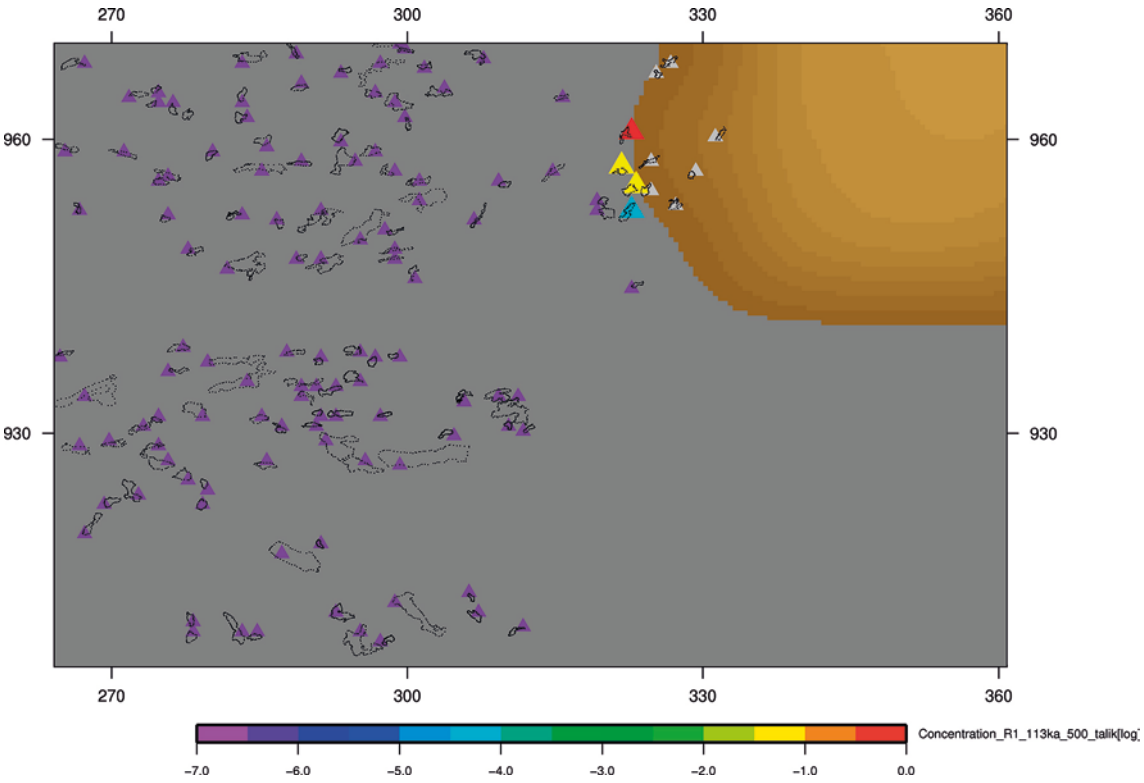

Figure 7-27. *Case 1: glacial meltwater concentration at talik (expressed in log [mass fraction]) at −113 ka, after 500 years of transport,* ***period of glacial build up****, projected top horizontal cut (coordinates in km); brown colours depict ice location and thickness. The taliks underneath the ice sheet are marked with a grey triangle and are excluded from the statistics.*

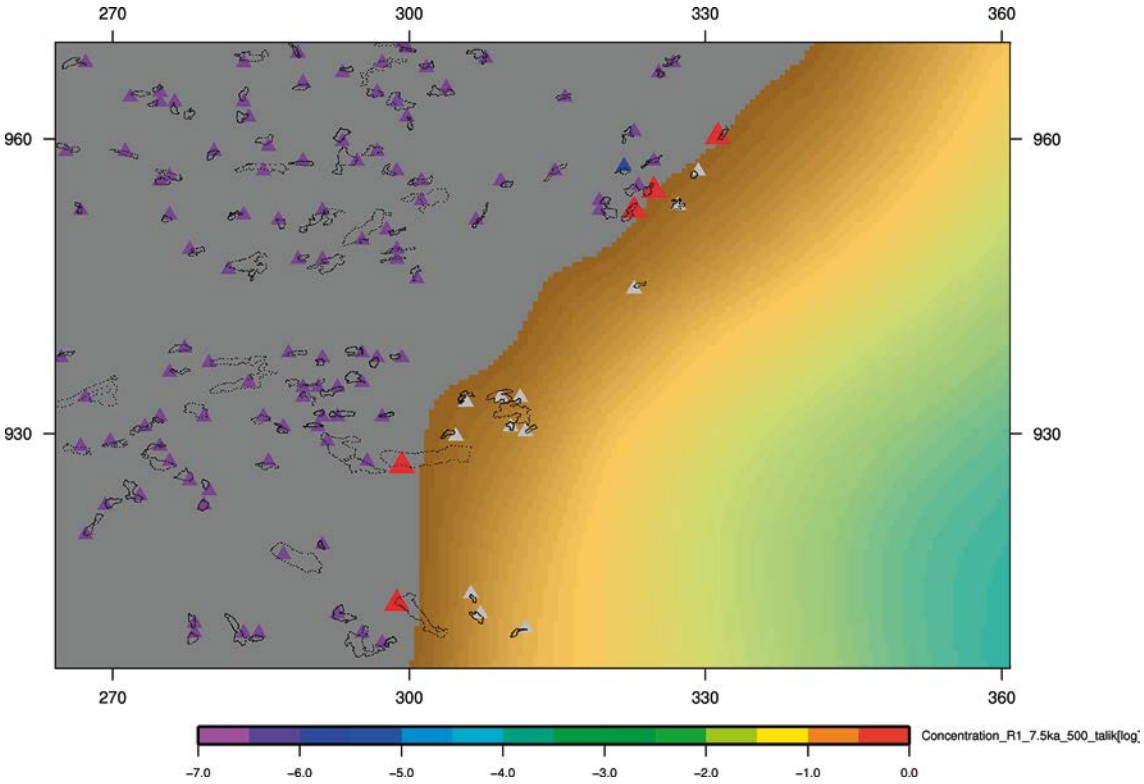

Figure 7-28. *Case 1: glacial meltwater concentration at talik (expressed in log [mass fraction]) at −7.5 ka, after 500 years of transport,* ***period of glacial retreat****, projected top horizontal cut (coordinates in km); brown colours depict ice location and thickness. The taliks underneath the ice sheet are marked with a grey triangle and are excluded from the statistics.*

Cases 2 and 3, when compared to the case 1, present similar talik results during the period of glacial retreat; some differences appears for the period of glacial build up, likely explained by their differences in hydraulic conductivity in the top layers (cf. Tables 5-1, 5-2 and 5-3). Finally, the variation in the number of taliks reached by glacial meltwater observed for cases 4 and 5, in comparison to the case 1, is related to the location of the ice margin (Figure 7-29 and cf. Figure 28; with a position for the ice margin located about 20 km further west for case 4 in comparison to the case 1); due to changes in the displacement velocity of the ice sheet, depending on the glaciation scenario. For case 5, the "Talik Lake" is close enough to the ice margin to be reached by glacial meltwater (Figure 7-30).

For the periods of glacial build up and retreat, the mean value of glacial meltwater concentration estimated at taliks lies in the range 2.7×10^{-4}–0.505; the percentage of taliks observed with glacial meltwater is between 1 and 16 % for the investigated domain during these periods (cf. Table 7-5).

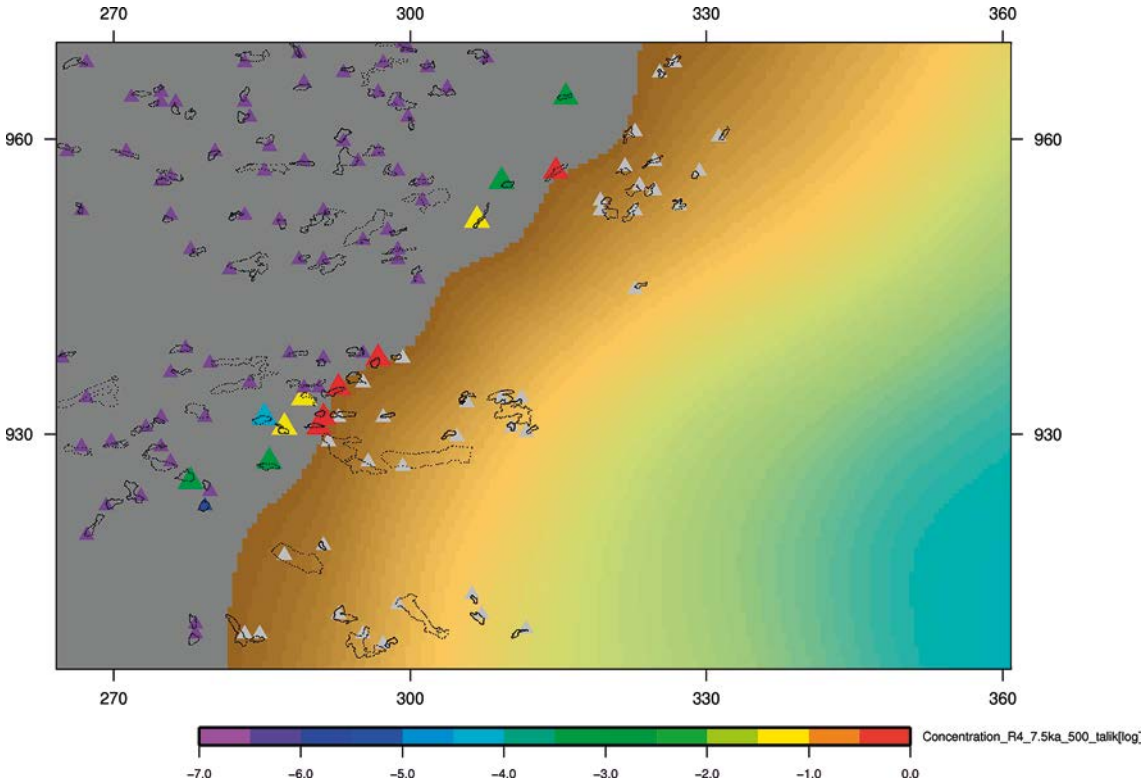

Figure 7-29. *Case 4: glacial meltwater concentration at talik (expressed in log [mass fraction]) at −7.5 ka, after 500 years of transport,* ***period of glacial retreat****, projected top horizontal cut (coordinates in km); brown colours depict ice location and thickness. The taliks underneath the ice sheet are marked with a grey triangle and are excluded from the statistics.*

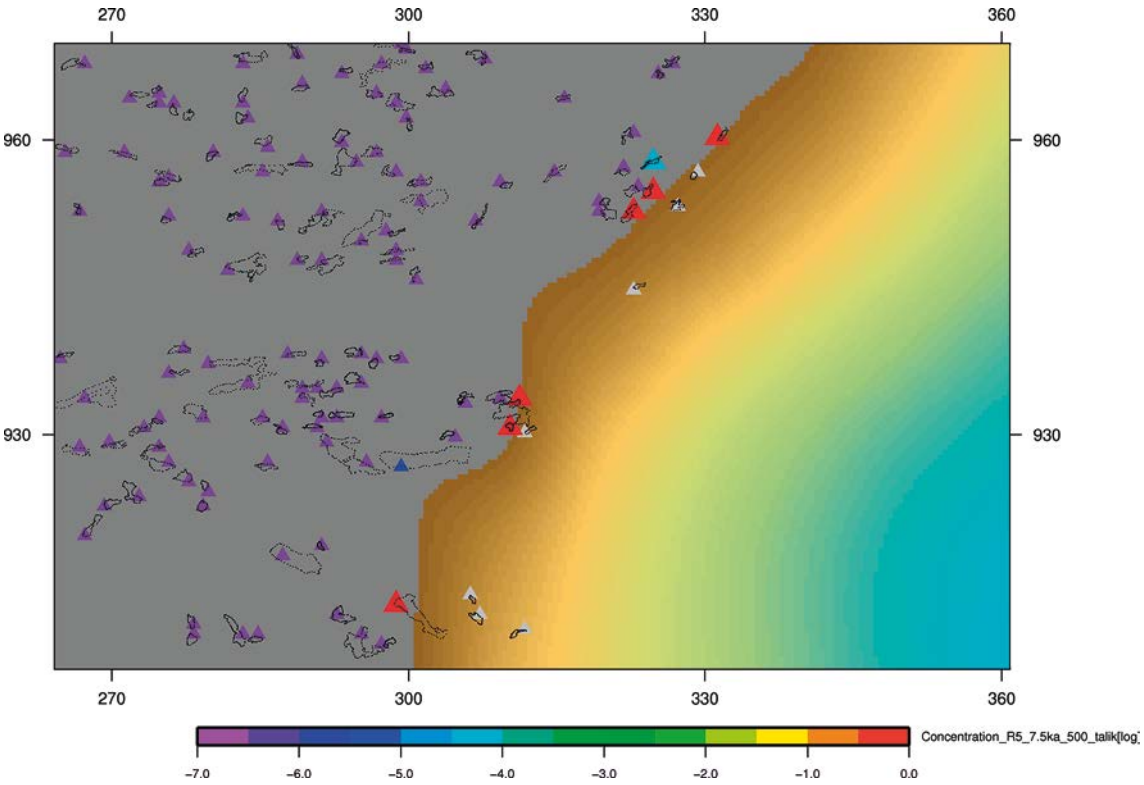

Figure 7-30. *Case 5: glacial meltwater concentration at talik (expressed in log [mass fraction]) at −7.5 ka, after 500 years of transport,* ***period of glacial retreat****, projected top horizontal cut (coordinates in km); brown colours depict ice location and thickness. The taliks underneath the ice sheet are marked with a grey triangle and are excluded from the statistics.*

8 Summary, conclusions, recommendations and perspectives

Within the framework of the GAP project, this third phase of groundwater flow modelling under transient ice sheet conditions in Greenland has enabled the assimilation of transient data from dynamic ice sheet modelling into the simulations over time frames relevant to safety assessment. Modelling density-driven groundwater flow, heat transfer and permafrost using transient boundary conditions representing ice sheet displacement was performed during a complete glacial cycle (from −115 to −1 ka before 2000 AD) in Greenland. Detailed subglacial topography, subglacial layer, deformation zones, borehole data and talik location were integrated in the model.

The geological medium with conductive deformation zones was modelled as a 3D continuum with stochastically generated hydraulic properties. Using glaciological concepts and GAP data: seismic reflection, ice borehole data and the GAP DEM for the bedrock topography, a stochastic model was developed for the geometric and hydraulic description of the permeable subglacial layer. The density-driven groundwater flow system is considered to be governed by infiltration of glacial meltwater in heterogeneous faulted crystalline rocks in the presence of permafrost and taliks. The characterisation of the permafrost-depth distribution was achieved using a coupled description of flow and heat transfer under transient conditions. A complete glacial cycle was considered with periods of glacial build up, completeness and retreat: ice thickness and basal temperatures – provided by the dynamic ice sheet model SICOPOLIS – were assimilated as boundary conditions into the groundwater flow model.

The major improvements are related to the capabilities of assimilating ice sheet modelling data into a density driven groundwater flow model with heat transfer at time scales relevant to safety assessment. For the first time, the choice for the subglacial boundary conditions, i.e. as basal hydraulic pressure, could be justified by field data provided by ice boreholes drilled in the Greenland ice sheet during the GAP project.

The impact of various hydraulic parameterisations for the rock domain and deformation zones was investigated based on data from three sites located in the Fennoscandian shield (Laxemar, Forsmark and Olkiluoto); and, as well as the effect of specific glaciation scenarios given by the dynamic ice sheet model. The tracing of meltwater from the ice sheet was modelled in order to determine the depth range likely reachable by glacial meltwater for the various sensitivity cases. The key findings of this modelling phase, in relation to major impacts and performance measures, are given below.

8.1 Major impacts

The periods of glacial build up and retreat of the ice sheet lead to an increase in the regional hydraulic gradient that could likely become stronger during glacial retreat, due to the rapid displacement of the ice sheet towards the east. The periglacial and the subglacial topography (i.e. hills and troughs) strongly influences the flow field in the western part of the modelled domain. The subglacial layer plays a key hydraulic role in draining meltwater underneath the ice sheet; and below the surface, groundwater flow is governed by the hydraulic parametrisation of the rock domain, the deformation zones and the permafrost. Because of its higher value hydraulic parametrisation, the case 1 (Laxamar) is remarkably different from cases 2 and 3 related respectively to the Forsmark and Olkiluoto sites, particularly in terms of the concentration of glacial meltwater at 500 m depth. Some subglacial permafrost remains during the periods of glacial build up, completeness and retreat. The distribution of salinity is mainly influenced after the period of glacial build up, less during the period of retreat; and it is driven by the hydraulic properties and enhanced by the western steeper topography. The mean surface Darcy velocity increases about 3–4 orders of magnitude during glacial periods, but decreases by several orders of magnitude at 500 m depth. The lowest Darcy velocities values at a depth of 500 m are found for the Forsmark analogue. Glacial meltwater is likely to reach depths that exceed 500 m whatever the glacial period considered. During the periods of glacial build and retreat, solely the taliks located within a few kilometres of the ice margin can be reached by glacial meltwater; i.e. the taliks located further away cannot be attained by glacial meltwater.

8.2 Fluxes

Whatever the glacial period considered, for the Forsmark and Olkiluoto cases, the flux values remains below 10 mm/a at depth (below an elevation of -300 m). The flux is sensitive to the hydraulic conductivity field (cf. Laxemar case with higher flux values at depth); but it is not sensitive to variations in boundary conditions given by the ice sheet model; i.e. to the various glaciation scenarios considered for the glacial cycle.

The recharge at depth is influenced by the type of glacial boundary conditions selected; i.e. dynamic fluid pressure versus meltwater rate. However, for most situations, the application of dynamic fluid pressure boundary conditions, based on ice overburden hydraulic pressure is justified; in particular, for present day conditions (in Greenland), as shown by the GAP observations and conceptual considerations. But care should be taken, when a full glacial cycle is under consideration, since dynamic fluid boundary conditions are likely to provide overestimation of recharge at depth, in particular for glacial periods with limited water supply.

8.3 Depth of permafrost

The mean depth of permafrost lies in the range 509–617 m when only a part of the domain is recovered by the ice sheet during the periods of glacial build up and retreat. The depth of permafrost appears to be slightly sensitive to the hydraulic conductivity field and sometimes to the glacial period. The depth range obtained for the permafrost is higher than that found in the GAP boreholes (350–400 m); but, the comparison is not straightforward since the modelling was performed using temperature data from a time series ending at −1 ka before 2000 AD.

During the period of glacial completeness, permafrost can partially remain underneath the ice sheet or even totally disappear for a short duration. During the period of glacial retreat, the permafrost is likely to disappear in ca. 1 000 years, depending on climatic conditions. In case of adequate temperature conditions, the permafrost can remain under the ice sheet close to the ice margin; and, it can likely stretch up to tens of kilometres under the ice sheet.

8.4 Concentration of glacial meltwater at 500 m depth

Glacial meltwater is likely to reach depths that exceed 500 m whatever the glacial period considered. These results are in accordance with the findings of the GAP project (Claesson Liljedahl et al. 2016). The mean value for the concentration of glacial meltwater evaluated at the depth of 500 m is sensitive to the glacial periods and the hydraulic conductivity field. The mean value for glacial meltwater concentration ranges from 0.082 to 0.398 at 500 m depth. The lowest mean values for the meltwater concentration were estimated for the Forsmark case; and the highest values with the Laxemar hydraulic parametrisation.

8.5 Concentration of glacial meltwater at taliks

Only the taliks located within a few kilometres of the ice margin can be reached by the glacial meltwater produced by the ice sheet. Larger mean values of concentration are obtained for the period of glacial retreat, as well as an augmentation in the number of taliks reached by glacial meltwater; the "Talik Lake" can be reached by glacial meltwater (Johansson et al. 2015). For the periods of glacial build up and retreat, the mean value of glacial meltwater concentration estimated at taliks lies in the range $2.7 \cdot 10^{-4}$–0.505; and, the percentage of taliks with glacial meltwater is between 1 and 16 %.

8.6 Assumptions

The present study is founded on several assumptions related to the conceptual model, the data and the groundwater flow model. A list of the key assumptions made is given below.

Conceptual assumptions

The conceptual assumptions undertaken for the groundwater flow modelling are the following:

- The geological medium is considered as a 3D stochastic continuum with conductive deformation zones.
- The horizontal deformation zones are described by horizontal patches of a few square kilometres in size; the number of horizontal patches decreases with depth; and, the value of their hydraulic conductivity is increased by a factor 10, in comparison to its previous value related to the rock mass domain.
- The subglacial layer is considered as a discontinuous permeable layer in melted state, located at the bedrock/ ice interface, likely to exist within the major troughs underneath the ice sheet. Its spatial distribution in terms of geometry and hydraulic properties controls subglacial drainage. The subglacial layer potentially plays a major hydraulic contribution in carrying meltwater infiltrating in the subsurface. Its description in the central and eastern parts of the domain is achieved using a stochastic model.
- The transient surface boundary conditions (ice thickness and temperature) for the groundwater flow model are taken from a dynamic ice sheet model. The movement of the ice sheet – involving glacial build up and retreat – is therefore taken into account.
- The groundwater flow system is considered under transient conditions and governed by infiltration of glacial meltwater in heterogeneous faulted crystalline rocks in the presence of permafrost.
- The spatial variability of the permafrost is described using subglacial temperature boundary conditions – given by the dynamic ice sheet model –, the groundwater flow system and the geothermal flux from the Earth interior. Surface cover effects, such as vegetation and snow cover, likely to increase the ground temperature were neglected. The evolution of permafrost is described by neglecting latent heat effects. Hydraulic conductivity and porosity are related to the proportion of ice in the pore space. No dependence is assumed between the dynamic viscosity of water and the temperature. During period of glacial build up, depending on the climatic conditions the permafrost is continuous in the periglacial environment, except at the location of the taliks. Beneath the ice sheet, some permafrost regions can likely occur depending on the temperature conditions underneath the ice sheet, in particular during the periods of glacial build up and completeness.
- Density-driven flow as induced by the variable salinity of the groundwater is taken into account. The influence of the far away ocean is neglected; i.e. there are no fluctuations in ocean level as well as no supply of salt from the Davis Strait.
- The impact of the ice sheet loading in terms of rock deformation leading to variations in porosity, hydraulic conductivity and pore pressure is not included in the present modelling approach.
- Two types of water are distinguished: glacial meltwater produced by the ice sheet and groundwater circulating at depth under density-driven flow conditions. The description of the medium heterogeneity in terms of a stochastic continuum enables the characterisation of the spatial variability for the fluid velocity and therefore captures the effects of kinematic dispersion. The effects of matrix diffusion were not considered.

Data assumptions

The assumptions related to the data are as follows:

- Bedrock elevation and ice thickness are described using the GAP DEM with various data resolution: 30 m (west of the ice margin), 250–500m (underneath the ice sheet; east of the ice margin), 1 km (underneath the ice sheet; eastern part of the domain). All lakes with a size similar or greater than the "Talik lake" are considered as a potential talik in the groundwater flow model. The description of the perimeter and surface elevation of these through taliks was obtained using satellite data.
- The current topography, given by the GAP DEM, is taken as constant for the complete glacial cycle.
- The observed potential deformation zones are extrapolated under the subglacial domain of the groundwater flow model.

- The hydraulic properties for the rock domain and the deformation zones are taken from sites in the Fennoscandian shield (Laxemar, Forsmark and Olkiluoto). The hydraulic conductivity of the rock domain is assumed to follow a log-normal distribution with an anisotropic exponential variogram. The correlation scale is assumed to remain constant for the five hydrogeological units considered.
- The temperature values applied as surface boundary conditions in the absence of the ice sheet are taken from ice core data from central-Greenland.
- The geothermal heat flux value taken from the borehole DH-GAP03 is assumed as a constant value and therefore is not spatially variable.
- The initial salinity conditions are extracted from three sites (Laxemar, Forsmark and Olkiluoto).

Model assumptions

The assumptions related to the model are given below:

- The discretisation is performed using an unstructured Cartesian grid system. The grid resolution is 500 m in the horizontal directions. The discretisation in the vertical direction varies between 25, 50 or 100 m when approaching the topographic surface. The model contains about 4 338 000 cells.
- The numerical resolution of the heat transfer, flow, salt transport and equations is weakly coupled by linearising the equations. At each iteration, the simulation is carried out as follows: (a) solving of heat transfer under permafrost conditions, then modifications of hydraulic conductivity and porosity according to the temperature field, (b) solving of flow with update of density according to salinity, and (c) solving of salt transport. For each time step, this iterative procedure is repeated sequentially; and, then stopped when the values for the convergence criteria are reached for the time step.
- The use of transient prescribed pressure and temperature boundary conditions to describe respectively flow and temperature effects of the ice sheet and its displacement on the groundwater flow model. For the lateral west boundary of the model, hydrostatic boundary conditions are set to a given surface elevation. No flow conditions are applied for the other lateral boundaries of the model.
- The characterisation of the proportion of ice in the pore space as function of the temperature is described using an exponential function.

Among the various assumptions cited above, the ones that were analysed and tested using the different model cases are the following:

- The use of transient boundary conditions, taken from a dynamic ice sheet model, for the groundwater flow model.
- The application of dynamic fluid pressure, meltwater rate and temperature as prescribed boundary conditions for the hydrogeological description of the ice-bedrock boundary.
- The simulation of permafrost with simplified physics and its consequences on the modelling results.
- The use of various hydraulic parameterisations for the rock domain and deformation zones.
- The application of three glaciation scenarios, given by the dynamic ice sheet model, providing different boundary conditions for the groundwater flow modelling.
- The tracing of glacial meltwater by distinguishing two types of water for the evaluation of the penetration depth and the concentration of glacial meltwater.

Sources of uncertainty

Confidence improvement in relation to the assessment of performance measures requires reduction of uncertainty. Therefore, the following sources of uncertainty need to be improved in terms of their characterisation:

1. The coarse resolution topography underneath the ice sheet eastward; it cannot capture the likely existing troughs.
2. The spatial distribution of the subglacial layer in terms of geometry and hydraulic properties, and consequently, its hydraulic contribution in carrying meltwater infiltrating in the subsurface.
3. The description of the permafrost evolution, modelled using simplified physics.
4. The spatial variability of the geothermal heat flux that may exist at the scale of the investigated domain.
5. The lack of data from the three sites (Laxemar, Forsmark, Olkiluoto) at depths below 1 000 m leading to additional uncertainty in relation to the characterisation of the hydraulic properties for the rock domain and deformation zones at these depths.
6. The variability of the glaciation scenarios provided by different dynamic ice sheet models (e.g. a sensitivity analysis in relation to extreme climatic scenarios). The low spatial and temporal resolution of the results from ice sheet models.
7. In terms of phenomenology, the impact of matrix diffusion and hydro-mechanical couplings.

8.7 Future work

Therefore future modelling, driven by the aim of reducing uncertainty, should address the following topics.

Integration of post-GAP data

Data acquisition will be continued beyond the duration of the GAP project, in case of relevance for the groundwater flow model, these data should be integrated in the model in order to assess their impact on the performance measures.

Fennoscandian groundwater flow modelling

The new findings of the GAP project should be integrated into groundwater flow models under ice sheet conditions during a complete glacial cycle for the sites in Sweden and Finland.

Permafrost characterisation

The description of the formation/ melting of the permafrost, using more detailed physics together with a spatially variable geothermal heat flux is needed in order to simulate its impact on the groundwater flow patterns and the resulting performance measures.

Phenomenology

Matrix diffusion needs to be included as a retardation process likely to influence the penetration depth of meltwater. In addition, the importance of hydro-mechanical couplings needs to be evaluated with respect to their consequences on the modelling results.

The presented groundwater flow calculations constitute the third modelling phase with progress towards data integration and groundwater flow system understanding under realistic transient ice sheet conditions during a complete glacial cycle in Greenland. This groundwater flow modelling phase constitutes a well founded base for future modelling issues aiming at the reduction of the uncertainty associated with performance measures.

References

SKB's (Svensk Kärnbränslehantering AB) publications can be found at www.skb.com/publications.

Applegate P J, Kirchner N, Stone E J, Keller K, Greve R, 2012. An assessment of key model parametric uncertainties in projections of Greenland Ice Sheet behavior. The Cryosphere 6, 589–606.

ASTER, 2009. ASTER GDEM Readme file – ASTER GDEM Version 1. Available at: http://www.cz/images/upload/6fbe0_aster-gdem-readme-ev1-dot-0.pdf

Bamber J L, 2001. Greenland 5 km DEM, ice thickness, and bedrock elevation grids, version 1. Boulder, CO: NASA National Snow and Ice Data Center Distributed Active Archive Center. doi:10.5067/01A10Z9BM7KP

Bamber J L, Griggs J A, Hurkmans R T W L, Dowdeswell J A, Gogineni S P, Howat I, Mouginot J, Paden J, Palmer S, Rignot E, Steinhage D, 2013. A new bed elevation dataset for Greenland. The Cryosphere 7, 499–510.

Bartholomew I, Nienow P, Sole A, Mair D, Cowton T, King M A, 2012. Short-term variability in Greenland Ice Sheet motion forced by time-varying meltwater drainage: implications for the relationship between subglacial drainage system behavior and ice velocity. Journal of Geophysical Research 117, F03002. doi:10.1029/2011JF002220

Booth A D, Clark R A, Kulessa B, Murray T, Carter J, Doyle S, Hubbard A, 2012. Thin-layer effects in glaciological seismic amplitude-versus-angle (AVA) analysis: Implications for characterising a subglacial till unit, Russell Glacier, West Greenland. The Cryosphere 6, 909–922.

Brinkerhoff D J, Johnson J V, 2013. Data assimilation and prognostic whole ice sheet modelling with the variationally derived, higher order, open source, and fully parallel ice sheet model VarGlaS. The Cryosphere 7, 1161–1184.

Brinkerhoff D J, Meierbachtol T W, Johnson J V, Harper J T, 2011. Sensitivity of the frozen/melted basal boundary to perturbations of basal traction and geothermal heat flux: Isunnguata Sermia, western Greenland. Annals of Glaciology 52, 43–50.

Chen J L, Wilson C R , Tapley B D, 2006. Satellite gravity measurements confirm accelerated melting of Greenland ice sheet. Science 313, 1958–1960.

Chilès J-P, Delfiner P, 2012. Geostatistics: modeling spatial uncertainty. 2nd ed. Hoboken, NJ: Wiley.

Claesson Liljedahl L, Kontula A, Harper J, Näslund J-O, Selroos J-O, Pitkänen P, Puigdomenech I, Hobbs M, Follin S, Hirschorn S, Jansson P, Kennell L, Marcos N, Ruskeeniemi T, Tullborg E-L, Vidstrand P, 2016. The Greenland Analogue Project: Final report. SKB TR-14-13, Svensk Kärnbränslehantering AB.

Cuffey K M, Paterson W S B, 2010. The physics of glaciers. 4th rev. ed. Amsterdam: Butterworth-Heinemann.

Dansgaard W, Johnsen S J, Clausen H B, Dahl-Jensen D, Gundestrup N S, Hammer C U, Hvidberg C S, Steffensen J P, Sveinbjörnsdóttir A E, Jouzel J, Bond G, 1993. Evidence for general instability of past climate from a 250-kyr ice-core record. Nature 364, 218–220.

Dow C F, Hubbard A, Booth A D, Doyle S H, Gusmeroli A, Kulessa B, 2013. Seismic evidence of mechanically weak sediments underlying Russell Glacier, West Greenland. Annals of Glaciology 54, 135–141.

Emery X, 2004. Testing the correctness of the sequential algorithm for simulating Gaussian random fields. Stochastic Environmental Research and Risk Assessment 18, 401–413.

Emery X, Lantuéjoul C, 2006. TBSIM: A computer program for conditional simulation of three-dimensional Gaussian random fields via the turning bands method. Computers & Geosciences 32, 1615–1628.

Engström J, Paananen M, Klint K E, 2012. The Greenland Analogue Project. Geomodel version 1 of the Kangerlussuaq area on Western Greenland. SKB P-11-38, Svensk Kärnbränslehantering AB.

Fausto R S, Ahlstrøm A P, van As D, Bøggild C E, Johnsen S J, 2009. A new present-day temperature parametrisation for Greenland. Journal of Glaciology 55, 95-105.

Ferry M, 2016. DarcyTools – Ice model. TR-16114. MFDRC. SKBdoc 1875709 ver 1.0, Svensk Kärnbränslehantering AB.

Follin S, Stigsson M, Rhén I, Engström J, Klint K E, 2011. Greenland Analogue Project – Hydraulic properties of deformation zones and fracture domains at Forsmark, Laxemar and Olkiluoto for usage together with Geomodel version 1. SKB P-11-26, Svensk Kärnbränslehantering AB.

Greve R, Blatter H, 2009. Dynamics of ice sheets and glaciers. Berlin: Springer.

Greve R, Weis M, Hutter K, 1998. Palaeoclimatic evolution and present conditions of the Greenland ice sheet in the vicinity of Summit: an approach by large-scale modelling. Palaeoclimates 2, 133–161.

Greve R, Saito F, Abe-Ouchi A, 2011. Initial results of the SeaRISE numerical experiments with the models SICOPOLIS and IcIES for the Greenland ice sheet. Annals of Glaciology 52, 23–30.

Gow A J, Meese D A, 1996. Nature of basal debris in the GISP2 and Byrd ice cores and its relevance to bed processes. Annals of Glaciology 22, 134–140.

Harper J, Hubbard A, Ruskeeniemi T, Claesson Liljedahl L, Kontula A, Hobbs M, Brown J, Dirkson A, Dow C, Doyle S, Drake H, Engström J, Fitzpatrick A, Follin S, Frape S, Graly J, Hansson K, Harrington J, Henkemans E, Hirschorn S, Humphrey N, Jansson P, Johnson J, Jones G, Kinnbom P, Kennell L, Klint K E, Liimatainen J, Lindbäck K, Meierbachtol T, Pere T, Pettersson R, Tullborg E-L, van As D, 2016. The Greenland Analogue Project: Data and processes. SKB R-14-13, Svensk Kärnbränslehantering AB.

Harper J T, Humphrey N F, Meierbachtol T W, Graly J A, Fischer U H, 2017. Borehole measurements indicate hard bed conditions, Kangerlussuaq sector, western Greenland Ice Sheet. Journal of Geophysical Research: Earth Surface 122, 1605–1618.

Harrington J A, Humphrey N F, Harper J T, 2015. Temperature distribution and thermal anomalies along a flowline of the Greenland ice sheet. Annals of Glaciology 56, 98–104.

Hartikainen J, Kouhia R, Wallroth T, 2010. Permafrost simulations at Forsmark using a numerical 2D thermo-hydro-chemical model. SKB TR-09-17, Svensk Kärnbränslehantering AB.

Hellä P, Pikänen P, Löfman J, Partamies S, Vuorinen U, Wersin P, 2014. Safety case for the disposal of spent nuclear fuel at Olkiluoto – Definition of reference and bounding groundwaters, buffer and backfill porewaters. Posiva Report 2014-04, Posiva Oy, Finland.

Henriksen N, Higgins A K, Kalsbeek F, Pulvertaft T C R, 2000. Greenland from Archean to Quaternary: Descriptive text to the geological map of Greenland, 1:2 500 000. Geology of Greenland Survey Bulletin 185.

Hewitt I J, 2013. Seasonal changes in ice sheet motion due to melt water lubrication. Earth and Planetary Science Letters 371–372, 16–25.

Hills B H, Harper J T, Meierbachtol T W, Humphrey N F, Johnson J V, 2016. Modeling heat transfer to explain observed temperature anomalies in near-surface ice, Greenland Ice Sheet ablation area. Abstract C31C-08 presented at AGU Fall Meeting, San Francisco, CA, 12–16 December 2016.

Howat I M, Joughin I, Tulaczyk S, Gogineni S, 2005. Rapid retreat and acceleration of Helheim Glacier, east Greenland. Geophysical Research Letters 32, L22502. doi:10.1029/2005GL024737

Howat I M, Negrete A, Smith B E, 2014. The Greenland Ice Mapping Project (GIMP) land classification and surface elevation data sets. The Cryosphere 8, 1509–1518.

Hutter K, 1983. Theoretical glaciology: material science of ice and the mechanics of glaciers and ice sheets. Dordrecht: D. Reidel; Tokyo: Terra Scientific.

Jaquet O, 1998. Modèle stochastique de la géométrie des réseaux karstiques. PhD thesis. Lausanne University.

Jaquet O, Namar R, Jansson P, 2010. Groundwater flow modelling under ice sheet conditions. Scoping calculations. SKB R-10-46, Svensk Kärnbränslehantering AB.

Jaquet O, Namar R, Siegel P, Jansson P, 2012. Groundwater flow modelling under ice sheet conditions in Greenland (phase II). SKB R-12-14, Svensk Kärnbränslehantering AB.

Jarvis G T, Clarke G K C, 1974. Thermal effects of crevassing on Steele Glacier, Yukon Territory, Canada. Journal of Glaciology 13, 243–254.

Johansson E, Gustafsson L-G, Berglund S, Lindborg T, Selroos J-O, Claesson Liljedahl L, Destouni G, 2015. Data evaluation and numerical modeling of hydrological interactions between active layer, lake and talik in a permafrost catchment, Western Greenland. Journal of Hydrology 527, 688–703.

Johnsen S J, Clausen H B, Dansgaard W, Gundestrup N S, Hammer C U, Andersen U, Andersen K K, Hvidberg C S, Dahl-Jensen D, Steffensen J P, Shoji H, Sveinbjörnsdóttir E, White J W, Jouzel J, Fisher D, 1997. The $\delta^{18}O$ record along the Greenland Ice Core project deep ice core and the problem of possible Eemian climatic instability. Journal of Geophysical Research 102, 26397–26410.

Krabill W, Abdalati W, Frederick E, Manizade S, Martin C, Sonntag J, Swift R, Thomas R, Wright W, Yungel J, 2000. Greenland Ice Sheet: High-elevation balance and peripheral thinning. Science 289, 428–430.

Kukkonen I, Kivekäs L, Vuoriainen S, Kääriä M, 2011. Thermal properties of rocks in Olkiluoto: results of laboratory measurements 1994–2010. Posiva Working Report 2011-17, Posiva Oy, Finland.

Lantuéjoul C, 1994. Non conditional simulation of stationary isotropic multigaussian random functions, Geostatistical simulations. In Armstrong M, Dowd P A (eds). Geostatistical simulations: proceedings of the Geostatistical Simulation Workshop, Fontainebleau, France, 27–28 May 1993. Dordrecht: Kluwer Academic,147–177.

Lantuéjoul C, 2002. Geostatistical simulation: models and algorithms. Berlin: Springer.

Lindbäck K, Pettersson R, Doyle S H, Helanow C, Jansson P, Savstrup Kristensen S, Stenseng L, Forsberg R, Hubbard A L, 2014. High-resolution ice thickness and bed topography of a land-terminating section of the Greenland Ice Sheet. Earth System Science Data Discussions 7, 129–148.

Luckman A, Murray T, de Lange R, Hanna E, 2006. Rapid and synchronous ice-dynamic changes in East Greenland. Geophysical Reseearch Letters 33, L03503. doi:10.1029/2005GL025428

Luthcke S B, Zwally H J, Abdalati W, Rowlands D D, Ray R D, Nerem R S, Lemoine F G, McCarthy J J, Chinn D S, 2006. Recent Greenland ice mass loss by drainage system from satellite gravity observations. Science 314, 1286–1289.

Lüthi M, Funk M, Iken A, Gogineni S, Truffer M, 2002. Mechanisms of fast flow in Jakobshavn Isbrae, West Greenland: Part III . Measurements of ice deformation, temperature and cross-borehole conductivity in boreholes to the bedrock. Journal of Glaciology 48, 369–385.

MacGregor J A, Fahnestock M A, Catania G A, Aschwanden A, Clow G D, Colgan W T, Gogineni S P, Morlighem M, Nowicki S M J, Paden J D, Price S F, Seroussi H, 2016. A synthesis of the basal thermal state of the Greenland Ice Sheet. Journal of Geophysical Research: Earth Surface 121, 1328–1350.

Marsily G de, 1981. Hydrogéologie quantitative. Paris : Masson.

Matheron G, 1973. The intrinsic random functions and their applications. Advances in Applied Probability 5, 439–468.

Meierbachtol T, Harper J, Humphrey N T, 2013. Basal drainage system response to increasing surface melt on the Greenland ice sheet. Science 341, 777–779.

Meierbachtol T W, Harper J T, Johnson J V, Humphrey N F, Brinkerhoff D J, 2015. Thermal boundary conditions on western Greenland: Observational constraints and impacts on the modeled thermomechanical state. Journal of Geophysical Research: Earth Surface 120, 623–636.

Meierbachtol T W, Harper J T, Humphrey N F, Wright P J, 2016. Mechanical forcing of water pressure in a hydraulically isolated reach beneath Western Greenland's ablation zone. Annals of Glaciology 57, 62–70.

Morland L W, 1984. Thermomechanical balances of ice sheet flows. Geophysical & Astrophysical Fluid Dynamics 29, 237–266.

Ramillien G, Lombard A, Cazenave A, Ivins E R, Llubes M, Remy F, Biancale R, 2006. Interannual variations of the mass balance of teh Antarctica and Greenland ice shets from GRACE. Global and Planetary Change 53, 198–208.

Rhén I (ed), Gustafson G, Stanfors R, Wikberg P, 1997. Äspö HRL – Geoscientific evaluation 1997/5. Models based on site characterisation 1986–1995. SKB TR-97-06, Svensk Kärnbränslehantering AB.

Rignot E J, Kanagaratnam P, 2006. Changes in the velocity structure of the Greenland ice sheet, Science 311, 986–990.

Rignot E J, Gogineni S P, Krabill W B, Ekholm S, 1997. North and Northeast Greenland ice discharge from satellite radar interferometry. Science 276, 934–937.

Ryser C, Lüthi M P, Andrews L C, Catania G A, Funk M, Hawley R, Hoffman M, Neumann T A, 2014. Caterpillar-like ice motion in the ablation zone of the Greenland ice sheet. Journal of Geophysical Research: Earth Surface 119, 2258–2271.

Schoof C, 2010. Ice-sheet acceleration driven by melt supply variability. Nature 468, 803–806.

SKB, 2006. Climate and climate-related issues for the safety assessment SR-Can. SKB TR-06-23, Svensk Kärnbränslehantering AB.

SKB, 2014. Climate and climate-related issues for the safety assessment SR-PSU. SKB TR-13-05, Svensk Kärnbränslehantering AB.

Smellie J (ed), Pitkänen P, Koskinen L, Aaltonen I, Eichinger F, Waber N, Sahlstedt E, Siitari-Kauppi M, Karhu J, Löfman J, Poteri A, 2014. Evolution of the Olkiluoto Site: Palaeohydrogeochemical considerations. Posiva Working Report 2014-27, Posiva Oy, Finland.

Sundal A V, Shepherd A, Nienow P, Hanna E, Palmer S, Huybrechts P, 2011. Melt-induced speed-up of Greenland ice sheet offset by efficient subglacial drainage. Nature 469, 521–524.

Svensson U, Ferry M, 2010. DarcyTools version 3.4. User's guide. SKB R-10-72, Svensk Kärnbränslehantering AB.

Svensson U, Ferry M, Kuylenstierna H-O, 2010. DarcyTools version 3.4 – Concepts, methods and equations. SKB R-07-38, Svensk Kärnbränslehantering AB.

Vallot D, Applegate P, Kirchner N, Petterson R, 2012a. Preliminary report from the Ice Sheet Modeling Group, Stockholm University, to SKB: Identifying ice sheet model runs for possible use as input into hydrologic modeling of the area near the GAP borehole, Kangerlussuaq, west-central Greenland. SKBdoc 1875247 ver 1.0, Svensk Kärnbränslehantering AB.

Vallot D, Applegate P, Kirchner N, Petterson R, 2012b. Translating hydrologically relevant variables from the ice sheet model SICOPOLIS to the Greenland Analogue Project hydrologic modeling domain. SKBdoc 1882965 ver 1.0, Svensk Kärnbränslehantering AB.

Velicogna I, Wahr J, 2006. Acceleration of Greenland ice mass loss in spring 2004. Nature 443, 329–331.

Vidstrand P, 2003. Surface and subsurface conditions in permafrost areas – a literature review. SKB TR-03-06, Svensk Kärnbränslehantering AB.

Vidstrand P, Follin S, Zugec N, 2010a. Groundwater flow modelling of periods with periglacial and glacial climate conditions – Forsmark. SKB R-09-21, Svensk Kärnbränslehantering AB.

Vidstrand P, Rhén I, Zugec N, 2010b. Groundwater flow modelling of periods with periglacial and glacial climate conditions – Laxemar. SKB R-09-25, Svensk Kärnbränslehantering AB.

Waddington E D, 1987. Geothermal heat flux beneath ice sheets. In Waddington E D, Walder J S (eds). The physical basis of ice sheet modelling. (IAHS-AISH publication 170), 217–226.

Wallroth T, Lokrantz H, Rimsa A, 2010. The Greenland Analogue Project (GAP). Literature review of hydrogeology/hydrogeochemistry. SKB R-10-34, Svensk Kärnbränslehantering AB.

Walter F, Chaput J, Lüthi M P, 2014. Thick sediments beneath Greenland's ablation zone and their potential role in future ice sheet dynamics. Geology 42, 487–490.

Werder M A, Hewitt I J, Schoof C G, Flowers G E, 2013. Modeling channelized and distributed subglacial drainage in two dimensions. Journal of Geophysical Research: Earth Surface 118, 2140–2158.

Wright P J, Harper J T, Humphrey N F, Meierbachtol T W, 2016. Measured basal water pressure variability of the western Greenland Ice Sheet: Implications for hydraulic potential. Journal of Geophysical Research: Earth Surface 121, 1134–1147.

Appendix A

Stochastic simulation for 3D continuum

For modelling groundwater flow at the regional scale, the geological medium is considered as a 3D stochastic continuum, discretised by a regular grid of cells of uniform size. This approach is motivated since equivalent hydraulic properties at cell scale cannot be obtained using fracture data, because such data are not available for the modelled domain in Greenland. Therefore, the description of hydraulic properties for the geological medium is performed at cell scale using a stochastic simulation method which parameters are obtained from analogue sites in Sweden and Finland.

The turning bands method (Matheron 1973, Lantuéjoul 2002) is applied for the simulation of hydraulic properties. This stochastic method is based on geometrical considerations allowing the reduction of a multidimensional simulation in a series of one-dimensional simulations. These simulations are performed along lines sequentially distributed in the working space for homogeneous discretisation purpose. Along each line, a Gaussian stationary random function is simulated with mean 0, variance 1 and a given variogram model (Lantuéjoul 2002). The values of the random function in 3-dimensional space are obtained by a weighted sum of the projected values taken along each line.

The turning bands method besides performance advantages – 3D simulations at the CPU costs of 1D simulations – allows the generation of simulations with statistics that are consistent with the underlying theoretical model (Emery 2004).

The input of stochastic hydraulic properties for groundwater flow modelling using the DarcyTools simulator requires the following steps:

1. **3D stochastic simulation at face centres**
   The hydraulic conductivity is simulated by the turning bands method at face cell centres in directions X, Y and Z for the entire domain grid. The simulation parameters are: (a) anisotropic exponential variogram with horizontal and vertical correlation scales and (b) Gaussian distribution of log-hydraulic conductivity with zero mean and unit variance.
2. **Input and scaling of hydraulic conductivity**
   The simulated hydraulic conductivity is introduced in DarcyTools at centres of X-faces, Y-faces and Z-faces for the domain grid. Using parameters of Tables 5-1 to 5-3, the hydraulic conductivity is scaled for each hydrogeological unit according to depth.
3. **Attribution of permafrost hydraulic conductivity**
   This step consists in attributing the hydraulic conductivity value (10^{-15} m/s) for the permafrost, located west of the ice margin, up to a depth of 350 m (cases 6 and 7).
4. **Calculation of porosity**
   Using Equation (5-6) and X-face hydraulic conductivity, porosity is calculated at cell centres for the domain grid.
5. **Introduction of deformation zones**
   The deformation zones are introduced in the model domain using their hydraulic and geometric parameters (cf. Section 5.9).

Step 1 was performed using a program written by Lantuéjoul (1994). This program had to be modified by Jaquet (1998); i.e. calls to IMSL functions and subroutines were replaced for portability reasons. For the realisation of steps 2 to 5, specific FORTRAN routines were written by In2Earth which were used with DarcyTools.

Appendix B

Additional steady state cases

Framework and objectives

The two steady state cases 6 and 7 (cf. Table 6-2) applies the following data sets:

- Meltwater rate for the present day conditions from the ice sheet model VarGlaS (cf. Section 3).
- Ice thickness and bed topography from the GAP DEM (cf. Section 5.2).
- Horizontal deformation zones (cf. Section 5.9)
- Absence of subglacial layer.

And, in terms of the process involved, solely groundwater flow is considered for these two cases.

The objectives are: first, to compare the modelling results with the reference case of the groundwater flow modelling of phase II (Jaquet et al. 2012), and second to evaluate the impact of the horizontal deformation zones in view of their application to the transient cases.

Boundary conditions

Surface of the model (underneath the ice sheet): a spatially variable meltwater rate is applied, where the values are provided by an ice sheet simulation from VarGlaS (Brinkerhoff and Johnson 2013) representative of the present day conditions. The total meltwater rate is estimated as follows:

$$TMR = 0.3\ SMR + BMR \tag{B-1}$$

where:

TMR: total meltwater rate

SMR: surface meltwater rate from the ice sheet simulation with a 500 m resolution

BMR: basal meltwater rate from the ice sheet simulation with a 500 m resolution.

Since steady state conditions are considered, a weighting coefficient is applied to the surface meltwater rate, (Jaquet et al. 2012), a value of 0.3 was chosen, because surface meltwater occurs only during the summer period (i.e. the melt season : cf. Section 5-4). The total meltwater rate is used as input to a mixed boundary condition; i.e. the prescribed flux equals the total meltwater rate expressed in terms of dynamic fluid pressure constrained by the ice thickness, as follows:

$$q_{BC}\ if\ P_{BC}^{0} < P_{BC}^{ice}\ \ else\ P_{BC} = P_{BC}^{ice} \tag{B-2}$$

where:

q_{BC}: prescribed flux; i.e. total meltwater rate from the ice sheet model

P_{BC}^{0}: computed dynamic fluid pressure at boundary

P_{BE}^{ice}: dynamic fluid pressure corresponding to the ice thickness contribution

P_{BC}: prescribed dynamic fluid pressure.

With the dynamic fluid pressure, corresponding to the ice thickness contribution, written as (cf. Section 6.1):

$$P_{BC}^{ice} = \rho_{ice} g h_{ice} + \rho_{water} g z \tag{B-3}$$

where:

ρ_{ice}: ice density (= 917 kg/m^3)

h_{ice}: ice thickness

ρ_{water}: water density

z : elevation.

Surface of the model (west of the ice margin): at talik location, a dynamic fluid pressure $P_{talik} = p\ g\ z$ is prescribed, where z corresponds to talik surface elevation. Outside of taliks, conditions of no-flow are prescribed for the topographic surface.

Lateral west boundary: a hydrostatic condition is prescribed using a dynamic fluid pressure where the surface elevation z is set to a constant value equal to 37.5 m; this value corresponds to the mean elevation of the topography along the boundary.

$$P_{BC}^{west} = \rho_{ice}\ g\ mean\left(h_{ice}\left(x_B\right)\right) + \rho\ g\ 37.5 \qquad \text{(B-4)}$$

Lateral north+south+east and bottom boundaries: no-flow conditions are prescribed.

No additional boundary conditions are required since the only process considered is groundwater flow under steady state conditions. The permafrost is only located in front of the ice margin with the exception of the taliks; it has a constant thickness, equal to 350 m, and with a hydraulic conductivity set to 10^{-15} m/s. The hydraulic properties for the rock mass domain and the deformation zones are taken from the Laxemar site (cf. Sections 5.5. and 5.9).

Simulation

For the cases 6 and 7, groundwater flow simulation is performed under steady state conditions. Regarding the mixed hydraulic boundary conditions beneath the ice sheet, an iterative procedure is needed; using the specified flux values (i.e. the total meltwater rate), the head solution is calculated at each iteration. After each iteration, the solution is analysed: if boundary value(s) with hydraulic head higher than the ice thickness occur, the iteration is restarted with prescribed hydraulic head – equal to the ice contribution, cf. Equation (B-2) – for these boundary values. After the convergence of the mixed boundary conditions, a final run with fixed boundary conditions is performed in order to improve convergence, in terms of lowering the value of the residual mean square error.

The case 6 and the case 7 – with horizontal deformation zones – display similar flow fields at regional scale (Figures B-1, B-2 and B-3) when compared to the reference case of phase II (Jaquet et al. 2012). The main difference is related to the larger range of the prescribed pressure for the ice sheet; the simulations for these two cases are based on the GAP findings, i.e. the prescribed pressure equals the ice overburden hydraulic pressure (cf. Section 6.1). These GAP results were not known at the time of the groundwater flow model of phase II and a narrower range was applied for the ice prescribed pressure of the reference case (Jaquet et al. 2012).

The comparison of cases 6 and 7 shows some differences in hydraulic head due to the presence of the horizontal deformation located in the upper layers of the model domain (Figure B-4). Therefore, the horizontal deformation zones were considered for the modelling of the five transient cases (cf. Section 6).

Using case 7, average recharge and average discharge are calculated over a specified domain, for horizontal planes at a given elevation. The elevation values of the horizontal planes are located between the lowest surface elevation point of the model domain and −1 000 m; these horizontal planes are selected every 100 m. The specified domains for flux averaging are respectively located west of the ice margin and below the ice sheet (subglacial). The obtained results are given by domain in terms of average recharge/ discharge curves as function of elevation (Figures B-5 and B-6).

At high elevation, the subglacial domain presents the highest recharge and discharge values due to the amount of surface and basal meltwater provided by the ice sheet. This effect is damped when reaching a lower elevation; the two domains present similar behaviour in fluxes below an elevation of about −600 m.

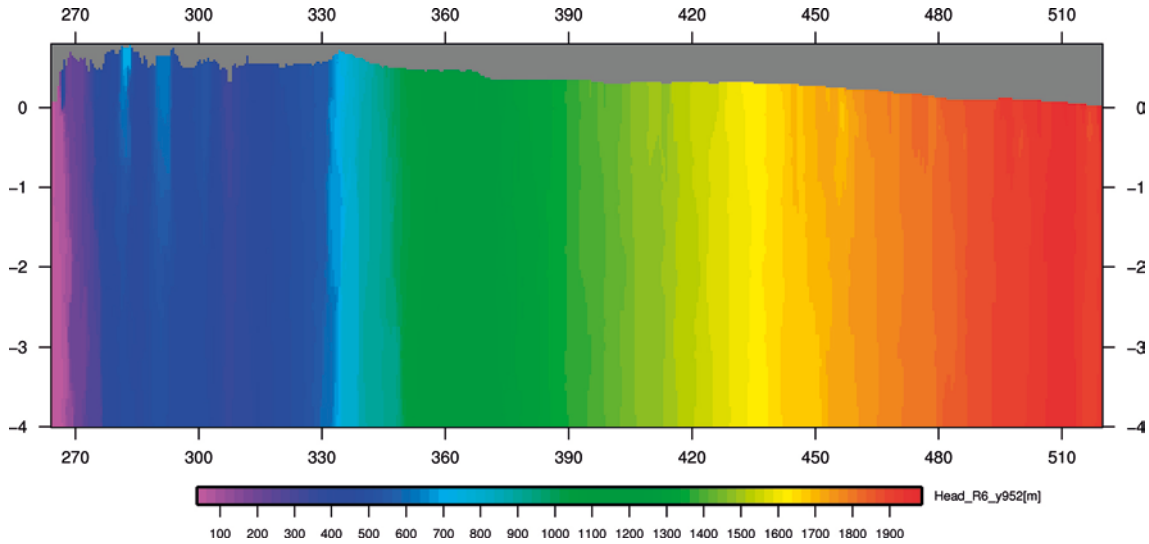

Figure B-1. *Case 6: hydraulic head [m], E-W vertical at Y = 952 km (coordinates in km).*

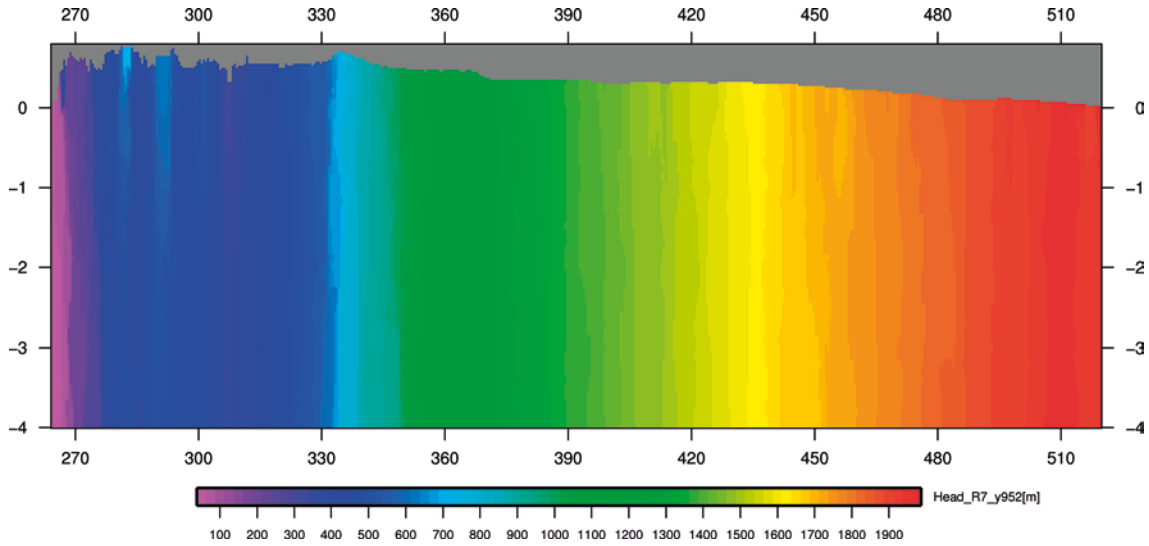

Figure B-2. *Case 7: hydraulic head [m], E-W vertical at Y = 952 km (coordinates in km).*

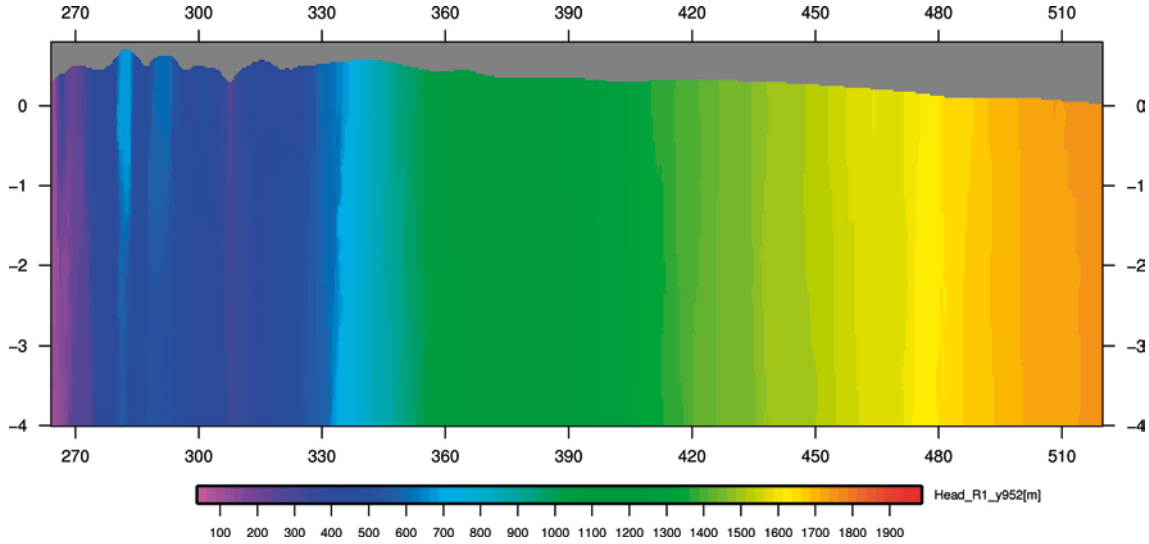

Figure B-3. *Reference case – phase II: hydraulic head [m], E-W vertical at Y = 952 km (coordinates in km).*

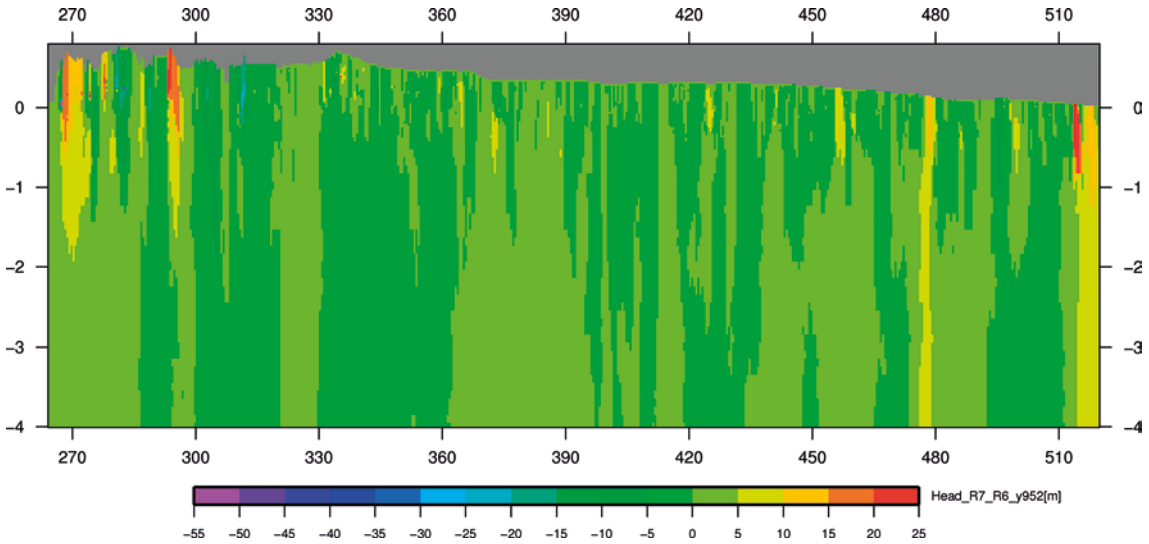

Figure B-4. *Case 7 – case 6: hydraulic head differences [m], E-W vertical at Y = 952 km (coordinates in km).*

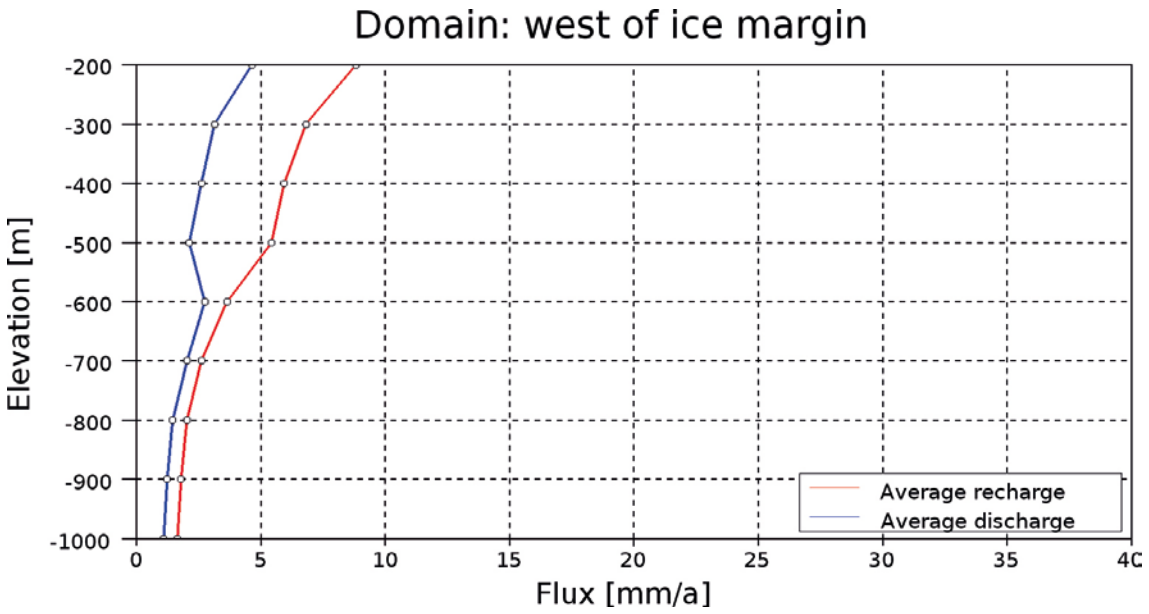

Figure B-5. *Case 7: average recharge/ discharge in terms of elevation, for the domain located west of the ice margin.*

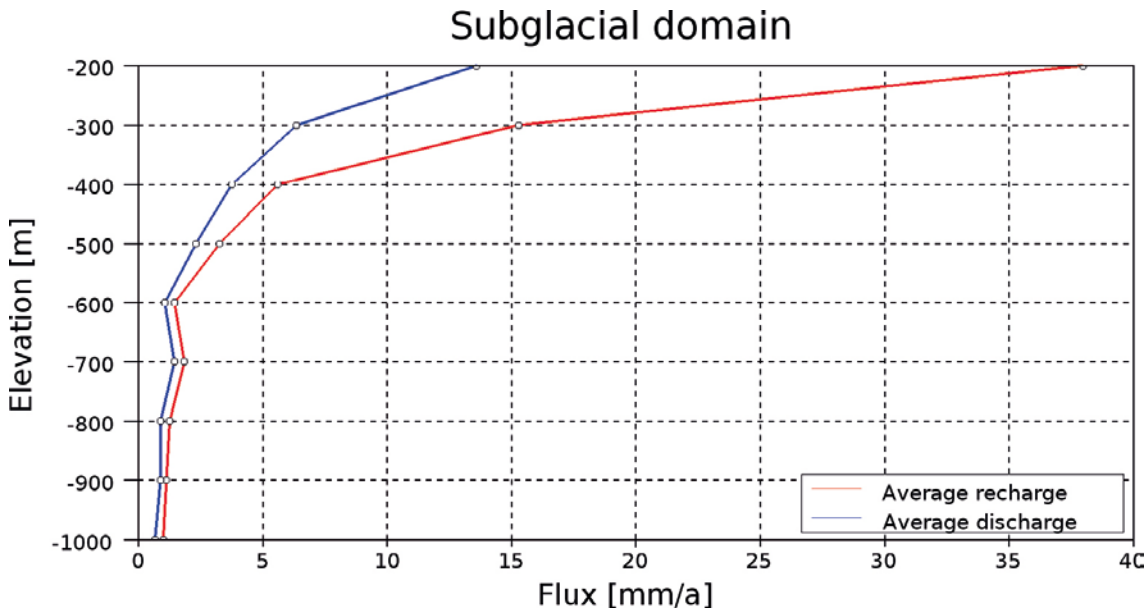

Figure B-6. *Case 7: average recharge/ discharge in terms of elevation, for the subglacial domain.*

Appendix C

Sensitivity analysis of subglacial boundary conditions

Objective

The aim is to compare the impact of two different types of subglacial boundary conditions in terms of recharge for the the case 1 – Laxemar; in relation to the ice sheet periods of build up, completeness and retreat.

Modelling cases

The case 1 with subglacial boundary conditions expressed in terms of dynamic fluid pressure was already calculated for the three ice sheet periods (cf. Section 6.1). Regarding the other type of boundary conditions, two additional cases (i.e. cases 8 and 9) are needed for comparison: they are simulated in terms of steady state groundwater flow, using subglacial boundary conditions taken from specific time steps of the SICOPOLIS ice sheet model (cf. Section 3), in relation to the ice sheet periods of build up and completeness. And for the period of ice sheet retreat, it corresponds to case 7, computed previously for present day conditions (cf. Appendix B) where the surface of the model domain, covered by the retreating ice sheet, is similar.

The following data sets and boundary conditions are used as input for the modelling of cases 8 and 9.

Data sets

The following data sets are applied:

- Bed topography from the GAP DEM (cf. Section 5.2).
- Hydraulic properties for the rock mass domain and the deformation zones from the Laxemar site (cf. Sections 5.5 and 5.9).
- Horizontal deformation zones (cf. Section 5.9).
- Surface and basal meltwater rates as well as ice thickness from the SICOPOLIS ice sheet model (glaciation scenario I for the Laxemar site (Vallot et al. 2012a, b): cf. Section 6.1 and Table 6-1) at time steps −110ka (i.e. build up period with the entire domain covered by ice sheet) and −102 ka (i.e. completeness period with the entire domain covered by the ice sheet at its maximum thickness).
- Absence of permafrost; the model domain being fully covered by the ice sheet at −110 ka and −102 ka. As for the case 7; absence of subglacial layer (cf. Appendix B).

Both bed topography and surface and basal meltwater rates were interpolated at the grid cell centres of the groundwater flow model (with a 500 m resolution: cf. Sections 5.2 and 6.1).

The surface and basal meltwater rates applied as input to the estimation of the boundary conditions are displayed for the ice sheet periods of build up and completeness at selected time steps (Figures C-1 and C-2). Both surface and basal meltwater rates exhibit larger values during the period of glacial completeness.

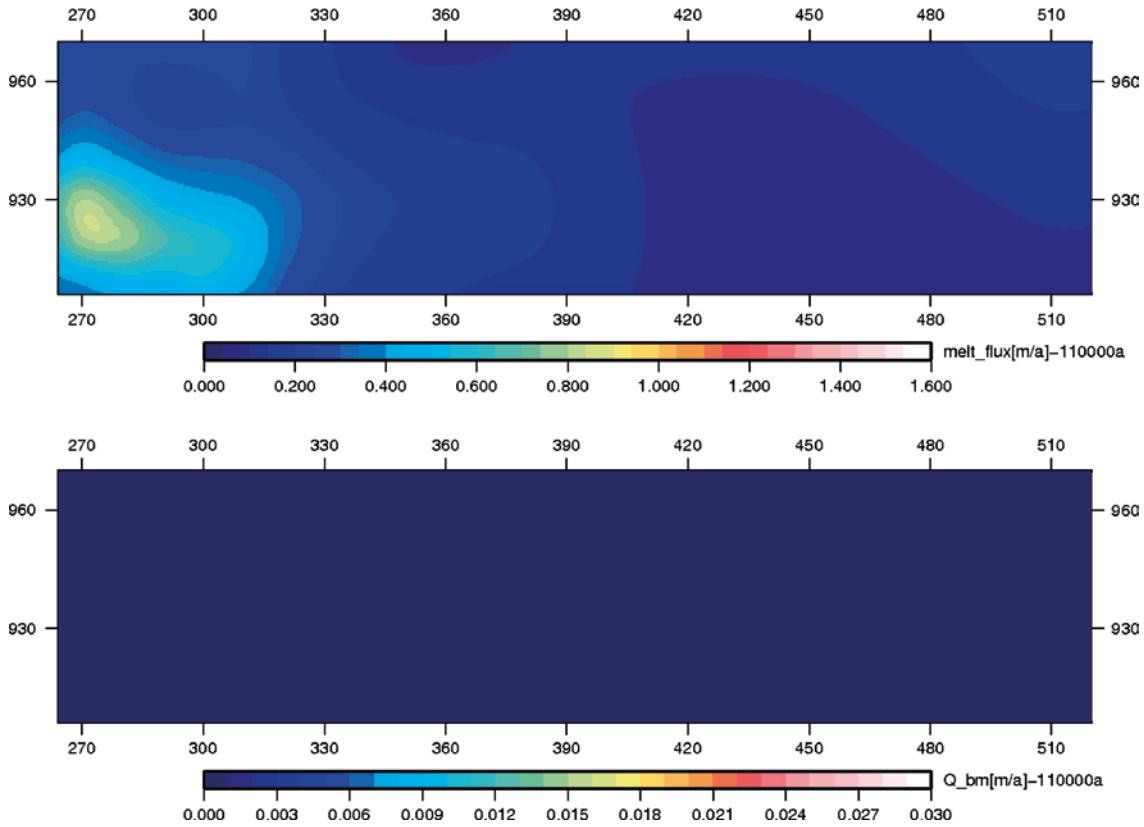

Figure C-1. *Period of glacial build up (−110 ka): surface meltwater rate (above) and basal meltwater rate (below), interpolated from the SICOPOLIS ice sheet model and expressed in [m/a]; coordinates in km.*

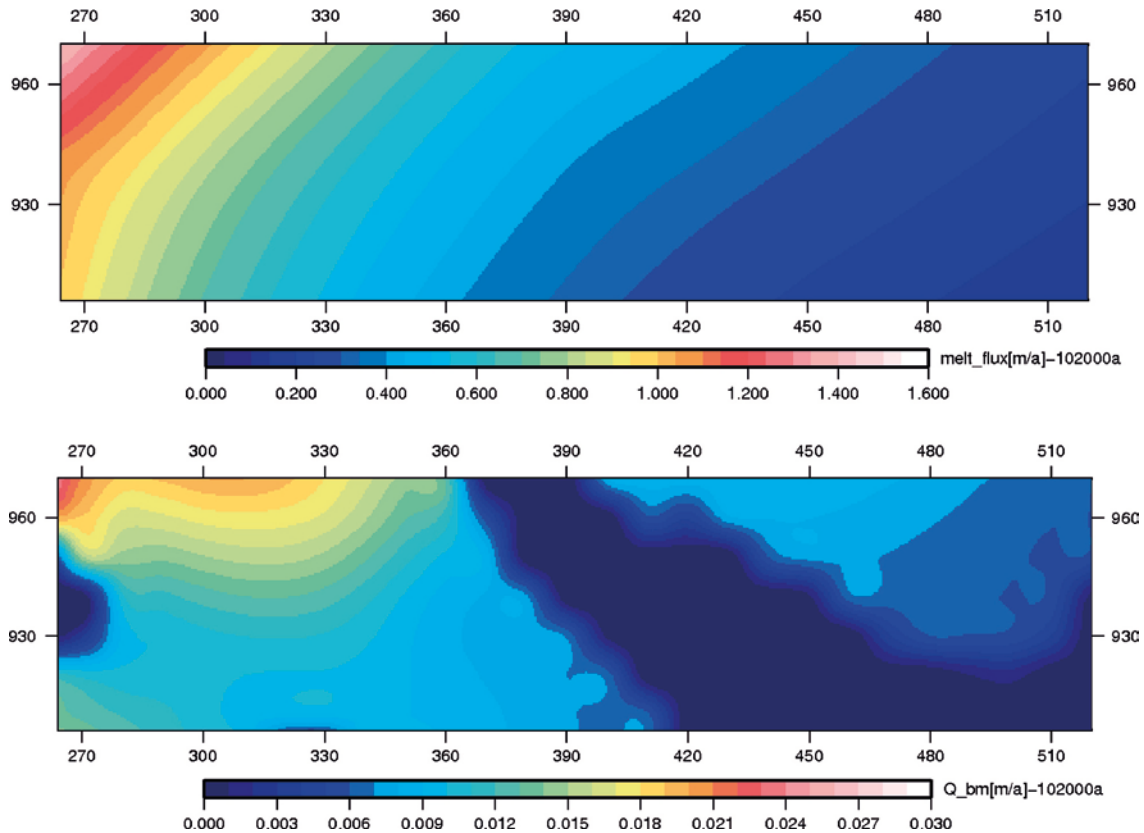

Figure C-2. *Period of glacial completeness (−102 ka): surface meltwater rate (above) and basal meltwater rate (below), interpolated from the SICOPOLIS ice sheet model and expressed in [m/a]; coordinates in km.*

Boundary conditions

Surface of the model (underneath the ice sheet): a spatially variable meltwater rate is applied, where the values are provided by an ice sheet simulation from SICOPOLIS, taken at two specific time steps representative of the glacial periods of build up and completeness (glaciation scenario I: respectively at −110 ka and −102 ka). The total meltwater rate is estimated as follows:

$$TMR = 0.3\ SMR + BMR$$

where:

TMR: total meltwater rate

SMR: surface meltwater rate from the ice sheet simulation

BMR: basal meltwater rate from the ice sheet simulation.

Since steady state conditions are considered, a weighting coefficient is applied to the surface meltwater rate (Jaquet et al. 2012), a value of 0.3 was chosen, because surface meltwater occurs only during the summer period (i.e. the melt season : cf. Section 5-4). The total meltwater rate is used as input to a mixed boundary condition; i.e. the prescribed flux equals the total meltwater rate expressed in terms of dynamic fluid pressure constrained by the ice thickness, as follows:

$$q_{BC}\ if\ P_{BC}^{0} < P_{BC}^{ice}\ \ else\ P_{BC} = P_{BC}^{ice}$$

where:

q_{BC}: prescribed flux; i.e. total meltwater rate from the SICOPOLIS ice sheet model

P_{BC}^{0}: computed dynamic fluid pressure at boundary

P_{BE}^{ice}: dynamic fluid pressure corresponding to the ice thickness contribution

P_{BC}: prescribed dynamic fluid pressure.

With the dynamic fluid pressure, corresponding to the ice thickness contribution, written as :

$$P_{BC}^{ice} = \rho_{ice} g h_{ice} + \rho_{water} g z$$

where:

ρ_{ice}: ice density (= 917 kg/m^3)

h_{ice}: ice thickness from the SICOPOLIS ice sheet model

ρ_{water}: water density

z: elevation.

Lateral west boundary: a hydrostatic condition is prescribed using a dynamic fluid pressure where the surface elevation z is set to a constant value equal to 37.5 m; this value corresponds to the mean elevation of the topography along the boundary.

$$P_{BC}^{west} = \rho_{ice}\ g\ mean\left(h_{ice}\left(x_B\right)\right) + \rho\ g\ 37.5$$

Lateral north+south+east and bottom boundaries: no-flow conditions are prescribed.

No additional boundary conditions are required since the only process considered is groundwater flow under steady state conditions.

Simulation

For the cases 8 and 9 (Table C-1), groundwater flow simulation is performed under steady state conditions using the data sets and boundary conditions, described in the above section. Case 8 disposes of boundary conditions related to the period of build up for the ice sheet (cf. Figure C-1); and regarding case 9, its boundary conditions corresponds to the period of glacial completeness (cf. Figure C-2).

Table C-1. Specifications for the two modelling cases.

Case	Processes	Hydraulic properties	Steady state boundary conditions (ice sheet)	Objectives
8	Flow steady state	Laxemar[1)] (with horizontal deformation zones)	Prescribed meltwater rate from the SICOPOLIS ice sheet model (build up period, − 110ka)	Impact of subglacial boundary conditions in terms of recharge
9	Flow steady state	Laxemar[1)] (with horizontal deformation zones)	Prescribed meltwater rate from the SICOPOLIS ice sheet model (completeness period, −102 ka)	Impact of subglacial boundary conditions in terms of recharge

[1)] Absence of permafrost and subglacial layer.

Fluxes

For the flux calculations, average recharge and discharge are calculated for each of the two cases over the studied domain, for horizontal planes at a given elevation. The elevation values of the horizontal planes are located between −200 m and −1 000 m; and, these horizontal planes are selected every 100 m. The obtained results are given for cases 7, 8 and 9 in terms of average recharge/ discharge curves as function of elevation (Figure C-3). These cases represent respectively the period of glacial retreat, build up and completeness. In term of recharge, the periods of glacial retreat (case 7) and build up (case 8) present similar behaviours, with decreasing values with depth. The period of glacial completeness (case 9) stands out in relation to the presence of higher meltwater rate (cf. Figure C2); i.e. the observed recharge values are significantly larger than the values of the other two glacial periods. But the recharge values for this period remain below 20 mm/a at the depth range of interest. The respective discharge values in relation to the different glacial periods present lower values; this systematic difference is due the the lateral west boundary (cf. Section Boundary conditions) where part of the flow can exit the model domain.

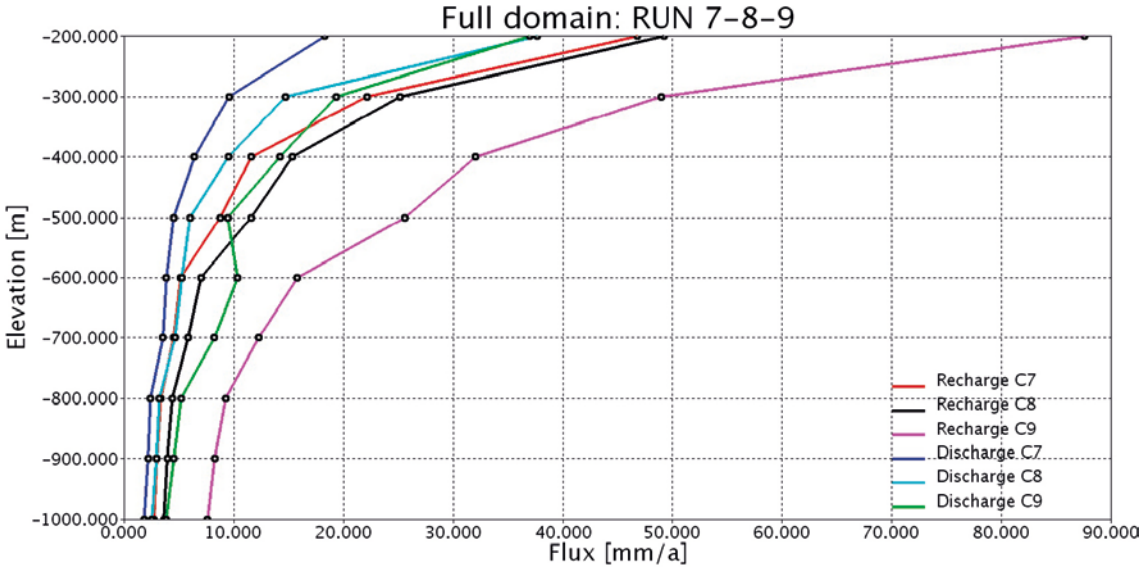

Figure C-3. *Cases 7, 8 and 9: respectively period of glacial retreat, build up and completeness, average recharge/ discharge, [mm/a], in terms of elevation, for the modelled domain.*

Comparison of subglacial boundary conditions

The recharge results for the steady state cases 8 (build up), 9 (completeness) and 7 (retreat), simulated with meltwater rate boundary conditions, are compared with those of the transient case 1, simulated with dynamic fluid pressure boundary conditions at specific time steps. As a reminder, case 1 is also representative of the Laxemar site (cf. Section 6.1) and flux calculations were already performed for the glacial periods of interest (cf. Section 7.1). The recharge results in relation to the two different types of boundary conditions and for the glacial periods of build up, completeness and retreat are displayed in Figure C-4.

For the case 1 with dynamic fluid pressure boundary conditions, the larger recharge values observed near the top are related to the high conductive subglacial layer (cf. Section 7.1). This amount of shallow recharge is directly link to the hydraulic conductivity of the subglacial layer, since the dynamic fluid pressure boundary conditions can provide unlimited water supply. These large recharge values disappear rapidly, at lower elevation, for the glacial periods of build up and retreat. However, for the period of glacial completeness, this decrease of the recharge values is more gradual with depth; i.e. the effect of the subglacial layer is decreased due to lower gradients of ice thickness during this glacial period and hence, more water is likely to penetrate at depth.

For the cases 8, 9 and 7 with meltwater rate boundary conditions, lower recharge values are observed near the top and the decrease of the recharge values with depth is more progressive. And, lesser variability in recharge observed between the different glacial periods. For these three cases, although the input data is the total meltwater rate, mixed boundary conditions are applied; i.e. in the presence of fluxes leading to a dynamic fluid pressure exceeding the corresponding ice thickness, the boundary conditions become of the dynamic fluid pressure type, and this for a significant part of the modelled domain (cf. Jaquet et al. 2012). Therefore, the shallow recharge values and the recharge behaviour at depth are influenced by the meltwater rate boundary conditions, limiting water supply; and to a lesser extent by the absence of the subglacial layer.

Finally, at the 500 m depth of interest (i.e. corresponding to an elevation of about −700 m, due to the potential presence of valleys and troughs), the variability range of the recharge lies between 1–23 mm/a, whatever the type of boundary conditions or glacial periods considered.

In conclusion, the recharge at depth is impacted by the choice of boundary conditions. However, for many situations, the application of dynamic fluid pressure boundary conditions, based on ice overburden hydraulic pressure (cf. Section 6.1), is justified; in particular, for present day conditions (in Greenland), as shown by the GAP observations and conceptual considerations (cf. Section 5.4). But care should be taken, when a full glacial cycle is under consideration, since dynamic fluid boundary conditions are likely to provide overestimation of recharge at depth, in particular for glacial periods with limited water supply.

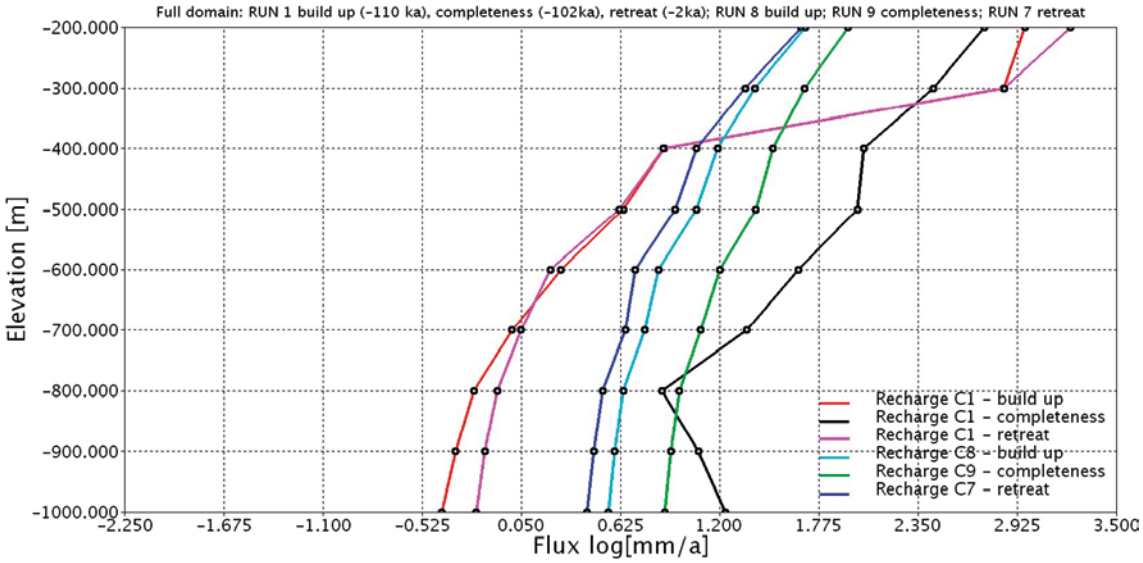

Figure C-4. *Comparison of boundary conditions : dynamic fluid pressure (case 1) versus meltwater rate (cases 8, 9 and 7) for the periods of glacial build up, completeness and retreat, average recharge, log[mm/a], in terms of elevation, for the modelled domain.*

Appendix D

Numerical parameters and procedure

For the iterative resolution of the system of coupled equations, the first criterion that is applied is the reduction of the normalised least square residual using the following reduction factor values for each equation:

- Heat transfer: 10^{-6}
- Mass conservation: 10^{-10}
- Salt transport: 10^{-6}

The second added criterion (not implemented in DarcyTools) is a verification of the non linear convergence with respect to results of consecutive iterations:

- Heat transfer: $\max | T_n - T_{n-1} | < 0.1$ °C
- Mass conservation: $\max | H_n - H_{n-1} | < 0.01$ m
- Salt transport: $\max | S_n - S_{n-1} | < 0.1$ %

For the mass conservation a large value for the reduction factor is required in order to obtain accurate results meeting the second convergence criteria. Such accuracy is required for solving the salt transport equation.

At each time step, each equation is linearly solved using DarcyTools with a specific number of iterations, *liter*, and then the non linear system is resolved with the help of 20 additional iterations or sweeps, until reaching the different criteria of convergence. Numerous convergence problems have emerged, the results obtained with the standard parameter values for the solver were not acceptable; i.e. the convergence criteria could not be met, even when using large numbers of iterations. These problems are caused by the strong variability of the permeability fields under permafrost conditions and the rapid changes in the ice boundary conditions, provided by the ice sheet model. By performing numerous tests, a careful selection of the solver parameter values (cf. Table C-1) has enabled to solve these convergence issues. And, the time discretisation (500 years) provided by the data from the ice sheet model could be kept, which has allowed to produce manageable run-times; however, well above one month of calculations for the simulation of the complete glacial cycle. Attempts to use smaller time steps have lead to unacceptable run-times with convergence problems. Finally, latent heat effects (cf. Equation 4-4) are not considered due to numerical problems; and, as mentioned in Section 4-3, the contribution of water freezing to heat transfer is minor when porosity for water-saturated rock is less than 1 % (SKB 2006).

Table C-1. Values of numerical parameters for the MIGAL solver* (Svensson and Ferry 2010); applied for all the five cases.

Equation	*nbrelax*	*relin*	*igmres*	*liter*	*alpha*	*ipreco*
Heat transfer	10	0.80	3	10	0	3
Mass conservation	10	0.75	80	200	0.25	1
Salt transport	10	0.75	10	10	0	3

*Algebraic multi-grid solver used in DarcyTools.

Arkitektkopia AB, Bromma, 2019

SKB is responsible for managing spent nuclear fuel and radioactive waste produced by the Swedish nuclear power plants such that man and the environment are protected in the near and distant future.

skb.se